

# THE APPLICATION OF METALLOINTERCALATORS IN RECOGNITION OF AND CHARGE TRANSPORT IN NUCLEIC ACIDS

Thesis by

Duncan T. Odom

*Submitted in Partial Fulfillment  
of the Requirements  
for the Degree of Doctor of Philosophy*

California Institute of Technology

Pasadena, California

2001

(Submitted 16 January 2001)

© 2001

Duncan T. Odom

All rights reserved.



## **ACKNOWLEDGEMENTS**

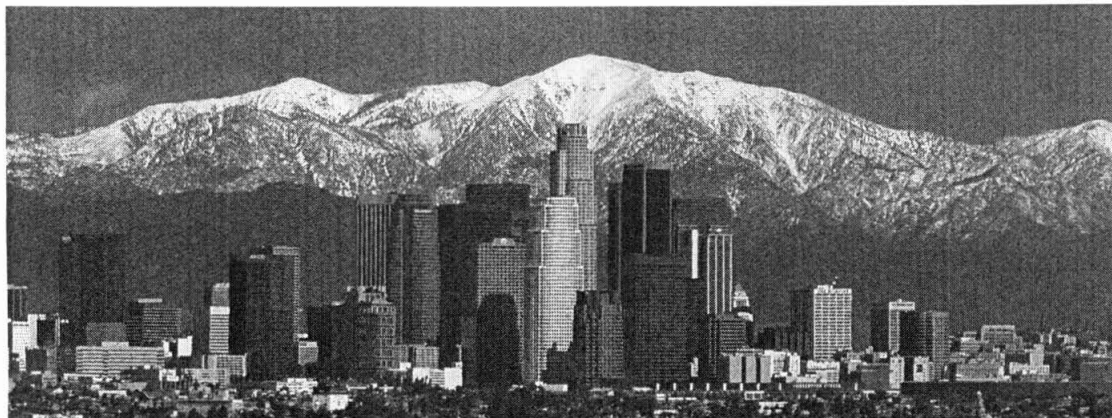
Over the last five years so many people and groups have contributed to my professional and personal development that I have a great deal of difficulty imagining even where to start. However, in the tradition of all good scientific analysis, I will start with the big and global and work my way down to the individual level, though, with a nod to my own persona, in a haphazard way.

Of course, without the generous funding of the NIH and the NRSA, none of the work in this dissertation would have been possible. The Parson's Foundation Fellowship supported me my last year at Caltech, and thanks goes out to them. The Gordon Conferences are one of the absolute best scientific venues to learn a frightening amount of material in a very short order of time. I was honored to have attended so many. ICBIC 6 and 9 offered a more broad band of appeal, and are one of the best overviews of an entire field that I think could ever be assembled. Harry Gray is an eternal source of inspiration and support, and Rick Young re-inspired me to continue in science with his talk on DNA microarrays. I am pleased and honored to be joining Rick's laboratory in a few months to pursue this subject. For all its problems (and it's got some pretty damn big ones!), it is hard to imagine a place that is as supportive and awesome as the California Institute of Technology, and MIT has a lot to live up to.

Jackie Barton has been a great, if at times exasperating, advisor, and I am glad that I have served in her laboratory. It is hard to adequately thank her for the opportunity to join the group, and the incredible scientific support I received while here. You truly do have the killer instinct, and I think I have absorbed a little of that while I have been here. And, yes, I admit that you have improved my writing, and my structuring of problems, not that you would know it from this acknowledgement. And I am extremely grateful for the generous opportunity to attend numerous conferences. The importance of learning about colleagues's work cannot be overstated, and her strong support of all of us in the group to attend scientific meetings is a great thing. Your unflagging interest in science and willingness to pursue unusual scientific interests is very inspiring.

Carl Parker has been a mentor to me, in many ways. The positive feedback and professional support that you gave me has kept me going, and kept my passion towards science from despair. After all, "It feels great when science works." Your laboratory was a haven for me. In addition to being a great source of scientific advice, I am honored to

have become friends with you, especially in the last year. I think that you make a great scientist and great friend. I look forward to working with you further. On a lighter note, thanks for lending me the Fly Room. 173 Braun must be completely weighted down with residual emotion from my travails--first candidacy, then my props, and now my thesis. But all jokes aside, without that private space to write and read and research, I never would have finished this Work in time, and certainly NOT been able to have imagined good research proposals.



Clearly, Caltech would not be Caltech without being in California. And for the first time I have lived somewhere where I feel part of the overall mainstream of the political, personal, and aesthetic currents. California is truly a nation in and of itself (secede now!!!), and I will always miss it. Los Angeles is the jewel in California's crown, and, as you may be able to tell, will always be my home. I will always miss the freeways and the sunsets and the mountains and the deserts and the ocean and Hollywood and the 3 a.m. Chinese food at FullHouse after long hard nights of dancing.

Thanks to the US Forestry Service for protecting, however imperfectly, the National Forests of Southern California (Los Padres, Angeles, Cleveland, San Bernardino) that so often kept me sane by being a peaceful and rugged escape from Pasadena. How do I even start—may your beauty be ever unmarred! The Theodore Payne Foundation and nursery allowed me to volunteer my life and time to the propagation of native California plants, and I am grateful for the opportunity to give back to this place that I love so much. Beyond Baroque Literary Arts Center in Venice, Midnight Special, and the Cobalt Café provided enormously needed distractions of poetry readings and workshops. LACMA, the Armory, Norton Simon, Huntington, Museum of Jurassic Technology, and ArtCenter have all given me great pleasure and often gotten rid of pesky visitors so I could work.

*All-Saint's Episcopal Church*, in addition to being a gorgeous place physically, is always part of me as an engine for social change.



The struggling bands that have meant so much to me: the late and lamented Congregation, and the Negro Problem, and Opie Gone Bad, and Candypants, and Itch, and Ann Magnuson, and Simon Stinger, and Jennifer Robin, and Jenna Music, and Gene Loves Jezebel. And most importantly of course, the all-powerful Space Team Electra, and its muse Infinity Starpants (a.k.a. Myshel Prasad), that have introduced me to so much wonderful literature and philosophy, and put to song so much of my own wonder, and our inability to comprehend anything. May you rise to the top--despite the weighty substance you are made of!

I would also like to thank the music venues and theaters and dance places I have spent so much time in. Some are awesome, some sleazy, some predatorial towards their artists, but all serve to advance music in some way. Luna Park (rest in peace), Silver Lake Lounge, the Dresden Room, 14 Below (I'll never forgive ya'll, though, for never paying your artists), both Gigs (Hollywood and Westside), the Mint, Jack's Sugar Shack, the Tiki-Ti, the Room, the Queen Mary (drag shows at their finest), the El Rey Theater, the Rialto, the ever-missed State Theater on Colorado, the Mayan, the Martini Lounge, the Whiskey-a-Go-Go, and of course, *Spaceland*. I swear to be a regular one of these days. Finally, I'd like to extend a special thanks to the Meister of the SF Bay Area area rock scene, the Paradise Lounge, pilgrimage site of my first insane trip to see Infinity and Space Team Electra, and of course Alpha-Omega Recording Studios in San Rafael for putting me up that night.

Trish Strickler for reminding me that true love is not impossible. Just maybe really, really difficult. If you ever read this, I apologize for not being who I should have been and want to be some day. Alyce Wittenstein for visiting and showing her movie "Multiple Futures." Sue Friedman for keeping me sane with so many band trips and late nights. You are one of the best friends I have ever had. Tashica Williams, my bay-mate. Your passion and fire are so wonderful. Just keep on the saddle with them, and they will lead you as far as anyone could ever want. Megan Nunez, my scientific sounding board and political

*bud. Thanks for the encouragement and reminder that I am not alone as a progressive here in this Institute. Liz Boon, one of the kindest people that I have ever met. Matthias and Sarah for being such a disgustingly happy couple. Dan Hall & Marilena Fitzsimons Hall, a couple of literal angels dropped on this earth. Your hospitality in Boston made my decision to come there so much easier. I hope I can somehow repay your kindness when I am there. Ai Ching Lim, Tim Johann, and Brian Hudson for being the social catalyst that pulled me into the Barton group. Brian Jackson for reminding me of how important it is to be forgiving and gracious. Jen Ottesen for early friendship at Caltech that made my transition from a New College hippie to a Techer much easier. Barbara Imperiali for being my initial advisor at Caltech, and encouraging me to extend myself intellectually. I regret that things did not work out well. Jennifer Johnson for saving me during one of the darkest times of my life. You were a lifeline from the Bjorkman lab when I was drowning and pulled me from the deep end of that damn pool. Bill Schrader again for early guidance and mentoring. Thanks for all the advice—it was among the best I have ever gotten. Sarah O'Connor, one of the brightest people that I have ever known, and good for you and Mo-Mo. Cathy Sarisky, also one of the smartest people that I know--again, sorry things got so bad. Congrats to you and Tim, hope Seattle is not too rainy. Chantal Morgan for being a wonderful and supportive friend from day one of my arrival at Caltech. More recently, for reminding me that there are options besides science that can be just as intellectually and personally rewarding. You have been a great role model. Scott Carter has also served as a great role model that way, not to mention being a hell of a nice guy. Stella Ota for making the last few months here a lot more fun.*

*Deepshikha Datta for a long and at times unusual friendship. I love your point of view, and our talks. Your husband is the luckiest guy in the world. Christine Davis-Rener for all the advice and friendship when I was first settling into the Barton group. Your wedding was a blast, even if it was “a fascist ritual to prove your love.” (!) Kitty Erkkila, my collaborator in so much, and dear friend. Your sense of humor and easy laughter will always warm me wherever I am. Amazing how resilient and enduring friendship can be, isn't it? Tianxin Cynthia Chen, a good friend. It was inspiring to watch you grow into who you are now. Dianne Sullivan, your strength and courage are an inspiration to me. This last year was without a doubt one of the most challenging of your life, and you have really risen to the occasion. You have saved yourself from destruction, and it is a pleasure to see you standing on your own. You have the best voice in the entire world, and I will see you this summer in Wales (I hope!).*

My mother and family have always been supportive, if slightly puzzled by why the hell I would ever want to go to school for a total of 25+ years. Let me assure you that I have yet to figure it out myself. But really, without you all, I would have had a much, much harder time getting here.

Now-professor Scott Rajski and Olav Schiemann served also as fantastic role models and were always there when I needed them. Scott taught me a great deal about how to view the world cynically and yet hopefully, and Olav taught me lots of hidden things. Those lessons too are invaluable.

For everyone else I may have missed (I just have run out of energy to type more), thanks for being there to support me, and to challenge me.





Henrik Junicke. You are one of the funniest and most brilliant guys that I have ever met, and I love you to death for it. The coffee, the scheming ('Evil plots don't just hatch themselves, you know'), all the lunches. You are one of the most loyal friends I have ever had. I will always remember the time that we have all spent together making barbeques—they are the most unallayed moments of companionship I have ever had. The mornings I arrived in lab to see your face, I knew that it was going to be a good day. You always had something interesting or funny to blow me away with. Writing this section hurts, because I really do not want this aspect of my life to end. I always want Jen and you and I to stay close. Well, I suppose that it is a good thing that flights to Europe are so cheap these days. And, no, I will not take a DC-10. I promise. Or the Concorde. I guess that that is a moot point, huh? We should make a barbeque sometime.

Jennifer Kisko. Ah, Jen. Save the best for last. Who would have guessed? Our friendship and comraderie has been the high point of the last six years. You are certainly the best friend that I have had in my life. I never imagined that I could miss a friend as profoundly and painfully as I miss you, even when we are only apart for mere days. Your friendship has been a rudder in the most violent of storms. We have to end up in the same city relatively soon, because I will go nuts without you there to rag on me and keep me in line. Besides, you look hilarious when you have been drinking, with fat red cheeks and that glazed look on your face; that always cheers me up whenever I feel bad. You know, I could not help but notice that your hair today really looks great!

I will always remember: Rick's. Grover. Grover's footprints. Boo! Spooky. Look who it is! Swing-Dance Smurf. Action Smurf. Sushi of Naples. Goth Barbie. Grover. Berries on the map. Ninja Training. 'Boyfriend' aka (Jason)<sub>n</sub>. San-Sui sushi. The Huntington ER. Sand-Dunes. A Pet Lynx. Napster. Dunconimus Gothicus I-IV. A'Float Sushi. Hidden PCR Micro-eppies. Sais. Thrill Kill Kult. Absynthe. Coven 13. Jerry's. Canter's. Astro. Floppy Black Hats. Smelly Feet. Elbow-Cancer. Banana-Hair. Carpeted doors. Candalabras. Candles. Reservoir-Dogs Café. The Ath. Ath Girl. Coffee and a coke. Making Barbeque. Jessica Rabbit. Bombed the World. *Oscar*.



## ABSTRACT

Metal complexes that utilize the 9,10-phenanthrene quinone diimine (phi) moiety bind to DNA through the major groove. These metallointercalators can recognize DNA sites and perform reactions on DNA as a substrate. The site-specific metallointercalator  $\Lambda$ -1-Rh(MGP)<sub>2</sub>phi<sup>5+</sup> competitively disrupts the major groove binding of a transcription factor,  $\gamma$ AP-1, from an oligonucleotide that contains a common binding site. The demonstration that metal complexes can prevent transcription factor binding to DNA site-specifically is an important step in using metallointercalators as therapeutics.

The distinctive photochemistry of metallointercalators can also be applied to promote long range charge transport in DNA. Experiments using duplexes with regions 4 to 10 nucleotides long containing strictly adenine and thymine sequences of varying order showed that radical migration is more dependent on the sequence of bases, and less dependent on the distance between the guanine doublets. This result suggests that mechanistic proposals of long range charge transport must involve all the bases.

RNA/DNA hybrids show charge migration to guanines from a remote site, thus demonstrating that nucleic acid stacking other than B-form can serve as a radical bridge. Double crossover DNA assemblies also provide a medium for charge transport at distances up to 100 Å from the site of radical introduction by a tethered metal complex. This radical migration was found to be robust to mismatches, and limited to individual, electronically distinct base stacks. In single DNA crossover assemblies, which have considerably greater flexibility, charge migration proceeds to both base stacks due to conformational isomers not present in the rigid and tightly annealed double crossovers.

Finally, a rapid, efficient, gel-based technique was developed to investigate thymine dimer repair. Two oligonucleotides, one radioactively labeled, are photoligated via the bases of a thymine-thymine interface; reversal of this ligation is easily visualized

by gel electrophoresis. This assay was used to show that the repair of thymine dimers from a distance through DNA charge transport can be accomplished with different photooxidants.

Thus, nucleic acids that support long range charge transport have been shown to include A-track DNA, RNA/DNA hybrids, and single and double crossovers, and a method for thymine dimer repair detection using charge transport was developed. These observations underscore and extend the remarkable finding that DNA can serve a medium for charge transport via the heteroaromatic base stack.



<b>CHAPTER 1: RECOGNITION AND REACTIVITY OF METALLOINTERCALATORS WITH DNA</b>	I-1
<b>1.1 INTRODUCTION</b>	I-2
<b>1.2 RECOGNITION OF DNA BY METALLOINTERCALATORS</b>	I-3
1.2.1 BACKGROUND – EARLY METAL COMPLEXES	I-3
1.2.2. INCREASING DNA AFFINITY AND DISCRIMINATION BY INTERCALATION	I-5
1.2.2.1. <i>Intercalation as a Platform for Binding</i>	I-5
1.2.2.2. <i>Metal Complexes of Dipyridophenazine and Triphenylene</i>	I-5
1.2.2.3. <i>Porphyrin Intercalation into DNA</i>	I-11
1.2.3. DNA RECOGNITION BASED ON SHAPE SELECTION BY PHI COMPLEXES	I-13
1.2.3.1. <i>[M(phen)<sub>2</sub>phi]<sup>3+</sup> Recognition of 5'-Py-Pu-3' Sites</i>	I-14
1.2.3.2. <i>[Rh(phen)<sub>2</sub>phi]<sup>3+</sup> as Probes of RNA Structure</i>	I-16
1.2.3.3. <i>Site-Specific Recognition of a Palindromic Octamer by [Rh(DPB)<sub>2</sub>phi]<sup>3+</sup></i>	I-18
1.2.3.4. <i>[Rh(bpy)<sub>2</sub>chrysi]<sup>3+</sup> Complexes and Mismatch Recognition</i>	I-20
1.2.4. DIRECT READOUT OF MAJOR GROOVE DNA FUNCTIONALITY	I-22
1.2.4.1. <i>Rhodium Amine Complexes as Intercalators</i>	I-22
1.2.4.2. <i>Predictive Design and Direct Readout of α-Δ-[Rh[(R,R)-Me<sub>2</sub>trien]phi]<sup>3+</sup></i>	I-23
1.2.4.3. <i>Rhodium Complex-Peptide Chimeras</i>	I-26
1.2.5. COMBINING DIRECT READOUT AND SHAPE SELECTION	I-27
1.2.5.1. <i>Site-Specific Recognition by [Rh(MGP)<sub>2</sub>phi]<sup>5+</sup></i>	I-27
1.2.5.2. <i>Λ-1-[Rh(MGP)<sub>2</sub>phi]<sup>5+</sup> as an Inhibitor of Transcription Factor Binding</i>	I-29
<b>1.3. REACTIONS OF METALLOINTERCALATORS WITH DNA</b>	I-30
1.3.1. DIRECT OXIDATIVE STRAND CLEAVAGE, REACTIONS WITH THE SUGAR	I-31
1.3.2. HYDROLYTIC STRAND CLEAVAGE	I-33

1.3.3. OXIDATIVE REACTIONS WITH DNA BASES	I-34
1.3.3.1. <i>Base Damage by Oxo Transfer</i>	I-35
1.3.3.2. <i>Guanine Oxidation by Singlet Oxygen</i>	I-35
1.3.3.3. <i>Guanine Oxidation by Long-Range Electron Transfer</i>	I-36
1.3.3.4. <i>Oxidative Repair of Thymine Dimers</i>	I-39
<b>1.4. SUMMARY</b>	I-41
<b>1.5. REFERENCES</b>	I-42

<b>CHAPTER 2: SITE-SPECIFIC INHIBITION OF TRANSCRIPTION FACTOR BINDING TO DNA BY A METALLOINTERCALATOR</b>	II-1
<b>2.1. INTRODUCTION</b>	II-2
<b>2.2. EXPERIMENTAL</b>	II-8
<b>2.3. RESULTS</b>	II-11
2.3.1. PURIFICATION OF RECOMBINANT TRANSCRIPTION FACTOR YAP-1	II-11
2.3.2. DESIGN OF TARGET OLIGONUCLEOTIDE	II-12
2.3.3. RECOGNITION OF TARGET OLIGONUCLEOTIDE BY $\Lambda$ -1-RH(MGP) <sub>2</sub> PHI <sup>5+</sup> AS VISUALIZED BY PHOTOCLEAVAGE	II-13
2.3.4. ISOMER SPECIFICITY OF COMPETITION BETWEEN METAL COMPLEXES AND TARGET OLIGONUCLEOTIDE	II-18
2.3.5. SITE SPECIFIC COMPETITION OF YAP-1 AND $\Lambda$ -1-RH(MGP) <sub>2</sub> PHI <sup>5+</sup>	II-22
<b>2.4. DISCUSSION</b>	II-23
2.4.1. TARGET OLIGONUCLEOTIDE DESIGN	II-23
2.4.2. SITE SPECIFICITY OF THE COMPETITION REACTION	II-23
2.4.3. ISOMER AND COMPLEX SPECIFICITY OF THE COMPETITION REACTION	II-24
2.4.4. MODEL FOR COMPETITION	II-25
2.4.5. A PROMISING NEW USE FOR INTERCALATORS	II-26
<b>2.5. REFERENCES</b>	II-27

<b>CHAPTER 3: LONG RANGE CHARGE TRANSPORT THROUGH RNA/DNA HYBRID DUPLEXES</b>	III-1
<b>3.1. INTRODUCTION</b>	III-2
<b>3.2. EXPERIMENTAL</b>	III-5
<b>3.3. RESULTS</b>	III-7
3.3.1. EXPERIMENTAL DESIGN	III-7

3.3.2. GUANINE OXIDATION IN AN RNA/DNA HYBRID DUPLEX BY PHOTOEXCITED ETHIDIUM	III-7
3.3.3. GUANINE OXIDATION IN A CNA/DNA HYBRID DUPLEX BY PHOTOEXCITED ETHIDIUM	III-12
3.3.4. OXIDATION IN DUPLEXES LACKING GUANINE DOUBLETS BY PHOTOEXCITED ETHIDIUM	III-14
3.3.5. ANALYSIS OF BASE-BASE OVERLAPS IN RNA/DNA AND DNA/DNA DUPLEXES	III-17
<b>3.4. DISCUSSION</b>	III-17
3.4.1. EFFICIENT RADICAL INJECTION IS A PREREQUISITE FOR LONG RANGE CHARGE TRANSPORT	III-19
3.4.2. PROPAGATION OF CHARGE THROUGH THE BASE STACK AND RADICAL TRAPPING	III-20
3.4.3. EFFECT OF RIBOSE•DEOXYRIBOSE JUNCTIONS ON ELECTRON TRANSFER	III-22
3.4.4. COMPARISON WITH PREVIOUS STUDIES	III-22
3.4.5. RADICAL MIGRATION AND BASE OVERLAP	III-24
3.4.6. CONCLUSIONS	III-25
<b>3.5. REFERENCES</b>	III-26
 <b>CHAPTER 4: LONG RANGE CHARGE TRANSPORT IN DNA DOUBLE CROSSOVER ASSEMBLIES</b>	IV-1
<b>4.1. INTRODUCTION</b>	IV-2
<b>4.2. EXPERIMENTAL</b>	IV-4
<b>4.3. RESULTS AND DISCUSSION</b>	IV-6
4.3.1. DESIGN OF DX ASSEMBLY TO PROBE CHARGE TRANSPORT	IV-6
4.3.2. CHARACTERIZATION OF DX ASSEMBLIES	IV-9
4.3.3. CHARGE TRANSPORT DOWN THE PRIMARY STACK OF THE DX ASSEMBLY	IV-12
4.3.4. ROBUST CHARGE TRANSPORT IN THE PRESENCE OF MISMATCHES	IV-14
4.3.5. INSULATION OF SEPARATE BASE PAIR STACKS IN THE DX ASSEMBLY	IV-15
<b>4.4. CONCLUSIONS</b>	IV-18
<b>4.5. REFERENCES</b>	IV-19

<b>CHAPTER 5: CHARGE TRANSPORT IN DNA SINGLE CROSSOVER ASSEMBLIES</b>	V-1
<b>5.1. INTRODUCTION</b>	V-2
<b>5.2. EXPERIMENTAL</b>	V-6
<b>5.3. RESULTS</b>	V-7
5.3.1. DESIGN OF FOUR WAY JUNCTIONS TO INVESTIGATE LONG RANGE CHARGE TRANSPORT	V-7
5.3.2. PHOTOINDUCED CLEAVAGE OF DNA FOUR WAY JUNCTIONS BY NONCOVALENTLY BOUND $\text{Rh}(\text{Ph})_2\text{DMB}^{3+}$	V-9
5.3.3. LONG RANGE CHARGE TRANSPORT THROUGH DUPLEX DNA BY PHOTOINDUCED ELECTRON TRANSPORT TO COVALENTLY BOUND $\text{Rh}(\text{Ph})_2\text{BPY}^{3+}$	V-11
5.3.4. LONG RANGE CHARGE TRANSPORT THROUGH THE CROSSOVER JUNCTION BY PHOTOINDUCED ELECTRON TRANSPORT TO COVALENTLY BOUND $\text{Rh}(\text{Ph})_2\text{BPY}^{3+}$	V-11
<b>5.4. DISCUSSION</b>	V-15
5.4.1. INTERCALATOR EXCLUSION FROM THE CROSSOVER CORE IN THE PRESENCE OF MAGNESIUM ION	V-15
5.4.2. LONG RANGE CHARGE TRANSPORT IN DUPLEX DNA ASSEMBLIES	V-17
5.4.3. LONG RANGE CHARGE TRANSPORT IN SINGLE CROSSOVER DNA ASSEMBLIES	V-18
5.4.4. MAGNESIUM EFFECTS ON LONG RANGE TRANSPORT	V-20
5.4.5. COMPARISON OF CHARGE TRANSPORT IN FOUR WAY JUNCTIONS TO DNA DOUBLE CROSSOVER ASSEMBLIES	V-21
5.4.6. CONCLUSIONS	V-21
<b>5.5. REFERENCES</b>	V-22
 <b>CHAPTER 6: OXIDATIVE REPAIR OF A THYMINE DIMER IN DNA BY A COVALENTLY ATTACHED, ORGANIC INTERCALATOR</b>	 VI-1
<b>6.1. INTRODUCTION</b>	VI-2
<b>6.2. EXPERIMENTAL</b>	VI-5
<b>6.3. RESULTS</b>	VI-8
6.3.1. HPLC EXPERIMENTS WITH NONCOVALENT NDI	VI-8

6.3.2. HPLC EXPERIMENTS WITH COVALENT NDI	VI-11
6.3.3. PHOTOLIGATION REVERSAL ASSAY FOR THYMINE DIMER REPAIR	VI-14
6.3.4. LONG DISTANCE REPAIR ASSAYED BY PHOTOLIGATION REVERSAL	VI-18
<b>6.4. DISCUSSION</b>	VI-21
6.4.1. REPAIR OF THYMINE DIMERS WITH NDI AND $[\text{Rh}(\text{PHI})_2(\text{BPY}') ]^{3+}$	VI-21
6.4.2. REDUCTIVE REPAIR OF THYMINE DIMERS WITH FLAVINS AT A DISTANCE	VI-22
6.4.3. ANTHRAQUINONES AND $[\text{Ru}(\text{PHEN})(\text{BPY}')(\text{DPPZ}) ]^{3+}$ LACK OF REACTIVITY	VI-22
6.4.4. MECHANISTIC CONSIDERATIONS AND FUTURE DIRECTIONS	VI-23
<b>6.5. REFERENCES</b>	VI-25
 <b>CHAPTER 7: CONCLUSIONS AND FURTHER DIRECTIONS</b>	 VII-1
 <b>APPENDIX 1: VARIATIONS IN DNA CHARGE TRANSPORT WITH NUCLEOTIDE COMPOSITION AND SEQUENCE</b>	 VIII-1

# LIST OF FIGURES AND TABLES

## CHAPTER 1:

Figure 1.1. Early octahedrally coordinated metal complexes used to probe DNA structure	I-3
Figure 1.2. Ancillary and intercalating ligands	I-4
Figure 1.3. dppz-like intercalating ligands, and a PHEHAT complex of Ru(II)	I-5
Figure 1.4. $[\text{Os}(\text{phen})_2\text{dppz}]^{2+}$ and the light switch effect	I-7
Figure 1.5. $[\text{Re}(\text{CO})_3(\text{py})\text{dppz}]^+$	I-8
Figure 1.6. Two proposed modes of binding of $\text{Ru}(\text{phen})_2\text{dppz}^{2+}$ to DNA through the major groove	I-9
Figure 1.7. Molecules used to show major groove intercalation of $\Delta\text{-Ru}(\text{phen})_2\text{dppz}^{2+}$	I-10
Figure 1.8. Minor groove intercalating metal complex $\Delta\text{-Ru}(\text{phen})_2\text{dpq}^{2+}$	I-11
Figure 1.9. Porphyrin hemi-intercalation into DNA	I-12
Figure 1.10. $[\text{Rh}(\text{phen})_2\text{phi}]^{3+}$ and $[\text{Rh}(\text{phi})_2\text{bpy}]^{3+}$ and illustration of their steric interactions	I-14
Figure 1.11. $\Delta\text{-}[\text{Rh}(\text{DPB})_2\text{phi}]^{3+}$ and the palindromic sequence recognized by cooperative dimer binding	I-19
Figure 1.12. Size comparison of chrysi and phi ligands	I-20
Figure 1.13. Plasmid based assay to test sensitivity of $[\text{Rh}(\text{bpy})_2\text{chrysi}]^{3+}$ to detect mismatches in plasmids	I-21
Figure 1.14. Phi complexes of Rh(III) with aliphatic ancillary ligands	I-22
Figure 1.15. Illustration of the recognition of TGCA by $\Delta\text{-}\alpha\text{-}[\text{Rh}[(\text{R},\text{R})\text{-Me}_2\text{trien}]\text{phi}]^{3+}$	I-24
Figure 1.16. Crystal structure of the DNA-bound metallointercalator $\Delta\text{-}\alpha\text{-}[\text{Rh}[(\text{R},\text{R})\text{-Me}_2\text{trien}]\text{phi}]^{3+}$	I-25
Figure 1.17. A rhodium-peptide chimera	I-26
Figure 1.18. Three conformational isomers of $[\text{Rh}(\text{MGP})_2\text{phi}]^{5+}$	I-28
Figure 1.19. Illustration of the inhibition of yAP-1 binding to DNA by $\Delta\text{-}1\text{-}[\text{Rh}(\text{MGP})_2\text{phi}]^{5+}$	I-29
Figure 1.20. Mechanistic scheme proposed for direct strand scission by phi complexes of Rhodium	I-32
Figure 1.21. Schematic drawing of a metallointercalator-peptide chimera with a coordinated $\text{Zn}^{2+}$	I-33

Figure 1.22. Two oxidative reaction pathways for ruthenium coupled DNA	I-37
Figure 1.23. $[\text{Rh}(\text{phi})_2\text{bpy}]^{3+}$ covalently tethered to a 15-mer oligonucleotide with proximal and distal 5'-GG-3' sites	I-38
Figure 1.24. Typical gel from a long range charge transport experiment using covalently tethered Rh-DNA	I-39
Figure 1.25. A 16-mer oligonucleotide covalently tethered to $[\text{Rh}(\text{phi})_2\text{bpy}]^{3+}$ and containing a thymine dimer lesion	I-40

## CHAPTER 2:

Figure 2.1. $\Lambda$ -isomers of metal complexes used in competition experiments	II-4
Figure 2.2. Schematic diagram of the recognition of 5'-CATATG-3' by $\Lambda$ -1- $\text{Rh}(\text{MPG})_2\text{phi}^{5+}$	II-5
Figure 2.3. Modifications made to the ARE to incorporate a metal complex binding site	II-7
Figure 2.4. Purification of the transcription factor yAP-1	II-11
Figure 2.5. Gel shift of yAP-1 with target and wild-type ARE	II-12
Figure 2.6. Photocleavage of the labeled target strand with $\Lambda$ -1- $\text{Rh}(\text{MPG})_2\text{phi}^{5+}$	II-14
Figure 2.7. Photocleavage of the labeled wild-type strand with $\Lambda$ -1- $\text{Rh}(\text{MPG})_2\text{phi}^{5+}$	II-15
Figure 2.8. Photocleavage of the labeled target strand with $\Lambda$ -2- $\text{Rh}(\text{MPG})_2\text{phi}^{5+}$	II-16
Figure 2.9. Photocleavage of the labeled wild-type strand with $\Lambda$ -1- $\text{Rh}(\text{MPG})_2\text{phi}^{5+}$	II-17
Figure 2.10. Competition between the protein yAP-1 and the metal complex $\Lambda$ -1- $\text{Rh}(\text{MPG})_2\text{phi}^{5+}$ for the target oligonucleotide duplex as visualized by gel mobility retardation assay	II-18
Figure 2.11. $\Lambda$ -2- $\text{Rh}(\text{MPG})_2\text{phi}^{5+}$ control competition reactions with the protein yAP-1 for the target oligonucleotide	II-19
Figure 2.12. Comparison of the fitted curves for competition between metal complexes and yAP-1	II-20
Figure 2.13. Competition reaction between yAP-1 and $\text{rac-Rh}(\text{phen})_2\text{phi}^{3+}$ for the target oligonucleotide	II-21

Figure 2.14. Competition reaction between yAP-1 and $\Lambda$ -2-Rh(MPG) <sub>2</sub> phi <sup>5+</sup> for the wild-type oligonucleotide	II-21
Figure 2.15. Comparison of the fitted curves for competition between yAP-1 and $\Lambda$ -1-Rh(MPG) <sub>2</sub> phi <sup>5+</sup> for the target oligonucleotide and the wild-type oligonucleotide	II-22
Figure 2.16. Schematic model of the competition between yAP-1 and $\Lambda$ -1-Rh(MPG) <sub>2</sub> phi <sup>5+</sup> for the target DNA	II-26

### CHAPTER 3:

Figure 3.1. Nucleic acid duplexes used to investigate long range radical migration	III-8
Figure 3.2. Long range guanine damage in RNA-GG duplexes and DNA-GG duplexes	III-9
Table 3.1. Partitioning between oxidatively damaged sites in RNA/DNA and DNA/DNA duplexes	III-10
Figure 3.3. Intercalation site and long range oxidative damage in RNA-GG and DNA-GG duplexes with appended metal complex	III-11
Figure 3.4. Long range oxidative damage in CNA-GG	III-12
Figure 3.5. Oxidative damage in DNA-AA and CNA-AA	III-14
Table 3.2. Base surface area overlap in idealized dinucleotides	III-15
Figure 3.6. Selected idealized dinucleotides base steps	III-16
Figure 3.7. Schematic illustration of the oxidative and direct damage in each duplex investigated	III-18

### CHAPTER 4:

Figure 4.1. Two types of DNA double crossover assemblies commonly used	IV-2
Figure 4.2. Schematic of a DNA duplex containing oxidatively sensitive 5'-GG-3' sites with a covalently attached metallointercalator	IV-7
Figure 4.3. Sequences of DX assemblies containing the spatially separated photooxidant and guanine doublets and triplets to be oxidized	IV-8
Figure 4.4. Phosphorimager of a native gel of the annealed double crossover assemblies	IV-9
Figure 4.5. A typical experiment testing charge transport in DX assemblies	IV-10



Figure 4.6. Long range oxidative damage in the intercalator bound stack of the DX assembly and comparison to damage in duplex DNA and with mismatches	IV-11
Figure 4.7. Graphs of the quantitation of the gels shown in Figure 4.6	IV-12
Figure 4.8. Targeting of strand distortion by noncovalently bound rhodium complex	IV-15
Figure 4.9. Test of cross coupling in electron transfer between the base stacks of the DX DNA assembly	IV-16
Figure 4.10. Molecular model of a DX assembly, emphasizing the base pair stacks	IV-17

## CHAPTER 5:

Figure 5.1. Crystal structures of four way junctions recently reported for all-DNA assemblies	V-4
Figure 5.2. AFM studies of four way junction arrays	V-5
Figure 5.3. Sequences of DNA assemblies used containing guanine doublets to be oxidized	V-8
Figure 5.4. Direct photocleavage and piperidine induced cleavage of four way junction DNA with noncovalently bound $\text{Rh}(\text{phi})_2\text{bpy}^{3+}$ as a function of magnesium concentration	V-10
Figure 5.5. Oxidation of a metallointercalator-bearing control duplex	V-11
Figure 5.6. Long range oxidation of DNA by covalently tethered $\text{Rh}(\text{phi})_2\text{bpy}^{3+}$ in four way junctions as a function of $\text{Mg}^{2+}$ concentration	V-13
Figure 5.7. Long range oxidation of DNA by covalently tethered $\text{Rh}(\text{phi})_2\text{bpy}^{3+}$ in four way junctions as a function of $\text{Mg}^{2+}$ concentration	V-14
Figure 5.8. Schematic illustration of the damage pattern, location, and intensity of direct photolysis induced oxidative damage in four way junction assemblies by noncovalent metal complex	V-17
Figure 5.9. Schematic illustration of the damage pattern, location, and intensity of direct photolysis induced oxidative damage in four way junction assemblies by covalently tethered metal complex	V-18

## CHAPTER 6:

Figure 6.1. Photoequilibration of a <i>cis-syn</i> thymine dimer in DNA	VI-3
Figure 6.2. Photoexcitable intercalators used in this study	VI-5
Figure 6.3. Sequence used to explore thymine dimer repair	VI-8
Figure 6.4. Photochemical repair of a thymine dimer in duplex DNA by noncovalently bound NDI	VI-9
Figure 6.5. Photochemical repair of a thymine dimer in duplex DNA by covalently bound NDI	VI-10
Figure 6.6. Anthraquinone-2,6-disulfonate mediated decomposition of DNA	VI-12
Figure 6.7. Control experiment demonstrating the intraduplex nature of the repair process	VI-13
Figure 6.8. Schematic diagram showing the template directed photoligation of oligonucleotides effected by cyclobutane dimer formation	VI-14
Figure 6.9. Sequences of the duplexes used to monitor the repair of photoligated thymine dimers	VI-15
Figure 6.10. Autoradiogram of the denaturing gel illustrating the reversal of the thymine dimer in duplex DNA that does not contain a phosphodiester linkage between the thymine dimer	VI-16
Figure 6.11. Guanine oxidation demonstrating noncovalent binding of anthraquinones	VI-17
Figure 6.12. Autoradiogram of the denaturing gel showing reversal of a thymine dimer with free and tethered rhodium complex	VI-19
Figure 6.13. Autoradiogram of the denaturing gel showing reversal of a thymine dimer with free and tethered NDI	VI-20

## APPENDIX 1:

Table 8.1. Long range oxidative damage in DNA functionalized with tethered metallointercalator	VIII-3
Figure 8.1. Sequence dependence of long range oxidative damage in assemblies containing tethered $\Delta\text{-Rh}(\text{phi})_2\text{bpy}^{3+}$	VIII-5
Figure 8.2. Plot of the distal/proximal ratio of guanine oxidation versus the distance of the intercalation site	VIII-6

# **CHAPTER 1**

## **Recognition and Reactivity of Metallointercalators with DNA\***

\*Adapted from K.E. Erkkila, D.T. Odom and J.K. Barton. *Chemical Reviews* **99** (1999)

2777-2796.

## 1.1 INTRODUCTION

The design of small metal complexes that bind to and react at specific sequences of DNA becomes more important as we begin to delineate, on a molecular level, how genetic information is expressed. A more complete understanding of how to target DNA sites with specificity will lead not only to novel chemotherapeutics, but also to a greatly expanded ability to probe DNA and to develop sensitive diagnostic agents.

Transition metal complexes are being used at the forefront of many of these new techniques. Stable, inert, and water-soluble complexes containing spectroscopically active metal centers are extremely valuable as probes of biological systems. Metal complexes have helped elucidate the mechanisms by which metalloproteins function, both as spectroscopic tags and as functional models for the active centers of proteins. More recently, such metal complexes have been used to probe both structural and functional aspects of nucleic acids.

In this introductory chapter, I describe the chemistry of metallointercalators that bind to and react with DNA. Intercalators are small molecules that contain a planar aromatic heterocyclic functionality which can insert and stack between the base pairs of double helical DNA.<sup>1</sup> Lippard and coworkers first established that square planar platinum(II) complexes containing an aromatic heterocyclic ligand could bind to DNA by intercalation.<sup>2</sup> In the Barton laboratory, metallointercalation was extended to three dimensions using stable octahedral complexes of late transition metals. Octahedral metallointercalators have permitted the targeting of the two species on a molecular level. Moreover, the photophysical and photochemical properties of the metallointercalators have allowed the development of spectroscopic and reactive probes of DNA. My review of this chemistry is intended to describe the characteristics of metallointercalators used in the work presented later in this thesis,

and to describe the reactions various types of DNA can undergo when oxidatively challenged by these metal complexes.

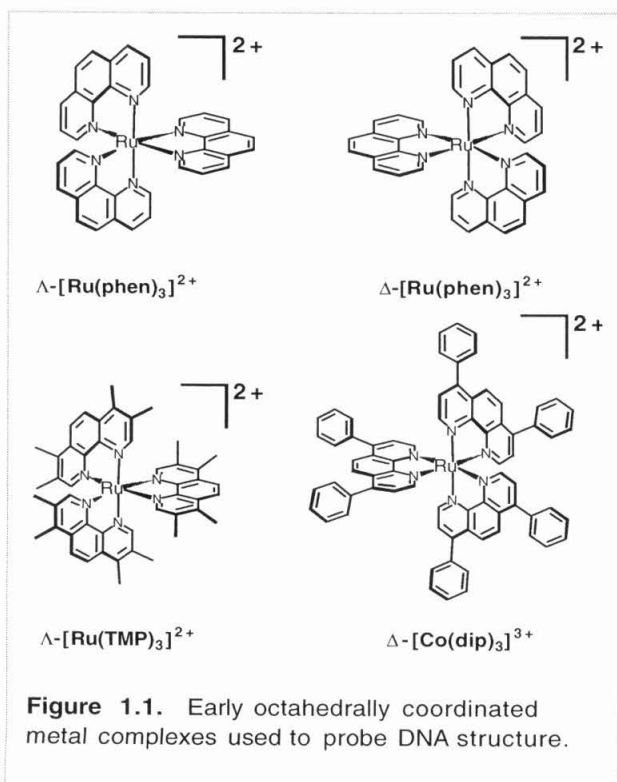
## 1.2 RECOGNITION OF DNA BY METALLOINTERCALATORS

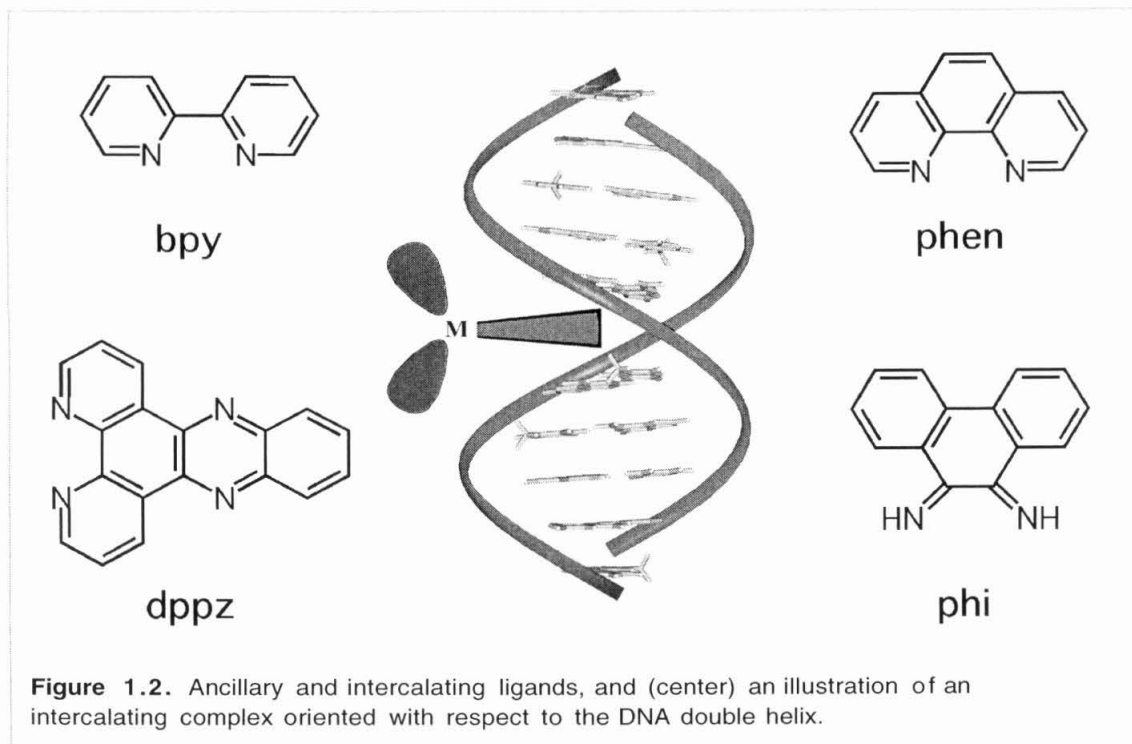
### 1.2.1 Background -- Early Metal Complexes

The first experiments describing the interaction of coordinatively saturated octahedral transition metal complexes with DNA involved the use of metal complexes that had been chemically well-characterized in many other contexts. These early studies focused on the binding of tris(phenanthroline) complexes of zinc, cobalt, and ruthenium to DNA<sup>3-11</sup> (Figure 1.1). Based upon photophysical and NMR studies, it was proposed that the cationic tris(phenanthroline) complexes bound to DNA through three non-covalent modes: (i) electrostatically; (ii) binding hydrophobically against the minor

groove; and (iii) by partial intercalation of one of the phenanthroline ligands into the DNA base stack from the major groove. Early experiments indicated a preference for the right-handed  $\Delta$ -isomers upon intercalation into right-handed DNA, while a slight preference for the  $\Lambda$ -isomers could be observed for binding in a complementary fashion against the right-handed groove.<sup>10</sup>

While the binding interactions of these complexes have been debated,<sup>12-14</sup> their enantiomeric preferences have





been seen consistently in derivative complexes investigated since those early experiments, as will be evident throughout this introduction. Chiral discrimination of this type clearly depends upon matching the symmetry of the metal complex with that of the double helix.

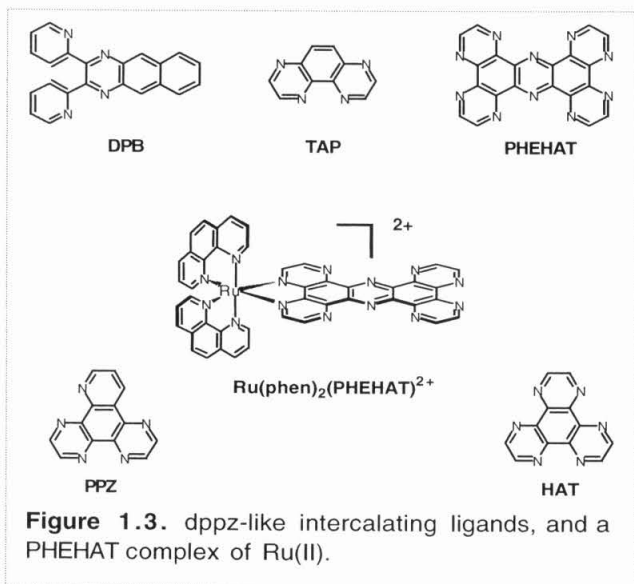
Studies with these simple complexes provided a basis for conceptualizing how octahedral complexes might interact non-covalently with DNA, and for exploring how the properties of the metal complexes, notably their photophysical and redox characteristics, might be utilized in developing novel probes for DNA. The binding affinities of these complexes for DNA were unimpressive, however, and the mixture of binding modes, depending upon DNA base sequence, salt, and temperature, was problematic. In order for octahedral metalointercalators to become useful in biological applications and assays, and indeed for intercalation to dominate as the mode of interaction, the intercalative binding affinities had to be significantly increased.

## 1.2.2. Increasing DNA Affinity and Discrimination by Intercalation

### 1.2.2.1. Intercalation as a Platform for Binding

Increasing the ligand surface area for intercalative stacking leads to a substantial increase in binding affinity. As a result metalointercalators which contain an expansive aromatic heterocyclic ligand can provide immensely powerful tools to probe nucleic acids.<sup>15-18</sup> By inserting and stacking between the base pairs, octahedral complexes containing the phenanthrenequinone diimine (phi) or dipyrido[3,2-a:2',3'-c]phenazine (dppz) ligand provide predictable, stable anchors in the major groove with a known orientation of all the functionalities on the metal complex, with respect to the DNA duplex (Figure 1.2). In combination with the stable ligand architecture of late transition metal complexes, this type of anchor can be exploited to generate chiral discrimination and sequence specificity comparable to that of DNA binding proteins.

### 1.2.2.2. Metal Complexes of Dipyridophenazine and Triphenylene



#### 1.2.2.2.1. dppz and dppz Derivatives

Bipyridyl and phenanthroline complexes of ruthenium containing the dppz ligand intercalate relatively non-specifically into B-form DNA with a slight preference for AT rich regions.<sup>19</sup> The dppz complexes, containing an expansive aromatic heterocyclic ligand, show extremely high affinity for DNA, with binding

constants  $>10^6 \text{ M}^{-1}$ .<sup>20</sup> Analogous ruthenium(II) complexes, with 1,4,5,8-tetraazaphenanthrene (TAP), 1,4,5,8,9,12-hexaazatriphenylene (HAT) and 1,10-

phenanthroline[5,6-b]1,4,5,8,9,12-hexaazatriphenylene (PHEHAT), also interact with DNA, and, like dppz complexes, show changes in photophysical properties upon binding to the DNA duplex (Figure 1.3).<sup>21</sup> Bimetallic complexes bridged by the 2,3-bis(2-pyridyl)-benzo[g]quinoxaline (dpb) ligand have also been shown to bind to DNA by intercalation.<sup>22</sup>

#### 1.2.2.2.2. Metal Complexes as Molecular Light Switches

$[\text{Ru}(\text{bpy})_2(\text{dppz})]^{2+}$  and related derivative complexes in organic solutions show solvatochromic luminescence to varying degrees. However, in aqueous solution, these complexes do not luminesce, due to the ability of water to non-radiatively deactivate the excited state by hydrogen bonding with the intercalating ligands.<sup>20,23,24</sup> Upon introduction of B-form double helical DNA to an aqueous solution of any of these metal complexes, photoluminescence is observed. This luminescence reflects the shielding of the intercalating ligand from bulk solvent, and would be akin to introducing a local organic solvent that shields the ring nitrogens on the intercalating ligand from protonation. It is this effect that has been extensively characterized and described as the "molecular light switch." In the case of  $[\text{Ru}(\text{phen})_2\text{dppz}]^{2+}$  bound to DNA, the excited state lifetime is approximately 200 ns, whereas free in aqueous solution, the lifetime of the excited state is only 200 ps.<sup>24</sup> This light switch effect provides the basis for a valuable photophysical probe of nucleic acids.  $[\text{Ru}(\text{phen})_2\text{PHEHAT}]^{2+}$  was also found to be a light switch, though it displayed a weaker luminescence when bound to calf thymus DNA than  $[\text{Ru}(\text{phen})_2\text{dppz}]^{2+}$ .<sup>25</sup>

$[\text{Ru}(\text{phen})_2\text{HAT}]^{2+}$ , unlike  $[\text{Ru}(\text{phen})_2\text{PHEHAT}]^{2+}$  and  $[\text{Ru}(\text{phen})_2\text{dppz}]^{2+}$ , luminesces in aqueous solution, but this luminescence is slightly enhanced in the presence of DNA.<sup>26</sup> The photophysics and photochemistry of both osmium(II) and ruthenium(II) complexes of HAT, PHEHAT, and several other, related polypyridyl ligands



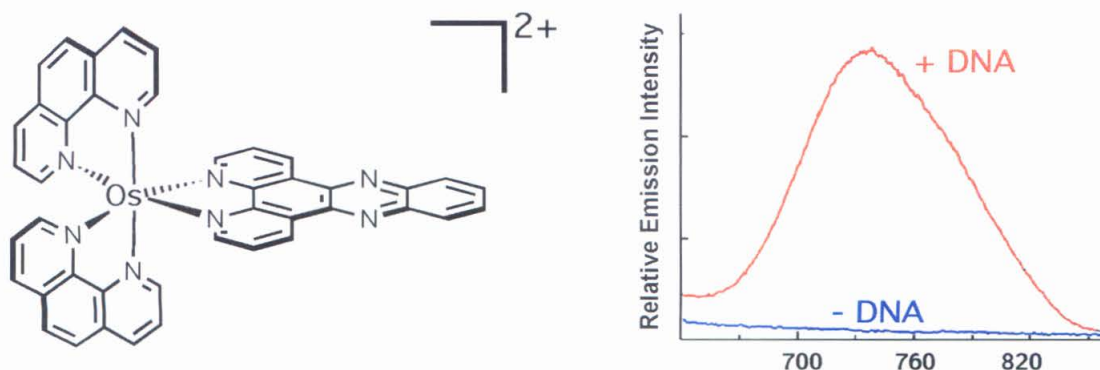


**Figure 1.4.**  $[\text{Os}(\text{phen})_2\text{dppz}]^{2+}$  and the light switch effect upon complex luminescence. In water the luminescence is quenched (blue) but in DNA, the ligand is protected from solvent quenching, giving rise to the luminescence shown in red.

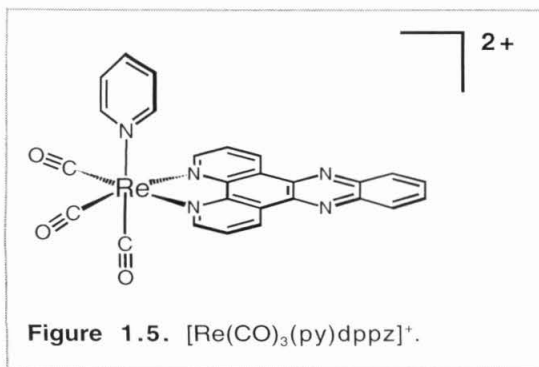
in the presence of DNA and single nucleotides is the subject of a recent review.<sup>21</sup>

Another study used fluorescence lifetimes to monitor chiral discrimination of DNA for  $\Delta$ - vs.  $\Lambda$ -isomers of  $[\text{Ru}(\text{bpy})_2\text{ppz}]^{2+}$ , where ppz = the intercalating ligand 4,7-phenanthroline-5,6-dipicolinate.<sup>28</sup>

#### 1.2.2.2.3. *Dppz Complexes and Derivatives as Luminescent Probes of DNA*

The systematic introduction of variations onto the terminal aromatic ring of the dppz ligand of  $[\text{Ru}(\text{phen})_2\text{dppz}]^{2+}$  has been carried out to provide a host of luminescent probes of DNA.<sup>29</sup> The complexes containing modified dppz ligands are not as sensitive to aqueous quenching of luminescence as the parent compound and so cannot be accurately described as light switches. The modified complexes, however, show a wide variety of spectroscopic profiles.

Replacement of the ruthenium with osmium as the central metal ion causes the luminescence observed for Ru(II) with a maximum of 620 nm to red-shift to 738 nm (Figure 1.4).<sup>30</sup> Hence,  $[\text{Os}(\text{phen})_2\text{dppz}]^{2+}$  can act as a red-emitting luminescent reporter for the presence of DNA. Recently, experiments varying the dppz ligand functionality similar to those performed for  $[\text{Ru}(\text{phen})_2\text{dppz}]^{2+}$  have been performed for osmium.<sup>31</sup>  $[\text{Co}(\text{phen})_2\text{dppz}]^{2+}$  and  $[\text{Ni}(\text{phen})_2\text{dppz}]^{2+}$  have also been constructed.<sup>32</sup>



$[\text{Co}(\text{phen})_2\text{dppz}]^{2+}$  binds to DNA with high affinity and is able to linearize plasmids when photoirradiated.<sup>25</sup> The Ni(II) analogue may prove to be useful in carrying out paramagnetic NMR experiments.

Finally, rhenium has also been used

in the construction of metallointercalators;  $[\text{Re}(\text{CO})_3(\text{py})\text{dppz}]^+$  has been shown to have the same “light switch” capabilities as Ru(II) dppz complexes (Figure 1.5).<sup>33</sup> This complex was also found to bind to calf-thymus DNA and, when irradiated, to promote strand scission on pBR322.<sup>34</sup>

#### 1.2.2.2.4. Intercalation of Metal Complexes of dppz through the Major Groove

Given the potential utility of the dppz complexes and their derivatives, it is important to develop a detailed structural understanding of how these complexes interact with the DNA helix. Both photophysical studies and linear dichroism studies provide support for intercalation.<sup>20,29,35-38</sup> Additionally, consistent with the early intercalative models,<sup>10</sup> it was observed that the  $\Delta$ -isomer showed greater luminescence bound to right-handed DNA than did the  $\Lambda$ -isomer. Calorimetry studies have established the high affinity of the dppz complexes in binding the DNA duplex.<sup>39</sup>

The luminescent characteristics of the dppz complexes bound to DNA in general showed a biexponential decay in emission, with the percentages of the two components varying as a function of DNA sequence. On this basis, two general orientations for intercalation of the complexes into DNA were proposed (Figure 1.6).<sup>29,35</sup> The longer-lived component was assigned to a “head-on” binding mode; in this mode both nitrogens of the phenazine ligand are equally protected by intercalation from solvent quenching. Similarly, the shorter component, more easily quenched, was assigned to a “side-on”

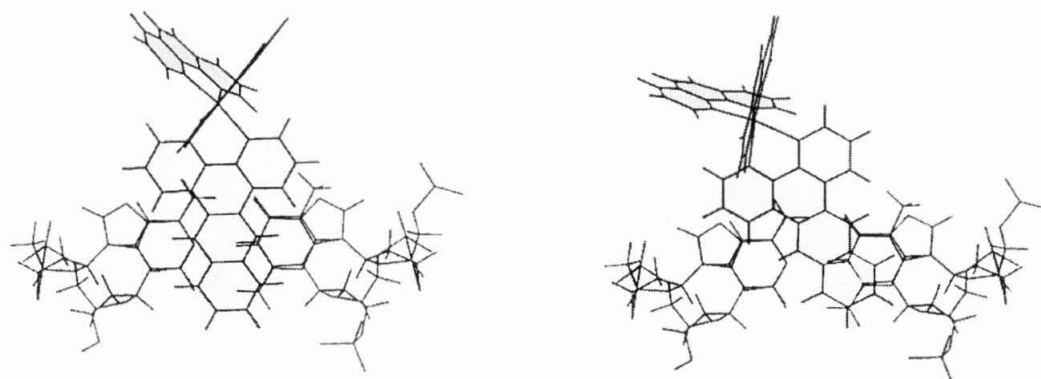


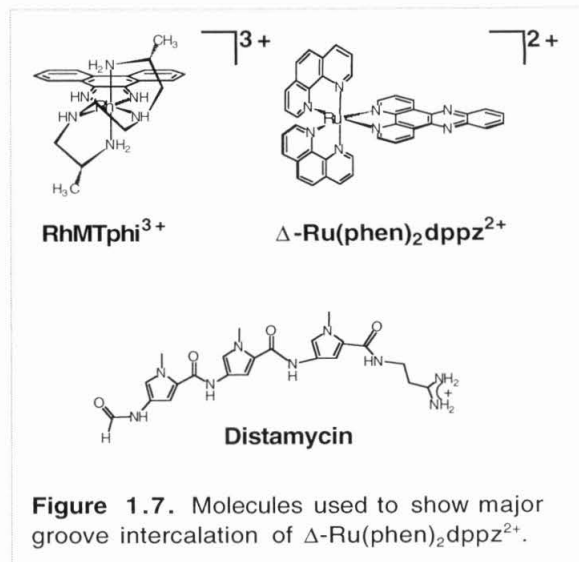
**Figure 1.6.** Two proposed modes of binding of  $\text{Ru}(\text{phen})_2\text{dppz}^{2+}$  to DNA through the major groove. The stacking of a dppz complex (shaded) on the base pair is shown down the helical axis. The side-on mode (right) is shown with one partially exposed phenazine nitrogen.

binding mode, where the dppz ligand was stacked at an angle with respect to the helical dyad axis.

While an intercalative mode of interaction was clear, some controversy has surrounded the groove position of the ruthenium intercalators on the DNA helix. Early NMR experiments that showed intermolecular NOE's to major groove protons supported a model in which the complex binds through the major groove.<sup>40</sup> However, other researchers reported photophysical studies showing that  $[\text{Ru}(\text{bpy})_2(\text{dppz})]^{2+}$  did not significantly decrease its luminescence when bound to T4-DNA, which is heavily glucosylated in the major groove by cytosine derivatization.<sup>36</sup> This observation, together with more indirect lines of evidence, seemed to suggest that the steric accessibility of the major groove was unimportant for  $[\text{Ru}(\text{bpy})_2(\text{dppz})]^{2+}$  binding, and hence that  $[\text{Ru}(\text{bpy})_2(\text{dppz})]^{2+}$  might instead intercalate *via* the minor groove.

In order to explore this issue more fully, direct competition experiments<sup>19</sup> were performed with the minor groove binding reagent distamycin and the well-characterized, major groove binding molecule  $\Delta\text{-}\alpha\text{-}[\text{Rh}[(\text{R,R})\text{-Me}_2\text{trien}]\text{phi}]^{3+}$ , where  $(\text{R,R})\text{-Me}_2\text{trien}$  = 2R,9R-diamino-4,7-diazadecane. For the latter compound, there is both a high resolution NMR structure,<sup>41</sup> and recently a full crystal structure<sup>42</sup> of this rhodium complex

intercalated into a DNA duplex from the major groove (*vide infra*) (Figure 1.7). These experiments showed that  $\Delta\alpha\text{-[Rh[(R,R)\text{-Me}_2\text{trien}]\text{phi}]^{3+}}$  directly displaced  $\Delta\text{-[Ru(phen)}_2\text{dppz}]^{2+}$  from the DNA helix. In contrast, distamycin competition experiments showed that the metal, when bound to various sequences of DNA, was unaffected by



the presence of excess minor groove binder. These results were therefore consistent with the DNA helix simultaneously accommodating  $[\text{Ru(phen)}_2\text{dppz}]^{2+}$ , a major groove binder, and distamycin, a minor groove binder. Additionally,  $[\text{Ru(phen)}_2\text{dppz}]^{2+}$  was shown to have a slight, but significant, preference for poly(AT) over poly(GC), which may resolve the apparent contradiction of major groove intercalation into T4-modified DNA.  $[\text{Ru(phen)}_2\text{dppz}]^{2+}$ , being preferentially intercalated into AT regions within the major groove, would not be seriously disrupted by major groove glucosylation of cytosines.

The NMR studies, which extended the original report of major groove intercalation based on selective deuteration of the dppz ligand, also confirmed the correlation of the biexponential decay of luminescence with the presence of two populations of intercalation geometries.<sup>43</sup> Two major orientations were proposed for the intercalation of this metal complex into B-form DNA. The first centers the dppz ligand symmetrically along the dyad axis of DNA affords even shielding of the phenazine ligand, whereas the second features canted intercalation that maximizes base overlap and greatly favors shielding primarily of only one half of the dppz intercalator. The latter orientation provides very different chemical environments for the 4' and 7' dppz protons, which are indistinguishable in the absence of DNA. These two modes of binding could

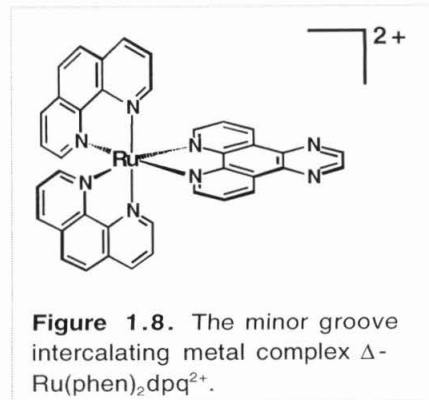
account for the biexponential decay of the dppz luminescence signal based on differential accessibility of the phenazine nitrogens to aqueous quenching in different binding orientations.<sup>35</sup>

#### 1.2.2.2.5. Minor Groove Binding of $\text{Ru}(\text{phen})_2\text{dpq}^{2+}$

Removal of the terminal aromatic ring on the dppz ligand makes dipyrido[2,2-d:2',3'-f]quinoxaline (dpq), a closely related analog to dppz (Figure 1.8).<sup>44,45</sup>  $[\text{Ru}(\text{phen})_2\text{dpq}]^{2+}$  also intercalates into DNA, but NMR studies similar to those described above for  $[\text{Ru}(\text{phen})_2\text{dppz}]^{2+}$  have shown that  $[\text{Ru}(\text{phen})_2\text{dpq}]^{2+}$  binds from the minor groove side.<sup>44-46</sup> It is remarkable how apparently minor changes in the ligand architecture and electronic structure can lead to profound influences on binding geometries. It is not simply a steric consideration which governs the groove position of the intercalator, as a crystal structure of a square planar platinum intercalator bound within a dinucleotide duplex shows intercalation of the coordinated ligand from the major groove side.<sup>47</sup> It will be important to predictably establish those factors which govern groove position for the intercalator.

#### 1.2.2.3. Porphyrin Intercalation into DNA

An additional large heterocyclic surface used for DNA intercalation is the porphyrin ring system. It has been long known that porphyrins bind to DNA.<sup>48</sup> Spectroscopic data indicate that porphyrins can bind to GC-rich sequences intercalatively, while in AT-rich regions they take on an external binding mode.<sup>49</sup> How such an intercalation can occur has been debated, however, given the substantial size of the porphyrin versus that of the base pair. Free porphyrins and porphyrins bound to metals which do not take on axial ligands, such as Cu(II) and Ni(II), were suggested to





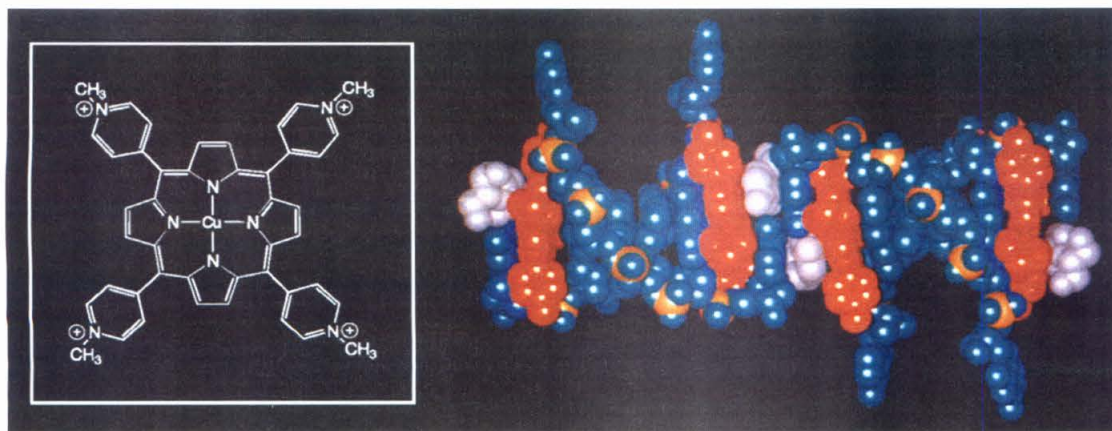


**Figure 1.9.** Porphyrin hemi-intercalation into DNA. The right box shows the copper porphyrin used to bind to duplex DNA. On the left is shown the structure of the porphyrin that hemi-intercalates into DNA, and displaces a cytosine. Adapted from reference 52.

intercalate into DNA,<sup>49-51</sup> while metallated porphyrins which have axial ligands such as Co(II), Fe(II), Zn(II), and Mn(II) did not appear to intercalate.<sup>50</sup>

A clearer understanding of how porphyrins interact with DNA emerged when the crystal structure of a copper porphyrin, [CuTMPPyP4] (copper(II)*meso*-tetra(*N*-methyl-4-pyridyl)porphyrin), intercalated into 5'-CGATCG-3' was solved.<sup>52</sup> The porphyrin was seen to hemi-intercalate at the end of the DNA oligomer by displacing a cytosine from the terminal GC base pair (Figure 1.9). The orphan cytosine then base pairs with a guanine in a separate double helix so that there are no non-paired extrahelical bases. Intercalation by a metal complex, in this view, represents a substantial perturbation of the DNA helix with base displacement being accompanied by binding. Indeed, in this instance, direct stacking of the porphyrin within the DNA helix does not occur. While subsequent high resolution views of  $\Delta\text{-}\alpha\text{-}[\text{Rh}[(\text{R},\text{R})\text{Me}_2\text{trien}]\text{phi}]^{3+}$  bound to DNA gave a picture of direct intercalation into the helix,<sup>42</sup> the porphyrin structure demonstrates that there are many different ways metal complexes can bind DNA.

### 1.2.3. DNA Recognition Based on Shape Selection by Phi Complexes

Due to their shape and polarity, different intercalating ligands stack with different orientations within the double helix and as such provide somewhat different strategies for the specific recognition of sites on DNA. Phenanthroline and bipyridine ligands are sterically compact, and metal complexes that have these ligands have relatively shielded surfaces. It was this steric shielding that prevents tris(phenanthroline) complexes from intercalating deeply into the B-form base stack and leads to its low binding affinities. Metal complexes containing a coordinated dppz ligand, in contrast, extend a heterocyclic ring system out from the central, compact  $[\text{Ru}(\text{bpy})_3]^{2+}$  core and in this manner provide a substantial aromatic surface for intercalation in DNA. Because of the large expanse of the ligand, a family of orientations within the stack appears to be available.

The 9,10-phenanthrenequinone diimine (phi) ligand provides different constraints and opportunities. When incorporated into an inert transition metal complex, the phi ligand projects far from the metal center, due to the use of imines as coordinating chelators (Figure 1.2). Hence, like dppz, phi also presents an intercalating aromatic system that is removed from the metal center, yet the geometry of the phi ligand provides an expanse of aromatic structure across the base pair rather than along the dyad axis. In fact, the phi ligand was first designed in an attempt to match the positioning of aromatic rings with those of the base pairs.<sup>53</sup> The non-intercalating, ancillary ligands are brought into position against the DNA base pairs, and as a result, specific non-covalent interactions between the ancillary ligand functionalities and functionality in the DNA groove can be made.

The phi complexes also differ from the dppz complexes in terms of their photochemistry, and thus, in terms of their utility. Phi complexes of both rhodium and ruthenium show no detectable photoinduced emission, and therefore no photophysical signature to exploit.<sup>54</sup> Nonetheless phi complexes of rhodium have a rich

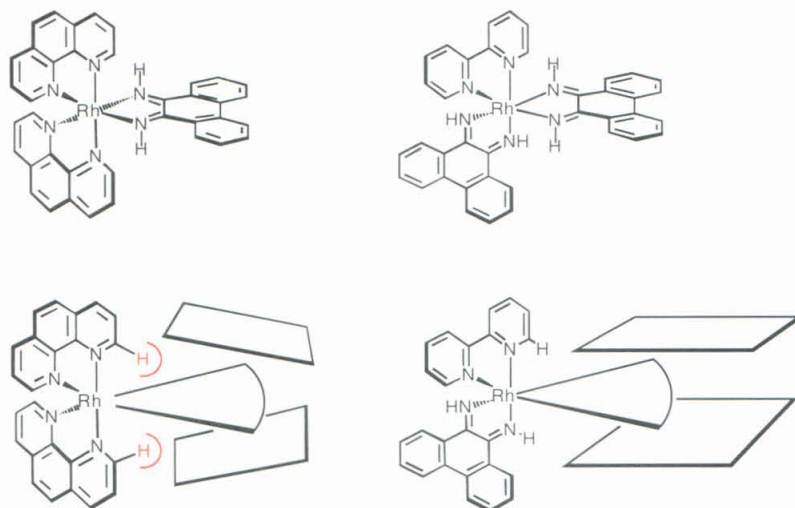


**Figure 1.10.**  $[\text{Rh}(\text{phen})_2\text{phi}]^{3+}$  (upper left) and  $[\text{Rh}(\text{phi})_2\text{bpy}]^{3+}$  (upper right) and illustration of steric interactions of  $[\text{Rh}(\text{phen})_2\text{phi}]^{3+}$  with propeller-twisted intercalation site (lower left) and  $[\text{Rh}(\text{phi})_2\text{bpy}]^{3+}$  with normally stacked intercalation site (lower right). The clash in the lower left panel between the phenanthroline hydrogen with the base stack is shown in red.

photochemistry. The ability of phi complexes of rhodium(III) to cleave DNA at the site of intercalation when irradiated with high energy light (310-320 nm) (*vide infra*) has been extensively used in researching how these complexes bind to DNA with specificity.

#### 1.2.3.1. Recognition of 5'-Py-Pu-3' Sites

One of the most extensively characterized and studied metal complexes that intercalates into DNA is  $[\text{Rh}(\text{phen})_2\text{phi}]^{3+}$  (Figure 1.10).<sup>53,55,56</sup> In this mixed ligand metallointercalator, phenanthrolines provide structural form to the complex, and the phi ligand serves to intercalate into the base stack of DNA by overlapping extensively with the  $\pi$ -stacked base pairs. In fact it is the shape of this complex, with phenanthroline ligands that partly occlude the phi ligand, which dominates its interactions with DNA.

Early studies showed that  $[\text{Rh}(\text{phen})_2\text{phi}]^{3+}$  binds to DNA with moderate site-selectivity whereas little specificity was evident with a close analog,  $[\text{Rh}(\text{phi})_2\text{bpy}]^{3+}$ .<sup>53</sup> It was proposed that the site selectivity of  $[\text{Rh}(\text{phen})_2\text{phi}]^{3+}$  was based upon shape



selection. Because of the steric bulk of the ancillary phenanthroline ligands hanging over the  $\phi$ , the complex could be considered to bind tightly only at sites which were more open in the major groove.<sup>53,56</sup> In addition, there appeared to be enantioselectivity favoring the  $\Delta$ -isomer.<sup>55</sup> Even moderate site-selectivity for this complex was remarkable, considering the lack of hydrogen bond donors or acceptors on the ancillary ligands.

Further study indicated that  $[\text{Rh}(\text{phen})_2\phi]^{3+}$  showed a preference for sites with high propeller twisting toward the major groove.<sup>55,57</sup> The metal complex preferentially cleaves at 5'-YYR-3' (where Y is pyrimidine and R is purine) sites, occasionally cleaves DNA at 5'-RYR-3' sequences, but never cleaves at sequences of the form 5'-RRY-3'. Comparison of crystal structures of three B-form DNA oligonucleotides to the photocleavage patterns for  $[\text{Rh}(\text{phen})_2\phi]^{3+}$  revealed the critical structural features for recognition.<sup>57</sup> Helical twist, rise, tilt, or roll, among other factors, were ruled out as important parameters. It was proposed that the propeller twisting that occurs in 5'-YYR-3' is critical to the shape selection by opening up the B-form DNA purines. This subtle architectural change permits facile intercalation of the  $\phi$  ligand while simultaneously removing the counterpart pyrimidines from positions that would sterically clash with the phenanthroline rings of the metal complex (Figure 1.10). In contrast, a 5'-RRY-3' site not only closes the major groove, but also places the pyrimidines in a highly unfavorable position with respect to the phenanthroline rings.  $[\text{Ir}(\text{phen})_2\phi]^{3+}$  has been shown to have similar sequence specificity.<sup>58</sup>

As mentioned above,  $[\text{Rh}(\phi)_2\text{bpy}]^{3+}$  shows almost no sequence or structure selectivity.<sup>56,59</sup> Inspection of the geometry of this metal complex shows that in this case, the non-intercalating  $\phi$  ligand is positioned away from possible steric clashes with the helix, as is the bpy ligand. The simple comparison of the shapes of these two metal complexes therefore highlights the idea that steric clashes, or their avoidance, can dominate site-selectivity.

### 1.2.3.2. $[\text{Rh}(\text{phen})_2\text{phi}]^{3+}$ as a Probe of RNA Structure

The observation that the site-selectivity for  $[\text{Rh}(\text{phen})_2\text{phi}]^{3+}$  depends upon somewhat open major grooves has been used most advantageously in the application of the complex in probing RNA structures. In general, metallointercalators that target major groove sites bind poorly to double stranded RNA.<sup>60-62</sup> One interpretation of this exclusion suggests that the very deep and narrow major groove of RNA duplexes would be largely inaccessible for stacking by the metal complex. Changes in tertiary structure of the RNA that serve to open the major groove could thus become possible targets for the rhodium complex.  $[\text{Rh}(\text{phen})_2\text{phi}]^{3+}$  would then act as a novel shape-selective probe for RNA tertiary structure. To test this possibility, the interactions of the rhodium complex with an RNA of well-characterized structure, tRNA, was examined, and thereafter understanding of its recognition characteristics was applied to probe other folded RNAs.

With photoactivation,  $[\text{Rh}(\text{phen})_2\text{phi}]^{3+}$  indeed promotes strand cleavage at sites of tertiary interaction in tRNA.<sup>60-63</sup> The rhodium complex yields no cleavage in double helical regions of the RNA nor in unstructured single-stranded regions. Instead  $[\text{Rh}(\text{phen})_2\text{phi}]^{3+}$  appears to target regions which are structured so that the major groove is open and accessible for stacking, as occurs where bases are triply bonded. Cleavage studies were conducted on two structurally characterized tRNAs, tRNA<sup>Phe</sup> and tRNA<sup>Asp</sup> from yeast, the unmodified yeast tRNA<sup>Phe</sup> transcript, a chemically modified tRNA<sup>Phe</sup>, as well as a series of tRNA<sup>Phe</sup> mutants.<sup>61</sup> There was a striking similarity in cleavage observed on these tRNAs, and the sites of cleavage mark regions of tertiary folding. Moreover, cleavage results on mutants indicated that it is the structure of the triply bonded array rather than the individual nucleotides that are being targeted.

Analogous experiments conducted on tDNA<sup>Phe</sup>, the DNA analog of tRNA<sup>Phe</sup>, showed that, although there were slight differences in photocleavage reactivity within the

putatively tertiary regions, within the double stranded regions of the stem regions of tDNA<sup>Phe</sup> strong photocleavage was indeed observed at 5'-YYR-3' sites, as is expected for B-form DNA.<sup>64</sup> Notably, these sites were not cleaved in the case of tRNA<sup>Phe</sup>, consistent with the A-form nature of the tRNA stem. Perhaps most importantly, the similarity in pattern at sites of tertiary interaction in tRNA indicated that the tDNA adopted a similarly folded structure, consistent with previous research.

The three-dimensional folding of *Xenopus* oocyte 5S rRNA was also examined using [Rh(phen)<sub>2</sub>phi]<sup>3+</sup> as a structural probe.<sup>65</sup> The sites targeted by the rhodium complex were mapped on the wild type *Xenopus* oocyte RNA, on a truncated RNA representing an arm of the molecule as well as on several single-nucleotide mutants of the 5S rRNA. Given the similarity observed in cleavage between the full 5S RNA and the truncated fragment, the results did not support folding models which involved long-range tertiary interactions. Cleavage results with [Rh(phen)<sub>2</sub>phi]<sup>3+</sup> did, however, indicate that the apposition of several noncanonical bases as well as stem-loop junctions and bulges could result in intimately stacked structures with opened major grooves. These distinctive structures might also be utilized for specific recognition by proteins.

The strong interactions [Rh(phen)<sub>2</sub>phi]<sup>3+</sup> showed with Hoogsteen bonded triples prompted a systematic investigation of the recognition that this complex shows towards synthetic triple helices.<sup>66</sup> Consistent with the recognition seen on tRNA, the metal complex seems to interact with triple helices in a structure-specific manner. Different cleavage patterns were seen with the Y•R-Y and R•R-Y motifs; cleavage was seen on both of the Watson-Crick strands of the former motif and primarily on the purine Watson-Crick strand of the latter motif with little cleavage on the Hoogsteen strand for either motif. Importantly, the metal complex showed no detectable cleavage on the A-form RNA duplex in the absence of the third Hoogsteen strand. Thus the cleavage patterns were consistent with an intercalated model for the metal complex in the triple helix.

Lastly, the Tat-binding site of the bovine immunodeficiency virus TAR RNA hairpin was examined using  $[\text{Rh}(\text{phen})_2\text{phi}]^{3+}$  as a photochemical probe of RNA tertiary structure.<sup>67</sup> The primary site cleaved by the rhodium complex, upon photoactivation, was found to be U24, a base which participates in the novel base triple (with bases A13 and U10) characteristic of this folded RNA.  $\Delta\text{-}[\text{Rh}(\text{phen})_2\text{phi}]^{3+}$  bound to this site with an affinity of  $2 \times 10^6 \text{ M}^{-1}$ . In mutants where the RNA oligomer was unable to form the base triple, site-specific cleavage by the rhodium complex was abolished. Moreover,  $[\text{Rh}(\text{phen})_2\text{phi}]^{3+}$  was found to inhibit specific binding of BIV-Tat peptide to its target site. Thus, the rhodium complex, in matching its shape to the opened major groove of the properly folded RNA, could not only target a specific site on a folded RNA, but could compete for binding with a functionally important Tat peptide.

#### 1.2.3.3. Site-Specific Recognition of a Palindromic Octamer by $[\text{Rh}(\text{DPB})_2\text{phi}]^{3+}$

Perhaps the most striking example of site-specific recognition by shape selection with bulky ancillary ligands was found in the enantiospecific targeting of an eight-base pair site by  $\Delta\text{-}[\text{Rh}(\text{DPB})_2\text{phi}]^{3+}$  (DPB = 4,4'-diphenylbpy) (Figure 1.11).<sup>59,68</sup> In doing so, this metallointercalator was found to mimic different aspects of DNA-binding proteins. Specific photocleavage was induced on irradiation by  $\Delta\text{-}[\text{Rh}(\text{DPB})_2\text{phi}]^{3+}$  at the highlighted cytosine in the self-complementary sequence 5'-CTCTAGAG-3'; in contrast,  $\Lambda\text{-}[\text{Rh}(\text{DPB})_2\text{phi}]^{3+}$  yielded no detectable photocleavage, even at concentrations 1000-fold higher. Additionally, a distinct footprint was observed at the 5'-CTCTAGAG-3' site for  $\Delta\text{-}[\text{Rh}(\text{DPB})_2\text{phi}]^{3+}$ , but not for  $\Lambda\text{-}[\text{Rh}(\text{DPB})_2\text{phi}]^{3+}$ .

As a monomer the metal complex is geometrically capable of spanning only six base pairs. Thus, similar to many DNA-binding proteins, specificity for the palindromic site appeared to depend upon dimerization. The palindromic target site could be considered as two overlapping 5'-CTCTAG-3' monomer sites on opposing strands;

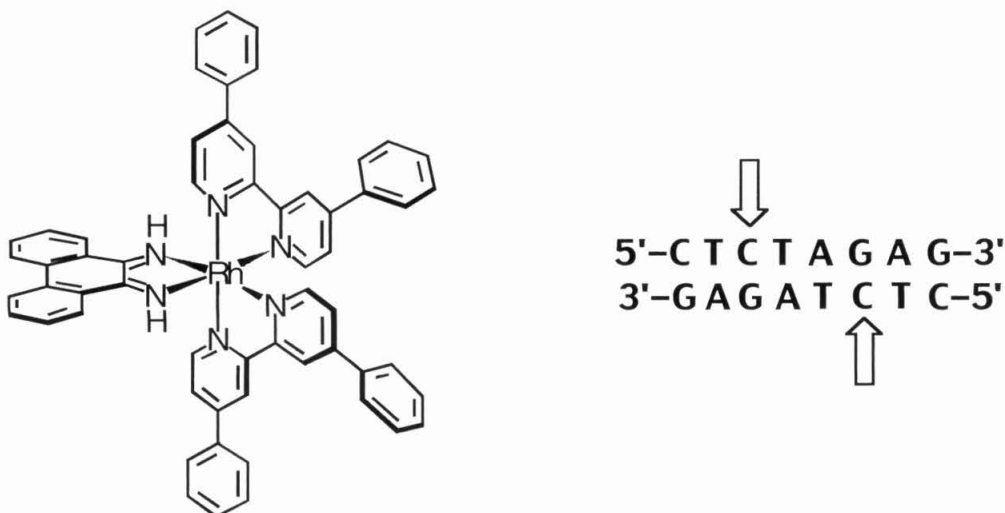


**Figure 1.11.**  $\Delta$ -[Rh(DPB)<sub>2</sub>phi]<sup>3+</sup> and the palindromic sequence recognized by cooperative binding of a dimer of this noncovalent dimer. The arrows indicate the sites of photocleavage.

simultaneous intercalation into the central 5'-CT-3' step of each monomer by  $\Delta$ -[Rh(DPB)<sub>2</sub>phi]<sup>3+</sup> would allow pendant phenyl groups from separate complexes to overlap over the central 5'-TA-3' base step. Evidence for this cooperative mechanism was obtained by comparing the binding curves between an isolated monomer of 5'-CTCTAG-3' with  $\Delta$ -[Rh(DPB)<sub>2</sub>phi]<sup>3+</sup> and the palindromic 5'-CTCTAGAG-3'. An enhancement of binding affinity for the palindromic site was observed, supporting a cooperative interaction of ~2 kcal between metal complexes within the 8-mer site.

Based on these observations, and its remarkable specificity,  $\Delta$ -[Rh(DPB)<sub>2</sub>phi]<sup>3+</sup> was then used to successfully inhibit XbaI restriction endonuclease activity at the palindromic site. No comparable inhibition was observed with a sequence-neutral DNA-binding metal complex, nor with [Rh(DPB)<sub>2</sub>phi]<sup>3+</sup> in competition with a restriction enzyme that binds an alternate site. Thus, a synthetic metallointercalator was found to bind to DNA with a level of specificity mimicking DNA-binding proteins and, in so doing, to inhibit site-specifically the reaction of the DNA binding protein.

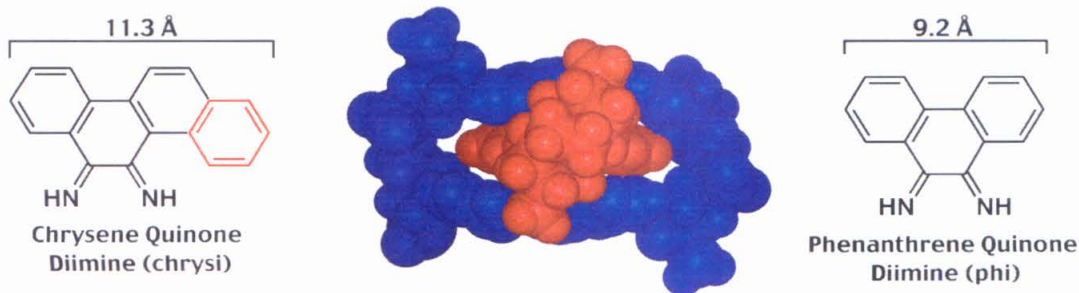


**Figure 1.12.** Size comparison of chrysi (left) and phi (right) ligands, and illustration of a DNA binding site containing  $\Delta\text{-}\alpha\text{-}[\text{Rh}[(\text{R,R})\text{-Me}_2\text{trien}]\text{phi}]^{3+}$ . The phi ligand fits tightly between the bases, leaving no room in B-form DNA for the extra chrysi ring (shown in red). Center structure courtesy of B. Hudson.

#### 1.2.3.4. $[\text{Rh}(\text{bpy})_2\text{chrysi}]^{3+}$ Complexes and Mismatch Recognition

Among the most recent of the metallointercalators explored as probes of DNA structure is  $[\text{Rh}(\text{bpy})_2\text{chrysi}]^{3+}$  (chrysi = 5,6-chrysenequinone diimine) (Figure 1.12).<sup>69,70</sup> This metal complex utilizes a somewhat different approach to DNA recognition. Here, recognition is still based upon steric exclusion, but now of the *intercalating* ligand. The strategy for shape-selective recognition of mismatched sites, irrespective of sequence, is based on the idea that expanding the size of the intercalating ligand by one aromatic group might restrict access to normal B-DNA but retain access to destabilized mismatches; the size of the chrysi aromatic ring makes it too sterically bulky to insert into standard B-form DNA.

This strategy holds, to first order. Specific DNA cleavage by  $[\text{Rh}(\text{bpy})_2\text{chrysi}]^{3+}$  is observed at over 80% of mismatch sites in all possible single base pair sequence contexts around the mispaired bases. Significantly, a correlation exists between the stability of the mismatch and the ability of the metal complex to photocleave the mismatch site. Moreover, the affinity of the metal complex for a C•A mismatch exceeds by almost three orders of magnitude that of the metal complex for matched B-form DNA.

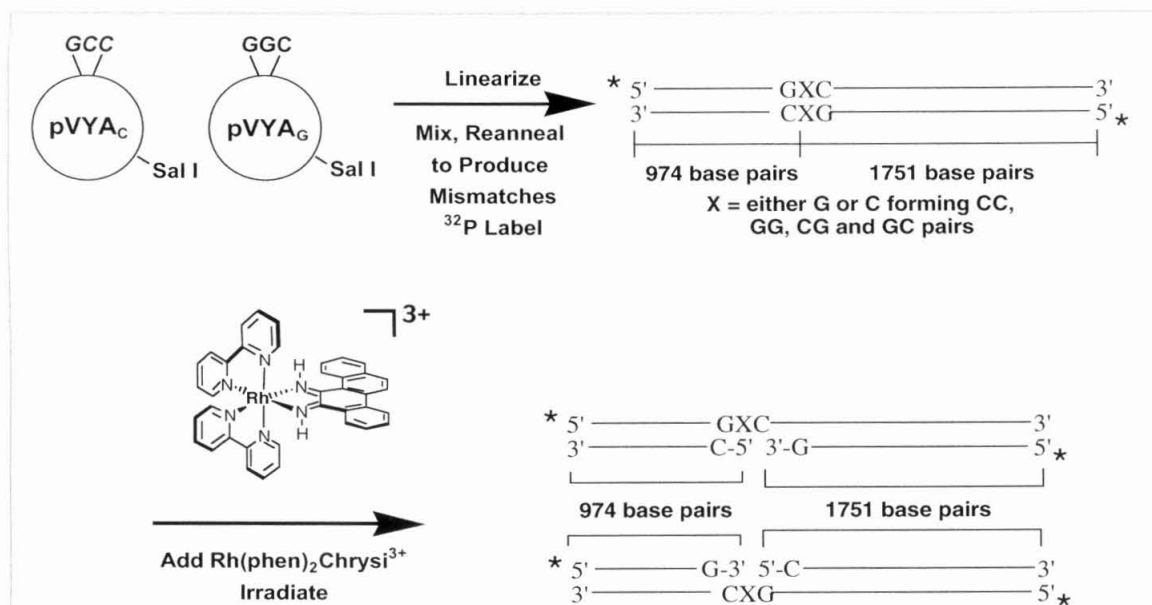


**Figure 1.13.** Plasmid-based assay to test sensitivity of  $[\text{Rh}(\text{bpy})_2\text{chrysi}]^{3+}$  to detect single mismatches in a 2.7 kb DNA strand. Two plasmids with a single base difference are linearized by a restriction endonuclease, mixed in equimolar amounts, denatured and reannealed. These strands are then irradiated in the presence of the metal complex, and the strand scission monitored by gel electrophoresis. Courtesy of B. Jackson.

This extremely high selectivity of  $[\text{Rh}(\text{bpy})_2\text{chrysi}]^{3+}$  for base mismatches has been demonstrated by targeting a single mismatch within a 2725 bp plasmid (Figure 1.13).<sup>70</sup> Following linearization of the two plasmids which differed in a sequence by only a single base, equimolar mixing and reannealing, a 2.7 kilo-base pair DNA strand was formed with a single mismatch at a known site. Low resolution mapping of this construct after irradiation with the metal complex showed cleavage of the DNA into a 974 bp fragment and a 1751 bp fragment, the appropriate sizes for scission at the mismatch site. Higher resolution mapping confirmed that the metal complex was binding exclusively to the mismatch site. Sterically demanding intercalators such as  $[\text{Rh}(\text{bpy})_2\text{chrysi}]^{3+}$  may have application both in mutation detection systems and as mismatch-specific chemotherapeutic agents.



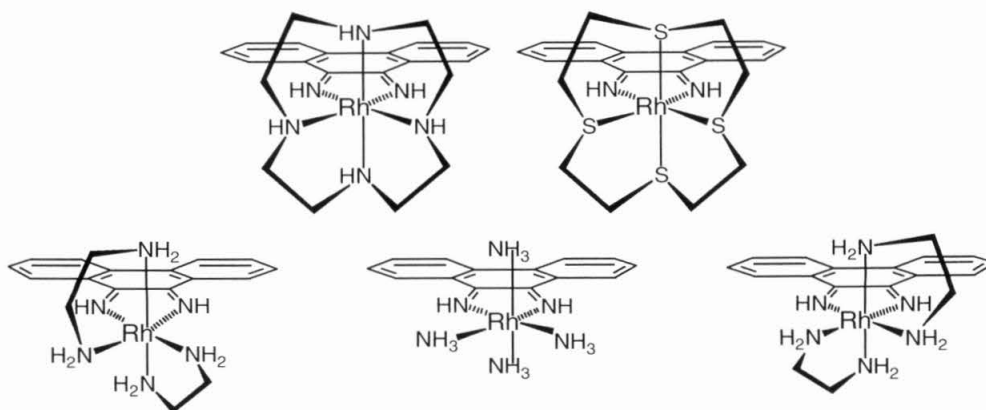


**Figure 1.14.** Phi complexes of Rh(III) with aliphatic ancillary ligands. From top right, clockwise,  $\text{Rh}[12]\text{aneN}_4\text{phi}^{3+}$ ,  $\text{Rh}[12]\text{aneS}_4\text{phi}^{3+}$ ,  $\Delta\text{-Rh}(\text{en})_2\text{phi}^{3+}$ ,  $\text{Rh}(\text{NH}_3)_4\text{phi}^{3+}$ ,  $\Lambda\text{-Rh}(\text{en})_2\text{phi}^{3+}$ .

## 1.2.4. Direct Readout of Major Groove DNA Functionality

### 1.2.4.1. Rhodium Amine Complexes as Intercalators

The ability of an octahedral metalointercalator to contact functionalities within the major groove by direct hydrogen bonding and/or specific van der Waals contacts provides another strategy for site-recognition. By designing metal complexes with functionality complementary to those of the base pairs arrayed three-dimensionally in the major groove, specificity can be achieved. Moreover, unlike shape-selection, in targeting B-DNA sites, site-specific metal complexes may be designed with a level of predictability.

A family of rhodium amine complexes containing the phi ligand was synthesized, and their selectivities for different sites were tested (Figure 1.14).<sup>71,72</sup> It was found that  $[\text{Rh}(\text{NH}_3)_4\text{phi}]^{3+}$ ,  $[\text{Rh}(\text{en})_2\text{phi}]^{3+}$ , and  $[\text{Rh}[12]\text{aneN}_4\text{phi}]^{3+}$  cleave strongly at 5'-GC-3' sites. Given the rigid structures of these complexes, and the orientation of these complexes when bound to DNA, models were made which indicated the possibility of hydrogen bond formation between axial amines of the metal complexes and the O6 of guanine. The C2 symmetry of the complexes should confer recognition of a 5'-GC-3' base step. A



metal complex,  $[\text{Rh}[\text{12}]_{\text{aneS}_4}\text{phi}]^{3+}$ , which lacks H-bond capability was synthesized and tested as a control in parallel experiments, and was seen to bind non-specifically.

Additional experiments using these phi complexes of rhodium which contain axial amines probed hydrogen bonding to guanine through the introduction of O6-methyl guanine in place of guanine on the targeted oligonucleotide. As expected, this modification disrupted binding to the site.<sup>73,74</sup> In contrast, replacement of guanine with deazaguanine did not disrupt recognition, suggesting that hydrogen bonding to the N7 of guanine is not an important factor in binding of these metal complexes. A related finding was that the  $\Delta$ - $[\text{Rh}(\text{en})_2\text{phi}]^{3+}$  enantiomer also bound to 5'-TX-3' sites, especially 5'-TA-3', due to a Van der Waals contact between the methylene groups on the backbone of the complex and the thymine methyl. The  $\Lambda$ -isomer of the complex showed no such preference in binding. Mutation of the thymine to deoxyuracil, which lacks the methyl group, abrogated binding by  $\Delta$ - $[\text{Rh}(\text{en})_2\text{phi}]^{3+}$  to the 5'-TX-3' sites.

#### 1.2.4.2. Predictive Design and Direct Readout by $\Delta$ - $\alpha$ - $[\text{Rh}[(R,R)\text{-Me}_2\text{trien}]\text{phi}]^{3+}$

Using the basic characterization of possible non-covalent contacts between phi intercalators containing amine ligands and DNA, a new complex,  $\Delta$ - $\alpha$ - $[\text{Rh}[(R,R)\text{-Me}_2\text{trien}]\text{phi}]^{3+}$ , was designed specifically to bind to a 5'-TGCA-3' site (Figure 1.15).<sup>75</sup> The targeting of this site was designed to generate hydrogen bonding contacts between the axial amines and the O6 of guanine, as well as potential van der Waals contacts between the pendant methyl groups on the metal complex and the methyl groups on the flanking thymines.<sup>71</sup> Photocleavage data indicates that the complex binds to the target site with a binding constant of  $9 \times 10^7 \text{ M}^{-1}$ .<sup>76</sup> A high resolution NMR structure,<sup>41,76</sup> and recently a crystal structure of the DNA-intercalated metal complex<sup>42</sup> all confirm that this complex targets the sequence 5'-TGCA-3' from the major groove, and, remarkably, that each of the predicted contacts are present.

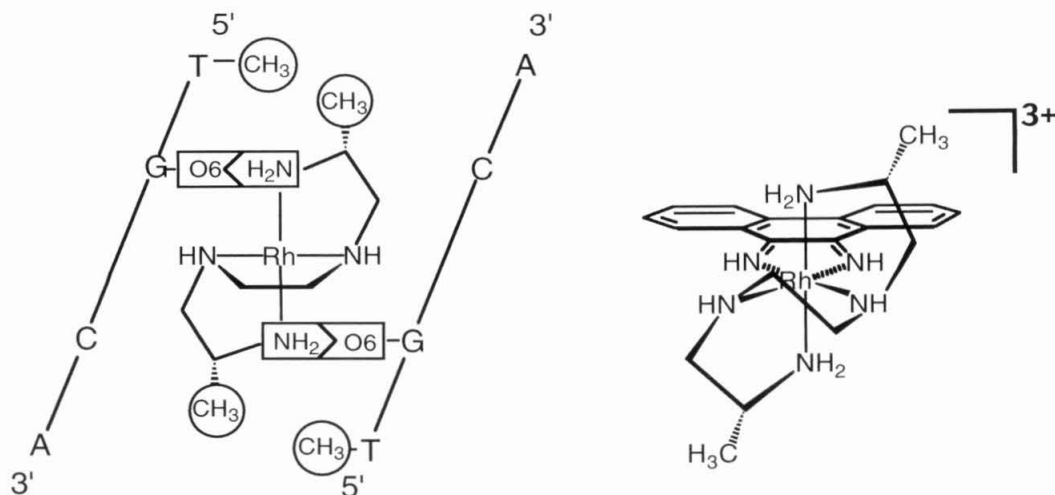


**Figure 1.15.** Illustration of the recognition of TGCA by  $\Delta\text{-}\alpha\text{-}[\text{Rh}[(\text{R},\text{R})\text{-Me}_2\text{trien}]\text{phi}]^{3+}$ .

The crystal structure of the rhodium intercalator  $\Delta\text{-}\alpha\text{-}[\text{Rh}[(\text{R},\text{R})\text{-Me}_2\text{trien}]\text{phi}]^{3+}$  bound specifically to the central 5'-TGCA-3' site of an eight base pair DNA oligonucleotide was solved at 2.0 Å resolution and represents the first crystallographically characterized high resolution view of a metalointercalator bound to a DNA duplex (Figure 1.16).<sup>42</sup> Five intercalated DNA duplexes in the asymmetric unit provide crystallographically independent views of the detailed interactions between the intercalator and the major groove binding site. The structure shows that the base pairs are well-stacked, the phi ligand is deeply intercalated, and the conformation of the deoxyribose sugars at the intercalation site is B-form. Indeed, metalointercalation here causes minimal structural perturbation to DNA. Essentially the intercalator resembles an inserted base pair. This structure provides a rational basis for expanding the current repertoire of sequence-specific intercalators and fundamental support for the strategy of utilizing octahedral metalointercalators in predictable site-specific design.

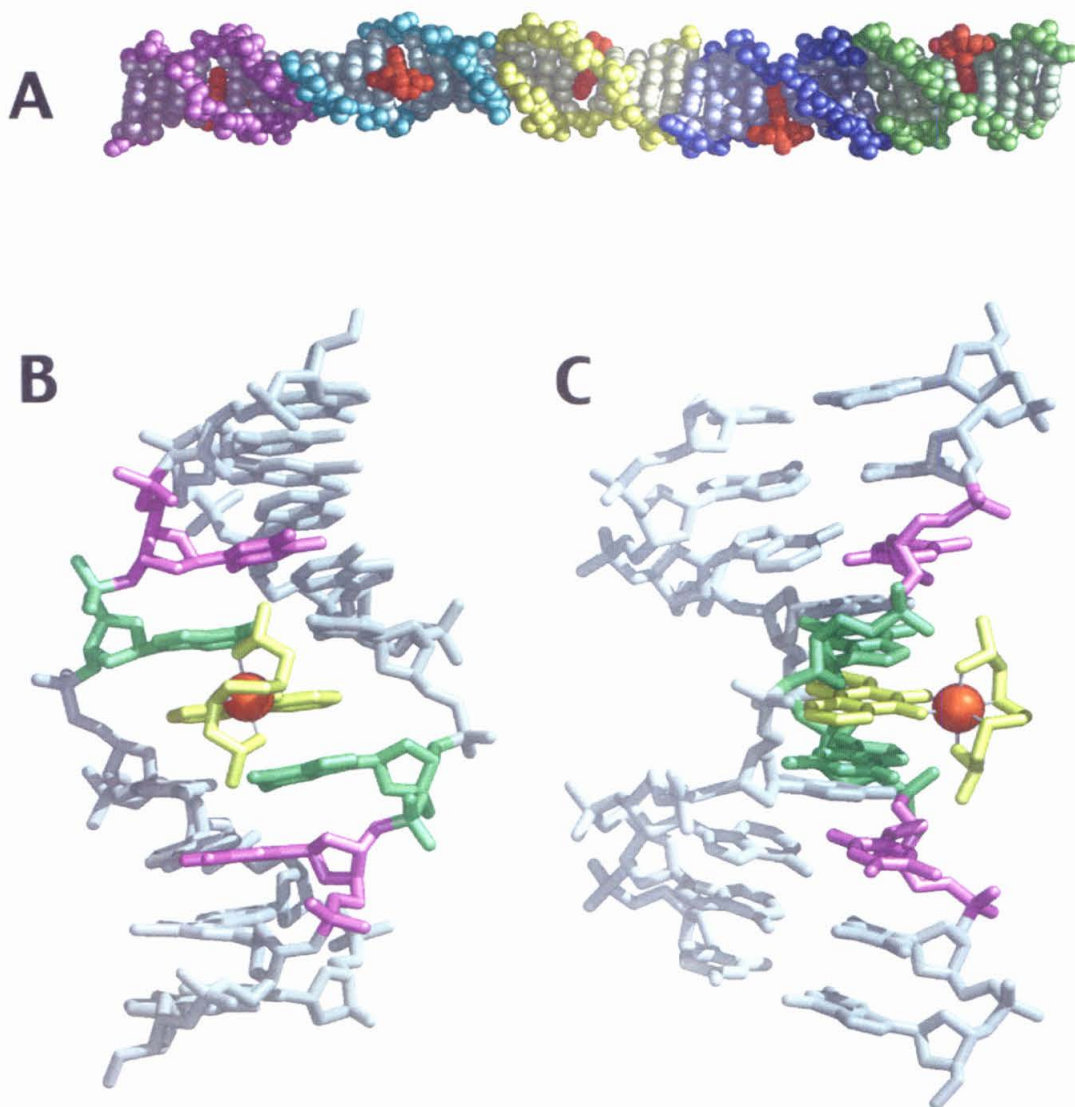


**Figure 1.16.** Crystal structure of the DNA-bound metallointercalator  $\Delta\text{-}\alpha\text{-}[\text{Rh}[(\text{R},\text{R})\text{-Me}_2\text{trien}]\text{phi}]^{3+}$  (red in A, gold in B and C) bound specifically to the central 5'-TGCA-3' site of an eight base pair DNA oligonucleotide. The five independent duplexes in the asymmetric unit are shown in A, and two 90° rotational views of one monomer from the asymmetric unit are depicted in B and C.

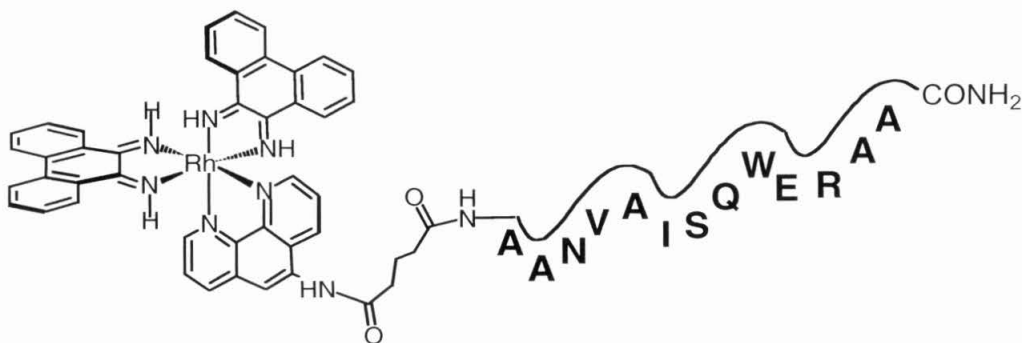


**Figure 1.17.** A  $[\text{Rh}(\text{phi})_2\text{phen}']^{3+}$ -peptide chimera.

#### 1.2.4.3. Rhodium Complex-peptide Chimeras

An entirely different strategy towards designing DNA binding agents utilizes a metallointercalator to provide non-specific affinity for DNA within a larger assembly of recognition elements. Proteins often use a significant percentage of their amino acids to provide a scaffold that has high non-specific affinity for DNA, while an appreciably smaller number of amino acids are actually used to contact the base pairs directly. Coupling of a derivative of  $[\text{Rh}(\text{phi})_2\text{bpy}]^{3+}$  to the peptide motif used as the contact region in a DNA binding protein can provide the same non-specific affinity with less steric bulk and complexity, while possibly maintaining the essential site recognition characteristics of the original motif.<sup>77</sup>

An example of this strategy uses the 13 amino acid DNA binding domain of phage P22 repressor coupled to  $[\text{Rh}(\text{phi})_2\text{bpy}]^{3+}$  (Figure 1.17).<sup>78</sup> Systematic variations in this motif revealed that the recognition characteristics of this molecule are critically dependent on a single glutamate. In cases where the glutamate was present, even with variations within the surrounding sequence, the chimera specifically recognized 5'-CCA-3'. However, changes as conservative as replacing glutamate with the isostere glutamine, or shortening the side-chain group by one methylene with aspartate, entirely destroyed the recognition characteristics of this metallointercalator. CD studies

indicated that this glutamate is essential to maintain the  $\alpha$ -helicity of the peptide; its removal disrupts the structure significantly. Hence, glutamate can act as a switch for recognition in this system, and its absence destroys both the secondary structure within the chimera peptide backbone and the DNA recognition of the ensemble.

Important issues still need to be established in effecting this design strategy. The metallopeptidases lack rigidity and often predictability in their structure. Moreover, the relationship between the peptide conformation in the chimera versus that in the DNA binding protein is also not necessarily strong. As such, while the construction of metallointercalator-peptide chimeras offers a whole new array of molecules to explore site-specific recognition, challenges remain in achieving predictable site-specificity with these complexes.

### 1.2.5. Combining Direct Readout and Shape Selection

#### 1.2.5.1. Site-Specific Recognition by $[Rh(MGP)_2\phi]^{5+}$

$[Rh(MGP)_2\phi]^{5+}$ , a derivative of  $[Rh(\text{phen})_2\phi]^{3+}$  containing pendant guanidinium groups on the phenanthroline ligand, was designed to target a subset of sites recognized by  $[Rh(\text{phen})_2\phi]^{3+}$ .<sup>79,80</sup> Because MGP (MGP = 4-(guanidylmethyl)-1,10-phenanthroline) is an asymmetric ligand, condensation of the ligand into two positions of an octahedral metallointercalator affords three possible positional isomers, each of which has two enantiomers (Figure 1.18). Based on modeling, it was predicted that 1-  $[Rh(MGP)_2\phi]^{5+}$  would target the subset of  $[Rh(\text{phen})_2\phi]^{3+}$  sites flanked by G•C base pairs, due to the potential hydrogen bonding to guanine sites that the MGP ligand afforded when this isomer is oriented along the major groove of DNA.

$\Delta$ -1- $[Rh(MGP)_2\phi]^{5+}$  was indeed found to target 5'-CATCTG-3' specifically, and NMR experiments showed that it binds to the target site in two modes canted from each other in the central base step.<sup>81</sup> Remarkably, however, the  $\Lambda$ -isomer also showed site-

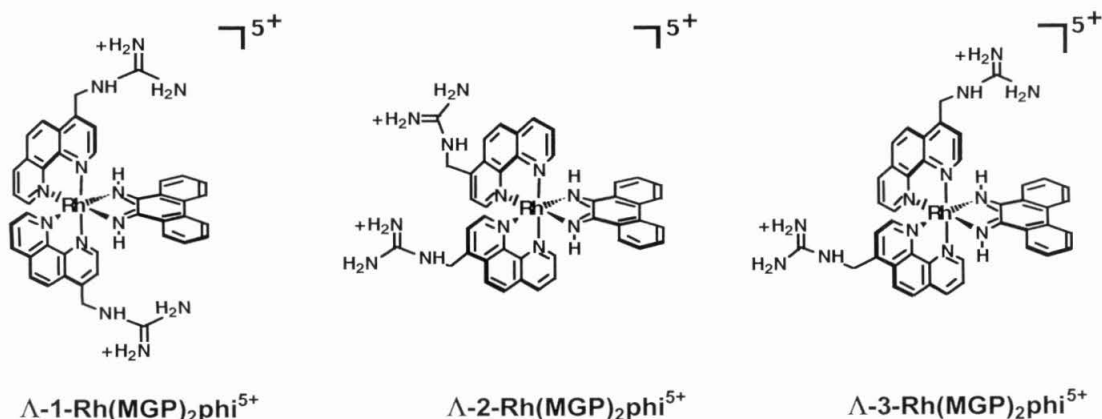


**Figure 1.18.** Three configurational isomers of  $[\text{Rh}(\text{MGP})_2\text{phi}]^{5+}$ .

specificity.  $\Lambda$ -1- $[\text{Rh}(\text{MGP})_2\text{phi}]^{5+}$  recognized the sequence 5'-CATATG-3' with high site-selectivity and affinity; systematic replacement of the bases of this motif showed that variation within this binding site caused a dramatic reduction in binding.<sup>79</sup> Since initial modeling studies had shown no possible specific interactions within a normal B-form site due to the left-handed symmetry of this metal complex, it was difficult to understand how this complex could bind B-DNA at all.

Additional modeling showed that if the complex bound to a significantly unwound DNA site, so as essentially to flatten the helix into a ladder at the binding site, specific binding to a six-base pair sequence by  $\Lambda$ -1- $[\text{Rh}(\text{MGP})_2\text{phi}]^{5+}$  was possible.<sup>79</sup> Plasmid unwinding assays were devised to test for this site-specific unwinding and indeed established that the complex bound to this DNA site which is marked by 70° unwinding. NMR studies provided additional support for this binding model.<sup>81</sup> It is in this conformation that the complex can span the entire six base pair binding site, and contact the N7 position of the flanking guanines with the pendant guanidinium groups. Replacement of these flanking guanines with deazaguanine showed that the absence of the N7 nitrogen removed selectivity for the site as seen by both NMR studies and photocleavage.<sup>81</sup> Therefore, it was proposed that the complex targeted its site by a

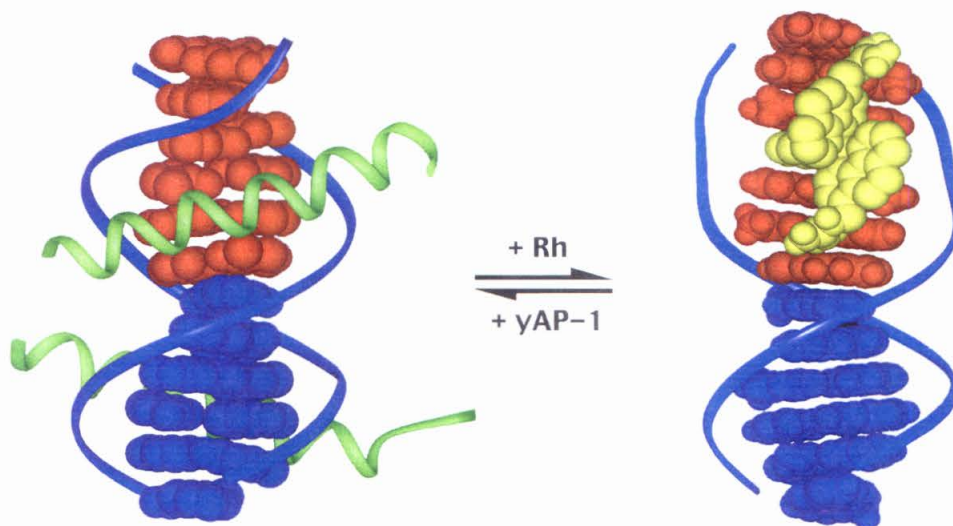


**Figure 1.19.** Illustration of the inhibition of transcription factor yAP-1 binding to DNA by  $\Lambda$ -1-[Rh(MGP)<sub>2</sub>phi]<sup>5+</sup>.

combination of direct readout and shape selection. While hydrogen bonding to guanine positions was critical, also important was the propensity of the 5'-ATAT-3' site for flexibility or "twistability." This explains the complete loss of recognition for the less flexible sequence 5'-CACGTG-3'. NMR studies supported a mechanism of recognition based on trapping of the target site by the complex in an unwound conformation. It is notable that this complex, in contrast to most other complexes described here, shows a higher binding affinity by the  $\Lambda$ -isomer ( $\sim 10^{-8} \text{ M}^{-1}$ ) for its target site than does the  $\Delta$ -isomer ( $\sim 10^{-7} \text{ M}^{-1}$ ) for its site. This combination of shape-selection and direct readout can be powerful and highly specific.

#### 1.2.5.2. $\Lambda$ -1-Rh(MGP)<sub>2</sub>phi]<sup>5+</sup> as an Inhibitor of Transcription Factor Binding

Given its high affinity and specificity,  $\Lambda$ -1-[Rh(MGP)<sub>2</sub>phi]<sup>5+</sup> has additionally been used to inhibit site-specifically a transcription factor from binding to a modified activator recognition region (Figure 1.19, and Chapter 2 of this Thesis).<sup>82</sup> In competition experiments with yeast Activator Protein 1 (yAP-1), the metal complex competed with



the protein for a binding domain that included both a yAP-1 binding region and a  $\Lambda$ -1- $[\text{Rh}(\text{MGP})_2\text{phi}]^{5+}$  binding site. The concentration of metal complex required for this site-specific inhibition was 120 nM. In the absence of the metal binding region, the inhibition required 30 fold higher metal complex. Furthermore, the use of the parent complex  $[\text{Rh}(\text{phen})_2\text{phi}]^{3+}$  in identical competition experiments required over three orders of magnitude more metal complex to afford the same competitive disruption of protein gel shift. This reaction was additionally seen to be isomer-specific, as the symmetric isomer 2- $[\text{Rh}(\text{MGP})_2\text{phi}]^{5+}$ , in which the guanidinium groups are projected away from the phi ligand, showed no competitive binding with the protein. These results demonstrated the utility of metallointercalators, not only as biochemical probes of nucleic acid structures but also, potentially, as therapeutical agents in gene regulation.

### 1.3. REACTIONS OF METALLOINTERCALATORS WITH DNA

Since metal complexes are amenable to many spectroscopic techniques, their utility as spectroscopic probes in biological systems has been the subject of increasing research. However, transition metal complexes also offer an unusual range of reactivity, particularly in the context of redox chemistry, and this chemistry can also be harnessed advantageously by metallointercalators to yield a variety of interesting reactions with DNA. It is, in fact, this reactivity that has helped in establishing the site-specificity of many of the metallointercalators, as already described. Indeed, the redox reactivity of even nonspecifically bound metallointercalators can be used in footprinting assays to determine the sequence preference of other DNA-binding molecules. The first such footprinting agent was MPE-Fe(II), a complex constructed by bringing together an organic intercalator, ethidium, and a redox active metal complex, FeEDTA.<sup>83</sup>



Here I highlight some of the different reactions of coordinatively saturated metalointercalators. Because there are an ever increasing number of reports of metal complexes reacting with various nucleic acids, in this introduction each subject is given a relatively broad overview. The reactions DNA and nucleic acids undergo with metalointercalators are explored more fully in the background of each of the relevant chapters.

### **1.3.1. Direct Oxidative Strand Cleavage, Reactions with the Sugar**

Strand cleavage by abstraction of a hydrogen atom from a sugar adjacent to the binding site is a mechanism by which many DNA binding agents degrade DNA. Minor groove binding molecules such as bis-(1,10-phenanthroline)copper(I), Fe(II)•bleomycin, and metal-centered porphyrins all display direct DNA strand scission consistent with hydrogen abstraction from the C1', C4' and C5' of the ribose ring, and studies of the reactivity by these molecules has been the subject of a recent review.<sup>84</sup> In contrast, C3' and C2' hydrogen atoms are only accessible for attack to complexes binding in the major groove, and because there are very few oxidative cleaving agents which bind to DNA via the major groove, there has been little opportunity to study this reaction. Phi complexes of Rh(III) are major groove intercalators, and their photoinduced strand-cleaving reactivity is quite distinctive from that of alternate DNA-damaging agents.

It was proposed that ultraviolet irradiation of an intercalated phi complex of Rh(III) leads to the generation of a radical on the phi ligand via ligand-to-metal charge transfer.<sup>56</sup> The ligand in turn can abstract a C3' hydrogen from the adjacent deoxyribose, and as a result the sugar radical degrades, leading to DNA strand cleavage and generating several degradation products (Figure 1.20).

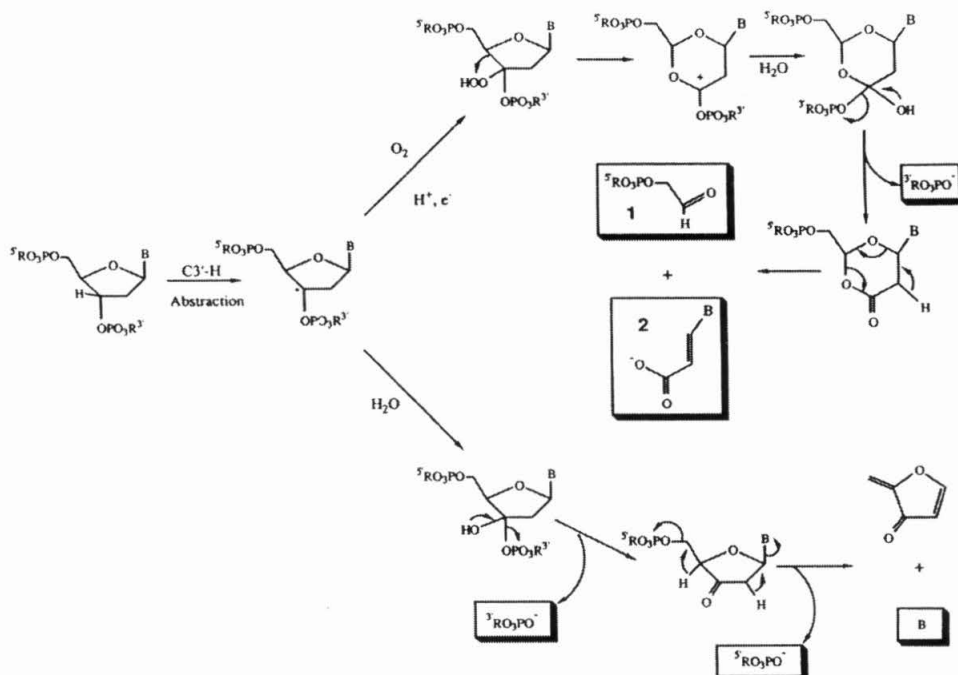


**Figure 1.20.** Mechanistic scheme proposed for direct strand scission by phi complexes of rhodium photoirradiated at 313 nm. Adapted from reference 56.

Photolysis of  $[\text{Rh}(\text{phen})_2\text{phi}]^{3+}$  or  $[\text{Rh}(\text{phi})_2\text{bpy}]^{3+}$  bound to DNA yields DNA strand cleavage and, in the absence of O<sub>2</sub>, results in the formation of 3' phosphate and 5' phosphate termini, and free bases. The presence of oxygen leads to different products: this is also direct strand cleavage, but now products include the 5' phosphate terminus, base propenoic acid, and a 3' phosphoglycaldehyde. By analogy with reactions of bleomycin at the C4' position, these products are consistent with radical chemistry at the C3'-position.

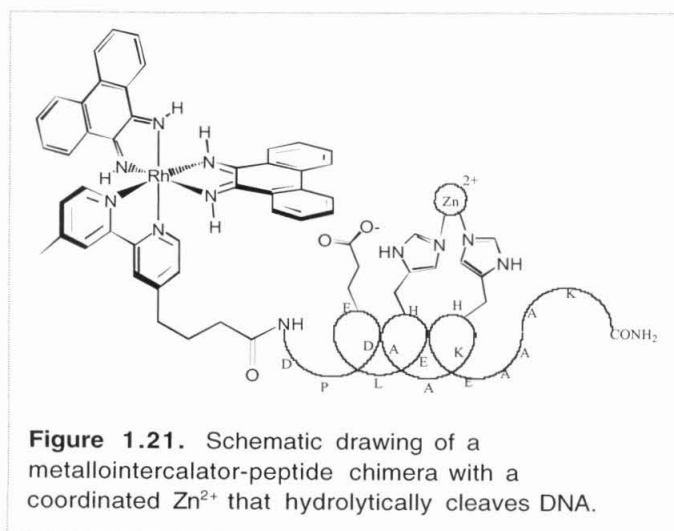
Recent NMR and crystallographic studies suggest a close association between the phi ligand and the C2' position.<sup>41,42,76</sup> Therefore, the initial reaction may be with the C2'-H followed by H-migration to form the C3'-radical with subsequent degradation. More detailed analysis will be required to precisely determine this mechanism. Certainly it is the orientation of the metallointercalator within its major

groove site that determines this chemistry. Intimate contact with DNA is required, and no diffusible radical species is involved in the DNA strand cleavage.

It should be noted here that much of what is known about how phi complexes of rhodium(III) recognize specific sites was derived first from DNA photocleavage experiments. Confirmation of recognition and greater structural definition would emerge later from NMR studies. Thus despite the very low quantum yields for photocleavage by these complexes, the fact that reactivity was localized, not involving a diffusible species, and essentially independent of sequence (a characteristic of reactions on the deoxyribose ring) led to a valuable nucleic acid probe. In a straightforward fashion, this reactivity has been used generally to mark the sites of binding by rhodium intercalators.

### 1.3.2. Hydrolytic Strand Cleavage

The search for complexes that mimic certain proteins, binding selectively to specific DNA sites and cleaving by hydrolysis of the phosphate was the subject of a recent review.<sup>85</sup> Here, too, metallointercalators have been employed, specifically, a metallointercalator-peptide chimera. An assembly consisting of a peptide tethered



covalently to the 4,4'-dimethyl-2,2'-bipyridine ligand of a  $[\text{Rh}(\text{phi})_2\text{dmb}]^{3+}$  was designed to explore hydrolytic DNA cleavage.<sup>86</sup> In this strategy, once the metal complex is bound to DNA by intercalation of the phi ligand, the peptide is delivered to the backbone of

DNA, where it cleaves the DNA by a hydrolytic mechanism (Figure 1.21). The 16-residue peptide chain was designed *de novo*, based upon studies of the active sites of several metallic hydrolases. In this design the peptide has a propensity to adopt an  $\alpha$ -helical conformation with two histidines on one face to coordinate a  $\text{Zn}^{2+}$ . It was hoped that that delivery of the  $\text{Zn}^{2+}$  would yield hydrolytic reactivity on the sugar-phosphate backbone. Cleavage products of the complex were analyzed by gel electrophoresis, where control sequencing lanes were run alongside product lanes. Band migration of the cleavage products showed that the cleaved DNA termini contained hydroxyl ends, rather than phosphates. The presence of only 3' hydroxyl termini, rather than a mixture of terminal products, suggests that the peptide cleaves stereospecifically, which might be a result of the complex's major groove binding orientation.

The reactivity of this metallointercalator-peptide chimera represented a first step in the development of a true synthetic nuclease. While sequence specificity was not achieved by this assembly, the possibility remains that similar short peptides which are tethered to more specific intercalators can serve as synthetic, sequence-specific restriction enzymes.

### 1.3.3. Oxidative Reactions with the DNA Bases

Oxidative damage to DNA bases generally occurs at guanines, which have the lowest oxidation potential of all the DNA bases. Damage to this base does not cause direct strand scission, however, so reactions must be post-treated with miperidine or aniline in order to analyze the reactivity of the oxidants. The oxidative damage to DNA can occur by one of four mechanistic pathways: (i) by direct electron transfer from the guanine to bound metal complex (already described above for TAP and HAT complexes of  $\text{Ru(II)}$ );<sup>21</sup> (ii) by oxo transfer (such reactions have been used in assays

of base accessibility with intercalators well-stacked into the helix); (iii) as a result of reaction with singlet oxygen, which is formed on sensitization of a DNA bound metallointercalator (exploitation of this type of damage has been the basis of phototherapeutic strategies);<sup>87</sup> and (iv) over a long range by DNA-mediated electron transport.<sup>88</sup>

#### 1.3.3.1. Base Damage by Oxo Transfer

Many examples of DNA cleavage using Mn porphyrin activated with persulfate or other oxygen donors have been reported, and these reactions yield oxidative damage both to the sugars and DNA bases.<sup>89,90</sup> Whether it is an intercalated metalloporphyrin that is reactive in these cases is not likely, however, since it is an axially bound oxo that is delivered to the DNA sugar or base.

Direct oxidation of DNA bases has also been accomplished by activation of Ru(II) complexes such as  $[\text{Ru}(\text{bpy})_3]^{2+}$  and  $\text{trans-}[\text{Ru}(\text{O}_2)(4\text{-Ome-Py})_4]^+$  electrochemically.<sup>91,92</sup> Reactivity can be enhanced by coordinating an intercalating ligand, as with  $[\text{Ru}(\text{tpy})\text{dppz}\text{O}]^{2+}$ ,<sup>93</sup> but here too reaction is likely not from the intercalative mode of binding. Oxidative reaction is evident preferentially at guanines. This chemistry has been exploited as a probe of DNA and RNA hybridization.<sup>92</sup>

#### 1.3.3.2. Guanine Oxidation by Singlet Oxygen

Singlet oxygen as a source of oxidative damage to DNA bases is well documented.<sup>94</sup> There are several examples of DNA-binding metal complexes that can generate the singlet oxygen species via a triplet energy transfer from the excited state of the metal complex to  $\text{O}_2$ . Such reactions with DNA involving porphyrins, Ru(II) complexes of HAT, TAP, and bpz, and Vanadium(V) complexes are discussed in a recent review.<sup>95</sup>

The high efficiency of singlet oxygen sensitization by  $[\text{Ru}(\text{bpy})_3]^{2+}$  derivatives was originally exploited to probe A-form nucleic acids.<sup>62,96</sup> In these cases, while the metal complexes were not bound by intercalation, the  $^1\text{O}_2$  generated locally by the surface bound metal complex could be used to probe the location of the bound metal. Because the reactivity of singlet oxygen is largely directed to guanines, and because  $^1\text{O}_2$  can diffuse along the helix, this reaction is not ideal for marking binding sites of metal complexes. However, in the absence of alternative methods, this type of reaction can be useful. This technique has been used extensively with ruthenium complexes to investigate helix binding locations. Ruthenium (II) dppz complexes, for example, with shorter excited-state lifetimes than  $[\text{Ru}(\text{bpy})_3]^{2+}$  when bound to DNA, are only moderate sensitizers of  $^1\text{O}_2$ .<sup>31</sup> However, this reaction has proven to be critical in marking sites of intercalation of tethered dppz complexes along DNA nucleotides.<sup>97</sup>

#### 1.3.3.3. Guanine Oxidation by Long-Range Electron Transport

DNA-mediated electron transfer has been a much debated topic of research.<sup>88</sup> Of particular interest to this introduction is the sensitivity of DNA-mediated electron transfer reactions to stacking. Metallointercalators which are able to intercalate into the DNA base stack and oxidize DNA bases are able to do so from a distance.

Oxidative damage to DNA by one-electron transfer occurs at guanines, in particular at the 5'-G's of 5'-GG-3' doublets. Calculations have shown that in general these guanines have a particularly low oxidation potential.<sup>98,99</sup> Following one-electron oxidation, the guanine radical can react both with  $\text{O}_2$  and  $\text{H}_2\text{O}$  to form a series of irreversible products, and some of these oxidation products can be revealed in biochemical experiments as strand cleavage events upon treatment with piperidine.<sup>100</sup> The piperidine-sensitive reaction of a range of species at the 5'-G of 5'-GG-3' sites has come to be regarded as a signature for electron transfer in DNA.

**Figure 1.22.** Two oxidative reaction pathways for ruthenium coupled DNA. On the left is the singlet oxygen based, intercalation site marking reaction; on the right is the long range charge transport reaction. Both require piperidine treatment to reveal base lesions.

Figure 1.22 illustrates two oxidative reactions of a Ru(II) intercalator tethered to DNA.<sup>97</sup> As mentioned above, photoexcited ruthenium(II) complexes can sensitize the formation of  $^1\text{O}_2$ , which react preferentially at nearby guanine residues, causing damage at the metal binding site. However, the photoexcited Ru(II) can also be quenched by electron transfer to a surface-bound quencher such as  $[\text{Ru}(\text{NH}_3)_6]^{2+}$  or methyl viologen. Once quenched, the Ru(III) intercalator, generated *in situ*, becomes a potent ground state oxidant. Ru(III) intercalators generated through this flash-quench technique can then be employed to damage DNA from a distance by electron transport, yielding reaction at the 5'-G of 5'-GG-3' sites. This flash-quench

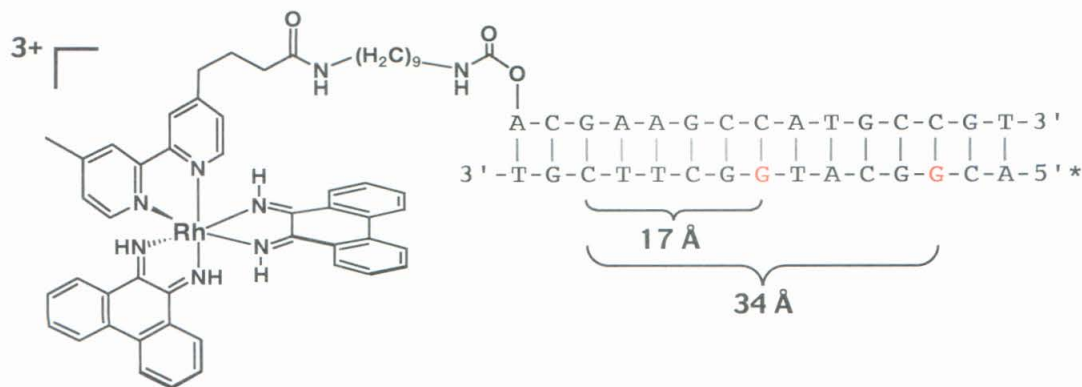


**Figure 1.23.**  $[\text{Rh}(\text{phi})_2\text{bpy}']^{3+}$  covalently tethered to a 15-mer oligonucleotide with proximal and distal 5'-GG-3' sites. 5'-guanines were oxidized by excitation of the intercalated metal complex, followed by long range charge transport through the  $\pi$ -stack.

methodology has also been exploited using non-covalently bound  $[\text{Ru}(\text{phen})_2\text{dppz}]^{2+}$  with poly-d(GC) to spectroscopically characterize the guanine radical formed in the DNA duplex.<sup>101</sup>

Damage to DNA sites from a distance was first demonstrated in assemblies containing a tethered phi complex of rhodium(III) as the photooxidant, which is spatially separated from the site of oxidation.<sup>102</sup> It had earlier been seen that low energy photolysis of the complex produced a potent photooxidant ( $\sim 2$  eV).<sup>103</sup>  $[\text{Rh}(\text{phi})_2\text{bpy}']^{3+}$  was covalently tethered to a 15 base pair strand of DNA and annealed to a complement which contained two 5'-GG-3' sites, one 17 Å and one 34 Å from the intercalation site of the metal complex, beyond a feasible distance for direct electron transfer (Figure 1.23). The Rh-DNA assembly was irradiated at 313 nm to induce direct strand cleavage, marking the site of rhodium intercalation near the tethered end. Separate Rh-DNA samples were also irradiated at 365 nm, treated with hot piperidine, and examined by gel electrophoresis (a typical experiment is shown as an example in Figure 1.24). Quantitation of the gel bands after photooxidation revealed that both the proximal and distal 5'-GG-3' doublets were equally damaged, and



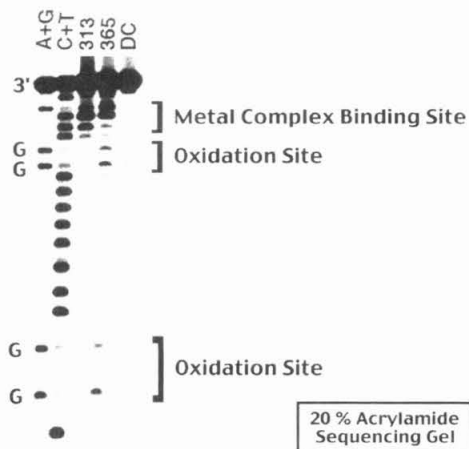


**Figure 1.24.** Typical gel from a long range charge transport experiment using covalently tethered Rh-DNA.

controls showed that the reaction was intraduplex. Hence, this experiment established oxidative damage to DNA from a distance via long range electron transfer.

Preferential oxidation was seen with the  $\Delta$ -diastereomer, consistent with the sensitivity of the reaction to deep intercalation of the oxidant. Subsequent studies also

showed the sensitivity of the reaction to the intervening base pair stack; assemblies containing bulges inserted in the DNA between the proximal and distal 5'-GG-3' doublets showed a diminution in oxidation at the distal site.<sup>104</sup> Long range oxidation was also shown to be modulated by proteins that bind DNA and perturb stacking at an intervening site.<sup>105</sup> Recently, damage has been reported at sites that are up to 200 Å away from the site of intercalation of the metal oxidant.<sup>106</sup>

#### 1.3.3.4. Oxidative Repair of Thymine Dimers

The oxidative chemistry of rhodium intercalators has also been used to repair thymine dimers in DNA.<sup>107,108</sup> The thymine dimer is the most common photochemical lesion in DNA, and is a result of the 2+2 cycloaddition reaction between neighboring thymines on the same DNA strand upon photolysis with ultraviolet light. In bacterial cells, thymine dimers are repaired reductively by the enzyme photolyase, but model studies had shown that thymine dimers can also be repaired oxidatively.

DNA duplexes were synthesized containing a site-specifically incorporated thymine dimer and then photolyzed with visible light in the presence of non-covalently

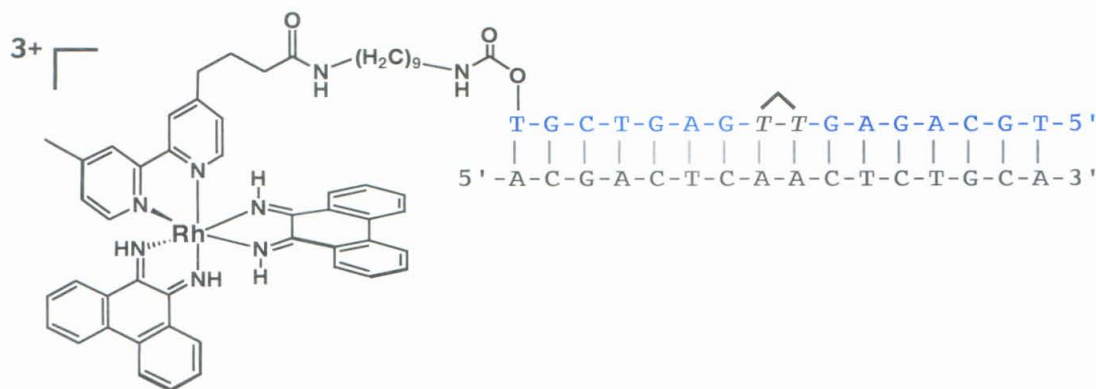


**Figure 1.25.** A 16-mer oligonucleotide covalently tethered to  $[\text{Rh}(\text{phi})_2\text{bpy}']^{3+}$  and containing a thymine dimer lesion.

bound  $[\text{Rh}(\text{phi})_2\text{bpy}']^{3+}$ .<sup>107</sup> High temperature HPLC showed the quantitative repair of the DNA promoted by the metal complex without any damage to the complementary strand. Moreover, only catalytic amounts of  $[\text{Rh}(\text{phi})_2\text{bpy}']^{3+}$  per DNA duplex were required, consistent with an oxidative repair mechanism. Indeed, quantitative repair could be seen with micromolar concentrations of  $[\text{Rh}(\text{phi})_2\text{bpy}']^{3+}$  and exposure of samples simply to sunlight.

The repair of thymine dimers in DNA by photolysis of the metallointercalators was next demonstrated at a distance with 16- to 19-base strands of DNA that contained a single TT sequence with no adjacent pyrimidines. These target strands were irradiated with ultraviolet light to induce the thymine dimer, the lesion containing strand was purified by HPLC, and this damaged strand was then annealed to a complementary strand which contained a covalently tethered  $[\text{Rh}(\text{phi})_2\text{bpy}']^{3+}$  complex with an intercalation site 19 Å to 26 Å from the damage site (Figure 1.25). The damaged Rh-DNA assembly was then irradiated with light at 400 nm, and as  $[\text{Rh}(\text{phi})_2\text{bpy}']^{3+}$  oxidized the thymine dimer, the conversion from damaged to repaired DNA was monitored by HPLC.

The repair efficiency of  $[\text{Rh}(\text{phi})_2\text{bpy}]^{3+}$  was about equal whether the complex was to the 5' or to the 3' side of the lesion. Several different lengths of DNA were used, and, interestingly, the repair efficiency increased from 67% to 100% as the distance increased from 19 to 26 Å. This may reflect the increased stability associated with stacking of the longer DNA duplexes. Another experiment introduced kinks into the DNA helix *via* extra, unpaired bases in order to determine if disruption of the DNA  $\pi$ -stack would affect the repair of the thymine dimer. Indeed, the repair efficiency was reduced by half. This experiment shows again that long range electron transfer requires good stacking within the base pairs of nucleic acids.

## 1.4. SUMMARY

This chapter has served as an introduction to the chemistry and biochemistry of metal complexes as they relate to nucleic acids. Metallointercalators have been prepared with a diversity of functions, from luminescent probes for DNA, to structural probes of RNA, or photochemical reagents for thymine dimer repair. Complexes have been designed which target a diversity of sites on double-helical DNA, as well, whether through shape-selection, direct read-out, or a combination. Indeed, even mismatches in DNA can now be targeted by metallointercalator recognition with high specificity. The possible utility of such metallointercalators as probes and diagnostic agents is obvious.

However, much work needs to be done to develop the therapeutic potential of these complexes. Metallointercalators rank among the few synthetic complexes which target the DNA major groove with specificity and, indeed, we have already observed that such site-specific targeting can lead to the selective inhibition of DNA-binding proteins, as will be further discussed in a later chapter. Attempts to use metallointercalators as therapeutics, whether as direct inhibitors of DNA binding

molecules in a cell, or as reactants to induce charge transport in cells, face considerable challenges. Additional work described in this dissertation represents significant progress towards the application of metal complexes *in vivo*, and towards understanding precisely what requirements need to be met to permit long range charge transport.

---

## 1.5 REFERENCES

- 1) Lerman, L. S. *J. Mol. Biol.* **1961**, 3, 18.
- 2) Jennette, K. W.; Lippard, S. J.; Vassiliades, G. A.; Bauer, W. R. *Proc. Nat. Acad. Sci. USA.* **1974**, 71, 3839.
- 3) Barton, J. K.; Dannenberg, J. J.; Raphael, A. L. *J. Am. Chem. Soc.* **1982**, 104, 4967.
- 4) Barton, J. K.; Danishefsky, A. T.; Goldberg, J. M. *J. Am. Chem. Soc.* **1984**, 106, 2172.
- 5) Kumar, C. V.; Barton, J. K.; Turro, N. J. *J. Am. Chem. Soc.* **1985**, 107, 5518.
- 6) Barton, J. K.; Goldberg, J. M.; Kumar, C. V.; Turro, N. J. *J. Am. Chem. Soc.* **1986**, 108, 2081.
- 7) Barton, J. K.; Raphael, A. L. *Proc Nat. Acad. Sci. USA* **1985**, 82, 6460.
- 8) Rehmann, J. P.; Barton, J. K. *Biochemistry* **1990**, 29, 1701.
- 9) Rehmann, J. P.; Barton, J. K. *Biochemistry* **1990**, 29, 1710.
- 10) Barton, J. K. *Science* **1986**, 233, 727.
- 11) Yamagishi, A. *J. Chem. Soc. Chem. Comm.* **1983**, 572.
- 12) Satyanarayana, S.; Dabrowiak, J. C.; Chaires, J. B. *Biochemistry* **1992**, 31, 9319.
- 13) Satyanarayana, S.; Dabrowiak, J. C.; Chaires, J. B. *Biochemistry* **1993**, 32, 2573.
- 14) Eriksson, M.; Leijon, M.; Hiort, C.; Norden, B.; Graslund, A. *Biochemistry* **1994**, 33, 5031.

- 15) Pyle A. M.; Barton, J. K. In *Progress in Inorganic Chemistry: Bioinorganic Chemistry*, Lippard, S.J., Ed.; John Wiley & Sons, Inc.: New York, 1990; Vol. 38, pp 413—475.
- 16) Johann, T. W.; Barton, J. K. *Phil. Trans. Royal Soc. (London)* **1996**, 354, 299.
- 17) Chow, C. S.; Barton, J. K. *Meth. Enzym.* **1992**, 212, 219.
- 18) Murphy, C. J.; Barton, J. K. *Meth. Enzym.* **1993**, 226, 576.
- 19) Holmlin, R. E.; Stemp, E. D. A.; Barton, J. K. *Inorg. Chem.* **1998**, 37, 29.
- 20) Friedman, A. E.; Chambron, J.-C.; Sauvage, J.-P.; Turro, N. J.; Barton, J. K. *J. Am. Chem. Soc.* **1990**, 112, 4960.
- 21) Moucheron, C.; Kirschdemesmaeker, A; Kelly, J.M. *J. Photochem. Photobiol. B.* **1997**, 40, 91.
- 22) Carlson, D. L.; Huchital, D. H.; Mantilla, E. J.; Sheardy, R. D.; Murphy, W. R. *J. Am. Chem. Soc.* **1993**, 115, 6424.
- 23) Turro, C.; Bossmann, S. H.; Jenkins, Y.; Barton, J. K.; Turro, N. J. *J. Am. Chem. Soc.* **1995**, 117, 9026.
- 24) Olson, E. J. C.; Hu, D.; Hormann, A.; Jonkman, A. M.; Arkin, M. R.; Stemp, E. D. A.; Barton, J. K.; Barbara, P. F. *J. Am. Chem. Soc.* **1997**, 119, 11458.
- 25) Moucheron, C.; Kirsch-De MesMaeker, A.; Choua, S. *Inorg. Chem.* **1997**, 36, 584.
- 26) Jacquet, L.; Kirsch-De MesMaeker, A. *J. Chem. Soc. Faraday Trans.* **1992**, 88, 2471.
- 27) Arkin, M. R.; Stemp, E. D. A.; Holmlin, R. E.; Barton, J. K.; Hormann, A. E.; Olson, E. J. C.; Barbara, P. F. *Science* **1996**, 273, 475.
- 28) Tysoe, S. A.; Morgan, R. J.; Baker, D.; Strekas, T. C. *J. Phys. Chem.* **1993**, 97, 1707.
- 29) Hartshorn, R. M.; Barton, J. K. *J. Am. Chem. Soc.* **1992**, 114, 5919.
- 30) Holmlin, R. E.; Barton, J. K. *Inorg. Chem.* **1995**, 34, 7.
- 31) Holmlin, R. E.; Yao, J. A.; Barton, J. K. *Inorg. Chem.* **1999**, 38, 174.

- 32) Arounaguiri, S.; Maiya, B.G.; *Inorg. Chem.* **1996**, 35, 4267.
- 33) Stoeffler, H. D.; Thornton, N. B.; Temkin, S. L.; Schanze, K. S. *J. Am. Chem. Soc.* **1995**, 117, 7119.
- 34) Yam, V. W.-W.; Lo, K. K.-W.; Cheung, K.-K.; Kong, R. Y.-C.; *J. Chem. Soc. Dalton Trans.* **1997**, 3, 2067.
- 35) Jenkins, Y.; Friedman, A. E.; Turro, N. J.; Barton, J. K. *Biochemistry* **1992**, 31, 10809.
- 36) Tuite, E.; Lincoln, P.; Norden, B. *J. Am. Chem. Soc.* **1997**, 119, 239.
- 37) Hiort, C.; Lincoln, P.; Norden, B. *J. Am. Chem. Soc.* **1993**, 115, 3448.
- 38) Lincoln, P.; Broo, A.; Norden, B. *J. Am. Chem. Soc.* **1996**, 118, 2644.
- 39) Haq, I.; Lincoln, P.; Suh, D.C., Norden, B., Chowdhry, B.Z.; Chaires, J.B. *J. Am. Chem. Soc.* **1995**, 117, 4788.
- 40) Dupureur, C. M.; Barton, J. K. *J. Am. Chem. Soc.* **1994**, 116, 10286.
- 41) Hudson, B. P.; Barton, J. K. *J. Am. Chem. Soc.* **1998**, 120, 6877.
- 42) Keilkopf, C. L.; Erkkila, K. E.; Hudson, B. P.; Barton, J. K.; Rees, D. C. *Nat. Struct. Biol.* **1999**, 7, 117.
- 43) Dupureur, C. M.; Barton, J. K. *Inorg. Chem.* **1997**, 36, 33.
- 44) Greguric, I.; Aldrichwright, J.R.; Collins, J.G. *J. Am. Chem. Soc.* **1997**, 119, 3621.
- 45) Fry, J.V.; Collins, J.G. *Inorg. Chem.* **1997**, 36, 2919.
- 46) Collins J. G.; Sleeman A. D.; Aldrich-Wright J. R.; Greguric I.; Hambley T. W. *Inorg. Chem.* **1998**, 37, 3133.
- 47) Wang, A. H. J.; Nathans, J.; van der Marel, G.; van Boom, J. H.; Rich, A. *Nature* **1978**, 276, 471.
- 48) Fiel, R. J.; Howard, J. C.; Mark, E. H.; Datta Gupta, N. *Nuc. Acids Res.* **1979**, 6, 3093.

- 49) Pasternack, R.F.; Garrity, P.; Ehrlich, B.; Davis, C.B.; Gibbs, E.J.; Orloff, G.; Giartosio, A.; Turano, C. *Nuc. Acids. Res.* **1986**, *14*, 5919.
- 50) Pasternack, R.F.; Gibbs, E.J.; Villafranca, J. J.; *Biochemistry* **1983**, *22*, 2406.
- 51) Kelly, J. M.; Murphy, M. J.; McConnell, D. J.; OhUigin, C. *Nuc. Acids. Res.* **1985**, *13*, 167.
- 52) Lipscomb, L. A.; Zhou, F. X.; Presnell, S. R.; Woo, R. J.; Peek, M. E.; Plaskon, R. R.; Williams, L.D. *Biochemistry* **1996**, *35*, 2818.
- 53) Pyle, A. M.; Long, E. C.; Barton, J. K. *J. Am. Chem. Soc.* **1989**, *111*, 4520.
- 54) Pyle, A. M.; Rehmann, J. P.; Meshoyrer, R.; Kumar, C. V.; Turro, N. J.; Barton, J. K. *J. Am. Chem. Soc.* **1989**, *111*, 3051.
- 55) Pyle, A. M.; Morii, T.; Barton, J. K. *J. Am. Chem. Soc.* **1990**, *112*, 9432.
- 56) Sitlani, A.; Long, E. C.; Pyle, A. M.; Barton, J. K. *J. Am. Chem. Soc.* **1992**, *114*, 2303.
- 57) Campisi, D.; Morii, T.; Barton, J. K. *Biochemistry* **1994**, *33*, 4130.
- 58) Erkkila, K. E.; Barton, J. K. manuscript in preparation.
- 59) Sitlani, A.; Barton, J. K. *Biochemistry* **1994**, *33*, 12100.
- 60) Chow, C. S.; Barton, J. K. *J. Am. Chem. Soc.* **1990**, *112*, 2839.
- 61) Jenkins, Y.; Friedman, A. E.; Turro, N. J.; Barton, J. K. *Biochemistry*, **1992**, *31*, 10809.
- 62) Chow, C. S.; Barton, J. K. *Biochemistry* **1992**, *31*, 5423.
- 63) Chow, C. S.; Behlen, L. S.; Uhlenbeck, O. C.; Barton, J. K. *Biochemistry* **1992**, *31*, 972.
- 64) Lim, A. C.; Barton, J. K. *Biochemistry* **1993**, *32*, 11029.
- 65) Chow, C. S.; Hartmann, K. M.; Rawlins, S. L.; Huber, P. W.; Barton, J. K. *Biochemistry* **1992**, *31*, 3534.
- 66) Lim, A. C.; Barton, J. K. *Biochemistry* **1998**, *37*, 9138.
- 67) Lim, A. C.; Barton, J. K. *Bioorg. Med. Chem.* **1997**, *5*, 1131.

- 68) Sitlani, A.; Dupureur, C. M.; Barton, J. K. *J. Am. Chem. Soc.* **1993**, *115*, 12589.
- 69) Jackson, B. A.; Barton, J. K. *J. Am. Chem. Soc.* **1997**, *119*, 12986.
- 70) Jackson, B. A.; Alekseyev, V. Y.; Barton, J. K. *Biochemistry* **1999**, *38*, 4655.
- 71) Krotz, A. H.; Kuo, L. Y.; Shields, T. P.; Barton, J. K. *J. Am. Chem. Soc.* **1993**, *115*, 3877.
- 72) Krotz, A. H.; Kuo, L. Y.; Barton, J. K. *Inorg. Chem.* **1993**, *32*, 5963.
- 73) Shields, T. P.; Barton, J. K. *Biochemistry* **1995**, *34*, 15037.
- 74) Shields, T. P.; Barton, J. K. *Biochemistry* **1995**, *34*, 15049.
- 75) Krotz, A. H.; Hudson, B. P.; Barton, J. K. *J. Am. Chem. Soc.* **1993**, *115*, 12577.
- 76) Hudson, B. P.; Dupureur, C. M.; Barton, J. K. *J. Am. Chem. Soc.* **1995**, *117*, 9379.
- 77) Sardesai, N. Y.; Barton, J. K. *J. Biol. Inorg. Chem.* **1997**, *2*, 762.
- 78) Sardesai, N. Y.; Zimmermann, K.; Barton, J. K. *J. Am. Chem. Soc.* **1994**, *116*, 7502.
- 79) Terbrueggen, R. H.; Barton, J. K. *Biochemistry* **1995**, *34*, 8227.
- 80) Terbrueggen, R. H.; Johann, T. W.; Barton, J. K. *Inorg. Chem.* **1998**, *37*, 6874.
- 81) Franklin, S. J.; Barton, J. K. *Biochemistry* **1998**, *37*, 16093.
- 82) Odom, D. T.; Parker, C. S.; Barton, J. K. *Biochemistry* **1999**, *38*, 5155.
- 83) Dervan, P. B.; *Science* **1986**, *232*, 464.
- 84) Pogożelski, W. K.; Tullius, T. D.; *Chem. Rev.* **1998**, *98*, 1089.
- 85) Hegg, E. L.; Burstyn, J.N.; *Coord. Chem. Rev.* **1998**, *173*, 133.
- 86) Fitzsimons, M. P.; Barton, J. K. *J. Am. Chem. Soc.* **1997**, *119*, 3379.
- 87) Le Doan, T.; Perrouault, L.; Rougee, M.; Bensasson, R.; Helene, C. *In Photodynamic Therapy of Tumors and Other Diseases*, Jori, G., Perria, C., Eds.; Libreria Progetto: Padova, Italy, 1985; pp. 56—58.
- 88) Holmlin, R. E.; Dandliker, P. J.; Barton, J. K. *Angew. Chem.* **1997** Germ. Ed. *109*, 2830; Int'l Eng. Ed. *36*, 2714.
- 89) Pratviel, G.; Bernadou, J.; Meunier, B. *Metal Ions in Biol. Sys.* **1996**, *33*, 399.



- 90) Vialas, C.; Pratviel, G.; Claparols, C.; Meunier, B. *J. Am. Chem. Soc.* **1998**, *120*, 11548.
- 91) Johnston, D. H.; Cheng, C.-C.; Campbell, K. J.; Thorp, H. H. *Inorg. Chem.* **1994**, *33*, 6388.
- 92) Napier, M. E.; Loomis, L. R.; Sistare, M. F.; Kim, J.; Eckhardt, A. E.; Thorp, H. H. *Bioconjug. Chem.* **1997**, *8*, 906.
- 93) Carter, P. J.; Cheng, C.-C.; Goll, J. G.; Campbell, K. J.; Thorp, H. H. *J. Am. Chem. Soc.* **1998**, *120*, 632.
- 94) Foote, C. S.; Shook, F. C.; Abakerli, R. B. *Meth. Enzym.* **1984**, *105*, 36.
- 95) Armitage, B. *Chem. Rev.* **1998**, *98*, 1171.
- 96) Mei, H. Y.; Barton, J. K. *Proc. Nat. Acad. Soc. USA* **1988**, *85*, 1339.
- 97) Arkin, M. R.; Stemp, E. D. A.; Coates-Pulver, S.; Barton, J. K. *Chem. Biol.* **1997**, *4*, 389.
- 98) Saito, I.; Takayama, M.; Sugiyama, H.; Nakatani, K.; Tsuchida, A.; Yamamoto, M. *J. Am. Chem. Soc.* **1995**, *117*, 6406.
- 99) Prat, F.; Houk, K. N.; Foote, C. S. *J. Am. Chem. Soc.* **1998**, *120*, 845.
- 100) Burrows, C. J.; Muller, J. G. *Chem. Rev.* **1998**, *98*, 1109.
- 101) Stemp, E. D. A.; Arkin, M. R.; Barton, J. K. *J. Am. Chem. Soc.* **1997**, *119*, 3379.
- 102) Hall, D. B.; Holmlin, R. E.; Barton, J. K. *Nature* **1996**, *382*, 731.
- 103) Turro, C.; Evanhuysen, A.; Bossmann, S. H.; Barton, J. K.; Turro, N. J. *Inorg. Chim. Acta* **1996**, *243*, 101.
- 104) Hall, D. B.; Barton, J. K. *J. Am. Chem. Soc.* **1997**, *119*, 5045.
- 105) Rajski, S. R.; Kumar, S.; Roberts, R. J.; Barton, J. K. *J. Am. Chem. Soc.* **1999**, *121*, 5615.
- 106) Nunez, M. E.; Hall, D. B.; Barton, J. K. *Chem. Biol.* **1999**, *6*, 85.
- 107) Dandliker, P. J.; Holmlin, R. E.; Barton, J. K. *Science* **1997**, *275*, 1465.

- 108) Dandliker, P. J.; Nunez, M. E.; Barton, J. K. *Biochemistry* **1998**, 37, 6491.

## **CHAPTER 2**

### **Site Specific Inhibition of Transcription Factor Binding to DNA by a Metallointercalator\***

\*Adapted from D.T. Odom, C.S. Parker, J.K. Barton. *Biochemistry* **38** (1999) 5155-5163.

## 2.1 INTRODUCTION

Proteins that interact with DNA are the subjects of great interest in developing potential targets for therapeutic treatment. Since transcription factors modulate the expression of genes by binding to and interacting with specific DNA sequences, one frequent target for drug design and biochemical modification has been the DNA binding sites of transcription factors. One method for altering transcription regulation both *in vivo* and *in vitro* is to modify the DNA bases of the protein binding site. Enzymatic base methylation,<sup>1</sup> the formation of cisplatin lesions,<sup>2-4</sup> and chemical alkylation<sup>5,6</sup> have been used successfully to affect the binding of proteins to DNA. However, these covalent modifications frequently show little sequence specificity beyond that of individual base preferences. The lack of extended sequence selectivity effectively prevents targeting specific genes and functions *in vivo*.

Alternatively, agents which bind DNA non-covalently may be used to interfere competitively with DNA binding proteins. One method for targeting specific genetic loci has been to use complementary protein nucleic acids (PNAs); however, these molecules may lack the cell permeability that is needed to make them effective therapeutic agents.<sup>7</sup> The oligosaccharide derivative calicheamicin as well as some derivatives have been shown to bind sequence-selectively to the minor groove of DNA and to inhibit transcription factor binding;<sup>8-10</sup> calicheamicin *in vivo* cleaves the sugar phosphate backbone of DNA.

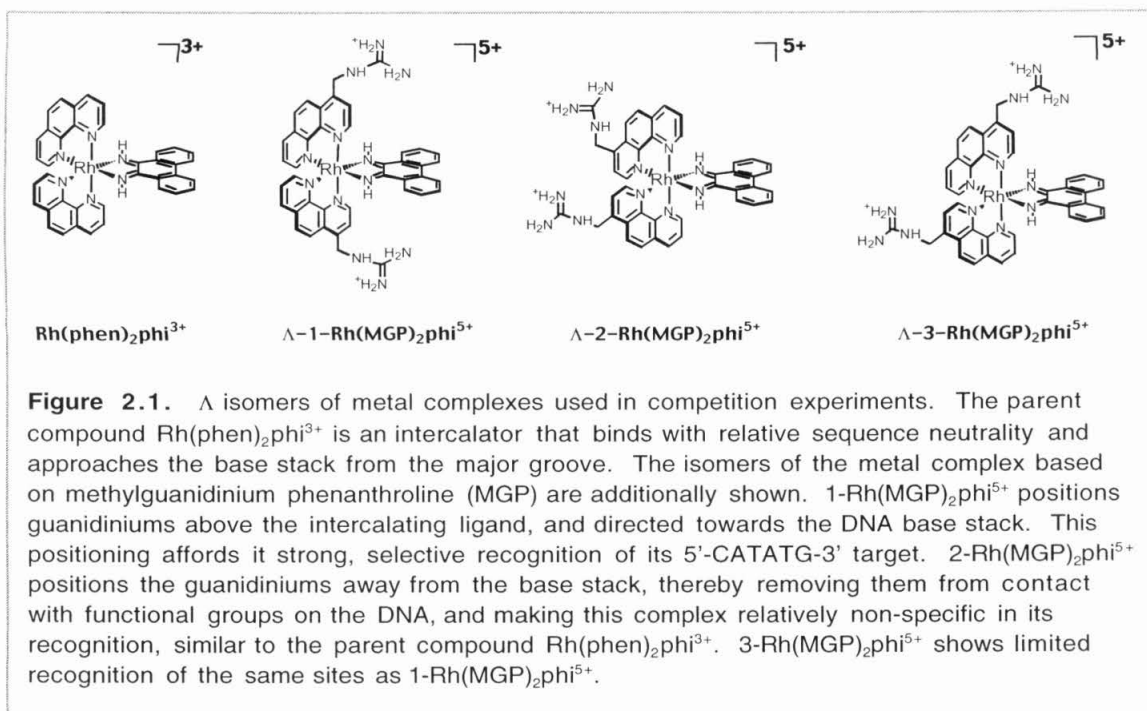
Currently, few strategies exist that utilize the major groove directly as a surface for recognition by small molecules to inhibit the initiation of transcription. Because the major groove is preferentially recognized by transcription factors,<sup>7</sup> small molecules that recognize specified regions within the major groove might be especially effective in blocking DNA binding. The steric accessibility of the wide and deep major groove, the greater range of functionality within the major groove versus the minor groove, and the

possibility of cooperative, multiple protein-DNA contacts in the major groove make it an attractive target for therapeutic design.

Our research has focused on the development of metallointercalators that bind to DNA in the major groove.<sup>11,12</sup> 9,10-Phenanthrenequinone diimine (phi) complexes of rhodium, such as  $\text{Rh}(\text{phen})_2\text{phi}^{3+}$  and  $\Delta\text{-}\alpha\text{-}[\text{Rh}[(\text{R,R})\text{-Me}_2\text{trien}]\text{phi}]^{3+}$  ( $\text{Me}_2\text{trien}$ =2,9-diamino-4,7-diazadecane) are octahedral complexes which are coordinatively saturated and inert to ligand substitution. The phi ligand, an extended aromatic, heterocyclic surface, preferentially intercalates between the DNA base pairs, and, in so doing, the intercalated phi orients the rigid complex with respect to the helix. All phi complexes of rhodium examined thus far appear to intercalate into the major groove side of the DNA duplex.<sup>11-15</sup> The ancillary ligands of these phi complexes can be tuned to provide sequence specificity through the geometrical positioning of functional groups on the ligands relative to the DNA bases to create an ensemble of sequence-determining interactions in the major groove. Upon irradiation with ultraviolet light of the phi complexes of rhodium bound to DNA, direct DNA strand scission occurs in a reaction consistent with radical abstraction of a sugar hydrogen; this photochemistry is useful in marking sites of specific binding by the complex on DNA.<sup>16</sup>

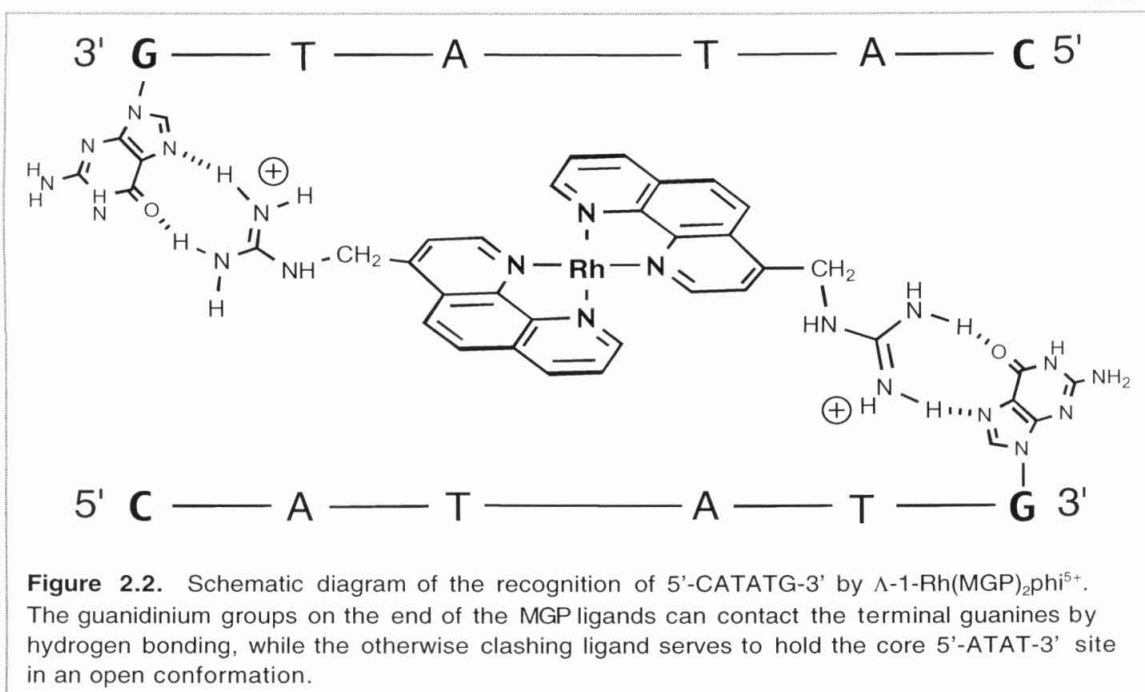
Here our focus is on phi complexes of rhodium that have functionalized phenanthrolines as ancillary ligands (Figure 2.1). These complexes exploit a combination of direct readout and shape selectivity to recognize sites in DNA.<sup>11,17</sup>  $\text{Rh}(\text{phen})_2\text{phi}^{3+}$ , the parent complex of this series, recognizes sites based upon shape-selection, notably 5'-pyrimidine-purine-3' steps.<sup>16,18</sup> The sites recognized are those which are somewhat more open in the major groove relative to B-form DNA. These openings better accommodate the large ligand array displayed by  $\text{Rh}(\text{phen})_2\text{phi}^{3+}$ . Nonetheless, this shape matching provides only a small amount of sequence-selectivity.

The pendant guanidiniums on the ancillary phenanthroline rings of  $\text{Rh}(\text{MGP})_2\text{phi}^{5+}$  (MGP = 4-guanidylmethyl-1,10-phenanthroline) lead instead to a high



level of DNA site specificity (Figure 2.1). The guanidinium groups of arginine side chains are exploited frequently by proteins in targeting guanine residues of DNA.<sup>19</sup> Because the MGP ligand is asymmetrically functionalized, multiple regioisomers of the complex exist. There are 3 geometric isomers, each of which has two stereoisomers, and each of these different isomers exhibits quite different recognition of DNA, demonstrating that the metal complex binding is dependent upon the alignment of functional groups. Notably, the symmetric isomer 2, with guanidiniums pointing away from the phi ligand, shows sequence selectivity resembling that of  $\text{Rh}(\text{phen})_2\text{phi}^{3+}$ .

Of particular interest, the symmetric isomer  $\Lambda\text{-1-Rh}(\text{MGP})_2\text{phi}^{5+}$ , with guanidinium arms that extend axially from the intercalating phi plane forward over the phi ligand, displays strong and site-selective binding to DNA.  $\Lambda\text{-1-Rh}(\text{MGP})_2\text{phi}^{5+}$  binds preferentially to the site 5'-CATATG-3' with nanomolar affinity (Figure 2.2). Although there is some tolerance for differences at the outermost positions in the 6 base pair site,<sup>11</sup> any variation of the central 5'-ATAT-3' disfavors metal complex intercalation. Molecular modelling shows that, in the absence of DNA distortion, the stereochemistry of



the guanidinium groups on the complex does not permit the bases at the extremities to be contacted by the guanidiniums, yet binding experiments in which guanines were replaced with deazaguanine have shown that terminal guanine-guanidinium contacts occur. DNA cyclization assays established that the intercalation of the metal complex is associated with a 70° unwinding at the DNA site, and this unwinding explains how the positioning of guanine-guanidinium contacts can occur. NMR evidence further suggests that the metal complex traps the DNA site in an unwound form, hence the strict requirement for a central TA-rich stretch.<sup>20</sup>

The six base pair recognition of a DNA site by this small synthetic complex, as well as the unwinding and exchange kinetics associated with binding, may resemble the interactions of many proteins that bind to DNA site-specifically. Significant bend angles are often found in DNA remodeling proteins, like for instance, TATA box binding protein (TBP).<sup>21,22</sup> Not only is  $\Lambda$ -1-Rh(MGP)<sub>2</sub>phi<sup>5+</sup> similar to TBP in that it uses guanidinium functionalities to generate a network of hydrogen bonds within the major groove, but with both TBP and the synthetic metal complex, significant unwinding (70° vs. 108° for TBP)

and kinking of the bound site occurs. Indeed, the preferential recognition of sites by TBP that contain TA-rich stretches may share mechanistic features with the targeting of  $\Lambda$ -1-Rh(MGP)<sub>2</sub>phi<sup>5+</sup> to its preferred binding site.<sup>11</sup>

One of the prominent classes of proteins that site specifically interact with DNA is the bZIP transcription factors.<sup>23</sup> Several of these proteins bound to their target DNA sites have been structurally characterized, among them the transcription factor GCN4, and in these structures a common structural motif is apparent. Most prominent is the dimerization domain which includes a coiled coil  $\alpha$ -helical region stabilized by the packing of leucine side chains; the dimerization domain is capped by a highly basic, DNA binding region. Separate regions either upstream or downstream of the bZIP DNA binding motif regulate transcriptional activation and signaling. Another member of this class of transcription factors is the yeast analog of mammalian AP-1, yAP-1, which is 70 kD in size.<sup>24</sup> yAP-1 shows sequence homology to other bZIP transcription factors, and the isolated DNA binding region from yAP-1 shows the induction of an  $\alpha$ -helix upon binding to its DNA recognition site, consistent with the leucine zipper motif.<sup>25</sup> Functionally, yAP-1 regulates pleiotropic drug resistance, and has been shown to be non-essential for cell viability under normal circumstances.<sup>26</sup>

yAP-1 has a strong affinity for the site 5'-AATTAGTCAGCA-3', known as the activator recognition element (ARE). Aspects of how yAP-1 recognizes its target site have been determined by chemical probing with dimethyl sulfate (DMS), DNase I, and methidiumpropylEDTA iron digestion (MPE) (Figure 2.3, top sequence).<sup>27</sup> Footprinting with MPE suggests that the yAP-1 binding domain spans the consensus site, but DMS digestion of DNA in the presence of yAP-1 reveals that there are a number of base pairs within the core of the consensus region that do not appear to be in intimate contact with the protein. This apparent lack of contact at particular locations within the site suggested that the target site could be mutated to contain an overlapping site for  $\Lambda$ -1-Rh(MGP)<sub>2</sub>phi<sup>5+</sup> without affecting the ARE specific binding of the protein. Such a DNA



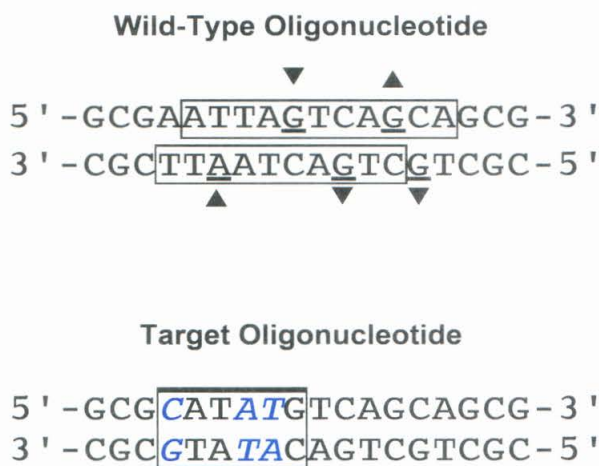


**Figure 2.3.** Modifications made to the ARE to incorporate a metal complex binding site (adapted from Ref. 14). The top oligonucleotide sequence (labelled wild-type) is the wild-type ARE, capped with GCG triplets. The boxed regions show protection against MPE footprinting in the presence of yAP-1. The solid triangles indicate increases or decreases in sensitivity in DMS labile sites when footprinted in the presence of yAP-1. The target strand, below, has incorporated a 5'-CATATG-3' site with no disruption of the footprinted nucleotides. The bases modified are shown in blue italics.

site would allow competitive assays to be carried out between yAP-1 and  $\Lambda$ -1-

$\text{Rh}(\text{MGP})_2\text{phi}^{5+}$ .

The notion of establishing functional similarities between  $\Lambda$ -1- $\text{Rh}(\text{MGP})_2\text{phi}^{5+}$  and DNA binding proteins such as yAP-1 in targeting a specific site is interesting to consider in light of the much smaller size and relative simplicity of the transition metal complex. If this metal complex could be used to inhibit the binding of a protein to DNA by recognition of a common site, this reactivity would strengthen the possible application of metallointercalators as competitive agents to alter transcription. The findings reported herein demonstrate that indeed  $\Lambda$ -1- $\text{Rh}(\text{MGP})_2\text{phi}^{5+}$  can be used to inhibit site-specifically the binding of a transcription factor to a promoter site *in vitro*. We show that this interaction is dependent both on the identity of the metal complex and on the presence of a metal complex binding site.

## 2.2 EXPERIMENTAL

*General Materials and Methods.* All chemicals and biochemicals were from commercial sources. Beckman JA2-21 and JA-4 centrifuges were used for general purposes. A Branson Sonifier 450 was used to lyse cell preparations. All enzymes were purchased from commercial sources unless otherwise noted. All proteins were stored at -20°C in protein buffer that consisted of 10% glycerol, 25 mM HEPES pH 7.4, 1 mM EDTA, 50 mM KCl, 0.1% Nonidet-40.

*Synthesis and Purification of DNA and Metal Complexes.* All DNA was synthesized with a terminal trityl group on an ABI 392 DNA/RNA synthesizer with reagents from Glen Research. HPLC purification and subsequent de-tritylation used standard techniques. All labeled oligonucleotides were 5'-endlabelled using standard protocols with polynucleotide kinase (New England Biolabs) and  $\gamma$ -<sup>32</sup>P-ATP. The labeled DNA was purified by denaturing gel electrophoresis on a 20% acrylamide gel, followed by crush and soak elution in 10 mM Tris HCl, pH 7.4, 1mM EDTA. The purified labeled material was then annealed to a ten-fold excess of complement, and native gel electrophoresis performed on a 10% polyacrylamide gel containing 90 mM Tris borate, pH 8.3, 1 mM EDTA. The synthesis and purification of the metal complexes followed previously reported procedures.<sup>17,28</sup>

*Preparation of Recombinant yAP-1 Expression Vector.* The plasmid pUC19 containing the complete open reading frame of the *YAP1* gene in 2.5 kB of yeast cDNA was digested with EcoRI, and the *YAP1* gene was isolated by agarose gel electrophoresis. pBluescript IISK(-) was digested with EcoRI and calf alkaline phosphatase, and gel purified. The previously isolated *YAP1* gene was ligated into this pBS vector, and successful ligations were selected by ampicillin resistance in DH5 $\alpha$  *E. Coli* cells. Plasmids from this step were harvested and inserted into CJ236 (*dut*-, *ung*-) cells. K07 helper phage and kanamycin selection was used with this construction to generate a ssDNA template for site-directed mutagenesis.<sup>29</sup> A 3' Sall restriction site and

a 5' NsiI restriction site were introduced into the YAP1 gene. The gene was excised, isolated, and ligated into a thioredoxin fusion expression vector pThioHisA (Invitrogen). The 5' and 3' termini of pThioHis(yAP-1) were sequenced, verifying proper framing and mutagenesis.

*Expression and Purification of Recombinant yAP-1 Protein.* The vector pThioHis(yAP-1) was transfected into DE3 cells (BL21) and four to five colonies were selected from an LB-ampicillin plate incubated overnight at 37°C. These colonies were used to directly infect 1 L of LB media with 40 µg/mL ampicillin with shaking at 200 rpm at 37°C. At OD<sub>595</sub> = 0.6, 10 mL of 100 mM isopropylthiogalactoside was added to a final concentration of 1 mM, and the cells were transferred to a 30°C shaker. After 3 hours of induction, the cells were harvested by 15 minute centrifugation at 1000g, and frozen overnight at -80°C. The cell pellet was rinsed with and then resuspended into 20 mL of protein buffer with 1 mM α-toluenesulfonyl fluoride. To this, 40 mg lysozyme was added, and the solution was incubated at 23°C for 20 minutes. This solution was then sonicated at 50% duty cycle for 2 minutes on ice, followed by immediate 12000 g, 10 minute centrifugation of cellular debris. The pellet was discarded, and the lysate was treated with 10% polyethyleneimine to a final concentration of 0.5%. After 20 minutes of room temperature incubation, the precipitated nucleic acids were spun down at 35000 g for 25 minutes at 0°C. Ammonium sulfate was then added to a concentration of 1.0 M and the solution was placed on ice for 30 minutes. The protein pellet was obtained by centrifugation at 35000 g for 20 minutes, and was redissolved into 10 mL of protein buffer at 0°C. All remaining steps were performed at 4°C. After filtration through a 0.22 µm filter, this material was loaded onto a 5 mL Heparin column (Pharmacia), thoroughly pre-rinsed with 100 mL of protein buffer. yAP-1 eluted at 700 mM NaCl on a continuous, linear 200 mL 0.01 M to 2.00 M NaCl gradient with protein buffer as the FPLC carry buffer. The resultant material was >90% pure as visualized by gel electrophoresis and Coomassie Blue staining. This band was positive to Western antibody probes to both

yAP-1 and thioredoxin, and highly active in DNA/protein gel retardation assays.

*Photocleavage Reactions.* Photocleavage reactions were performed using 5'-end-labeled oligonucleotides purified as described earlier. Cold carrier duplex was made using HPLC-purified oligonucleotides. The photocleavage reactions contained 50 mM NaCl, 10 mM sodium cacodylate pH 7.0, with a 10:1 ratio of DNA to rhodium complex. A five minute pre-incubation in the dark was followed by 8 minute irradiations at 313 nm. Samples lacking metal complexes were irradiated 15 minutes. Immediately after irradiation, each sample was frozen at -80°C, and lyophilized. They were resuspended in formamide loading buffer, and directly run on a denaturing polyacrylamide sequencing gel (8 M urea, 20% polyacrylamide).

*Competition Experiments to Measure Protein Binding.* Metal complexes were freshly dissolved into doubly distilled, de-ionized water, and the concentrations of the stock solutions were determined by measuring absorbance ( $\epsilon_{360} = 1.94 \times 10^4 \text{ M}^{-1}\text{cm}^{-1}$ ). Protein concentrations were established by dilution from a stock dialyzed against protein buffer that had been quantitated by 280 nm absorbance to have 6.25  $\mu\text{M}$  protein. Each reaction had final concentrations as follows: 40 nM yAP-1, 2% Ficoll, 50 mM KCl, 25 nCuries of labeled oligonucleotide (~2 nM final concentration of duplex DNA), 1  $\mu\text{M}$  bovine serum albumin as non-specific carrier, and 15 mM Tris pH 7.4. The amount of protein buffer included in the reaction varied among the experiments but never exceeded 2% of the final volume (v/v). The incubations were equilibrated for three to six hours, and were then loaded directly onto a running 5.5% native acrylamide gel buffered with 45 mM tris-borate buffer with 1 mM EDTA at pH 8.3. Order of incubation was varied and found to be unimportant. The electrophoresis was performed for 1 hour at 100 V, after which the gels were vacuum dried onto Whatman paper and exposed overnight to a Phosphorimager plate. Results were quantitated in ImageQuant, and data fitting was performed on Kaleidograph software, using the equation

$\theta = 1 - (K_a)(Rh_T) / [1 + (K_a)(Rh_T)]$ , where  $K_a$  is the association constant,  $Rh_T$  is the

rhodium concentration, and  $\Theta$  is the fraction DNA bound (derived from equations in reference 30).

## 2.3 RESULTS

### 2.3.1. Purification of Recombinant

#### *Transcription Factor yAP-1.* Previous

investigations using recombinant yAP-1 relied on the activity of crude bacterial cell lysates of bacterial cells carrying the gene on a

constitutively producing locus.<sup>27</sup> Introduction of

the *YAP1* gene to the pThioHis vector generated

a thioredoxin/yAP-1 fusion protein. This fusion protein was additionally placed under the *lacZ*

promoter, which allows controlled induction of

protein production in engineered bacterial cells. The thioredoxin domain increased the

temperature stability of yAP-1 so that the fusion protein was stable in protein buffer at

60°C for up to three hours with no discernable effect on DNA binding. Purifications from

cell lysate by polyethylimine precipitation of cellular nucleic acids and a 25% ammonium

sulfate cut yielded crude yAP-1 separation from the bulk of the cellular proteins. The last

step of a Heparin agarose affinity column resulted in >90% purity (Figure 2.4). As

expected, gel shift assays showed that the addition of the thioredoxin fusion domain did

not interfere with yAP-1 binding to oligonucleotides. Because of this full biological

activity, combined with previous research demonstrating the relatively innocuous nature

of the thioredoxin domain,<sup>31</sup> the fusion protein was directly used in assays. Additionally,

this fusion generated a second epitope for antibody detection, so that the purification

steps could be monitored with commercially available antibodies.

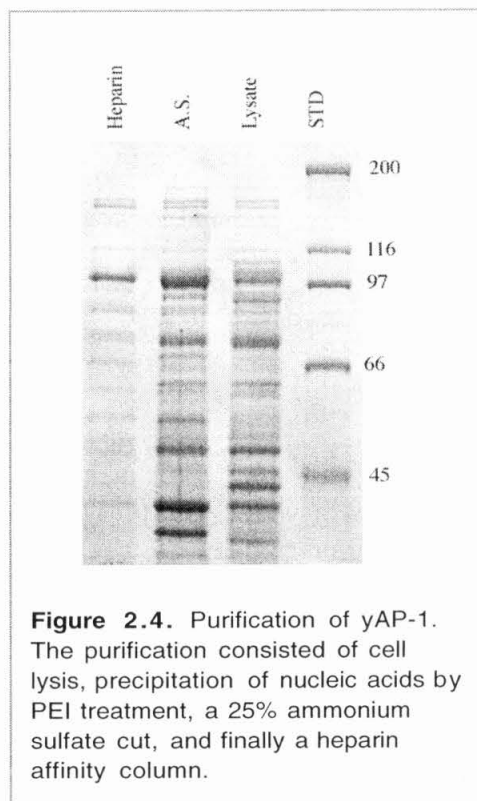


**Figure 2.4.** Purification of yAP-1. The purification consisted of cell lysis, precipitation of nucleic acids by PEI treatment, a 25% ammonium sulfate cut, and finally a heparin affinity column.

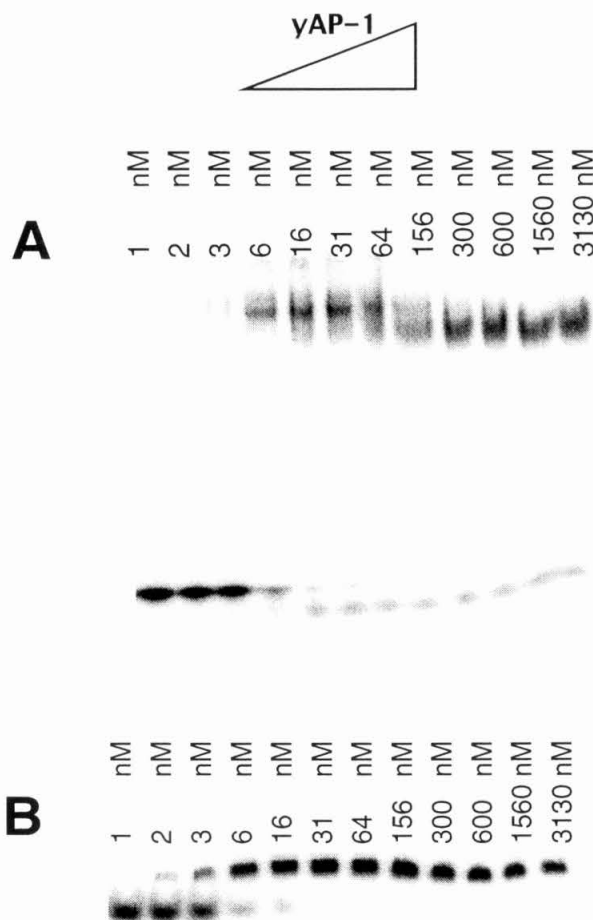


**Figure 2.5.** Gel shift of yAP-1 with target and wild-type ARE. Each 20  $\mu$ L, 10 minute incubation reaction contained, in addition to the concentration of yAP-1 indicated above each lane, 2% Ficoll, 15 mM Tris pH 7.4, 50 mM KCl, 25 nCuries 5'-<sup>32</sup>P labeled wild-type (A) or target (B) oligonucleotide duplex (2-3 nM DNA duplex), and 1  $\mu$ M BSA.

**2.3.2. Design of Target Oligonucleotide.** The contacts yAP-1 makes to the native AP-1 recognition element (ARE) have been well-characterized biochemically, and are shown along with the target oligonucleotide in Figure 2.3.<sup>27</sup> To permit binding of  $\Lambda$ -1- $\text{Rh}(\text{MGP})_2\text{phi}^{5+}$  in a site also recognized by yAP-1, a minimum number of nucleotides not directly contacted by the protein were modified to introduce the recognition site preferred by the metal complex, 5'-CATATG-3'. The three base pair alterations needed to introduce 5'-CATATG-3' into the wild type ARE removed only one AT base pair from the AT rich tract that dominates half the ARE, and inverted two others. yAP-1 interacts with

both the modified sequence of the target oligonucleotide and the native sequence with a dissociation constant that is less than 5 nM (Figure 2.5).

*2.3.3. Recognition of Target Oligonucleotide by  $\Lambda$ -1-Rh(MGP)<sub>2</sub>phi<sup>5+</sup> as Visualized by Photocleavage.* Having established strong interaction between the transcription factor and the target oligonucleotide sequence, DNA photocleavage studies were used to probe the interaction of the metal complexes and oligonucleotides used in this study. As in previous studies, the metal complexes were pre-equilibrated for five minutes with the photocleaved oligonucleotide before irradiation to ensure equilibration.<sup>17</sup> NMR studies suggest, though, that the equilibration is much more rapid than this.<sup>20</sup> Upon irradiation,  $\Lambda$ -1-Rh(MGP)<sub>2</sub>phi<sup>5+</sup> exhibited strong recognition of the site introduced into the transcription promoter region (Figure 2.6) as seen through photocleavage. Alternatively, very little cleavage was observed for wild type ARE below micromolar concentrations (Figure 2.7). As described previously, the cleavage seen is a strong doublet at the central AT step of the CATATG binding site.<sup>11</sup> The binding at this sequence has previously been shown to occur in only one binding mode,<sup>20</sup> and irradiation at 313 nm in all phi complexes of rhodium strongly favors direct damage of DNA at the site of intercalation.<sup>16</sup> We estimate a dissociation constant of 25 nM  $\pm$  10 nM by the cleavage at this doublet as a function of concentration, consistent with previous values,<sup>17</sup> based on curve fitting done with a modification of equation 1. Photocleavage quantum yields for these metal complexes are rather low,<sup>16</sup> and quantitation of the photocleavage bands showed that the photocleavage efficiency had peaked well under 1  $\mu$ M. The splitting of the 5' T into a double band is occasionally seen with photocleavage on small oligonucleotides with  $\Lambda$ -1-Rh(MGP)<sub>2</sub>phi<sup>5+</sup>.<sup>32</sup> No strong sites of photocleavage activity in either oligonucleotide were observed for the metal complexes *rac*-Rh(phen)<sub>2</sub>phi<sup>3+</sup> (data not shown) or  $\Lambda$ -2-Rh(MGP)<sub>2</sub>phi<sup>5+</sup> (Figure 2.8 and 2.9) at concentrations lower than 10<sup>-5</sup> M.

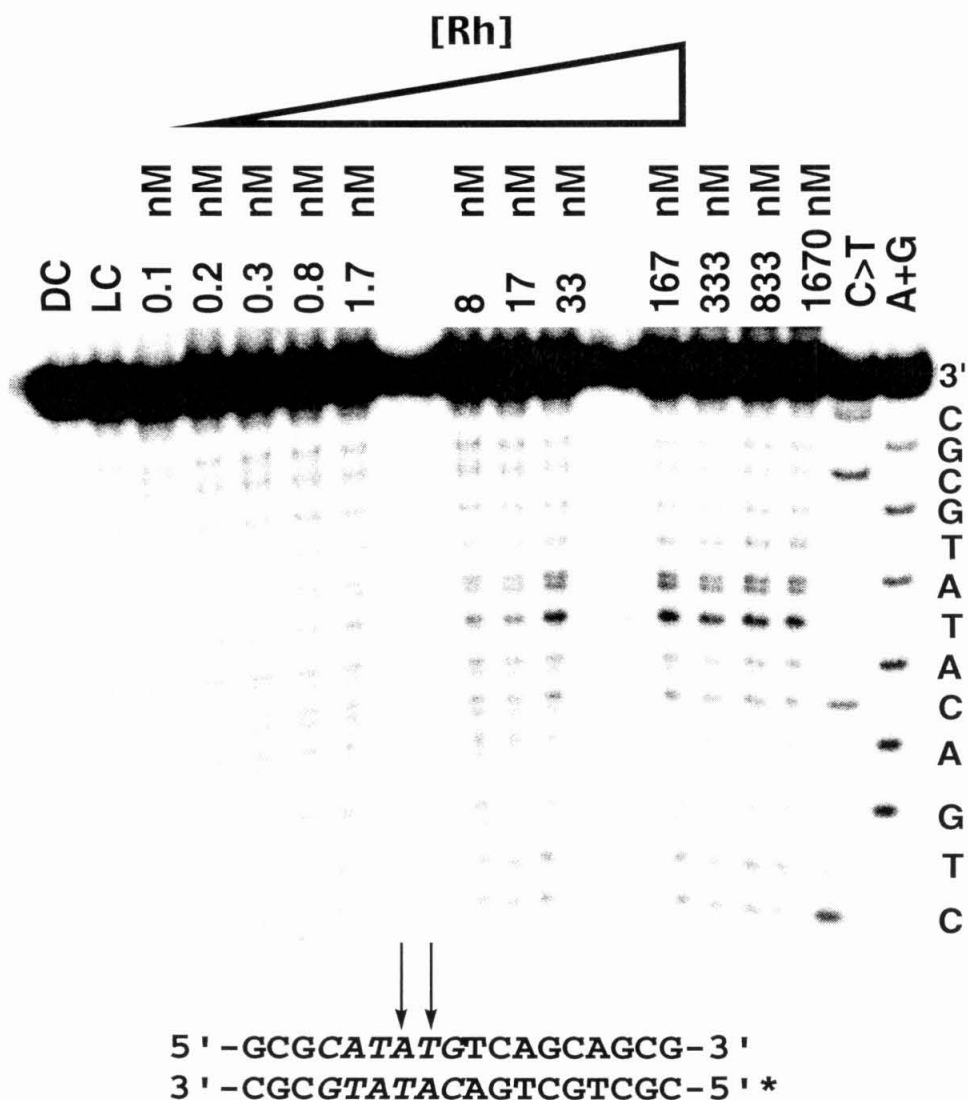


**Figure 2.6.** Photocleavage of 5'-<sup>32</sup>P labeled target by  $\Lambda$ -1-Rh(MGP)<sub>2</sub>phi<sup>5+</sup>. The top of the gel shows the concentration of Rh used in each lane. Final duplex DNA concentrations were exactly one order of magnitude higher than the Rh concentrations for each irradiation reaction. Each sample was irradiated for 8 minutes at 313 nm. Maxam-Gilbert A+G and C>T sequencing lanes are shown to the far right. The buffer concentrations were 10 mM sodium cacodylate and 50 mM NaCl. Introduced target sites are shown in the sequence below the gel in *italics* and cleavage sites are indicated by arrows.



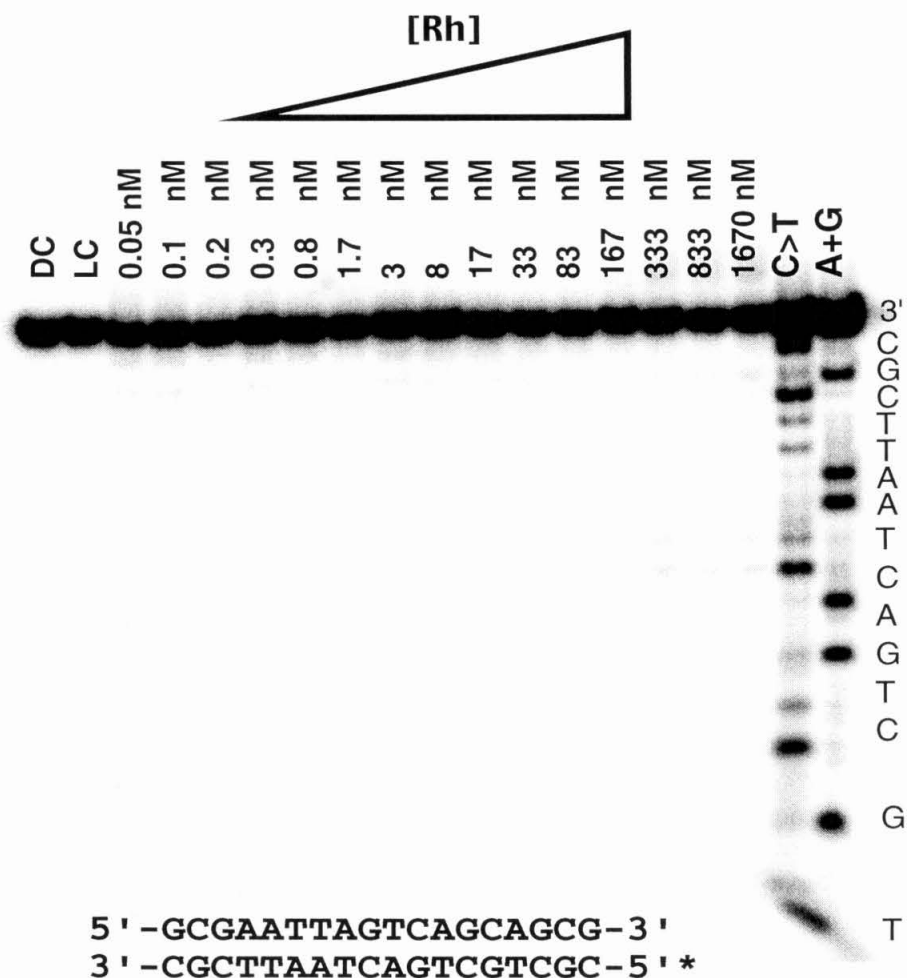


**Figure 2.7.** Photocleavage of 5'-<sup>32</sup>P labeled, wild-type strand by  $\Lambda$ -1-Rh(MGP)<sub>2</sub>phi<sup>5+</sup>. The top of the gel shows the concentration of Rh used in each lane. Final duplex DNA concentrations were exactly one order of magnitude higher than the Rh concentrations for each irradiation reaction. Each sample was irradiated for 8 minutes at 313 nm. Maxam-Gilbert A+G and C>T sequencing lanes are shown to the far right. The buffer concentrations were 10 mM sodium cacodylate and 50 mM NaCl.

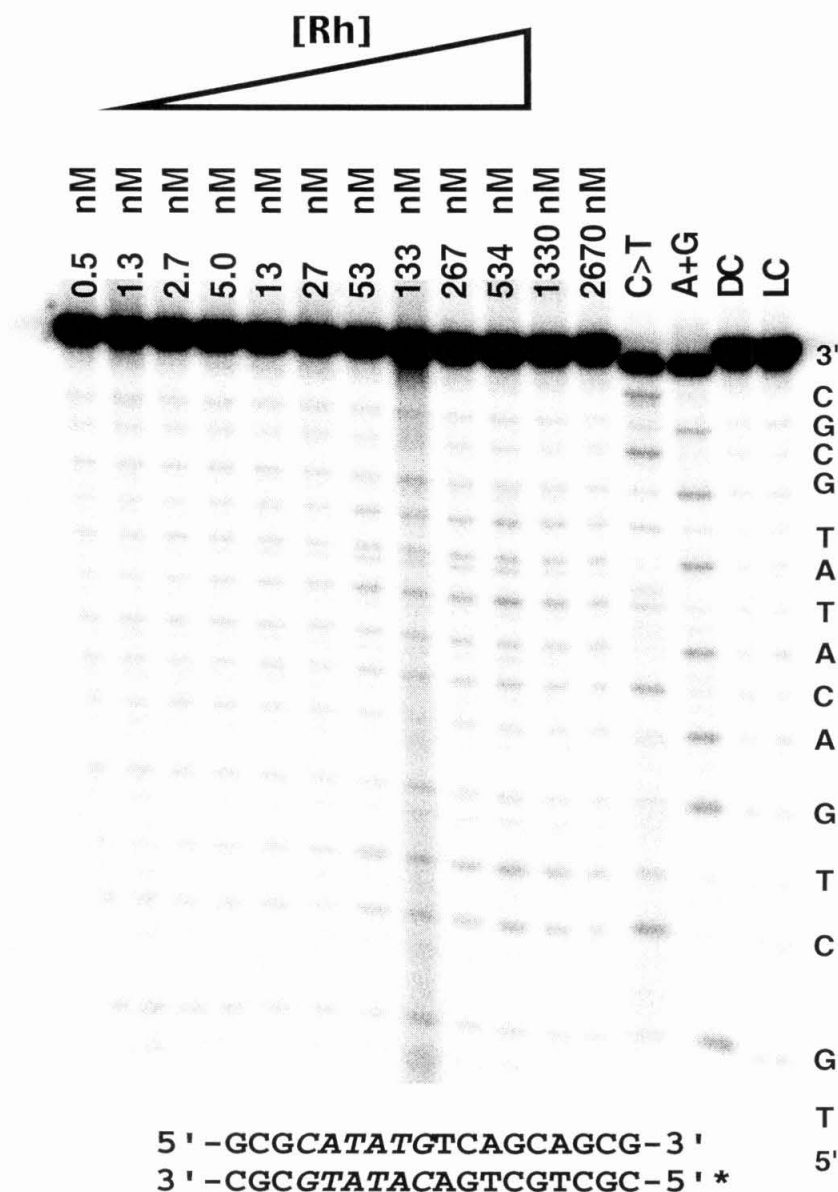


**Figure 2.8.** Photocleavage of 5'-<sup>32</sup>P labeled target oligonucleotide by  $\Lambda$ -2-Rh(MGP)<sub>2</sub>phi<sup>5+</sup>. The top of the gel shows the concentration of Rh used in each lane. Final duplex DNA concentrations were exactly one order of magnitude higher than the Rh concentrations for each irradiation reaction. Each sample was irradiated for 8 minutes at 313 nm. Maxam-Gilbert A+G and C>T sequencing lanes are shown to the far right. The buffer concentrations were 10 mM sodium cacodylate and 50 mM NaCl. Introduced target sites are shown in the sequence below the gel in italics.

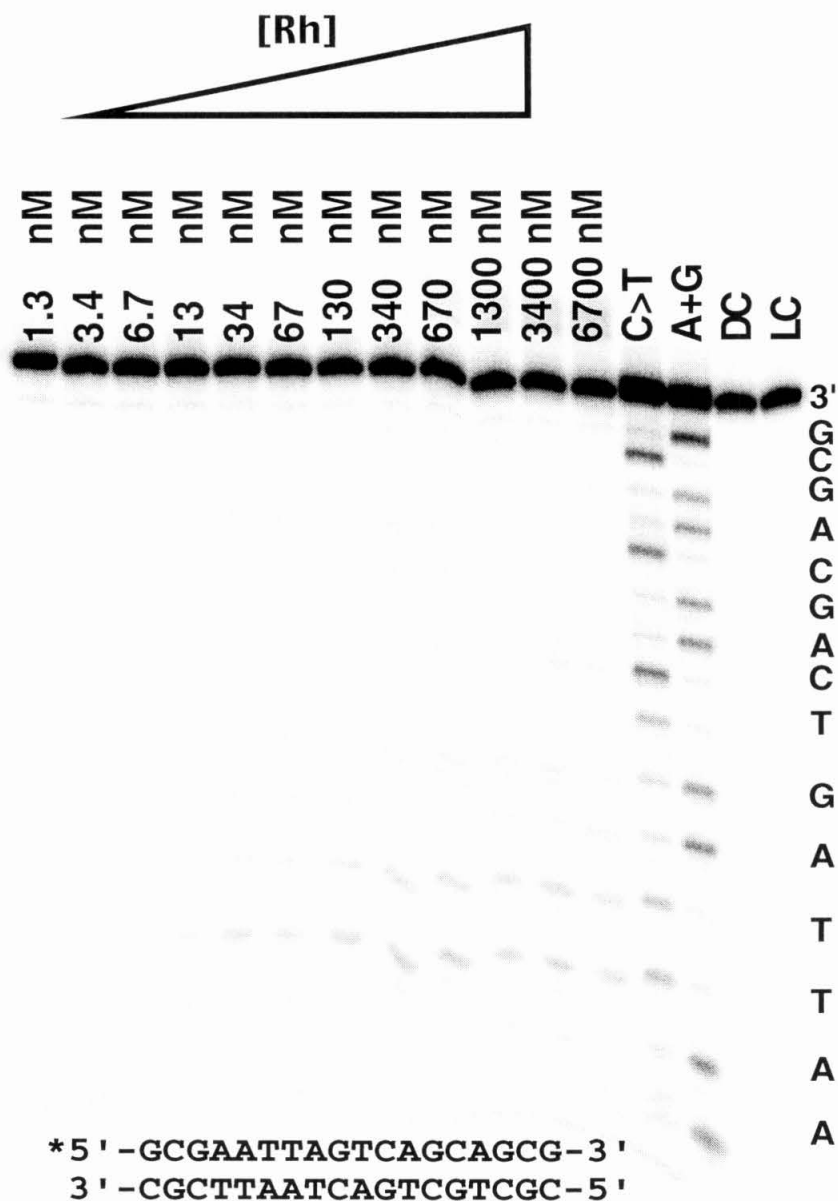


**Figure 2.9.** Photocleavage of 5'-<sup>32</sup>P labeled wild-type oligonucleotide by  $\Delta$ -2-Rh(MGP)<sub>2</sub>phi<sup>5+</sup>. The top of the gel shows the concentration of Rh used in each lane. Final duplex DNA concentrations were exactly one order of magnitude higher than the Rh concentrations for each irradiation reaction. Each sample was irradiated for 8 minutes at 313 nm. Maxam-Gilbert A+G and C>T sequencing lanes are shown to the right. The buffer concentrations were 10 mM sodium cacodylate and 50 mM NaCl.

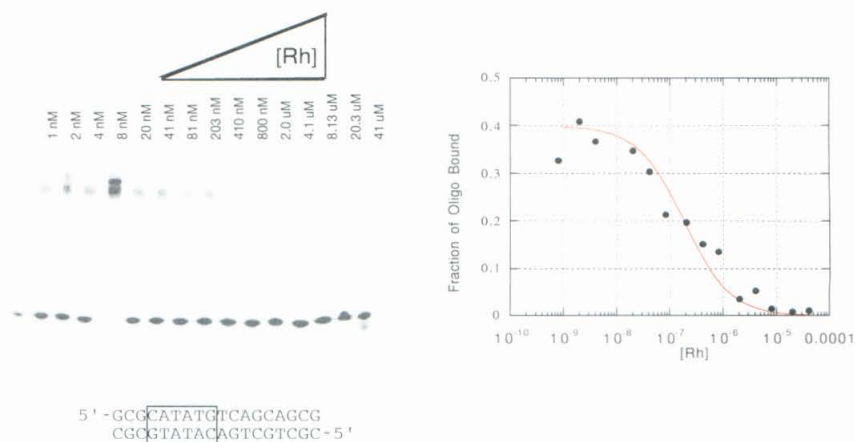


**Figure 2.10.** Competition between the protein yAP-1 and the metal complex  $\Lambda$ -1-Rh(MGP)<sub>2</sub>phi<sup>5+</sup> for the target oligonucleotide duplex as visualized by gel mobility retardation assay. Below the left gel is shown the target oligonucleotide strand used in the competition reaction, and the graph to the right shows the quantitation and curve fit of the data. In this experiment,  $\Lambda$ -1-Rh(MGP)<sub>2</sub>phi<sup>5+</sup> competitively disrupts 50% of the yAP-1/DNA binding complexes at 120 nM concentration. Each 30  $\mu$ L, 3 hour incubation reaction contained, in addition to the concentration of metal complex indicated above each lane, 40 nM yAP-1, 2% Ficoll, 15 mM Tris pH 7.4, 50 mM KCl, 25 nCuries 5'-<sup>32</sup>P labeled target oligonucleotide duplex (2 nM DNA duplex), and 1  $\mu$ M BSA. Competition reactions (10  $\mu$ L of the 30  $\mu$ L reaction) were directly loaded onto a running 5.5% non-denaturing polyacrylamide gel for 100 Volt-Hours, and then visualized by Phosphorimager plates.

#### 2.3.4. Isomer Specificity of Competition Between Metal Complexes and Target

*Oligonucleotide.* Competition for the target oligonucleotide between yAP-1 and either  $\Lambda$ -1-Rh(MGP)<sub>2</sub>phi<sup>5+</sup> or  $\Lambda$ -2-Rh(MGP)<sub>2</sub>phi<sup>5+</sup> was examined by titrating with the metal complexes using gel retardation assays (Figure 2.10 and 2.14). Reactions were loaded onto a running gel in our laboratory as standard procedure for all gel shift assays regardless of incubation time. Protein binding thus measured decreased in a sigmoidal fashion with increasing concentrations of the metal complex, albeit at different concentrations for different species of metal complex.

Curve fitting of the ratios of the bound oligonucleotide to total oligonucleotide showed that the concentration of  $\Lambda$ -1-Rh(MGP)<sub>2</sub>phi<sup>5+</sup> required to reach half-dissociation of the protein-DNA sites was 118 nM (Figure 2.10). The complex  $\Lambda$ -2-Rh(MGP)<sub>2</sub>phi<sup>5+</sup>, in contrast, showed no disruption of the DNA-protein complex at concentrations as high as

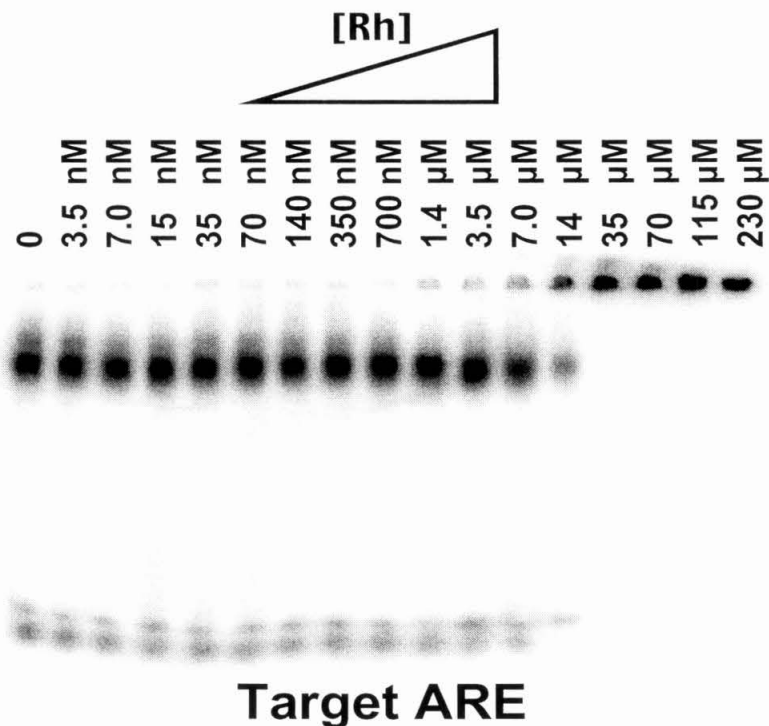


**Figure 2.11.**  $\Lambda$ -2-Rh(MGP)<sub>2</sub>phi<sup>5+</sup> control competition reactions with the protein yAP-1 for the target oligonucleotide.  $\Lambda$ -2-Rh(MGP)<sub>2</sub>phi<sup>5+</sup> shows no competition for the protein/DNA complex, but did show nonspecific aggregation above concentrations of 10  $\mu$ M. Gels were obtained with the conditions as in Figure 2.10.

10  $\mu$ M, but non-specific aggregation of the DNA-protein complexes was evident at higher rhodium concentrations (Figure 2.11). The aggregation did not occur until the metal complex was over 250 times more concentrated than yAP-1 in the binding reactions, and over 10 times higher in concentration than the non-specific carrier protein BSA. This behavior was not seen with  $\Lambda$ -1-Rh(MGP)<sub>2</sub>phi<sup>5+</sup> at concentrations as high as 40  $\mu$ M. The differential binding by  $\Lambda$ -1-Rh(MGP)<sub>2</sub>phi<sup>5+</sup> versus  $\Lambda$ -2-Rh(MGP)<sub>2</sub>phi<sup>5+</sup> clearly demonstrates isomer specificity in recognition by the metal complex (Figure 2.12). The geometric repositioning of the pendant guanidiniums (*e.g.*,  $\Lambda$ -1-Rh(MGP)<sub>2</sub>phi<sup>5+</sup> versus  $\Lambda$ -2-Rh(MGP)<sub>2</sub>phi<sup>5+</sup>) increases by over two orders of magnitude the amount of metal

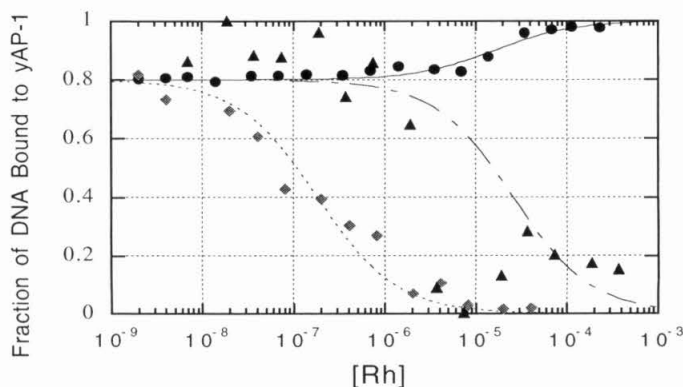


**Figure 2.12.** Comparison of fitted curves for competition between metal complexes and yAP-1. Gel shift assays were quantitated in ImageQuant and then graphed and fitted in Kaleidograph. The metal complexes  $\Lambda$ -1-Rh(MGP)<sub>2</sub>phi<sup>5+</sup> (diamonds),  $\Lambda$ -2-Rh(MGP)<sub>2</sub>phi<sup>5+</sup> (solid circles), and *rac*-Rh(phen)<sub>2</sub>phi<sup>3+</sup> (solid triangles) were used in competition experiments with yAP-1 for the target oligonucleotide.

complex needed to disrupt competitively specific protein-DNA complexes.

Binding reactions with the parent metal complex *rac*-Rh(phen)<sub>2</sub>phi<sup>3+</sup> were examined in similar competition experiments to explore the effect that a relatively sequence neutral intercalating metal complex has on yAP-1 and yAP-1/DNA complexes. *rac*-Rh(phen)<sub>2</sub>phi<sup>3+</sup> does not interfere with protein/DNA complexes directly, but competes at higher concentration sterically for sites in the major groove of the oligonucleotide (Figure 2.13). Competition on both wild-type and target oligonucleotides had half-site occupancy at 23  $\mu$ M metal complex (Figure 2.12 solid triangles, and data not shown). This value accurately reflects the lower overall binding affinity that *rac*-Rh(phen)<sub>2</sub>phi<sup>3+</sup>, compared to  $\Lambda$ -1-Rh(MGP)<sub>2</sub>phi<sup>5+</sup>, displays for DNA. Indeed, previous work has estimated the dissociation constant of this metal complex from DNA to be in the micromolar range,<sup>16</sup> and photocleavage experiments with the native and target oligonucleotides described herein show no strong photocleavage at concentrations of metal complex up to 20  $\mu$ M.

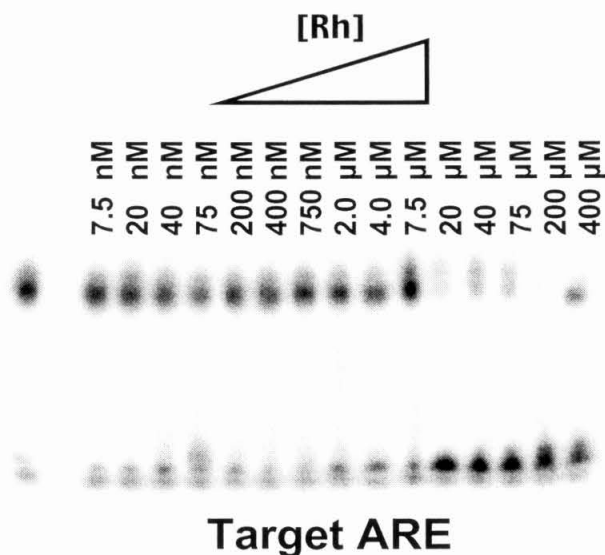


**Figure 2.13.** Competition reactions between the protein yAP-1 and  $\text{rac-Rh(phen)}_2\text{phi}^{3+}$  for the target oligonucleotide. When the guanidiniums are removed from the metal complex, the concentration needed to displace yAP-1 increases to over 20  $\mu\text{M}$ .

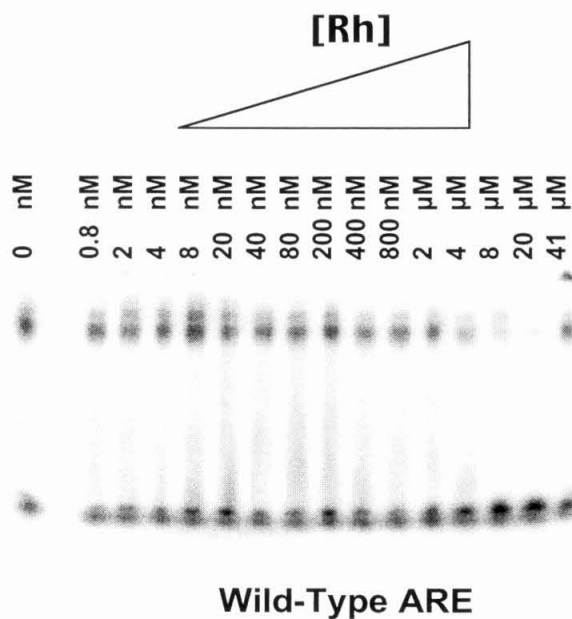


**Figure 2.14.** Competition reactions between the protein yAP-1 and  $\Lambda\text{-2-Rh(MGP)}_2\text{phi}^{5+}$  with the wild-type oligonucleotide. Remarkably, the concentration of metal complex needed to inhibit yAP-1 binding increases to  $\sim 3 \mu\text{M}$ .

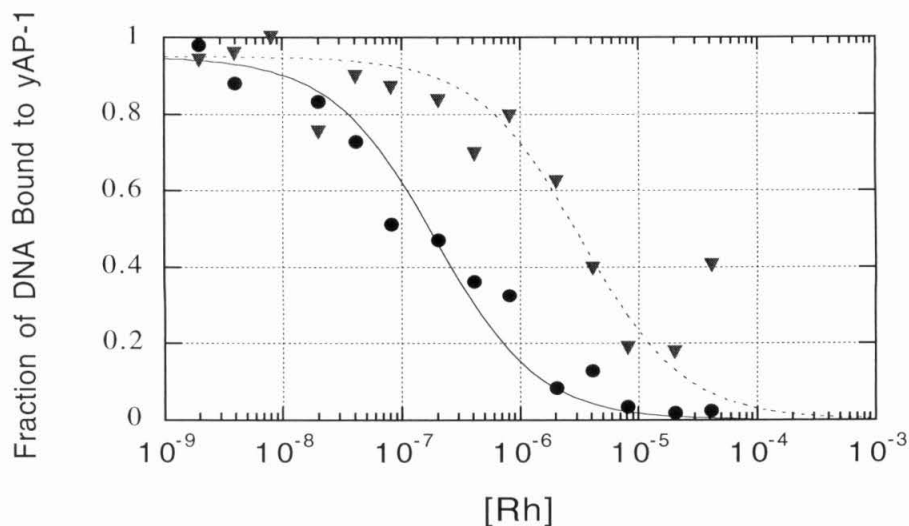


**Figure 2.15.** Comparison of fitted curves for competition between yAP-1 and  $\Lambda$ -1-Rh(MGP)<sub>2</sub>phi<sup>5+</sup> for the target oligonucleotide (solid circles) and the wild type oligonucleotide (inverted triangles). Gel shift assays were quantitated in ImageQuant and then graphed and fitted in Kaleidograph.

**2.3.5. Site Specific Competition of yAP-1 and  $\Lambda$ -1-Rh(MGP)<sub>2</sub>phi<sup>5+</sup>.** To demonstrate that successful competition between yAP-1 and  $\Lambda$ -1-Rh(MGP)<sub>2</sub>phi<sup>5+</sup> for a DNA binding site is dependent on the presence of a target 5'-CATATG-3' site, we performed identical competition experiments on both with the wild type ARE oligonucleotide and with the target oligonucleotide (Figure 2.14). In these experiments, competition experiments using an oligonucleotide lacking a binding site for  $\Lambda$ -1-Rh(MGP)<sub>2</sub>phi<sup>5+</sup> (as shown by photocleavage in Figure 2.7) was compared to experiments using the target oligonucleotide which contains the preferred binding site 5'-CATATG-3'.

If  $\Lambda$ -1-Rh(MGP)<sub>2</sub>phi<sup>5+</sup> were non-specifically interfering with the protein, identical behavior between these two different protein-DNA complexes would be expected. However, as seen in Figure 2.15,  $\Lambda$ -1-Rh(MGP)<sub>2</sub>phi<sup>5+</sup> disrupted 50% of the protein-target DNA complexes at a concentration of 120 nM, whereas over 3  $\mu$ M rhodium was required to compete similarly on the wild type oligonucleotide. This result represents an increase



of 30 times the concentration of  $\Lambda$ -1-Rh(MGP)<sub>2</sub>phi<sup>5+</sup> required to disrupt yAP-1-target oligonucleotide complexes. In effect, the removal of the binding site from the oligonucleotide increases the concentration of metal complex required for successful competition with yAP-1 by more than an order of magnitude.

## 2.4 DISCUSSION

*2.4.1. Target Oligonucleotide Design.* In general, the native ARE shows a great deal of tolerance for variation of the nucleotides within its binding site that are not closely contacted by the protein. However, attempts to introduce a metal complex binding site that disrupts one or more of the closely contacted base pairs resulted in a pronounced decrease in the binding affinity between yAP-1 and the modified ARE (not shown). Consistent with this notion, the mutation of the binding site to include a metal complex binding region without changing these essential base pairs, as shown in Figure 2.3, did not alter the binding of yAP-1 to the oligonucleotide. Gel retardation assays showed that, at an approximate 2:1 molar ratio in titration, the binding of the target oligonucleotide to the protein was quantitative at very low nanomolar concentrations (typically 8-10 nM of protein). Photocleavage with  $\Lambda$ -1-Rh(MGP)<sub>2</sub>phi<sup>5+</sup> confirmed that the metal complex strongly recognized the target oligonucleotide containing the three base pairs altered from the wild-type ARE.

*2.4.2. Site Specificity of the Competition Reaction.* The ability of a metal complex to compete specifically at low concentrations with a transcription factor for a promoter depends on the presence of an overlapping binding site for the two species. Competition between yAP-1 and  $\Lambda$ -1-Rh(MGP)<sub>2</sub>phi<sup>5+</sup> for the target oligonucleotide showed disruption at concentrations more than an order of magnitude lower than seen for competition between the same species for the wild type ARE. These controls show that the competitive disruption of the binding of yAP-1 to the ARE depends on the specific DNA sequence, and not on a non-specific interaction with yAP-1. Non-specific

interactions between  $\Lambda$ -1-Rh(MGP)<sub>2</sub>phi<sup>5+</sup> and the carrier BSA are also ruled out by the differential inhibition of yAP-1 binding to DNA by  $\Lambda$ -1-Rh(MGP)<sub>2</sub>phi<sup>5+</sup>. Interaction of the metal complex with BSA cannot account for the strongly sequence-specific competition between the transcription factor and  $\Lambda$ -1-Rh(MGP)<sub>2</sub>phi<sup>5+</sup> that occurs at concentrations of metal complex an order of magnitude below the concentration of BSA (Figure 2.15). There are pronounced differences in binding affinity for the two oligonucleotides and the metal complex  $\Lambda$ -1-Rh(MGP)<sub>2</sub>phi<sup>5+</sup>, as seen both by photocleavage and by competition with yAP-1 for an oligonucleotide. These differences show that the metal complex binding is specific to the sequence introduced into the ARE and is not a non-specific metal complex-protein interaction. The data furthermore show that the specific inhibition of protein binding is dependent on the presence of 5'-CATATG-3' within the promoter site.

*2.4.3. Isomer and Complex Specificity of the Competition Reaction.* The specificity in metal complex for  $\Lambda$ -1-Rh(MGP)<sub>2</sub>phi<sup>5+</sup> is demonstrated through the comparison between its competition reactions and those of related complexes. Other metal complexes showed non-specific interference in the binding of yAP-1 to the target oligonucleotide. Moreover, for other metal complexes the protein-promoter complex disruption was insensitive to the sequence of the DNA used. Both wild type ARE and the target ARE show approximately the same susceptibility to disruption, as is expected for a competition with metal that is not site-specific. Furthermore, titrations revealed that only concentrations of *rac*-Rh(phen)<sub>2</sub>phi<sup>3+</sup> above 20  $\mu$ M could disrupt DNA-protein complexes. These concentrations are well over two orders of magnitude greater than those seen for the specific competition of  $\Lambda$ -1-Rh(MGP)<sub>2</sub>phi<sup>5+</sup>.

The symmetrical isomer  $\Lambda$ -2-Rh(MGP)<sub>2</sub>phi<sup>5+</sup> also showed no disruption of protein-DNA complexes up to 20  $\mu$ M either with the wild type ARE or with the target ARE (Figure 2.12). However, as the concentration of the metal complex increased to over 250 times that of yAP-1 and over ten times that of the carrier BSA, aggregation in the

wells occurred. Importantly, the only difference between this series of reactions and those performed for  $\Lambda$ -1-Rh(MGP)<sub>2</sub>phi<sup>5+</sup> was the orientation of the pendant guanidiniums. Positioning these arms so that they no longer contact DNA removes all specificity for DNA recognition, as seen previously.<sup>17</sup> Inspection of the geometry of the two isomeric species (see Figure 2.1) shows that  $\Lambda$ -1-Rh(MGP)<sub>2</sub>phi<sup>5+</sup> directs its guanidinium functional groups into the DNA major groove. In contrast,  $\Lambda$ -2-Rh(MGP)<sub>2</sub>phi<sup>5+</sup> has both guanidiniums directed away from the intercalating phi ligand. The differences in orientation of hydrogen bonding substituents between the two complexes must be the source of the different biochemical interactions of these metal complexes; indeed the overall charge on the complexes and thus their electrostatic interaction with DNA is the same. The proximity of the two guanidiniums in  $\Lambda$ -2-Rh(MGP)<sub>2</sub>phi<sup>5+</sup> could be responsible for the increased inter-complex contacts between multiple protein-DNA complexes and possibly the carrier BSA we observe, and, hence, cause a non-specific aggregation not dissimilar to that used in ammonium sulfate precipitations of susceptible proteins in purification steps.

*2.4.4. Model for Competition.* yAP-1 shares many features with other bZIP transcription factors.<sup>33</sup> Comparison of our designed target site with the related oligonucleotide site in the crystal structure of the GCN4 DNA binding domain<sup>34</sup> suggests that the presence of a metal complex in the location of our introduced binding site would appear to sterically block one of the two dimer arms from making contacts with half of the semi-symmetrical core of the binding domain. All of the modifications to the ARE are located 5' to the pivotal G-C base pair, and hence on only one of the two dimer binding regions. Although there still exists some controversy regarding the dimerization and DNA binding pathway that proteins follow *in vivo*, recent models have suggested that bZIP proteins dimerize stepwise on some target sites of DNA.<sup>35,36</sup> The steric presence of a metal complex, and the concomitant unwinding of half of the target site may also prevent the dimerization step of protein binding. Whatever the intervening species, the

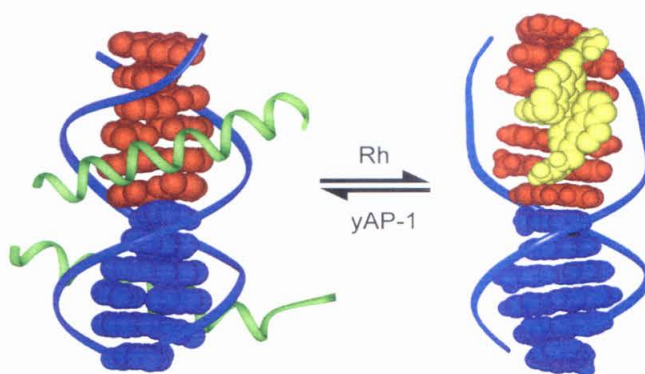


**Figure 2.16.** Schematic model of the competition between yAP-1 and  $\Lambda$ -1-Rh(MGP)<sub>2</sub>phi<sup>5+</sup> on the target DNA. The models were constructed in InsightII based on NMR models of  $\Lambda$ -1-Rh(MGP)<sub>2</sub>phi<sup>5+</sup> intercalation at 5'-CATATG-3' sites<sup>20</sup> and the GCN4 crystal structure parameters.<sup>33</sup> When occupied by the metal complex, the half site of the target site is unwound by 70° and sterically precludes protein association

equilibrium between the protein and metal complex bound states on DNA and the probable DNA conformations are shown modeled in Figure 2.16.

Nature offers many parallels to the type of competition  $\Lambda$ -1-Rh(MGP)<sub>2</sub>phi<sup>5+</sup> shows with yAP-1. By using direct competition at overlapping sites, often two repressor proteins modulate gene expression. In much the same way, the site-specific competition between metal complexes and transcription factors might be exploited to modulate expression.

*2.4.5. A Promising New Use for Metallointercalators.* Octahedral metallointercalators would have to satisfy many criteria to be candidates for possible therapeutic applications. Perhaps the first of these important criteria would be the site-specific inhibition of a transcription factor binding to an enhancer site. We have shown previously that metal complexes can inhibit restriction endonucleases, and that metal complexes can mimic the binding characteristics of transcription factors.<sup>11,37</sup> We have now shown that a metallointercalator can compete directly with a transcription factor in

the major groove for its target site. This is a fundamental first step towards controlling gene expression therapeutically using metallointercalators.

---

## 2.5 REFERENCES

- 1) Ahmad, I., Rao, D. N. (1996) *Crit. Rev. Biochem. Mol. Biol.* 31, 361-380.
- 2) Donahue, B. A., Augot, M., Bellon, S. F., Treiber, D. K., Toney, J. H., Lippard, S. J., Essigmann, J. M. (1990) *Biochemistry* 29, 5872-5880.
- 3) Pil, P. M., Lippard, S. J., (1992) *Science* 256, 234-237.
- 4) Whitehead, J. P., Lippard, S. J. (1996) *Metal Ions Biol. Sys.* 32, 687-726.
- 5) Tomasz, M., Palom, Y. (1997) *Pharmaceuticals and Therapeutics* 76, 73-87.
- 6) Poltev, V. I., Bruskov, V. I., Shulyupina, N. V., Rein, R., Shibata, M., Ornstein, R. L., Miller, J. (1993) *Mol. Biol.* 27, 447-462.
- 7) Denison, C., Kodadek, T. (1998) *Chem. Biol.* 5, R129-R145.
- 8) Liu, C., Smith, B. M., Ajito, K., Komatsu, H., GomezPaloma, L., Li, T. H., Theodorakis, E. A., Nicolaou, K. C., Vogt, P. K. (1996) *Proc. Natl. Acad. Sci. USA* 93, 940-944.
- 9) Nicolaou, K. C., Tsay, S. C., Suzukit, T., Joyce, G. F. (1992) *J. Am. Chem. Soc.* 114, 7555-7557.
- 10) Nicolaou, K. C., Dai, W. (1991) *Angew. Chem.* 30, 1387-1416.
- 11) Terbrueggen, R. H., Barton, J. K. (1995) *Biochemistry* 34, 8227-8234.
- 12) Johann, T. W., Barton, J. K. (1996) *Phil. Trans. R. Soc. Lond. A* 354, 299-324.
- 13) Hudson, B. P., Barton, J. K. (1998) *J. Am. Chem. Soc.* 120, 6877-6888.
- 14) David, S. S., Barton, J. K. (1993) *J. Am. Chem. Soc.* 115, 2984-2985.
- 15) Keilkopf, C. L.; Erkkila, K. E.; Hudson, B. P.; Barton, J. K.; Rees, D. C. *Nat. Struct. Biol.* 1999, 7, 117.

- 16) Sitlani, A., Long, E. C. Pyle, A. M., Barton, J. K. (1992) *J. Am. Chem. Soc.* 114, 2303-2312.
- 17) Terbrueggen, R. H., Johann, T. W., Barton, J. K. (1998) *Inorg. Chem.* 37, 6874-6883.
- 18) Campisi, D., Morii, T., Barton, J. K. (1994) *Biochemistry* 33, 4130-4139.
- 19) Pabo, C. O., Sauer, R. T. (1992) *Ann. Rev. Biochem.* 61, 1053.
- 20) Franklin, S. J., Barton, J. K. (1998) *Biochemistry* 37, 16093-16105.
- 21) Kim, J. L., Nikolov, D. B., Burley, S. K. (1993) *Nature* 365, 520-527.
- 22) Kim, Y. C., Geiger, J. H., Hahn, S., Sigler, P. B. (1993) *Nature* 365, 512-520.
- 23) Oshea, E. K., Klemm, J. D., Kim, P. S., Alber, T. (1991) *Science* 254, 539-544.
- 24) Moye-Rowley, W. S., Harshman, K. D., Parker, C. S. (1988) *Cold Spring Harbor Symp. Quant. Biol.* LIII, 711.
- 25) Moye-Rowley, W. S., Harshman, K. D., Parker, C. S. (1989) *Genes and Development* 3, 283-292, and unpublished results in the Parker lab.
- 26) Wemmie, J., Wu, A.-L., Harshman, K. D., Parker, C. S., Moye-Rowley, W. (1994) *J. Biol. Chem.* 269, 14690.
- 27) Harshman, K. D., Moye-Rowley, W. S., Parker, C. (1988) *Cell* 53, 321-330.
- 28) Chow, C. S., Barton, J. K. (1992) *Meth. Enzym.* 212, 219-242.
- 29) Kunkel, T. A. (1985) *Proc. Natl. Acad. Sci. USA* 82, 488-492.
- 30) Singleton, S., Dervan, P. B. (1992) *J. Am. Chem. Soc.* 114, 6957.
- 31) LaValle, E. R., DiBlasio, E. A., Kovacic, S., Grant, K. L., Schendel, P. F., McCoy, J. M. (1993) *Bio/Technology* 11, 187-193.
- 32) Johann, T. W. California Institute of Technology, *Ph.D. Dissertation*.
- 33) Vinson, C. R., Sigler, P. B., McKnight, S. (1989) *Science* 246, 911.
- 34) Ellenberger, T. E., Brandl, C. J., Struhl, K., Harrison, S. C. (1992) *Cell* 71, 1223-1237.
- 35) Metallo, S. J., Schepartz, A. (1997) *Nature Structural Biology* 4, 115-117.
- 36) Weiss, M. A. (1990) *Biochemistry* 29, 8020-8024.

- 37) Sitlani, A., Dupureur, C. M., Barton, J. K. (1993) *J. Am. Chem. Soc.* 115, 12589-12590.

## **CHAPTER 3**

### **Long Range Charge Transport Through RNA/DNA Hybrid Duplexes**



### 3.1 INTRODUCTION

Recently, the ability of DNA to both sustain and participate in long range electron transport has been the subject of considerable research.<sup>1-12</sup> Oxidative damage to DNA is suspected to play significant roles in diseases as disparate as aging and cancer, and understanding the molecular basis of genetic degradation has become an important research goal.<sup>13-15</sup> In addition, recent nanotechnological research has focused on the possible uses of DNA duplexes as possible one dimensional quantum wires and templates for directed material deposition,<sup>16</sup> and larger nucleotide assemblies as building blocks for nanoscale structures and signaling devices.<sup>17-20</sup> Dissecting possible roles that the  $\pi$ -stack can play in long range charge transport, and what the precise parameters are for this reaction are of fundamental interest.

Given the A•T and G•C pairing rules, nucleic acid duplex regions are easily designed. The development of phosphoramidite chemistry in the last twenty years has further allowed high yield synthesis of single strand oligonucleotides up to 100-mer length. Thus, nucleic acids are an ideal medium for systematic chemical studies of charge transport, and, indeed, considerable literature exists delineating many facets of nucleic acid chemistry.<sup>21</sup> Crystal structures have been solved for a number of duplex DNA's, both alone and complexed with various DNA-binding molecules.<sup>22,23</sup> Diverse methods additionally exist to footprint, sequence, crosslink, and otherwise characterize DNA and its interactions with other molecules.<sup>24</sup>

Much research has focused on the role that the heteroaromatic  $\pi$ -stack of duplex DNA plays in facilitating long range charge transport to effect oxidative damage to DNA at a distant site.<sup>1-8</sup> In the standard technique used extensively, a photooxidant is appended covalently to one site of a duplex, and electronic holes can be injected into the base stack by these oxidants at a known location. In our laboratories, we have focused on appending metallointercalators to stack near the terminus of the DNA duplex.<sup>4</sup> As a result of long range charge transport, the injected radical then can localize onto the 5'-

guanine of 5'-GG-3' doublets, the most oxidatively sensitive sites.<sup>25</sup> Subsequent trapping of the radical with H<sub>2</sub>O or O<sub>2</sub> leads to formation of an irreversible lesion that is easily visualized by using denaturing gel electrophoresis after treatment with base.<sup>26</sup> Many different covalently attached photooxidants have been used to cause this type of long range damage, including metallointercalators,<sup>27</sup> ethidium derivatives,<sup>28</sup> anthraquinone derivatives,<sup>29,30</sup> flavins,<sup>31</sup> and naphthalamide derivatives.<sup>32</sup> All of these photooxidants can easily access the electronic structure of the base stack by intercalating into or stacking on the end of the DNA helix, and photooxidants that cannot electronically access the base stack in this manner have not been observed to damage the 5'-guanine of a guanine doublet. Although considerable discussion exists as to the exact mechanism of radical migration through the base stack,<sup>2,5,33-38</sup> electron and hole hopping between bases and domains is almost certainly involved.<sup>33,39-40</sup> Studies have shown modifying the structure of the base stack, for instance by the introduction of bulges,<sup>41</sup> mismatches,<sup>42,43</sup> or protein binding,<sup>44,45</sup> can affect charge transport.

Long range radical migration has also been investigated in non-B-form DNA. It was found that migrating charges can access single strand overhangs from a duplex region that has had a radical injected into it.<sup>46</sup> Interestingly, the preference for 5'-guanine damage in a guanine doublet was eliminated; instead, guanines were evenly damaged regardless of surrounding base identity. Similar experiments have shown that triple stranded DNA, both in short oligonucleotides<sup>47</sup> and in plasmid fragments,<sup>48</sup> can promote charge transport over significant distances.

Other experiments have applied fluorescence quenching to investigate the rate of electron transport in DNA.<sup>49,50</sup> DNA base analogs that have donor and acceptor properties, but that still form hydrogen bonds to complementary bases, can be introduced into DNA at known locations.<sup>49</sup> Because these bases retain their usual base-pairing properties, the duplexes they are in are in standard B-form, and the distance and orientation between donor and acceptor is precisely known. By varying the location and

orientation of these two species, it was found that fluorescence quenching as a function of distance decreases much less rapidly when both donor and acceptor are on the same strand than when they are on opposing strands, suggesting that charge transport is more efficient in B-form DNA when localized to one strand of the DNA duplex.

In solution, heteroduplexes of RNA and DNA assume conformations between the A-form of RNA duplexes and the B-form of DNA duplexes, and are central to genetic biochemistry.<sup>51-56</sup> Reverse transcriptases, most prominently HIV reverse transcriptase, produce RNA/DNA hybrids when replicating viral genomes. RNA/DNA hybrids are also found during transcription of a DNA template into an mRNA transcript. Furthermore, in DNA replication, lagging strand synthesis is initiated by synthesis of a short RNA oligonucleotide by primase, from which are formed Okazaki fragments.

Some research investigating long range charge transport in RNA/DNA hybrids and part ribose, part deoxyribose containing chimeric nucleic acid (CNA)/DNA hybrids has been carried out.<sup>57</sup> These studies focused on oxidative damage that occurs on DNA strands in a DNA/RNA or DNA/CNA hybrid. Long range oxidative damage of guanines was observed at 35°C, but not at 20°C, and no preference was observed for oxidative lesions to localize on the 5'-G of a 5'-GG-3' doublet. The low levels of strand cleavage were rationalized to be due to the hydrophobic nature of the A-like structure of the RNA/DNA hybrid duplex. No inspection of the damage that may occur on the RNA strand or segment was conducted.

Here, we describe experiments demonstrating that long range transport occurs efficiently through the RNA strand of an RNA/DNA duplex to the 5' guanine of 5'-GG-3' doublets. We utilized constructs previously successful in exploring the role of the DNA/DNA  $\pi$ -stack as a bridge for remote oxidation.<sup>28</sup> An ethidium derivative was covalently attached to the 5'-end of a DNA strand, which could then be annealed to a complement consisting of DNA, RNA, or CNA. This assembly could subsequently be photoirradiated to inject holes into the base stack, and treated with hot base to reveal

oxidative damage. As in previous studies, our results indicate that RNA/DNA hybrids can indeed act as a bridge for electron transfer. However, in contrast to previous results, we find that radical migration occurs in similar amounts to that found in DNA duplexes at ambient temperature, and that the resultant oxidative damage is overwhelmingly localized to the 5'-guanine of a 5'-GG-3' doublet.

## 3.2 EXPERIMENTAL

*Materials.* All chemical reagents and starting materials were purchased from commercial sources and used as received. N-8-glycyl ethidium (Et') and its methyl ester were synthesized as previously described.<sup>50</sup>

Oligodeoxynucleotides were synthesized on an ABI 392 RNA/DNA synthesizer and purified in the trityl on form by C18 reverse phase HPLC. These oligonucleotides were then detritylated and HPLC purified a second time. Ethidium-modified<sup>50</sup> and rhodium-modified<sup>58</sup> oligodeoxynucleotides were prepared according to published procedures, and stored in dried aliquots at  $-70^{\circ}\text{C}$  until needed.

*RNA Synthesis.* RNA oligonucleotides and chimeric RNA•DNA hybrids were prepared on an ABI 392 RNA/DNA synthesizer entirely with fresh reagents, and deprotected using standard techniques. These deprotected, desilanized sequences were purified using a preparative scale non-denaturing 10% polyacrylamide gel. The desired sequence was visualized by rapid UV shadowing, cut from the gel, crushed, and eluted at  $4^{\circ}\text{C}$  overnight into 10 mL of RNase-free 50 mM Tris•HCl pH 7.5 with 1 mM EDTA (TE). This solution was loaded onto a 12 cc Sep-Pak cartridge using standard procedures, rinsed extensively with water and the oligonucleotide eluted with 10 mL of 50% aqueous acetonitrile. The purified oligonucleotide was stored in aliquots at  $-70^{\circ}\text{C}$  as a dry solid, and redissolved as needed.

*RNA and DNA Techniques and Photoirradiation Experiments.* The oligonucleotides used were labeled by addition of a 5'-<sup>32</sup>P group using polynucleotide

kinase. The reaction mixture was desalted, treated for 30 minutes with either 1 M piperidine at 90°C (DNA), or 1 M aniline acetate at 60°C (RNA and RNA•DNA hybrids), and purified on a 20% non-denaturing acrylamide gel. The desired band was cut from the gel, and soaked in 3x1 mL of TE buffer, and isolated by use of NENsorb 20 oligonucleotide columns (Dupont) using standard procedures. Samples used in irradiations were annealed on a thermocycler by heating to 90°C for 5 minutes, followed by linear cooling to 4°C over 90 minutes. Noncovalent intercalators, when used, were added after duplex annealings were complete.

Irradiations were performed at 22°C on 10 µL samples in pre-siliconized 1.5 mL Eppendorf tubes using a 1000 W Hg/Xe arc lamp with a monochromator. Samples were buffered with 17 mM NaPO<sub>4</sub> at pH 7.0, 50 mM NaCl, and contained 10 µM duplex strands. In experiments where intercalator was bound non-covalently to the duplex, the concentration of Et'OMe was also 10 µM. After irradiation, the samples were dried by vacuum concentration, and then either directly diluted into formamide gel loading buffer or heated for 30 minutes in a total volume of 100 µL in the presence of 1 M piperidine (90°C), or 1 M aniline acetate (60°C) for all-DNA and RNA-containing samples, respectively, to reveal oxidative damage, then dried *in vacuo* and redissolved into denaturing, formamide-based gel loading buffer. Sequencing gels were 20% denaturing polyacrylamide containing 8 M urea, and were analyzed by phosphorimager.

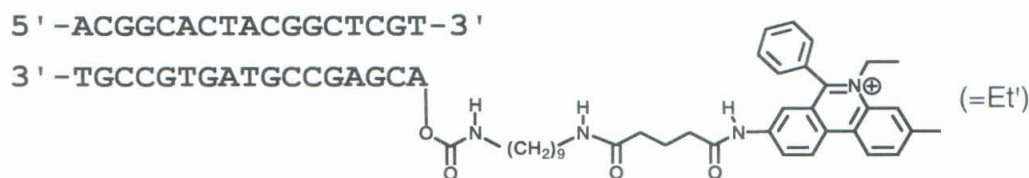
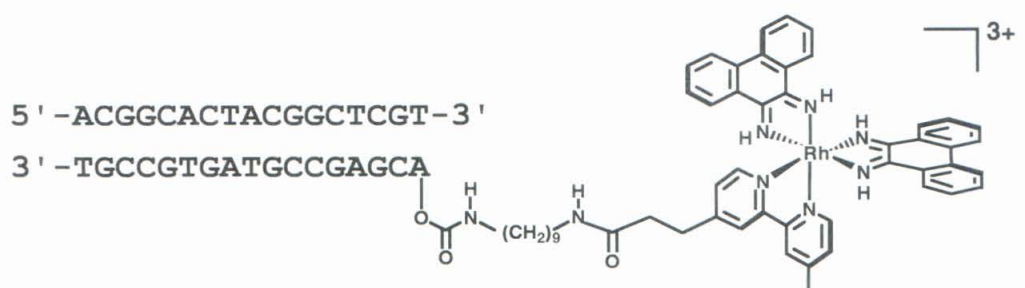
*Calculation of Base-Base Overlaps.* Using an O<sub>2</sub> SGI workstation and InsightII software with Biopolymer Module, idealized stick drawn B-form DNA dinucleotides were assembled. These nucleotides were centered down the dyad axis, and frame pictures taken. After exporting to a Macintosh G3, these pictures were opened by Adobe Photoshop, and the overlap between the stacked bases shaded. Hard copy prints of these photographs were made, and the stick structures cut out and weighed to determine the partitioning of overlap between neighboring bases. The same procedure was followed for the DNA/RNA hybrid duplexes, using the A-form DNA/RNA tool.

### 3.3 RESULTS

*3.3.1. Experimental Design.* In order to investigate the ability of RNA/DNA hybrids to sustain long range hole transfer, ethidium was used as a photooxidant in many of our experiments. Ethidium and its conjugates can intercalate into both A- and B-form DNA, as seen by luminescence enhancement when this intercalator is bound to either duplex RNA or B-form DNA.<sup>59</sup> Because of the non-B-form structure of the duplexes used in this study, the ability to intercalate into A-form, B-form and forms intermediate to these two was an essential requirement for the photooxidant. Previous studies in our laboratory have shown that ethidium when photoexcited can cause radical migration into DNA, and subsequent guanine oxidation at a distance.<sup>28</sup> Here, as previously, covalently bound ethidium showed significant damage at the guanine located at its intercalation site after irradiation at 313 nm, consistent with the direct formation of a covalent lesion at the site of intercalation. Rhodium conjugates of the same sequence were used to compare the effect photooxidant stacking has on the ability of an intercalator to introduce radicals into the base stack, as rhodium complexes of phi are not expected to intercalate effectively into non-B-form nucleic acids.<sup>60,61</sup>

In order to facilitate comparison with previous work, base sequences identical to those found in earlier reports<sup>28</sup> were utilized in these studies (Figure 3.1). The sugar identity of the strand complementary to the one bearing tethered photooxidants was varied to focus on the role(s) that conformation plays in enabling long range oxidation. The strands were synthesized as phosphoramidites, and purified by nondenaturing gel electrophoresis. The strand integrity was verified by radiolabeling with polynucleotide kinase, and inspecting the band pattern on a denaturing 20% polyacrylamide sequencing gel.

*3.3.2. Guanine Oxidation in an RNA/DNA Hybrid Duplex by Photoexcited Ethidium.* DNA-GG duplexes with tethered ethidium as a photooxidant showed, as



*5' -ACGGCACTACGGCTCGT-3'		
3' -TGCCGTGATGCCGAGCA-5' (-Et' or Rh)		DNA-GG
*5' - <i>acggcacuacggcucgu</i> -3'		
3' -TGCCGTGATGCCGAGCA-5' (-Et' or Rh)		RNA-GG
*5' -A <i>cggc</i> ACTA <i>cggc</i> TCGT-3'		
3' -TGCCGTGATGCCGAGCA-5' (-Et')		CNA-GG
*5' -ACAACACTACAAC TCGT-3'		
3' -TGTTGTGATGTTGAGCA-5' (-Et')		DNA-AA
*5' -A <i>caac</i> ACTA <i>caac</i> TCGT-3'		
3' -TGTTGTGATGTTGAGCA-5' (-Et')		CNA-AA

**Figure 3.1.** Nucleic acid duplexes used to investigate long range radical migration. The assemblies are named based on the sugar composition of the second strand, followed by the base composition of the sites of oxidation, and can have ethidium, Rh(phi)<sub>2</sub>bpy<sup>3+</sup>, or no photooxidant covalently tethered to the 5' end of one of the strands. Thus, DNA-GG represents an assembly where the strand complementary to the intercalator is entirely DNA with guanine doublets. RNA-GG has a complementary strand entirely of ribose sugars and guanine doublets; CNA-GG has a chimeric mixture of RNA and DNA with guanine doublets; DNA-AA contains a DNA strand with adenines in place of guanines; and CNA-AA contains a chimeric strand with adenine doublets.

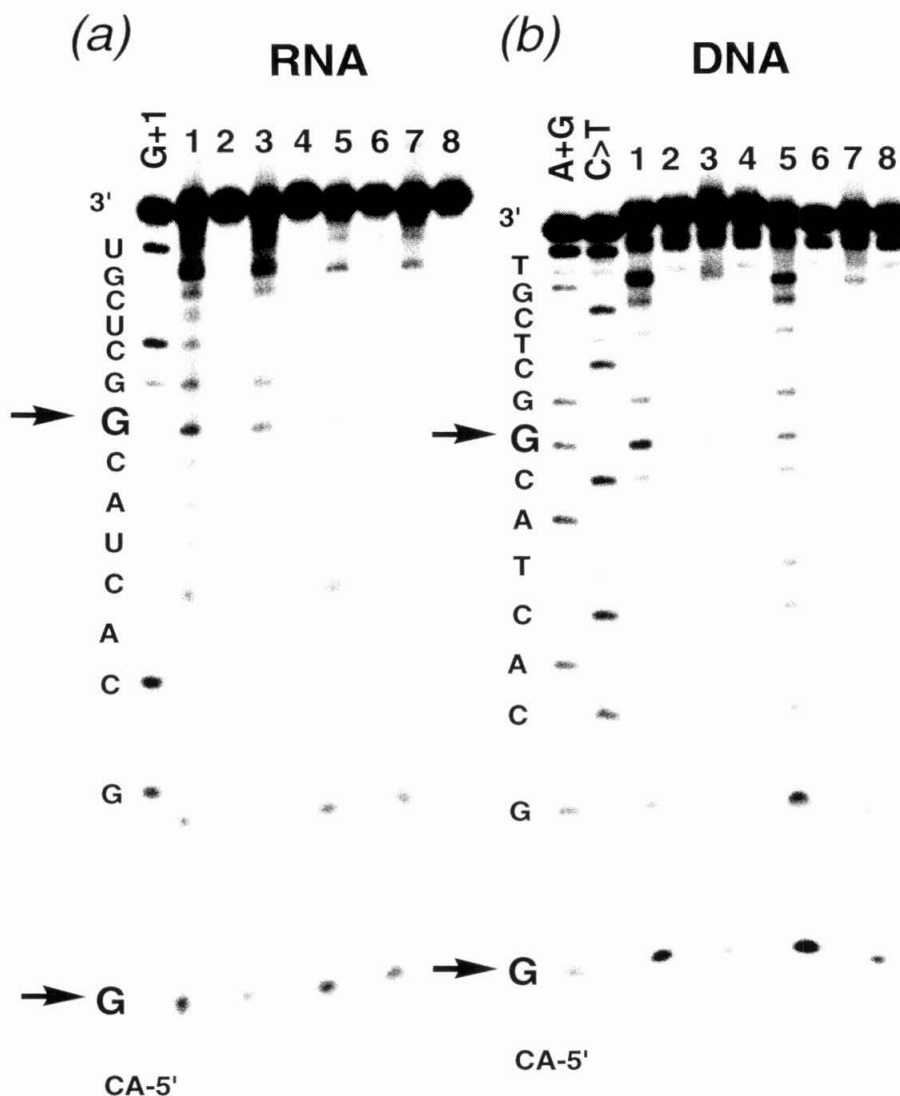


**Figure 3.2.** Long range guanine damage in RNA-GG duplexes (a) and DNA-GG duplexes (b) with covalently attached ethidium'. Shown is the phosphorimager of a representative 20% denaturing gel. Lanes are as follows: G+1, RNase T1 digestion, A+G, C>T Maxam-Gilbert sequencing reactions, lane 1 is 313 nm irradiation with hot base treatment (10% piperidine at 90°C with DNA, 1 M aniline acetate at 60°C for RNA), lane 2 is nonirradiated duplex with base treatment, lane 3 is 313 nm irradiated duplex without base treatment, lane 4 is nonirradiated duplex without base treatment, lanes 5 to 8 are identical to 1 to 4, but with non-covalent ethidium used with unmodified duplexes, instead of covalently joined intercalator constructs. All irradiations were performed for one hour, and the following concentrations were used: duplex 10  $\mu$ M, sodium phosphate pH 7.0 buffer 17 mM, ethidium' methyl ester 10  $\mu$ M in experiments with noncovalent intercalator. The sequence of the oligonucleotides is shown to the left of each panel, with the reactive guanines in slightly larger font, bold, and indicated by arrows.



**Table 3.1.** Partitioning Between Oxidatively Damaged Sites in RNA/DNA and DNA/DNA Duplexes<sup>a</sup>

2 <sup>nd</sup> Strand	RNA	DNA	CNA
Covalent Et' Distal/Prox	<b>0.63 (0.2)</b>	<b>1.1 (0.1)</b>	<b>0.9 (0.2)</b>
Covalent Et' Prox/Direct	<b>0.5 (0.2)</b>	<b>0.3 (0.05)</b>	<b>N/A</b>
Covalent Et' Dist/Direct	<b>0.3 (0.1)</b>	<b>0.3 (0.05)</b>	<b>N/A</b>

<sup>a</sup> The ratios were calculated from averages of three trials. Experimental conditions are described in the caption to Figure 3.2, and in the Experimental section of this chapter.

Direct damage to the guanine located at the ethidium intercalation site was also evident when photoirradiated at 313 nm for an hour (Figure 3.2). Hence, oxidation at the 5'-G of the guanine doublets was the result of a long range transport event. By annealing the same ethidium-bearing strand to a complementary RNA strand, RNA-GG was assembled (Figure 3.1). Subsequent photoirradiation and aniline treatment showed that, as with exclusively DNA assemblies, sites of greatest damage were the 5'-guanines in 5'-GG-3' doublets. Moreover, the ethidium intercalation site also shows damage that corresponds closely with that seen in DNA/DNA hybrids irradiated under the same conditions. This damage is due to the direct reaction of excited state ethidium with the adjacent guanine. Hence, as with DNA-GG, here too oxidative damage at the guanine doublets is the result of radical migration from a distance.

Notably, when either DNA-GG or RNA-GG are photoirradiated in the presence of non-covalently bound, equimolar ethidium, the proximal guanine doublet does not show any appreciable damage, though both the distal site and the intercalation site guanine still show oxidation. The reason for this lack of reaction at an oxidatively sensitive site is not clear. We also consistently found that the RNA systems employed showed higher

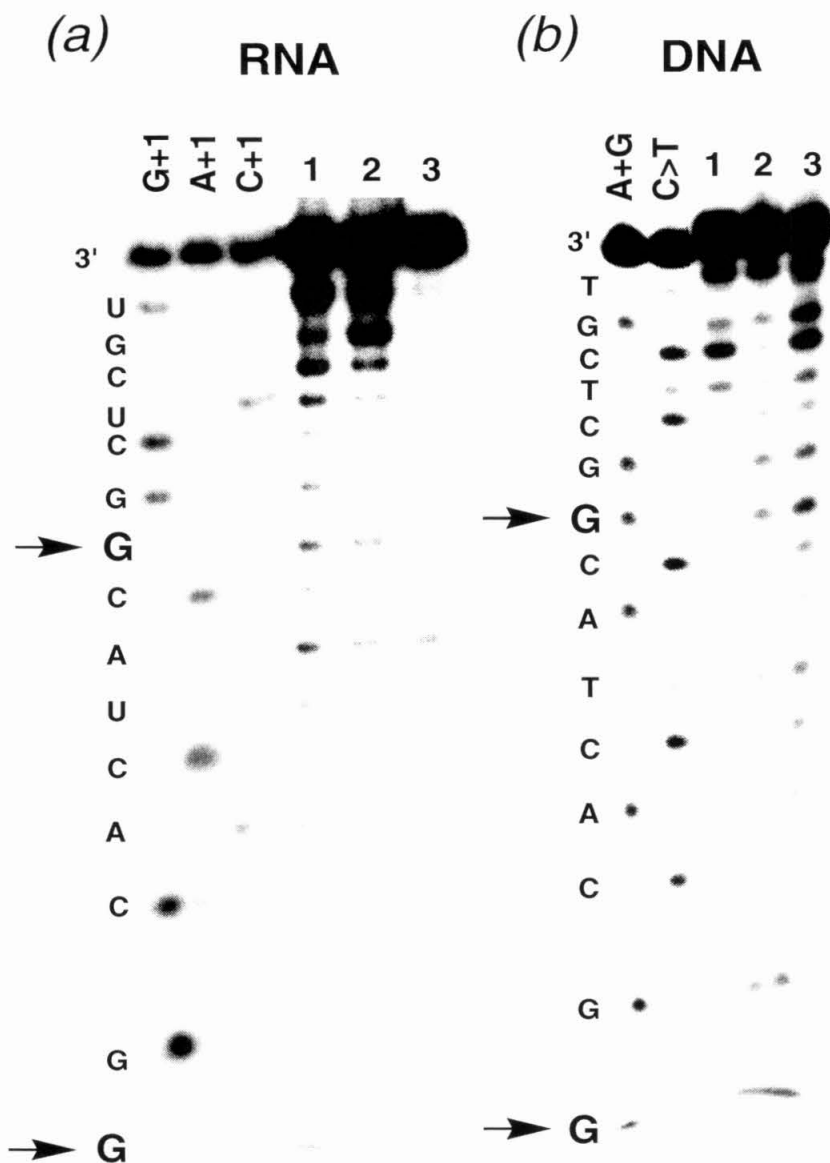


**Figure 3.3.** (a) Intercalation site and long range guanine oxidative damage in RNA-GG duplexes when  $\text{Rh}(\text{phi})_2\text{bpy}^{3+}$  is covalently appended, and (b) the same reactions in DNA-GG when  $\text{Rh}(\text{phi})_2\text{bpy}^{3+}$  is appended. Sequencing lanes are as in Figure 3.2. Other lanes are as follows: panel (a), lane 1, photoirradiation for 1 hour at 365 nm with aniline treatment; lane 2, photoirradiation for 10 minutes at 313 nm, no base treatment; lane 3, nonirradiated samples with aniline treatment; panel (b), lane 1, photoirradiation for 10 minutes at 313 nm, no base treatment; lane 2, nonirradiated samples with aniline treatment; lane 3, photoirradiation for 1 hour at 365 nm with aniline treatment. In all irradiations the following concentrations were used: duplex 10  $\mu\text{M}$ , sodium phosphate pH 7.0 buffer 17 mM.

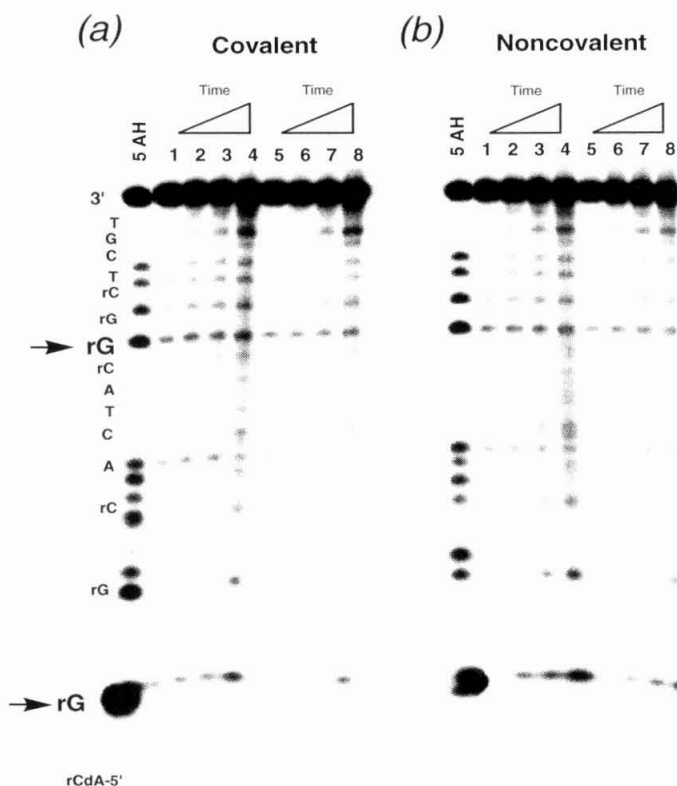


**Figure 3.4.** Long range oxidative damage at 5'-gg-3' cassettes in CNA-GG. Sample concentrations are as in Figure 2. The sequence, shown to the left of panel (a), was determined by alkaline hydrolysis (AH) of the RNA containing regions. AH lanes were exposed to 50 mM  $\text{Na}_2\text{CO}_3$ , pH 11 for 5 minutes. Sequencing hydrolysis cleavage occurs one base pair from the oxidative cleavage site. Lanes 1-4 of each panel are 15, 30, 60, and 120 minute irradiations followed by aniline acetate treatment of the samples, lanes 5-8 are the same irradiation times without aniline treatment.

### 3.3.3. Guanine Oxidation in an CNA/DNA Hybrid Duplex by Photoexcited

*Ethidium.* Having shown that RNA/DNA hybrids can efficiently support radical migration when the photooxidant is well-coupled into the base stack, we investigated also the effect that junctions between regions of ribose and deoxyribose sugars on one strand (CNA-GG) have on long range charge transport. The oxidatively sensitive 5'-CGGC-3' cassettes were replaced in the parent DNA sequence with the RNA cassette 5'-cggc-3', thus creating a strand with discrete regions of ribose and deoxyribose sugars. After annealing the strands to form the duplex CNA-GG that contains a covalently attached ethidium, photoirradiations were performed, as previously. After photooxidation, the

guanine doublets appear to show some damage in this construction, but it is modest (Figure 3.4). Considerable nonspecific damage also occurs in these constructs. Notably, the guanine most proximal to the intercalated ethidium shows lower than expected damage from direct reaction with the excited photooxidant. It is important to note that we have assigned the damage observed to reaction at the guanine sites by comparison with the sequencing reactions.

Sequencing reactions were performed by alkaline hydrolysis of the RNA containing regions. Basic hydrolysis marks a site that is one base upstream of the site of strand scission by base-liberated oxidative damage. Damage to the heterocyclic base and subsequent cleavage causes loss of the sugar-phosphate attached to it. In contrast, intramolecular hydrolysis at the 3'-hydroxyl attached to the same base leaves the sugar-phosphate intact. Thus, direct hydrolysis of the 3'-hydroxyl affords a fragment that is one base longer than oxidative reactions. Alkaline hydrolysis was performed by heating the labeled CNA strand to 90°C with carbonate buffer (pH 11) for a short time.

In contrast to the relatively modest damage that occurs at the intercalation site, the sites damaged most severely comigrate with the expected location for guanine oxidation. Thus, a significant percentage of these lesions likely represent guanine lesions that occurs after radical migration. This assumption is further supported by the dependence on aniline treatment that much of this damage shows (Figure 3.4). All analyses subtracted the non-irradiated samples as controls; these non-irradiated lanes should account for any associated hydrolysis that the stringent aniline treatment causes. In addition, experiments where the CNA-GG duplex was incubated with noncovalent ethidium, and long range transfer reactions performed, showed that aniline dependent damage occurred at the same sites, further supporting the contention that these are the sites of oxidative susceptibility. Nevertheless, it is important to note that the strands cleaved by hydrolysis at the junction comigrate with the expected location where strands generated by aniline treatment of oxidative guanine lesions would appear.

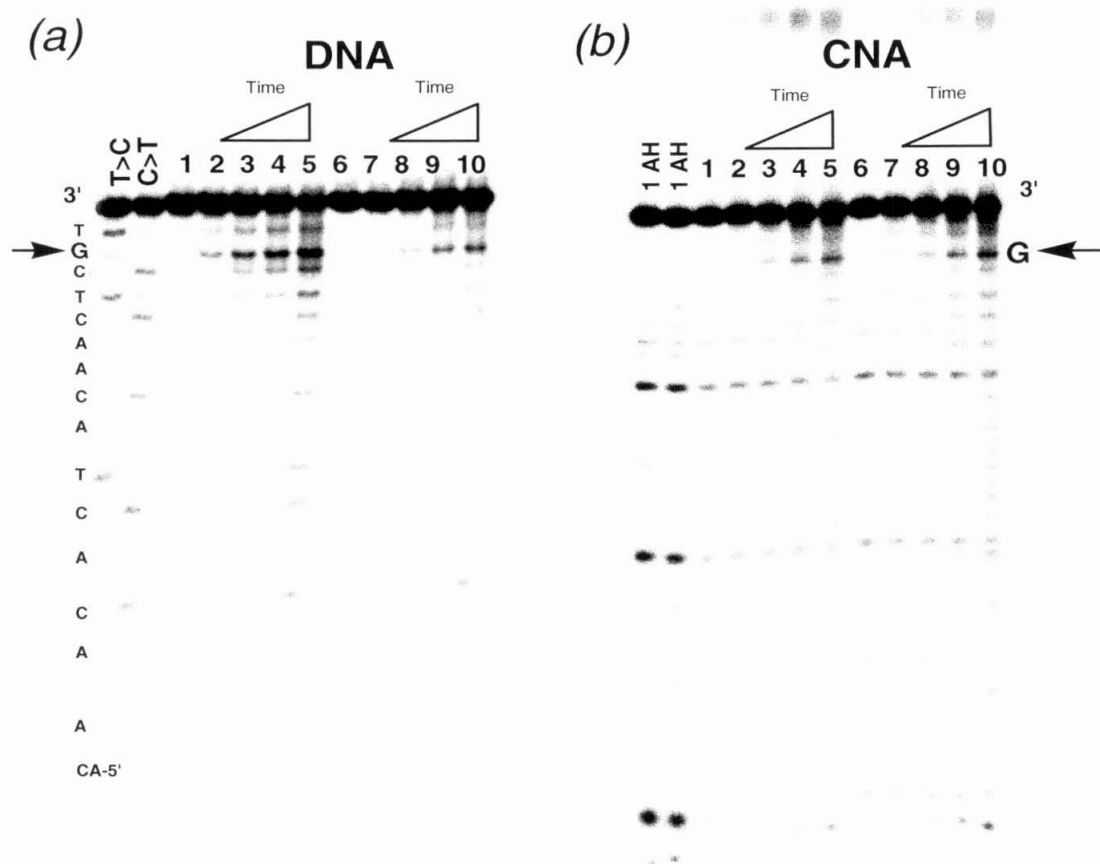


**Figure 3.5.** Oxidative damage found in the absence of guanine doublets in (a) ethidium tethered DNA-AA and (b) the equivalent result in CNA-AA. No damage is apparent in either case, except at the guanine located at the intercalation site.

#### 3.3.4. Oxidation in a Duplex Lacking Guanine Doublets by Photoexcited

*Ethidium.* In order to verify that the damage seen here is indeed specific to guanine, the 5'-CGGC-3' cassettes were replaced with 5'-CAAC-3' cassettes to afford DNA-AA and CNA-AA target strands. As can be seen in Figure 3.5, neither construct, when annealed with its complement and photoirradiated, showed any significant damage except at the lone remaining guanine at the intercalation site. This corresponds to the site of lowest oxidation potential; the result confirms that the damage seen earlier is indeed guanine specific.

**Table 3.2.** Base Surface Overlap in Idealized Dinucleotides

A-form <sup>a</sup>	% 5'-Base (Intrastrand) <sup>b</sup>	% 3'-Base (Intrastrand) <sup>b</sup>	% 3'-Base (Interstrand) <sup>b</sup>	% 3'-Base (Interstrand) <sup>b</sup>	B-form <sup>a</sup>	% 5'-Base <sup>b</sup>	% 3'-Base <sup>b</sup>
5'-AA-3'	26	26	-	-	5'-AA-3'	27	27
5'-AG-3'	26	26	-	-	5'-AG-3'	29	28
5'-GA-3'	28	29	-	-	5'-GA-3'	28	28
5'-GG-3'	28	28	-	-	5'-GG-3'	33	33
5'-AT-3'	42	67	-	-	5'-AT-3'	20	33
5'-AC-3'	37	59	-	-	5'-AC-3'	25	37
5'-GT-3'	42	29	-	-	5'-GT-3'	21	52
5'-GC-3'	43	72	-	-	5'-GC-3'	22	36
5'-TT-3'	0	0	-	-	5'-TT-3'	5	5
5'-TC-3'	0	0	-	-	5'-TC-3'	4	4
5'-CT-3'	0	0	-	-	5'-CT-3'	4	4
5'-CC-3'	0	0	-	-	5'-CC-3'	3	3
5'-CG-3'	-	-	19	19	5'-CG-3'	0	0
5'-CA-3'	-	-	18	18	5'-CA-3'	0	0
5'-TG-3'	-	-	18	18	5'-TG-3'	0	0
5'-UA-3'	-	-	26	26	5'-TA-3'	0	0

<sup>a</sup>Dinucleotides of the sequences listed below were generated as idealized duplexes in Insight II using the Biopolymer Module. Since both strands are fitted to ideal parameters, the overlap found in the dinucleotides of both strands of the RNA/DNA hybrid duplexes are identical.

<sup>b</sup>Base area overlaps were obtained as follows. Photographs of the dinucleotides were obtained by centering the view directly down the dinucleotide axis in InsightII. The pictures were exported into Photoshop 4.0.1, classified as overlap or nonoverlap base area, and then cut out and weighed. These weights were assumed to correspond directly to area, and used to calculate the percentage overlap. Errors in measurement are estimated to be 5%.

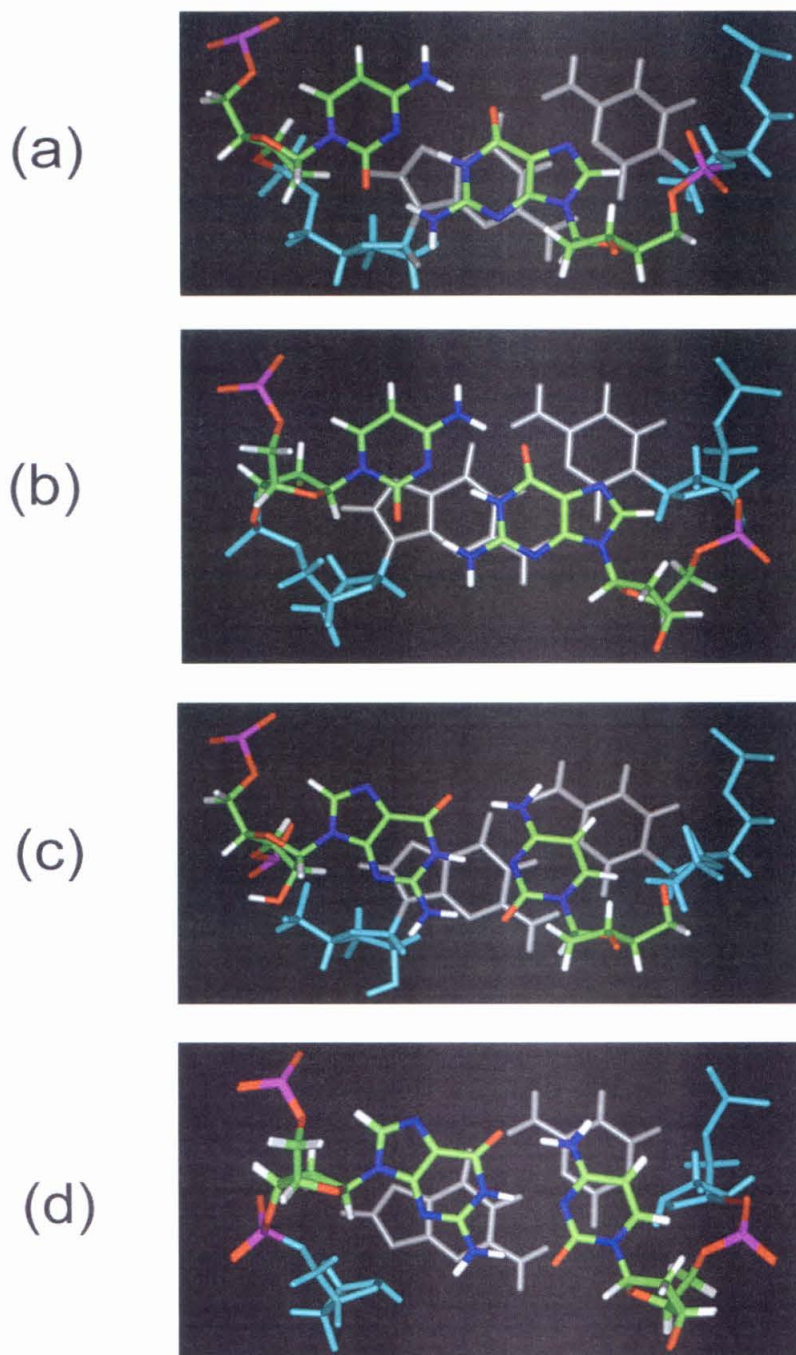


**Figure 3.6.** Selected ideal dinucleotide base overlaps in A-form and B-form nucleic acids. The 5' base and sugar are colored by atom type, and the 3' 'underlying' base is colored light blue for the sugar and gray for the base. Views are directly down the helical axis. (a) A-form 5'-CG-3', (b) B-form 5'-CG-3', (c) A-form 5'-GG-3', (d) B-form 5'-GG-3'.

### 3.3.5. Analysis of Base-Base Overlaps in RNA/DNA and DNA/DNA Duplexes.

Using the InsightII program to generate the structures of idealized dinucleotides, we calculated the base-base overlaps that occur in different canonical duplexes (Table 3.2). It is important to note that these dinucleotides only represent static snapshots of idealized configurations for nucleic acids in solution. Further, our calculations of these overlaps give preference to the occlusion of the ring systems, as the stick bonds used trace the shortest line, and presumably the highest electron density, between atom centers. In heteroaromatic bases of nucleic acids, this assumption in effect biases the overlap calculations, not towards simple van der Waals contacts, which are clearly present between the bases in all the dinucleotides, but towards the ability of these ring systems to stack with their  $\pi$ -clouds overlapping.

As is evident in Table 3.2, purine-purine (R-R) steps are extremely well stacked, with typical intrastrand overlaps of their aromatic rings greater than 1/4 of the surface area. In the case of RNA/DNA duplexes, the overlap of each of the purines in the R-R step is even greater with typical values of ~40%. Purine-pyrimidine (R-Y) steps show intrastrand overlaps comparable to those for R-R steps on the purine base, but with even greater coverage (exceeding 50% of the surface area in some cases) for the pyrimidine base. Pyrimidine-pyrimidine (Y-Y) junctions in all cases show minimal to no overlap. Most interestingly, however, pyrimidine-purine (Y-R) steps, which in DNA/DNA duplexes show no overlap, show appreciable *intrastrand* overlap between the guanines on opposite strands when in an idealized A-form RNA/DNA duplex. Two base steps, 5'-CG-3' and 5'-GG-3' are shown in Figure 3.6 in both A-form and B-form conformations.

## 3.4 DISCUSSION

The ability of photooxidants to damage guanine at a distance by long range charge transport in ribose-containing nucleic acids is governed by three separate factors. First, radical injection must occur efficiently. Second, this generated radical



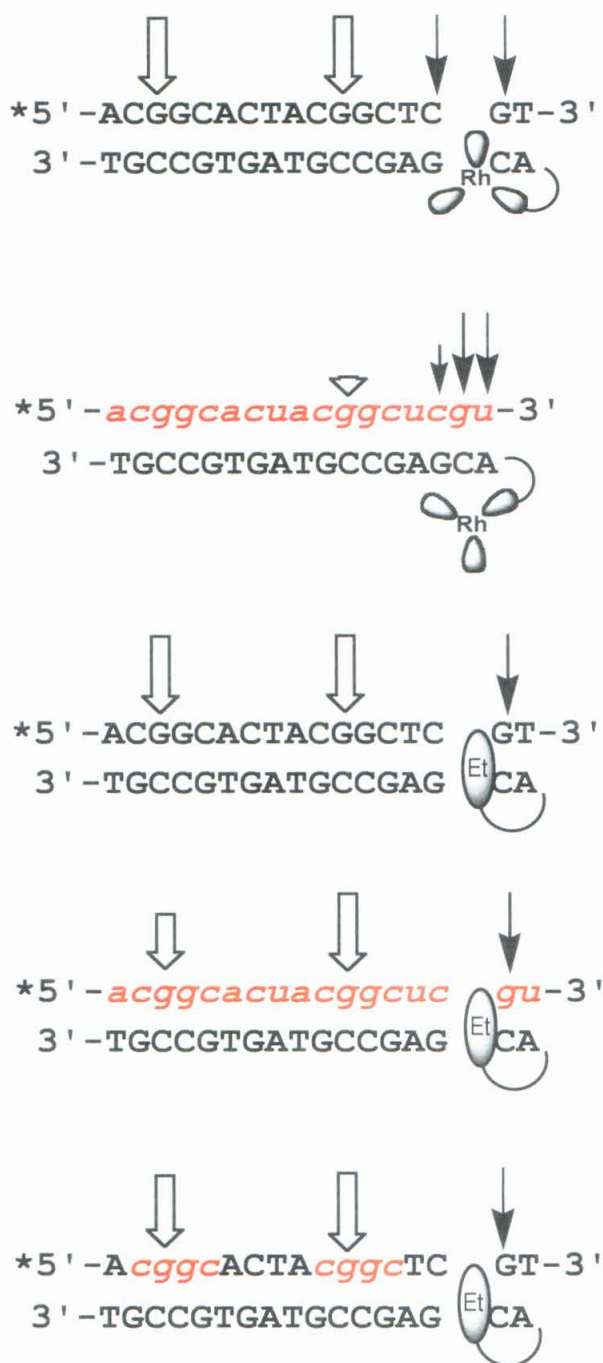


**Figure 3.7.** Schematic illustration of the oxidative and direct damage seen in each duplex investigated here. Hollow arrows indicate long range guanine damage from radical migration. Black arrows indicate sites of direct damage from either hydrogen abstraction (in the rhodium complex case) or direct base reaction (with ethidium).

timescale of the radical lifetime, and a lesion must be formed that can be visualized by chemical or biochemical means. Figure 3.7 summarizes the results obtained; the experiments conducted in this study provide considerable information about the relationship of nucleic acid conformation and identity to all three factors.

#### 3.4.1. *Efficient Radical Injection is a Prerequisite for Long Range Charge*

*Transport.* Clearly, without efficient radical injection into the base stack, charge transport is not possible. The differing ability of ethidium and  $[\text{Rh}(\text{phi})_2\text{bpy}]^{3+}$  to induce guanine oxidation at a distance when conjugated to duplexes of the same sequence demonstrates this dependence. Previous studies investigated the guanine oxidation that occurs in DNA duplexes conjugated to ethidium, and the results here for DNA-GG coupled to ethidium are, as expected, in line with previous reports, including the damage yield and partition ratios between sites (Table 3.1). In RNA-GG with covalently tethered ethidium, long range charge transport occurs to the same locations as in DNA-GG and with roughly the same yield (Figure 3.2 and Table 3.1), unambiguously demonstrating efficient radical injection. The similarity in yield is consistent with the fact that ethidium is an efficient and well-coupled organic photooxidant with different nucleic acid conformations. The facile intercalation and high affinity binding of ethidium in both A-form and B-form nucleic acids means that, upon photoirradiation, this intercalator can efficiently inject a radical into the base stack, regardless of the stacking orientation and sugar conformation(s).

In contrast, the irradiation of similar duplexes, but with  $[\text{Rh}(\text{phi})_2\text{bpy}]^{3+}$  covalently tethered to the end of the duplex in place of ethidium, affords considerably different results. In normal B-form DNA, 313 nm irradiation of phi complexes of rhodium cleaves DNA backbone sugars at intercalative binding sites *via* direct hydrogen abstraction from the sugar ring.<sup>62</sup> Using this convenient photochemistry to mark the sites of binding for these assemblies, it is evident that the metal complex is bound to the top of the duplex when the second strand is RNA. Photoirradiation of  $[\text{Rh}(\text{phi})_2\text{bpy}]^{3+}$  tethered DNA

duplexes at 365 nm leads to injection of a high energy radical into the base stack. Migration of this charge, and subsequent localization onto an oxidatively sensitive site causes irreversible lesions that can be revealed with hot base treatment. In DNA-GG, photoirradiating this duplex at 365 nm affords roughly equal partitioning of oxidative damage between the proximal and distal sites. In contrast, RNA-GG, when tethered to  $[\text{Rh}(\text{phi})_2\text{bpy}]^{3+}$ , shows almost no oxidative damage at the 5'-gg-3' sites that were strongly damaged at a distance by photoexcited ethidium (Figure 3.3). The low yield of guanine oxidation at a distance in RNA-GG, despite appreciable damage at the site of metal complex binding, is probably due to covalently tethered  $[\text{Rh}(\text{phi})_2\text{bpy}]^{3+}$  groove binding non-intercalatively. This type of binding is more driven by simple charge affinity than by stacking interactions and shape selection. The metal complex is not tightly stacked between the bases in the case of RNA-GG because it cannot fit into the narrow major groove associated with A-like conformation of the nucleic acid, in contrast to the wide major groove of B-form duplex DNA. The reaction of the groove bound rhodium complex may be favored in tethered assemblies; it was not seen in previous studies of this metal complex when noncovalently bound to tRNA.

#### *3.4.2. Propagation of Charge Through the Base Stack and Radical Trapping.*

Estimates of the charge transport efficiency, once a radical is successfully introduced into the base stack, can be made by comparing the distal versus proximal ratios of guanine oxidation. This ratio is determined by the ability of a charge to migrate through the base stack between the two sites, and directly reflects the capacity for a nucleic acid to act as a bridge for radical migration. In addition, the ratio of the direct damage caused by ethidium at its site of intercalation to the damage seen at oxidatively sensitive sites located a distance from the binding site of the photooxidant can also be calculated and used to determine absolute yields. Notably, this estimate of absolute yield assumes that radical trapping is comparable between RNA and DNA strands. Our data suggest that this assumption is correct, based on the high levels of long range guanine oxidation that

occurs with ethidium coupled RNA-GG, and the similarities between the RNA and DNA distal/proximal ratios and overall yield of oxidative damage. Although this supposition appears to be valid for RNA-GG and DNA-GG for the reasons outlined, CNA-GG duplexes appear to be less specifically damaged at the ethidium intercalation site. This lower level of damage may represent a conformation at the binding site that is less favorable towards direct reaction.

Distal/proximal ratios can be calculated for each of the ethidium tethered constructs, DNA-GG, RNA-GG, and CNA-GG. As expected, the ethidium tethered DNA-GG has a partition ratio of equality, within error bars. Notably, ethidium tethered RNA-GG, which contains a second strand of purely ribonucleic acid, shows slightly more damage at the proximal guanine doublet than does its ethidium tethered DNA-GG counterpart. Taking into account the uncertainty defined by the error bars in this series of experiments, RNA-GG has a somewhat lower distal/proximal ratio compared to DNA-GG. These data suggest that RNA is a viable conduit for charge transport but perhaps poorer than the B-form DNA duplex. Certainly the closeness of the ratios suggests that the stacking interactions in the core of the duplex are more important to radical migration than the identity of the sugar and subsequent global conformation of the assembly. Not unexpectedly, the distal to proximal ratio for CNA-GG is between that of RNA-GG and DNA-GG. It seems likely that the base stack of CNA-GG may have more B-form character than that of RNA-GG.

The absolute yield of charge migration can be estimated by normalizing the guanine oxidation that occurs remotely at the distal site to the direct damage induced by photoexcited ethidium at its binding site, as described above. Taking the ratio of the distal doublet to the direct damage as a benchmark measure, covalently bound ethidium is seen in both RNA-GG and DNA-GG to be a very efficient photooxidant. Typically, guanine doublets located distal to the site of intercalation show approximately 30% of the guanine oxidation that occurs by direct contact with photoexcited ethidium. Thus, a

significant percentage of the radicals introduced into the base stack by photoexcited ethidium, when either DNA or RNA is the complementary strand, migrate to a remote site and are irreversibly trapped. The absolute yield of long range guanine oxidation, however, is negligible when the rhodium intercalator is used as a photooxidant in RNA-GG. This diminution, as discussed above, is most likely the result, not of an inability of the nucleic acid to transport charge, but of poor electronic coupling between the metallointercalator and the RNA-GG base stack.

*3.4.3. Effect of Ribose•Deoxyribose Junctions on Electron Transfer.* Ethidium tethered CNA-GG shows damage at a distance after photoirradiation. Interestingly, however, the site of intercalation is less damaged in CNA-GG by direct reaction with ethidium than it is in either RNA-GG or DNA-GG. The direct trapping of the radical at the binding site in CNA-GG may follow a different mechanism to that operative in RNA-GG or DNA-GG, or possibly the same mechanism has an appreciably lower yield. This low yield for the direct reaction precludes discussion of absolute yields in CNA-GG constructs, as without a reliable value for the direct damage, it is impossible to estimate the amount of intercalative binding by ethidium, and to relate this value to damage at a distance.

Previous research that introduced a single ribose sugar in an otherwise entirely DNA duplex can induce an entire duplex to assume an A-like conformation in the solid state,<sup>63,64</sup> but solution studies using NMR suggest somewhat more complicated conformations with deoxyribose sugars assuming a more B-like structure and ribose regions tending to A form.<sup>52</sup> Hence, CNA-GG may have a structural junction between regions of ribose versus deoxyribose sugars, but the overall stacking of the duplex bases is expected to be continuous. Clearly, the distal to proximal ratio demonstrates efficient charge migration to remote sites of oxidative sensitivity in this chimeric duplex.

*3.4.4. Comparison with Previous Studies.* Our results provide an interesting comparison and contrast to the damage on DNA strands of mixed oligonucleotides

reported previously.<sup>57</sup> Previous research showed that oxidative damage partitioned roughly equally between sites distal and proximal to a covalently linked anthraquinone when oligonucleotides were between A and B form. However, the absolute yield was decreased greatly, and the 5'-guanines of 5'-GG-3' doublets were no longer the most sensitive oxidatively. The low yield was attributed to trapping effects, and further experiments increasing the temperature and, thus, B-form characteristic of the hybrid duplexes seemed to increase the overall yield of oxidative damage. Presumably, the trapping of the generated guanine radical was greatly improved with increasing B-form character of the constructs. Indeed, in the most A-like structures previously investigated, no long range oxidative damage at all was seen in homosaccharide RNA/DNA duplexes on the DNA strands. No measure of anthraquinone binding was however provided for normalizing the reactions.

In contrast to the above described yield decrease, our duplexes show comparable yields of oxidative damage, as estimated based on ratios to the direct damage at the intercalation site. The partitioning of radical damage between oxidative sites in our duplexes, like those seen previously, seems to be largely independent of the sugar composition of the oligonucleotide. However, when in an entirely RNA/DNA hybrid duplex, long range charge transport and its trapping at susceptible guanines *on the RNA strand* seems to be almost identical in magnitude as for B-form DNA/DNA duplexes of the same base sequence. Similar experiments in previous studies that focused on the damage on the DNA strand of an RNA/DNA hybrid found considerably reduced yields at oxidatively sensitive guanine sites.<sup>57</sup>

Furthermore, RNA/DNA hybrids here display oxidative damage patterns on the RNA strand that are equivalent to those found when purely DNA/DNA hybrids are used. Other researchers have suggested that RNA/DNA hybrids, at least on the DNA strand bearing a photooxidant, lose the hallmark damage at the 5' guanine in 5'-GG-3' doublets. This may indeed occur in the DNA strand of hybrids, but the 5'-guanines in guanine

doublets on an RNA strand seem to retain their preferred oxidative susceptibility when in RNA/DNA hybrids.

*3.4.4. Radical Migration and Base Overlap.* In order to explore theoretically whether long range coupling through the stacked aromatic heterocycles of A-form nucleotides was feasible, molecular modeling was also used to estimate the overlap of idealized A-form RNA/DNA hybrid dinucleotides, and B-form DNA duplex dinucleotides. Although we found that the base-base overlaps on the whole were quite comparable, there were notable differences, as illustrated in Figure 3.6. Most importantly, B-form DNA has minimal interstrand overlap between the hydrogen bonded bases between the two separate molecules that make up the duplex. In contrast, in A-form nucleotides, significant *interstrand* base overlap is found in a number of cases, notably between the adjacent guanines in 5'-CG-3' steps (Figure 3.6A). Comparison of this base step, generated as an idealized A-form RNA/DNA hybrid, to its B-form analog shows that the same 5'-CG-3' step in standard conformation has negligible interstrand overlap between the neighboring guanines.

One implication of this interstrand overlap not directly explored here is the possibility that long range charge transfer, which is sensitive to stacking and also is strand specific in B-form DNA, may equilibrate between the two duplex strands when they are in conformations that approach the A-form. The potentially greater electronic coupling between the two strands could significantly change the pathway by which radicals propagate through the base stack. Previous results have posited that in duplex B-form DNA, charge migration favors the stack into which it is introduced. In fact, a difference of three orders of magnitude in rate was evident in comparing interstrand base-base electron transfer to intrastrand electron transfer. The results here suggest that this predilection may not hold in A-like conformations. Indeed, it is possible that ribose-containing nucleic acids may show a somewhat steeper distance dependence, as suggested by the proximal to distal ratios discussed earlier, due to the diffusion of the

*migrating radical* into the second strand. Any damage that occurred on the second strand to remove the radical would be undetectable by our methodology.

An equally important issue raised here is the relative susceptibility of guanine doublets towards oxidation in duplexes between A-form and B-form conformations. Again, in computer modeling of guanine doublets, the overlap seen between neighboring intrastrand guanines was quite significant in both A-form and B-form. However, the precise alignment of the two conformations differed somewhat (Figure 3.6C and 3.6D). Because of this, it is possible that the oxidation potentials are not equivalent in these two cases; however, it is clear that guanine doublets, experimentally, are found to be the most sensitive sites for oxidative damage on the RNA strand of RNA/DNA hybrids, as well as in B-form, duplex DNA. This suggests that even if the exact trapping mechanism is different between these two cases, the rate of trapping appears to be quite comparable between a B-form DNA strand and a more A-form RNA strand annealed to identical ethidium tethered DNA strands. Otherwise, the yields at the guanine doublets between different nucleic acid conformations would vary greatly, as previously reported for the DNA strand of RNA/DNA hybrids.

Our finding that mixed nucleotides can support radical migration efficiently is consistent with the effective stacking found in idealized A-form constructs. Hence, consistent with previous results, it appears that the most critical parameter that determines electronic coupling is the ability for the bases' aromatic surfaces to stack regularly and well, though the overall conformation of the sugar backbone and the three dimensional location and orientation of the base strands can vary quite widely.

**3.4.5. Conclusions.** In summary, RNA/DNA hybrids can act as conduits for long range electron transfer, comparable to DNA/DNA counterparts of an identical sequence. Hence, it is possible that oxidative damage can occur at a distance when a radical is introduced on the RNA strand generated by DNA-to-RNA transcription, polymerase priming, and Okazaki extensions. The results described here underscore the inherent



tendency for well-stacked nucleic acids to act as bridges for charge migration, regardless of the identity of the sugars. Remarkably, the overall yield and oxidative behavior of ribose containing nucleotides is extremely similar to that found in duplexes entirely composed of DNA, reflecting the significant pairwise stacking in RNA-containing duplexes.

---

### 3.5 REFERENCES

- 1) Núñez, M. E., Hall, D. B., Barton, J. K. *Chem. Biol.* **6**, 85-97 (1999).
- 2) Giese, B. *Acc. Chem. Res.* (2000), **33**, 631-636.
- 3) Giese, B., Meggers, E., Wessely, S., *et al.* *Chimia* (2000) **54**, 547-551.
- 4) Núñez, M. E., Barton, J. K. *Curr. Op. Chem. Biol.* (2000) **4**, 199-206.
- 5) Schuster, G. B. *Acc. Chem. Res.* (2000), **33**, 253-260.
- 6) Lewis, F. D., Liu, X. Y., Liu, J. Q., *et al.* *J. Am. Chem. Soc.* (2000) **122**, 12037-12038.
- 7) Lewis, F. D., Liu, X. Y., Liu, J. Q., *et al.* *Nature* (2000) **406**, 51-53.
- 8) Hall, D. B., Holmlin, R. E., Barton, J. K. Oxidative DNA damage through long-range electron transfer. *Nature* (1996) **382**, 731-735.
- 9) Porath, D., Bezryadin, A., de Vries, S., Dekker, C. *Nature* (2000) **403**, 635-638.
- 10) Fink, H. W., Schonenberger, C. *Nature* (1999) **398**, 407-410.
- 11) Wan, C., Fiebeg, T., Kelley, S. O., Treadway, C. R., Barton, J. K., Zewail, A. H. *Proc. Natl. Acad. Sci. USA* (1999) **96**, 6014-6019.
- 12) Holmlin, R. E., Dandliker, P. J., Barton, J. K., *Angew. Chem. Int. Ed. Engl.* (1997) **36**, 2714.
- 13) Ames, B. N., Shigenaga, M. K., Hagen, T. M. *Proc. Natl. Acad. Sci. USA* (1993) **90**, 7915-7922.
- 14) Piette, J. J. *Photochem. Photobiol. B* (1991) **11**, 241-260.
- 15) Simon, M. I., Vunakis, H. V. *J. Mol. Biol.* (1962) **4**, 488-499.

- 16) Storhoff, J. J., Mirkin, C. A. *Chem. Rev.* (1999) **99**, 1849-1862.
- 17) Li, X., Yang, X., Qi, J., Seeman, N. C. *J. Am. Chem. Soc.* (1996) **118**, 6131-6140.
- 18) Mao, C., Sun, W., Shen, Z., Seeman, N. C. *Nature* (1999) **397**, 144-146.
- 19) Winfree, E., Liu, F., Wenzler, L. A., Seeman, N. C. *Nature* (1998) **394**, 539-544.
- 20) Yang, X., Wenzler, L. A., Qi, L., Li, X., Seeman, N. C. *J. Am. Chem. Soc.* (1998) **120**, 9779-9786.
- 21) Saenger, W. *Principles of Nucleic Acid Structure*, Springer-Verlag: New York, 1984.
- 22) Dickerson, R. E. *Structure, Motion, Interaction, and Expression of Biological Macromolecules* (1998) 17-36.
- 23) Dickerson, R. E. *Nucleic Acids Res.* (1998) **26**, 1906-1926.
- 24) For a brief overview, see *Bioorganic Chemistry: Nucleic Acids*, edited by Hecht, S. M. New York : Oxford University Press (1996).
- 25) Sugiyama, H., Saito, I. *J. Am. Chem. Soc.* (1996) **118**, 7063-7068.
- 26) Burrows, C., Muller, J. G. *Chemical Reviews* (1998) **98**, 1109-1152.
- 27) Núñez, M. E., Rajski, S. R., Barton, J. K. *Meth. Enzymol.* (2000) **319**, 165-188.
- 28) Hall, D. B., Kelley, S. O., Barton, J. K. *Biochemistry* (1998) **37**, 15933-15940.
- 29) Ly, D., Kan, Y., Armitage, B., Schuster, G. B. *J. Am. Chem. Soc.* (1996) **118**, 8747-8748.
- 30) Breslin, D. T., Schuster, G. B. *J. Am. Chem. Soc.* (1996) **118**, 2311.
- 31) Ito, K. *J. Biol. Chem.* (1993) **268**, 13221-13228.
- 32) Núñez, M. E., Noyes, K. T., Gianolio, D. A., McLaughlin, L. W., Barton, J. K. *Biochemistry* (2000) **39**, 6190-6199.
- 33) Beratan, D. N., Priyadarshy, S., Risser, S. M. *Chem. Biol.* (1997) **4**, 3-8.
- 34) Bixon, M., Jortner, J. *J. Phys. Chem. B* (2000) **104**, 3906-3913.
- 35) Bixon, M., Giese, B., Wessely, S., Langenbacher, T., Michel-Beyerle, M. E., Jortner, J. *Proc. Natl. Acad. Sci. USA* (1999) **96**, 11713-11716.
- 36) Berlin, Y. A., Burin, A. L., Ratner, M. A. *J. Phys. Chem. A* (2000) **104**, 443-445.

- 37) Felts, A. K., Pollard, W. T., Friesner, R. A. *J. Phys. Chem.* (1995) **99**, 2929-2940.
- 38) Henderson, P. T., Jones, D., Hampikian, G., Kan, Y., Schuster, G. B. *Proc. Natl. Acad. Sci., USA* (1999) **96**, 8353-8358.
- 39) Williams, T. T., Odom, D. T., Barton, J. K. *J. Am. Chem. Soc.* (2000) **122**, 9048-9049.
- 40) Wan, C., Fiebig, T., Kelley, S. O., Treadway, C. R., Barton, J. K., Zewail, A. H. *Proc. Nat. Acad. Sci. USA* (1999) **96**, 6014-6019.
- 41) Hall, D. B., Barton, J. K. *J. Am. Chem. Soc.* (1997) **119**, 5045-5046.
- 42) Kelley, S. O., Boon, E. M., Barton, J. K., Jackson, N. M., Hill, M. G. *Nucleic Acids Res.* (1999) **27**, 4830-4837.
- 43) Boon, E. M., Ceres, D. M., Drummond, T. G., Hill, M. G., Barton, J. K. *Nature Biotech.* (2000) **18**, 1096-1100.
- 44) Rajski, S. R., Barton, J. K. *J. Am. Chem. Soc.* (1999) **121**, 5615-5616.
- 45) Rajski, S. R., Barton, J. K. *J. Biomol. Struct. Dynamics* (2000) **11**, 285-295.
- 46) Kan, Y., Schuster, G. B. *J. Am. Chem. Soc.* (1999) **121**, 10857-10864.
- 47) Kan, Y., Schuster, G. B. *J. Am. Chem. Soc.* (1999) **121**, 11607-11614.
- 48) Núñez, M. E., Noyes, K. T., Gianolio, D. A., McLaughlin, L. W., Barton, J. K. *Biochemistry* (2000) **39**, 6190-6199.
- 49) Kelley, S. O., Barton, J. K. *Science* (1999) **283**, 375-380.
- 50) Kelley, S. O., Barton, J. K. *Chem. Biol.* (1998) **5**, 413-418.
- 51) Roberts, R. W., Crothers, D. M. *Science* (1992) **258**, 1463-1470.
- 52) Salazar, M., Fedoroff, O. Y., Miller, J. M., Ribeiro, N. S., Reid, B. R. *Biochemistry* (1993) **32**, 4207-4215.
- 53) Gyi, J. I., Conn, G., Lane, A. N., Brown, T. *Biochemistry* (1996) **35**, 12538-12548.
- 54) Gyi, J. I., Lane, A. N., Conn, G., Brown, T. *Nucleic Acids Res.* (1998) **26**, 3104-3110.
- 55) Lesnick, E. A., Freier, S. M. *Biochemistry* (1995) **34**, 10807-10815.

- 56) Wang, A., Fujii, S., van Boom, J. H., van der Marel, G. A., Boeckel, S. A. A., Rich, A. *Nature* (1992) **299**, 601-604.
- 57) Sartor, V., Henderson, P. T., Schuster, G. B. *J. Am. Chem. Soc.* (1999) **121**, 11027-11033.
- 58) Holmlin, R. E., Dandliker, P. J., Barton, J. K. *Bioconjugate Chem.* (1999) **10**, 1122-1130.
- 59) Olmstead, J., Kearns, D. R. *Biochemistry* (1977) **16**, 3647-3654.
- 60) Lim, A. C., Barton, J. K. *Biochemistry* (1993) **32**, 11029.
- 61) Chow, C. S., Barton, J. K. *J. Am. Chem. Soc.* (1990) **112**, 2839.
- 62) Sitlani, A., Barton, J. K. *Biochemistry* (1994) **33**, 12100.
- 63) Egli, M., Usman, N., Zhang, S., Rich, A. *Proc. Natl. Acad. Sci. USA* (1992) **89**, 534-548.
- 64) Egli, M., Usman, N., Rich, A. *Biochemistry* (1993) **32**, 3221-3227.

## **CHAPTER 4**

### **Long Range Charge Transport in DNA Double Crossover Assemblies\***

\*Adapted from D.T. Odom, E.A. Dill, J.K. Barton. *Chemistry and Biology* **7** (2000) 475-

## 4.1 INTRODUCTION

The discovery and exploitation of molecular assemblies for the fabrication of nanoscale devices have been the focus of increasing attention. In this context, one polymeric structure of particular interest has been DNA. Molecular arrays constructed with DNA offer promise because of (i) the ability of DNA to self assemble; (ii) the inherent programmability of DNA through sequence; and (iii) its resistance to degradation.

Multiple-stranded DNA assemblies have been formed to yield micro- and mesoscale structural and functional arrays. In particular, DNA double crossover (DX) assemblies have been used to construct a nanoscale fluorescent signaling device.<sup>1</sup> These DX assemblies are composed of a collection of semi-complementary strands annealed into one supermolecule that has two coaxial and connected, but spatially separated, base stacks. Two common types of DX assemblies are shown in Figure 4.1. Initial experiments using semi-complementary strands to construct these DX assemblies understandably focused on characterization and classification of different possible conformers and architectures.<sup>2,3</sup> The DX assembly is more rigid than canonical duplex DNA, as demonstrated by its resistance to circularization by ligation, and this rigidity permits the self-assembly of structures that have visible regularity over micrometer distances.<sup>4,5</sup> Other studies have focused on the use of DNA architecture as a template for metal deposition,<sup>6-9</sup> thus suggesting the use of DNA as an easily removed template for forming submicroscale wires a few atoms thick. Studies of DNA conductivity and of long range charge transport through double

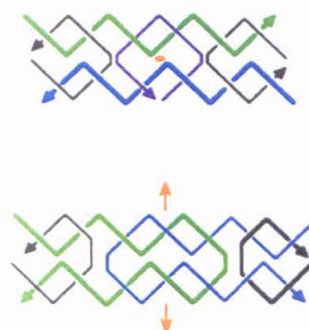


**Figure 4.1.** Two types of DNA double crossover assemblies commonly used. The top picture is of a double crossover, anti-parallel, even number of half turns between junctions (DAE); the bottom is the odd number of half turns between junctions (DAO). Gold dots and arrows indicate symmetry axes.

helical DNA have also been carried out. On the basis of conductivity measurements, the DNA duplex has been suggested to have properties of either a large or small band gap semiconductor, and these results have prompted speculations about DNA being exploited as a quantum wire in nanoscale electronic devices.<sup>12-14</sup>

With respect to DNA-mediated charge transport, perhaps most clearly established thus far is that charge transport through DNA can promote oxidative damage to guanine bases from a remote site.<sup>15-18</sup> In assays of oxidative DNA damage from a distance, the effects of intervening bulges,<sup>19</sup> of DNA-binding proteins,<sup>20</sup> and of variations of sequence and length<sup>21</sup> have been examined. Mechanisms proposed to describe this damage include hole hopping,<sup>22</sup> phonon-assisted polaron formation,<sup>23</sup> and tunneling.<sup>24</sup> Whether long range oxidative damage is an issue of physiological importance within the cell has yet to be determined.

This combination of interests in the DNA double helix as an electronic entity and as an architecture in nanoscale devices prompted us to examine charge transport through DX DNA assemblies. The potential application of DNA in nanoscale electronic devices would require the tight packing of helices in arrays controlled by sequence. Is charge transport efficient under these conditions? Do DX assemblies generate sufficiently well-stacked base pair arrays to promote charge transport? Moreover, are such base pair stacks electronically insulated from each other? Undesired crosstalk among circuits could completely abrogate the size advantages obtained by using these molecules as assembly units.

The exploration of electronic interactions between tightly packed helices is important to consider also in the context of understanding aspects of radical damage to DNA within the cell. The extremely tight packing of DNA either on a surface or in large scale, covalent arrays offer an interesting parallel to the structures found in genomic, packaged DNA. To prevent irreversible tangling of the chromosomes, these linear supermolecules are extensively wrapped into coiled coils on histones, which themselves

are assembled into higher levels of organization in chromatin.<sup>25</sup> Due to the limited nuclear volume of eukaryotic cells, the manipulation of and access to each layer of packaging is rigorously orchestrated to allow the highest possible density of the DNA helices. The resultant close proximity of many otherwise quite distant strands suggests that free radical induced damage in DNA could conceivably migrate across sugar phosphate bonds, and thus into oxidatively sensitive locations quite distant from the point of introduction.

Here we examine charge transport through a DX DNA assembly. DX molecules with two spatially and electronically decoupled base stacks provide a model system for interstack electronic coupling in packed arrays. Our results indicate that these tightly packed base pair arrays provide a robust medium for charge transport. These observations suggest that DNA duplexes organized within chromosomes, or potentially tightly packaged and arrayed within a nanoscale device, would mediate charge transport directly through the base stack, precluding oxidative damage migration across sugar phosphate backbones and onto abutting helices. Thus, DNA may indeed represent a promising molecular medium for nanofabrication.

## 4.2 EXPERIMENTAL

*Oligonucleotide Preparation.* Oligonucleotides were synthesized using phosphoramidite chemistry on an ABI 392 DNA synthesizer with a dimethoxy trityl protecting group on the 5' end. Purification on a Rainin Dynamax C18 column by reverse phase HPLC on a Waters HPLC (25 mM  $\text{NH}_4\text{OAc}$ , pH 7, 5 to 25%  $\text{CH}_3\text{CN}$  over 30 minutes) was followed by deprotection in 80% acetic acid for 15 minutes. Following deprotection, the oligonucleotides were purified a second time on the same C18 column by reversed-phase HPLC (25 mM  $\text{NH}_4\text{OAc}$ , pH 7, 2 to 20%  $\text{CH}_3\text{CN}$  over 30 minutes) and were quantitated by UV-visible absorption spectroscopy on a Beckman DU 7400 Spectrophotometer using the following extinction coefficients for single-stranded DNA:



(260 nm,  $M^{-1}cm^{-1}$ ) adenine (A) = 15,000; guanine (G) = 12,300; cytosine (C) = 7,400; thymine (T) = 6,700.

Strands used were each radioactively labeled at the 5'-end using  $\gamma$ - $^{32}P$ -ATP and polynucleotide kinase, then treated with hot piperidine to remove latent oxidative damage and purified on a 20% denaturing polyacrylamide gel. DX molecules and duplexes were made by mixing equimolar amounts of strands to a final concentration of 10  $\mu$ M, and annealed in 50 mM Tris-Acetate 1 mM EDTA and 12.5 mM  $Mg(OAc)_2$  pH 7.4 (1xTAEMg) using a temperature gradient of 90°C to 5°C over 1.5 hours. DNA strands with attached rhodium metallointercalators were prepared as previously described<sup>36</sup> and purified on a Dynamax C4 column by reverse phase HPLC (50 mM  $NH_4OAc$ , pH 7, 2 to 15%  $CH_3CN$  over 45 minutes). Both stereoisomers were combined and used in experiments. Quantitation for rhodium-DNA conjugates was based on using the DNA extinction coefficient value calculated at 260 nm, as described.

*Characterization of DX Assemblies.* Annealing of DX assemblies with one strand  $^{32}P$  end-labeled allowed characterization by non-denaturing gel electrophoresis. 10% acrylamide gels polymerized with a running buffer of 1xTAEMg were run in the same buffer at 100 V for 3.5 hours with 10  $\mu$ L of the 10  $\mu$ M annealing solutions. Each of the five strands was separately labeled, separately gel purified as single strands, and then alternately annealed into 50  $\mu$ L aliquots of a solution of 10  $\mu$ M final concentration of each oligonucleotide used to form the DX assembly. Typical results afforded > 95% of a single parent band on non-denaturing gels that migrated at an identical location regardless of the radioactively labeled strand. This location was considerably more retarded than the location of a duplex DNA of a similar length run side by side with the DX assemblies.

In addition, every experiment was performed with covalent Rh-DNA conjugates, noncovalently added  $[Rh(DMB)phi_2]^{3+}$ , and DX assemblies lacking any form of rhodium. The mismatch containing and the properly paired DX molecules and their corresponding

duplexes show moderate, relatively sequence neutral damage patterns identical to each other upon irradiation at 313 nm or 365 nm; this strongly suggests that assemblies containing double mismatches are in fact not in a distorted conformation.

*Photocleavage Reactions.* Photolysis reactions were performed in 1xTAEMg on 20  $\mu$ L samples using a 1000 W Hg/Xe lamp with a monochromator. Each sample irradiated at 313 nm was dried and resuspended into a volume of formamide loading buffer (determined by the sample radioactivity) to 10 kcts/ $\mu$ L. Samples irradiated at 365 nm and not irradiated (dark control) were dried, redissolved into 100  $\mu$ L of 10% piperidine in water, and heated to 90°C for 30 minutes. After drying *in vacuo*, these samples were resuspended into formamide loading buffer by radioactivity as above. Most of the samples required cold excess of the labeled strand to be added after irradiation and any chemical treatment but before redissolution into formamide to minimize reannealing of the highly stable double crossover assemblies. All 20% sequencing gels were run hot (>60°C). Samples in formamide were heated to 90°C for 5 minutes before being loaded immediately onto sequencing gels. Maxam-Gilbert sequencing reactions followed standard protocols.<sup>37</sup>

*Data Analysis.* Gels were exposed to Phosphorimager plates overnight and ImageQuant software was used to scan and analyze the collected data. Further data manipulations after band quantitation were performed in Microsoft Excel.

## 4.3 RESULTS AND DISCUSSION

*4.3.1. Design of DX Assembly to Probe Charge Transport.* A chemical assay now commonly employed to probe long range charge transport through DNA involves the construction of an assembly containing a photooxidant that is spatially well-separated from the DNA site being oxidized; the yield of long range ET is determined through measurements of oxidative damage,<sup>15</sup> as extensively discussed previously in this Dissertation. Figure 4.2 shows a representative assembly.

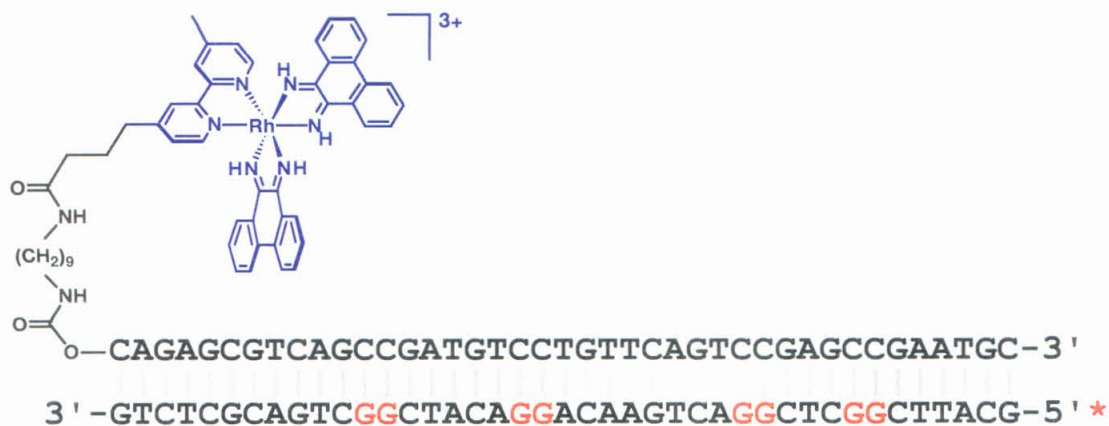


**Figure 4.2.** A schematic of a DNA duplex containing oxidatively sensitive 5'-GG-3' sites (in red) with a covalently attached derivative of  $[\text{Rh}(\text{phi})_2\text{DMB}]^{3+}$  (in blue). The 5'- $^{32}\text{P}$  label is also in red. Photolysis at 365 nm of the tethered rhodium complex intercalated in the duplex promotes oxidative damage to the 5'-G of guanine doublets by long range charge transport.

In these experiments, each B-DNA duplex is selectively functionalized on the 5' end of one strand with an intercalating photooxidant, here a phenanthrenequinone diimine (phi) complex of rhodium.<sup>15,21</sup> The complementary strand contains 5'-GG-3' sites, which are preferentially oxidized at the underlined guanine over any other sites. Empirical evidence and theoretical calculations<sup>26</sup> indicate that the oxidative potential of guanines in DNA is significantly lowered compared to other bases due to HOMO delocalization. When irradiated at 365 nm, although bound remotely, the photoexcited metallointercalator accepts an electron from the 5' guanine of a 5'-GG-3' pair in a reaction mediated by the base stack. The resultant guanine radical cation can either undergo recombination or, following deprotonation, be trapped irreversibly to form an oxidative lesion that is susceptible to strand cleavage by treatment with hot piperidine.<sup>15</sup> Irradiation of bound rhodium complex at 313 nm, in contrast, causes direct strand scission at sites of intercalation in duplex DNA by hydrogen atom abstraction from the sugar ring;<sup>27</sup> photolysis at this higher energy thus allows mapping of metal complex intercalation sites. We employ these photochemical assays here to conveniently monitor the path for charge transport.



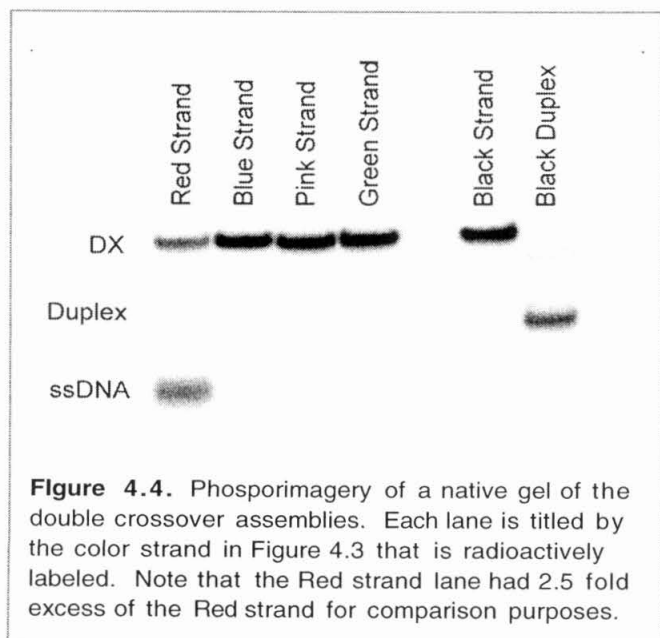
**Figure 4.3.** Sequences of DX assemblies containing the spatially separated photooxidant, the rhodium complex (as in Figure 2, gold in Figure 1), and guanine doublets or triplets to be oxidized (in bold). (a) Sequence and base pairing scheme for one DX assembly in which the location of the double mismatch is boxed in red; (b) Sequence and base pairing scheme for the DX molecule containing a longer second stack compared to that in (a) so as to rotate the most distal 5'-GGG-3' 180° from the orientation in (a).

An antiparallel double crossover assembly, containing an even number of helical half turns between junction overlap points, was therefore designed to have a pendant metalointercalator, in addition to well spaced guanine doublets on one base stack and guanine triplets on the second (Figure 4.3). Guanine triplets have been predicted to be oxidatively more sensitive than guanine doublets.<sup>28</sup> Our intent was to maximize sensitivity to potential oxidative damage on the base stack that is uncoupled to the tethered rhodium metalointercalator, while still allowing investigation of long range charge transport through the rhodium-bearing base stack.

The overall assembly contains five semi-complementary strands, two of which serve as “backbone” strands and permit easy comparison of duplex DNA to DX DNA by varying the complementary strand(s). The intercalator, which in B-form duplex DNA stacks deeply into the helix,<sup>29</sup> was tethered to the 5' end of one capping strand to permit intercalation into one base stack but not the other. In addition, we extended the length of the intercalated base stack six base pairs from the terminal end of the second, non-

metallated stack; molecular modeling indicated that this duplex elongation extends the metallintercalator well past the end of the second stack (Figure 4.3). Direct photocleavage reactions confirmed these intercalation restrictions experimentally (*vide infra*).

**4.3.2. Characterization of DX Assemblies.** Characterization of these assemblies, once synthesized using phosphoramidite chemistry and purified by HPLC and gel electrophoresis, was similar to that described previously, using gel shifts and chemical structural probes.<sup>2,30</sup> Figure 4.4 shows the gel shift of the double crossover, after annealing all five strands together. In addition, for each experiment, three separate sets of photoirradiations were performed simultaneously. In the first, covalent metal complex was used to investigate long range electron transport by injection of the radical cation into the base stack at a specific location. The second set of experiments used noncovalent metallointercalator. Photocleavage performed at 313 nm marked the preferred binding site(s) of the complex when it has unrestricted access to the base stack. Further, photoirradiations performed at 365 nm light verified the integrity of the base stack by showing that oxidation continued to cause damage at the 5' guanine of 5'-



GG-3' sites, despite the much larger assembly of strands in a double crossover. Finally, the double crossover assembly was irradiated in the complete absence of metal complex to verify that the assemblies were not unusually oxidatively sensitive in the absence of metallointercalator. A typical series of experiments is shown in Figure 4.5.

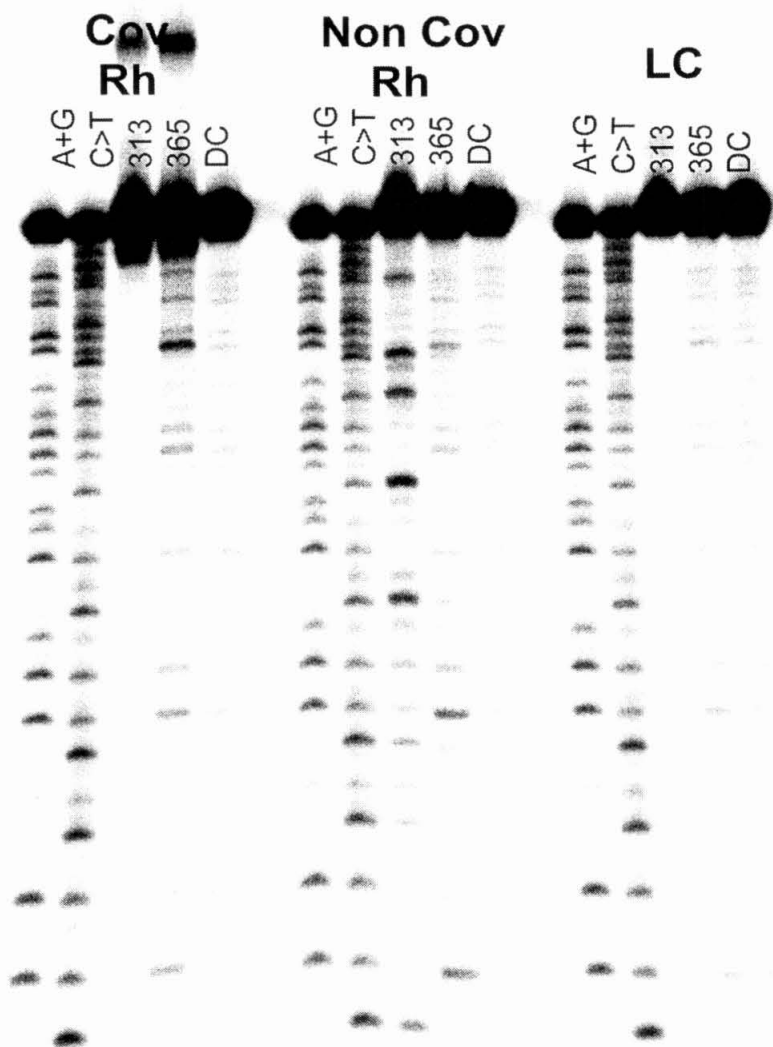


**Figure 4.5.** A typical experiment testing charge transport in DX assemblies. The left panel shows the results when a covalently tethered metal complex is photoirradiated. The center panel shows the effect of the same irradiations with noncovalently bound metal complex, and the right panel is the same irradiations with no rhodium. Maxam-Gilbert sequencing lanes are to the left of each panel.



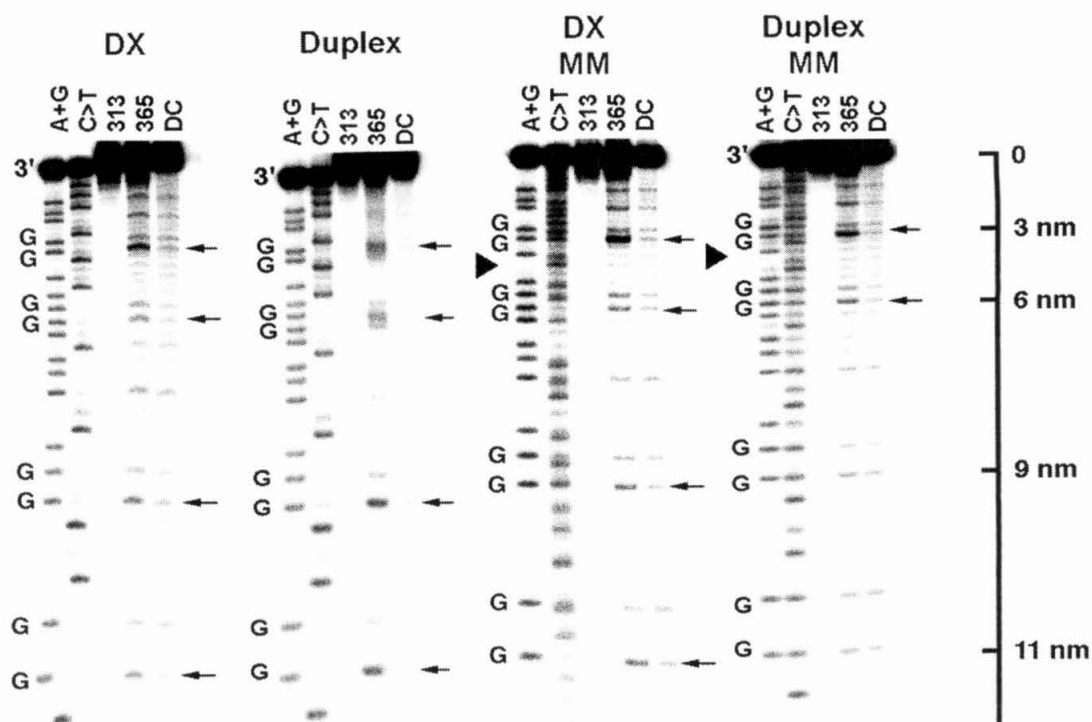


**Figure 4.6.** Long range oxidative damage in the intercalator-bound stack of the DX assembly and comparison to damage in duplex DNA and with mismatches. Shown is the phosphorimager after electrophoresis in a denaturing 20% polyacrylamide gel with 5'-<sup>32</sup>P- end-labeling of the strand complementary to the metalointercalator-tethered strand for (panels left to right): the DX DNA assembly shown in Figure 3a (navy strand labeled); the duplex DNA shown in Figure 2; the DX DNA assembly containing a double mismatch (red box in Figure 3a) and the duplex DNA counterpart with the double mismatch at the corresponding site. The mismatch sites are indicated by the solid triangle. Lanes for each panel correspond (left to right) to Maxam Gilbert A+G and C>T sequencing reactions, photolysis at 313 nm for 10 min, photolysis at 365 nm for one h followed by piperidine treatment, and the same labeled assembly without irradiation (dark control) followed by piperidine treatment.

The sites of potential oxidation upon irradiation at 365 nm are indicated by **GG** labels, and arrows highlight reaction at the 5'-G. Some background damage at purines is evident in dark control lanes, as a result of piperidine treatment. In addition, 365 and 313 nm lanes, though equal intensity by autoradiography, appear broader due to photocleavage at their intercalation sites. The DX assembly with or without an intervening double mismatch (MM) shows oxidative damage at the 5'-G of 5'-GG-3' sites up to 11 nm from the site of rhodium intercalation through long range ET. Approximate distances are marked on the right; these were determined based upon the number of bases separating the 5'-G site of oxidation and the rhodium intercalation site (established by 313 nm photocleavage) and assuming an interbase pair stacking distance of 3.4 Å. Substantial long range oxidative damage is evident also in the DNA duplex, but no significant oxidative damage above the control is apparent in the DNA duplex containing MM at sites 9 nm and 11 nm away from the metalointercalator.

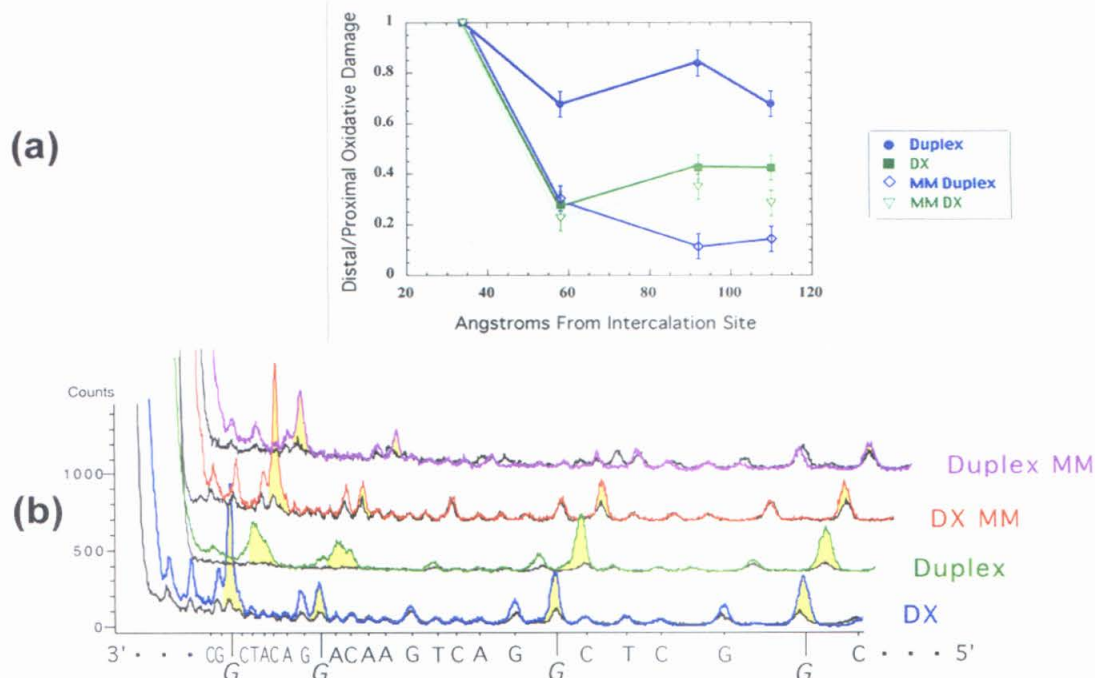


**Figure 4.7.** Quantitation of the gels shown in Figure 4.6. **(a)** Proximal to distal ratios of the oxidatively sensitive guanines normalized to the first proximal guanine as a function of distance. **(b)** Histograms made by linear scanning of the phosphoimager of samples after 365 nm irradiation (colors indicated to right) with corresponding dark controls (uniformly black) overlayed. The damage at 5'-G sites of guanine doublets above the control is highlighted by yellow shading.

**4.3.3. Charge Transport Down the Primary Stack of the DX Assembly.** An individual base stack, composed of four separate DNA strands, can serve as a conduit for long range charge transport. Radioactive labeling of the contiguous strand in the rhodium bound stack (navy strand in Figure 4.3) and photolysis of the DX assembly at 365 nm reveals significant oxidative damage at 5'-GG-3' doublets up to 11 nanometers from the site of intercalation, established by photolysis at 313 nm.

Figure 4.6 shows the results of photolysis experiments conducted on the assemblies shown in Figures 4.2 and 4.3. As evident in the 313 lane for the DX assembly, direct photocleavage is apparent only near the 3'-end of the labeled backbone strand; this appears here as a broadening of the parent bands with irradiation either at 313 or 365 nm. At higher gel resolution or using shorter oligonucleotides, this cleavage



maps directly to the intercalation site near the duplex terminus. Irradiation at 313 nm of DX assemblies alternately labeled on each strand, except for the rhodium-bearing strand that was not radioactively tagged, showed no damage.

Irradiation at 365 nm of the DX assembly shows oxidative damage at the 5'-G of guanine doublets. Long range damage is evident at guanine doublets located approximately 35, 54, 92, and 109 Å from the site of intercalation. In calculating the separation between the intercalator and the site of guanine damage, we assumed 3.4 Å interbase stacking distances. Some background damage at purines is also revealed upon piperidine treatment. The histogram shown in Figure 4.7, which includes an overlay of the lanes containing DX assemblies without irradiation at 365 nm but subjected to piperidine treatment (dark controls), clearly demonstrates significant damage over the controls at the 5'-G of the guanine doublets, the signature for electron transfer.

We can also compare reaction on the DX assembly to its duplex DNA counterpart. As with the DX assembly, its duplex counterpart shows long range damage at the 5'-G of guanine doublets upon irradiation at 365 nm. Some hyperreactivity is noteworthy at the site preceding the first crossover junction for the DX assembly but not for the duplex. This in effect reduces the distal to proximal ratios as seen in Figure 4.7a. Though the level of damage in the DX portion of the gel at the 5'-GG-3' closest to the rhodium complex compares well to that seen in the duplex strand visually, quantitation in Figure 4.7b, indicates that there is more damage at the proximal site in the DX case than in the case of the duplex. However, both systems show comparable damage at long range in the most distal sites.

As with duplex DNA, long range transport in the DX supermolecule occurs in an intra-molecular reaction. As in previous studies of long range damage,<sup>15,19,21</sup> no oxidative damage is seen on a radioactively labeled DX assembly that does not contain

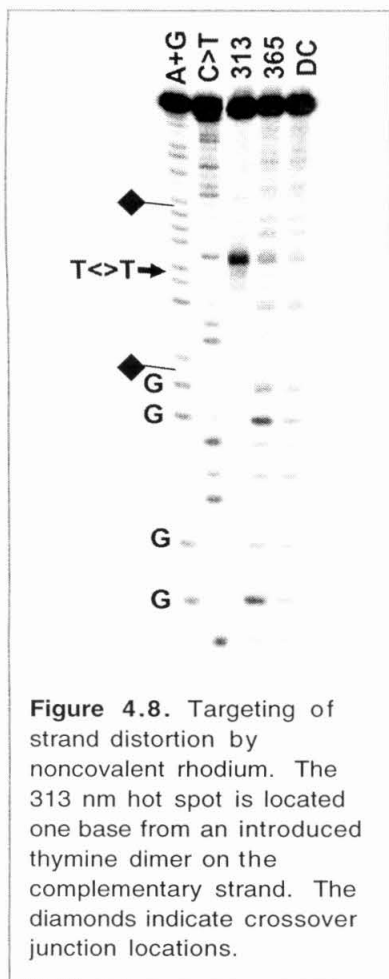
a pendant rhodium complex when incubated with an unlabeled DX bearing a covalently bound metallointercalator, even with twice the normal irradiation time (data not shown).

Thus, these data establish unambiguously that charge transfer proceeds down the  $\pi$ -stacked array of bases. The ability of the DX assembly to serve as a conduit for such long range transfer is in agreement with previous biochemical studies which suggest that the base stacking within the DX molecule is, in general, quite similar to that of B-form DNA.<sup>2</sup> However, our results further indicate that the DX base stack is *electronically* coupled over long range.

*4.3.4. Robust Charge Transport in the Presence of Mismatches.* Remarkably, DX assemblies act as more robust conduits for long range charge transfer than do their duplex counterparts. To test for the effects of stacking perturbations, we introduced mispairs into the assemblies (Figure 4.3, boxed in red). Previous experiments have noted that the presence of mismatches in DNA can completely abrogate long range charge transport.<sup>10,11</sup>

Here, introduction of a double mismatch into a DX assembly between the intercalator and the first of the two crossover junctions does not attenuate long range guanine oxidation down the intercalator-bearing stack at all (Figure 4.6). In contrast, the incorporation of the same double mismatch into identically base paired duplex DNA essentially eliminates long-range electron transfer past the mismatch, as expected. The damage at the most distal 5'-GG-3' in duplex DNA normalized to the proximal guanine oxidation site decreases sevenfold (average of 3 trials) upon introduction of the double mismatch, whereas in a DX assembly with these mismatches, the decrease is negligible (<10%) and within error bars of the experiment (Figure 4.7).

We considered whether the double mismatch within the DX assembly might significantly alter the structure of the DX assembly. As a test, here, as with the other DX assemblies examined, we irradiated the assembly at 313 nm in the presence of non-covalently bound  $[\text{Rh}(\text{DMB})\text{phi}_2]^{3+}$  (DMB = 4,4'-dimethyl 2, 2'-bipyridine) (not shown).



Hyperreactivity in direct photocleavage by this sequence-neutral metallointercalator would be expected to reveal any substantial alterations in structure.<sup>31</sup> Instead low levels of uniform cleavage with no unusual hot spots were observed after photoirradiation either at 313 nm or 365 nm. By comparison, introduction of a disruptive thymine dimer lesion into the core of a DX assembly using photoligation techniques<sup>32-34</sup> generated an intensely targeted hot spot when irradiated at 313 nm in the presence of noncovalent  $[\text{Rh}(\text{DMB})\text{phi}_2]^{3+}$  (Figure 4.8).

The double mismatch perturbation examined here is clearly more extreme than other disruptions that might be expected to occur during the routine application of a DX assembly in a nanoscale device. This experiment thus highlights the rugged character of the DX assembly. We suggest, based on the observations described here,

that the persistence of electronic coupling in this DX assembly is likely the result of tight packing of the sugar-phosphate backbones that dynamically constrains the nucleotides in the base stack.

**4.3.5. Insulation of Separate Base Pair Stacks in the DX Assembly.** Despite the tight packing of neighboring helices within a single DX molecule, the electronic structure of the two separate base stacks appears to be completely decoupled. Isotopic  $^{32}\text{P}$  end-labeling of the backbone strand that does not interact with covalently bound metal, (light blue strand, Figure 4.3) followed by 365 nm photolysis and piperidine treatment, afforded the same amount of damage at the 5'-GGG-3' triplets as the non-irradiated samples (Figure 4.9a). Moderate damage was found at the guanine triplet sites in this base stack

**Figure 4.9.** Test of cross coupling in ET between base stacks in the DX DNA assembly. Shown is the gel of the DX assembly shown in Figure 4.3 with 5'-<sup>32</sup>P-end-labeling of **(a)** the backbone strand (light blue in Figure 2a) opposite the rhodium bearing base stack with 5'-GGG-3' cassettes spaced evenly facing into the stack-stack contact surface, or **(b)** the contiguous strand on the same stack (light blue strand in Figure 2b) with one 5'-GGG-3' cassette rotated by 180° around the stack helical axis by insertion of a 5 bp spacer. Also shown in **(a)** and **(b)** is oxidative damage on the alternate stack with non-covalently bound rhodium complex. Within each panel, lanes are as in Figure 3, and almost all conditions are the same as Figure 3. Irradiations in **(b)** are doubled in duration. The sites of oxidation upon irradiation at 365 nm are indicated by **GGG** labels to the left of the gels.

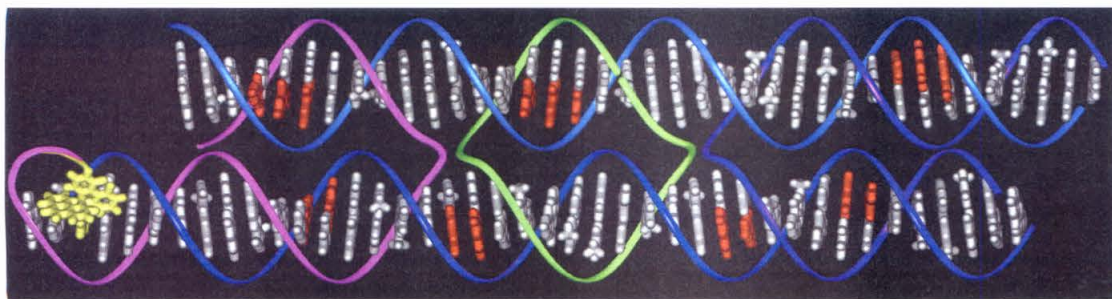


**Figure 4.10.** Molecular model of a DX assembly, emphasizing the base pair stacks. The base stack is shown in small space-filling display, whereas the sugar-phosphate backbone is portrayed as colored ribbons entwining the spatially distinct base stacks. The bottom stack has an appended rhodium metallointercalator that is constrained to intercalate specifically into the extended end of the lower base stack. Strands in this molecular model are colored as follows: top backbone, light blue; metallointercalator-bearing interstack, violet; core interstack, green; rightmost interstack, purple; bottom backbone, navy.

when irradiated at 365 nm with noncovalently added  $\text{Rh}(\text{DMB})\text{phi}_2^{3+}$ , most prominently in the guanine triplet located between the two crossover junctions. The locations of direct photocleavage reactions carried out at 313 nm on this strand were relatively sequence neutral, and entirely different than those seen in the 365 nm irradiation lanes.

Molecular modeling indicated that all three guanine triplets in this molecule are located at the interface between the two helices. In order to eliminate the possibility that the lack of damage observed at these sites was due to a closed orientation of the guanines, thus possibly making the oxidation sites inaccessible to irreversible trapping, another DX molecule with a guanine triplet shifted five base pairs down the duplex and therefore rotated by  $180^\circ$  was constructed (schematic in Figure 4.3b and molecular model in Figure 4.10). As with other DX molecules, strong oxidative damage was evident at the 5'-GG-3' sites on the stack into which the covalently attached rhodium complex was intercalated (not shown). However, the predicted sites of oxidative damage on the triplet-bearing base stack not containing the covalently attached metallointercalator are left completely undamaged after irradiation at 365 nm (Figure 4.9b). Like the shorter DX assembly, the longer DX assembly shows the most oxidative

damage at the core 5'-GGG-3' triplet when irradiated in the presence of non-covalently bound rhodium complex. The reactivity of the core guanine triplet persists despite the change in orientation afforded by the introduction of five additional base pairs between the core guanine triplet and the triplet 3' to it on the backbone strand.

Thus the lack of electronic communication between the two helices prevents the photoexcited metallointercalator, covalently bound to the first stack, from extracting an electron from the guanine triplets on the second stack. Indeed, the two stacks are not only spatially separated, as expected by molecular modeling of double crossovers, but the two base stacks within a DX molecule are also unique and insulated electronic entities.

A crystal structure of a single four way crossover junction was reported recently.<sup>35</sup> The electronic decoupling of the two stacks within the DX assembly is fully consistent with this structure; in the four way junction crystal structure, bases within the separate stacks are strictly localized to the stack to which they are canonically assigned, and do not show unexpected interhelix overlaps. These results bear also upon how damage may be directed within nucleosomes, where helices are closely and more rigidly packed than are DNA duplexes in solution. Radical damage that is introduced into systems such as the nucleosome or nanoscale DNA arrays would in essence be constrained to migration in a one-dimensional pathway—either upstream or downstream from the site of lesion introduction. Our results strongly suggest that radical migration within tightly packed arrays would be unable to jump helices, and thus would be limited to within approximately 100 linear base pairs.

## 4.4 CONCLUSIONS

DX DNA can therefore be applied both as a rugged and easily programmable nanomaterial and as an insulated charge conduit in long range signaling. In a DX assembly, the structure is determined by molecular recognition of complementary bases,



while the electronics are determined by stacking of the base pair array. The ability to construct spatially and electronically separate components in close proximity on a molecular scale therefore is feasible in DX assemblies through DNA synthesis.

---

## 4.5 REFERENCES

- 1) Mao, C., Sun, W., Shen, Z., Seeman, N.C. A nanomolecular device based on the B-Z transition of DNA. *Nature* **397**, 144-146 (1999).
- 2) Fu, T.-J., Seeman, N.C. DNA double crossover molecules. *Biochemistry* **32**, 3211-3220 (1993).
- 3) Li, X., Yang, X., Qi, J., Seeman, N.C. Antiparallel DNA double crossover molecules as components for nanoconstruction. *J. Am. Chem. Soc.* **118**, 6131-6140 (1996).
- 4) Winfree, E., Liu, F., Wenzler, L.A., Seeman, N.C. Design and self-assembly of two-dimensional DNA crystals. *Nature*. **394**, 539-544 (1998).
- 5) Yang, X., Wenzler, L. A., Qi, L., Li, X., Seeman, N.C. Ligation of DNA triangles containing double crossovers. *J. Am. Chem. Soc.* **120**, 9779-9786 (1998).
- 6) Storhoff, J.J., Mirkin, C.A. Programmed materials synthesis with DNA. *Chem. Rev.* **99**, 1849-1862 (1999).
- 7) Coffey, J.L., Bigham, S.R., Li, X., Pinizzotto, R.F., Rho, Y.G., Pirtle, R.M., Pirtle, I.L. Dictation of the shape of mesoscale semiconductor nanoparticle assemblies by plasmid DNA. *Appl. Phys. Lett.* **69**, 3851-3853 (1996).
- 8) Mucic, R.C., Storhoff, J.J., Mirkin, C.A., Letsinger, R.L. DNA-directed synthesis of binary nanoparticle network materials. *J. Am. Chem. Soc.* **120**, 12674-12675 (1998).
- 9) Braun, E., Eichen, Y., Sivaun, U., Ben-Yoseph, G. DNA-templated assembly and electrode attachment of a conducting silver wire. *Nature* **391**, 775-778 (1998).
- 10) Kelley, S.O., Jackson, N.M., Hill, M.G., Barton, J.K. Long range electron transfer through DNA films. *Angew. Chem. Intl. Ed. Engl.* **38**, 941-945 (1999).

- 11) Kelley, S.O., Boon, E.M., Barton, J.K., Jackson, N.M., Hill, M.G. Single-base mismatch detection based on charge transduction through DNA. *Nucleic Acids Res.* **27**, 4830-4837 (1999).
- 12) Fink, H.W., Schonenberger, C. Electrical conduction through DNA molecules. *Nature* **398**, 407-410 (1999).
- 13) Porath, D., Bezryadin, A., de Vries, S., Dekker, C. Direct measurement of electrical transport through DNA molecules. *Nature* **403**, 635-638 (2000).
- 14) Okahata, Y., Kobayashi, T., Tanaka, K., Shimomura, M. Anisotropic electric conductivity in an aligned DNA cast film. *J. Am. Chem. Soc.* **120**, 6165-6166 (1998).
- 15) Hall, D.B., Holmlin, R.E., Barton, J.K. Oxidative DNA damage through long-range electron transfer. *Nature* **382**, 731-735 (1996).
- 16) Arkin, M.R., Stemp, E.D.A., Coates-Pulver, S., Barton, J.K. Long-range oxidation of guanine by Ru(III) in duplex DNA. *Chemistry & Biology* **4**, 389-400 (1997).
- 17) Armitage, B., Ly, D., Koch, T., Frydenlund, H., Orum, H., Batz, H.G., Schuster, G.B. Peptide nucleic acid-DNA duplexes: Long range hole migration from an internally linked anthraquinone. *Proc. Nat. Acad. Sci. USA* **94**, 12320-12325 (1997).
- 18) Meggers, E., Kusch, D., Spichy, M., Wille, U., Giese, B. Electron transfer through DNA in the course of radical-induced strand cleavage. *Angew. Chem. Intl. Ed. Engl.* **37**, 460-462 (1998).
- 19) Hall, D.B., Barton, J.K. Sensitivity of DNA-mediated electron transfer to the intervening pi-stack: A probe for the integrity of the DNA base stack. *J. Am. Chem. Soc.* **119**, 5045-5046 (1997).
- 20) Rajski, S.R., Kumar, S., Roberts, R.J., Barton, J.K. Protein-modulated DNA electron transfer. *J. Am. Chem. Soc.* **121**, 5615-5616 (1999).
- 21) Núñez, M.E., Hall, D.B., Barton, J.K. Long range oxidative damage to DNA: effects of distance and sequence. *Chemistry & Biology* **6**, 85-97 (1999).



- 22) Meggers, E., Michel-Beyerle, M.E., Giese, B. Sequence dependent long range hole transport in DNA. *J. Am. Chem. Soc.* **120**, 12950-12955 (1998).
- 23) Henderson, P.T., Jones, D., Hampikian, G., Kan, Y., Schuster, G.B. Long-distance charge transport in duplex DNA: The phonon-assisted polaron-like hopping mechanism. *Proc. Natl. Acad. Sci., USA* **96**: 8353-8358 (1999).
- 24) Beratan, D.N., Priyadarshy, S., Risser, S.M. DNA: Insulator or wire? *Chemistry & Biology* **4**, 3-8 (1997).
- 25) Edmondson, D.G., Roth, S.Y. Chromatin and transcription. *FASEB Journal* **10**, 1173-1182 (1996).
- 26) Saito, I., Takayama, M., Sugiyama, H., Nakatani, K., Tsuchida, A., Yamamoto, M. Photoinduced DNA cleavage via electron transfer: demonstration that guanine residues located 5' to guanines are the most electron donating sites. *J. Am. Chem. Soc.* **117**, 6406-6407, (1995).
- 27) Sitlani, A., Long, E.C., Pyle, A.M., Barton, J.K. DNA Photocleavage by phenanthrenequinone diimine complexes of rhodium(III): shape-selective recognition and reaction. *J. Am. Chem. Soc.* **114**, 2303-2312 (1992).
- 28) Sugiyama, H., Saito, I. Theoretical studies of GG-specific photocleavage of DNA via electron transfer: significant lowering of ionization potential and 5'-localization of HOMO of stacked GG bases in B-form DNA. *J. Am. Chem. Soc.* **118**, 7063-7068 (1996).
- 29) Kielkopf, C.L., Erkkila, K.E., Hudson, B.P., Barton, J.K., Rees, D.C. Structure of a photoactive rhodium complex intercalated into DNA. *Nature Struct. Biol.* **7**, 117-121 (2000).
- 30) Erkkila, K.E., Odom, D.T., Barton, J.K. Recognition and reactivity of metalointercalators with DNA. *Chem. Rev.* **99**, 2777-2795 (1999).
- 31) Lim, A.C., Barton, J.K. Chemical probing of tDNA<sup>Phe</sup> with transition metal complexes. *Biochemistry* **32**, 11029-11034 (1993).

- 32) Vicic, D., Odom, D.T., Nunez, M.E., Gianolio, D.A., McLaughlin, L.W., Barton, J.K. Oxidative repair of a thymine dimer in DNA from a distance by a covalently linked organic intercalator. *J. Am. Chem. Soc.* **2000**, 122, 8603-8611.
- 33) Liu, J.Q., Taylor, J.S. Template-directed photoligation of oligodeoxyribonucleotides via 4-thiothymidine. *Nucleic Acids Res.* **26**, 3300-3304 (1998).
- 34) Lewis, R.J., Hanawalt, P.C. Ligation of oligonucleotides by pyrimidine dimers. *Nature* **298**, 393-396 (1982).
- 35) Ortiz-Lombardía, M., González, A., Eritja, R., Aymamí, J., Azorín F., Coll, M. Crystal structure of a DNA Holliday junction. *Nature Struct. Biol.* **6**, 913-917 (1999).
- 36) Holmlin, R.E., Dandliker, P.J., Barton, J.K. Synthesis of metallointercalator-DNA conjugates on a solid support. *Bioconjugate Chem.* **10**, 1122-1130 (1999).
- 37) Maxam, A.M., Gilbert, W. Sequencing DNA by labeling the end and breaking at bases. *Molecular Biology* **20**, 461-509 (1986).

## **CHAPTER 5**

### **Charge Transport in DNA Single Crossover Assemblies**

## 5.1 INTRODUCTION

DNA can both sustain and participate in long range electron transport. One ramification of this is that oxidative damage can occur at a distance from a site of radical introduction. Because oxidative damage to DNA appears to play significant roles in cancer and aging, understanding the molecular basis of genetic degradation is an important research goal.<sup>1-3</sup> In addition, recent nanotechnological research has focused on the possible application of DNA duplexes as one dimensional quantum wires,<sup>4-6</sup> and as a template for directed material deposition.<sup>7</sup> In the same arena, larger nucleotide assemblies like crossover junctions have been suggested and used as building blocks for nanoscale structures and signaling devices.<sup>8-11</sup> Understanding the molecular mechanisms of charge transport for these nanoscale building blocks is of fundamental importance to designing microarray electronics. Finally, dissecting possible roles that the  $\pi$ -stack can play in long range charge transport, and what the precise parameters are for this reaction are of basic scientific interest.

To investigate long range charge transport in DNA, photolysis of the covalently tethered intercalator  $\text{Rh}(\text{phi})_2\text{bpy}'^{3+}$  ( $\text{phi}$  = phenanthrenequinone diimine,  $\text{bpy}'$  = 4-butyric acid, 4'-methylbipyridine) can inject a radical cation directly into the DNA base stack when 365 nm light is used.<sup>12</sup> Subsequent migration of this radical cation through the base stack results in localization and irreversible damage to the 5'-guanine of a 5'-GG-3' doublet, the most oxidatively sensitive site in DNA.<sup>13</sup> This lesion can be revealed by treatment with hot piperidine or FPG enzyme. In contrast, photolysis at 313 nm causes direct strand scission of sites of intercalation by all  $\text{phi}$  complexes of rhodium without chemical treatment after irradiation. Thus, covalently tethering  $\text{Rh}(\text{phi})_2\text{bpy}'^{3+}$  to the end of a base stack also should restrict the damage that occurs by photoirradiation at 313 nm, which results in strand scission at the binding site for the metal complex, to be restricted to the top of the duplex to which the metal complex is tethered.<sup>14</sup>

Using this and similar techniques, long range charge transport has been shown to occur intramolecularly, and at distances up to 200 Å from a site of hole injection in duplex DNA.<sup>15</sup> Charge transport also has been seen in DNA double crossovers (DX),<sup>16</sup> RNA/DNA hybrid duplexes,<sup>17,18</sup> and DNA triple helices.<sup>19,20</sup> In addition, the ability of charge transport to migrate through regions of unusual structure, such as A-tracks, has also been demonstrated.<sup>21</sup> Modifications to duplex DNA that weaken the structural integrity of the base stack, such as base-base mismatches or insertion of aliphatic protein side chains in place of nucleobases, may adversely affect radical migration.<sup>22-24</sup>

In contrast, introduction of a double mismatch into an otherwise properly paired DX assembly does not disrupt radical migration.<sup>16</sup> A similar disruption in the proper base pairing of identically sequenced duplex DNA causes complete disruption of charge migration, as visualized by guanine oxidation. The different reactivity between the two species is likely due to the stabilization of base dynamics that occurs in DX assemblies from the packing of the sugar phosphate backbones into the major groove of the sister base stack.

Highly stable double crossovers are in essence two four way junctions joined together to greatly rigidify the base stacks of DNA.<sup>25</sup> When in isolation, however, single four way junctions have dramatically different stacking and stability than do DX assemblies.<sup>26-28</sup> In the absence of magnesium, the four way junctions adopt an extended conformation with an open core to minimize negative charge localization from the backbone strands. In the presence of >100 μM magnesium, or other highly charged cations, the four helix arms fold into two coaxial  $\pi$ -stacks in an antiparallel fashion. Four way DNA junctions have long been known in biology as flexible intermediates during homologous recombination of sister chromatids. Originally proposed by Holliday in 1964 (thus often called Holliday junctions),<sup>29</sup> they are composed of four strands of DNA that are partially complementary to each other to form parallel stacks of bases that can interchange between different stacking isomers. In nature, these junctions are unstable

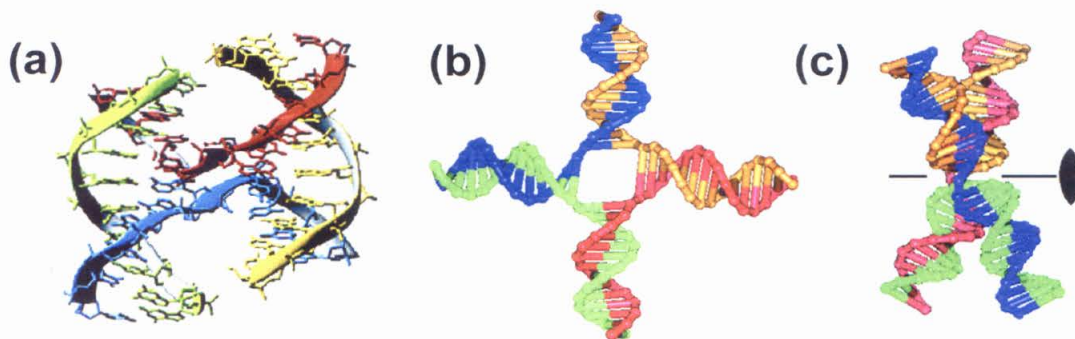


**Figure 5.1.** Crystal structures of four way junctions recently reported for all-DNA assemblies. (a) The first reported four way junction with a double A•G mismatch at the crossover point,<sup>35</sup> (b) Schematic of the four way junction in the absence of magnesium, and (c) crystal structure in the presence of magnesium<sup>36</sup> (adapted from references 35 and 36).

to migration, and, when formed during recombination events, can rapidly migrate *via* a zippering mechanism.

In order to study the structural architecture of these molecules, synthetic four way junctions can be made immobile to base-pairing migration by constructing each arm from non-complementary sequences (reviewed in 26-28, 30). The location of the crossover junction is dictated by the complementarity of the arms. These immobilized four way junctions, however, retain high conformer exchange rates. Solution studies have shown that the rate of interconversion between and the relative abundance of the two junction isomers is critically dependent on the sequence of the three base pair region in each arm that flank the crossover junction itself.<sup>31-34</sup> Indeed, by judicious choice of core, the four way junction can be made to partition evenly between crossover isomers,<sup>34</sup> or strongly prefer one or the other of these isomers.<sup>31</sup>

At present, two crystal structures have been reported in the literature for all-DNA four way junctions (Figure 5.1). Importantly, the base stacks found in both structures are evenly stacked through the junction. Though the sugar phosphate backbone is severely distorted at the crossover location, the bases across the junction are coplanar and show a base pair rise of 3.4Å per step, remarkably similar to those found in duplex DNA. Further, in both crystal structures, the alignment of the two base stacks is antiparallel,



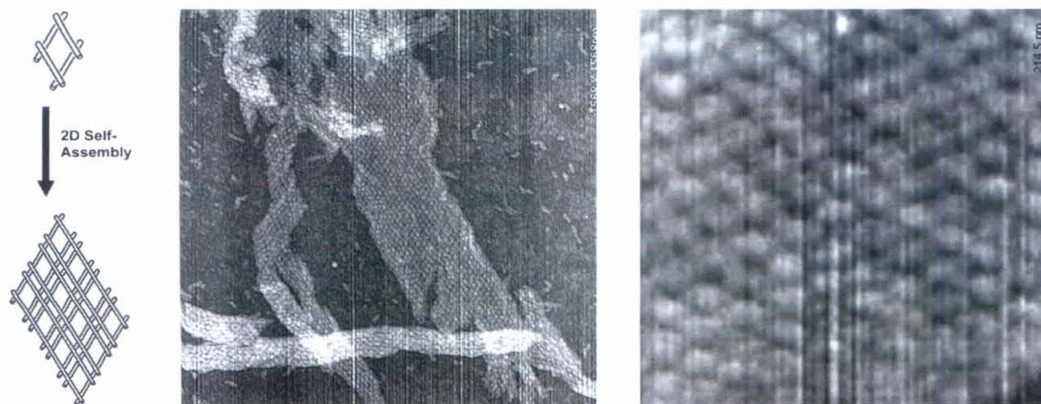


**Figure 5.2.** AFM studies of four way junction arrays. The angle between arms can be estimated using images like this one as  $\sim 60^\circ$  (adapted from reference 37).

and the two stack axes are rotated at angles of  $41.4^\circ$  and  $40^\circ$ .<sup>35,36</sup> These angle measurements are slightly smaller than those predicted in previous studies. AFM of crosslinked four way junctions<sup>37</sup> and other studies<sup>38-41</sup> proposed angles between the helical axes of approximately  $60^\circ$  (Figure 5.2). However, studies with FRET<sup>31</sup> and restriction nucleases<sup>39</sup> have indicated clearly that these four way junctions are fluxional, and are stacked in both possible anti-parallel conformations, though in differing proportions of each when dissolved in solution.

Interest in using various DNA constructs, including crossover junctions, to assemble architectural features in nanoconstruction has prompted us to investigate the electronic structure of crossover junctions. We have designed four way junctions based on previously-used core residues that were shown to maintain one isomeric stacking form preferentially.<sup>31</sup> Charge transport experiments employing this four way junction were conducted both with noncovalently bound metalointercalator and tethered metal complex. It was found that, as is the case with many other intercalators,  $\text{Rh}(\text{phi})_2\text{bpy}^{3+}$  strongly prefers to bind to bases in the core of the crossover junction, depending on conditions. In addition, charge transport between the tethered metalointercalator and the guanine doublet within the stacked arm bearing the metal complex was found to occur consistently, but that charge transport also occurred across the junction into the

isomer stacked arm and into the second helix. This contrasts with previous results with much more rigid DX assemblies,<sup>16</sup> and highlights the critical requirements for stable, well-defined architecture to control pathways of long range charge transport.

## 5.2 EXPERIMENTAL

*Oligonucleotide Preparation.* Oligonucleotides were prepared on an ABI392 DNA synthesizer using standard phosphoramidite chemistry. DNA was synthesized with a 5'-dimethoxytrityl (DMT) protective group, and purified on a Dynamax 300 Å reversed phase C4 column (10mm i.d. x 25 cm length) from Rainin. The DMT group was removed using an aqueous, 80% acetic acid solution to suspend the dried, protected DNA for 20 minutes. After evaporation *in vacuo* of the acetic acid, the DNA was repurified using the same Rainin C4 column. The purified DNA was dissolved into 10 mM Tris pH 7.4 with 1 mM EDTA (TE) to a standardized concentration of 100  $\mu$ M using extinction coefficients of (260 nm,  $M^{-1}cm^{-1}$ ) adenine (A) = 15,000; guanine (G) = 12,300; cytosine (C) = 7,400; thymine (T) = 6,700. Synthesis and tethering of Rh(phi)<sub>2</sub>bpy<sup>3+</sup> to DNA has been described elsewhere.<sup>42</sup>

*DNA Techniques and Photocleavage.* Each strand except the one tethered to the rhodium complex was alternately 5'-labeled with <sup>32</sup>P by use of polynucleotide kinase. P-6 BioRad Microspin columns were used to remove excess, unreacted  $\gamma$ -<sup>32</sup>P-ATP. This desalted solution was treated with 10% piperidine at 90°C for 30 minutes to remove latent guanine oxidation. After drying *in vacuo*, each oligonucleotide was purified on a 20% denaturing polyacrylamide gel, and the parent band extracted from the gel by elution at 37°C into TE. All rinses were pooled, dried, and resuspended into 50  $\mu$ L of TE, and then passed through a BioRad P6 column to remove urea and salts. Four way junctions and duplexes were assembled by annealing equimolar amount of each strand using a linear gradient of 90°C to 4°C over 90 minutes on a Perkin-Elmer Cetus Gene Amplifier. These four way junctions were characterized by gel shift analysis on 10%



non-denaturing gels in 10 mM  $\text{Mg}(\text{OAc})_2$  and 45 mM Tris-Acetate 1 mM EDTA pH 7.6 (1xTAEMg) buffer. In general, it was found that the four way junction made up >90% of the species visualized by the gel shift, regardless of the labeled strand. Noncovalent metallointercalators were added after annealing.

Irradiations were performed on 10-30  $\mu\text{L}$  samples in 1.7 mL presilanized Eppendorf tubes using a 1000 W Hg/Xe arc lamp equipped with a monochromator at 15°C. Unless otherwise noted, all reactions were performed in 1xTAE. When magnesium was present, it was 10 mM as  $\text{Mg}(\text{OAc})_2$ . After irradiation, samples were dried *in vacuo*, and samples to be treated with piperidine (*i.e.* all 365 nm irradiations and dark controls) were resuspended into 100  $\mu\text{L}$  of 10% piperidine and heated to 90°C for 30 minutes. After removal of this piperidine solution, all samples were diluted into denaturing 8 M urea buffer normalized to 10 kcts/ $\mu\text{L}$  by determining the amount of radioactivity of the samples in a scintillation counter. These samples were then analyzed on a 20% denaturing gel followed by phosphorimagery.

## 5.3 RESULTS

*5.3.1. Design of Four Way Junctions to Investigate Long Range Charge Transport.* Our design strategy was based on that used previously to construct a four way junction that would preferentially assume one isomeric conformation of an antiparallel stacked bundle of helices.<sup>31</sup> Using the six-base junction previously verified by FRET to preferentially assume one conformer regardless of the sequence farther removed from the crossover location, we designed the four way junction shown in Figure 5.3. The backbone strands, solvent exposed at the crossover point when the junction is properly folded in the presence of magnesium, are shown in purple and black. Rhodium complexes can be easily attached to the black strand by covalent tethering, thus allowing spatial control of the radical injection into the base stack. The crossover strands, which are tightly wrapped and thus largely solvent excluded in the presence of

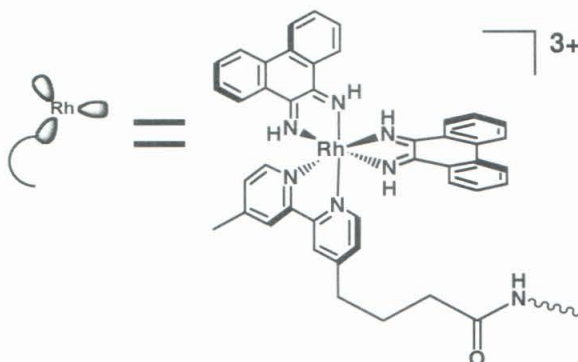
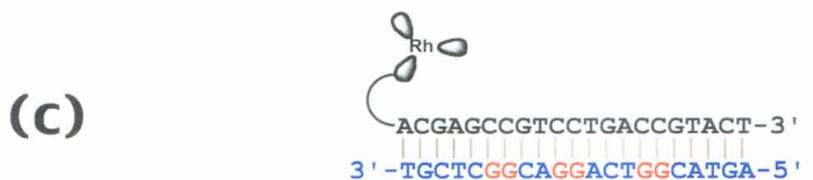
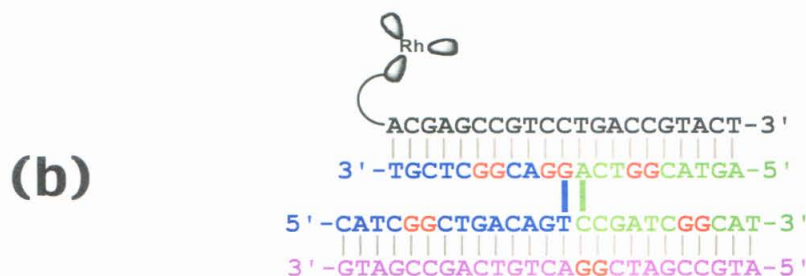
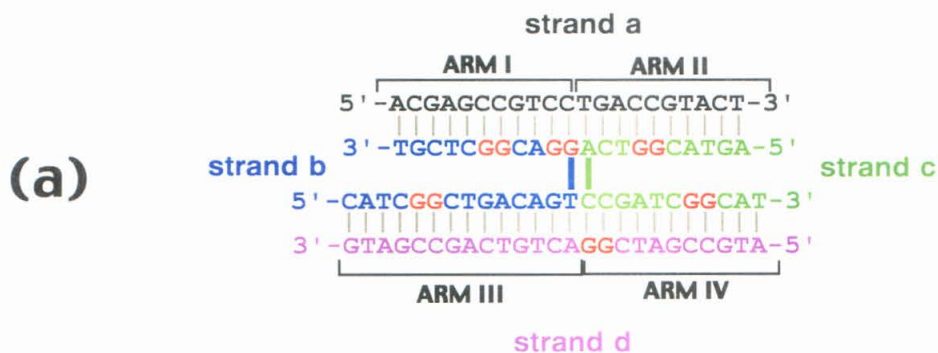


**Figure 5.3.** Sequences of DNA assemblies used containing guanine doublets to be oxidized in red. (a) The noncovalent four way junction assembly with its strands color coded and labeled with lower case letters. The stacked arms are labeled in capital Roman numerals. (b) Analog of the four way junction shown in (a) with covalently attached metal complex. The structure of the appended metallointercalator, which is shown schematically in this rendering, is given at the bottom of this figure. (c) Duplex of the same base-stacked sequence as the combined Arm I/II from (b) with covalently attached metallointercalator.

magnesium, as shown in the crystal structures<sup>35,36</sup> and radical footprinting experiments,<sup>39</sup> incorporate oxidatively sensitive guanine doublets at well-spaced locations along the helix. Because these strands extend across the junction and into both stacks, oxidative damage on different arms can be easily visualized in a single experiment.

*5.3.2. Photoinduced Cleavage of DNA Four Way Junctions by Noncovalently Bound Rh(phi)<sub>2</sub>bpy<sup>3+</sup>*. Previous research indicates that many organic intercalators preferentially bind to the core of four way junctions.<sup>44-47</sup> To distinguish preferred binding sites for noncovalently intercalated Rh(phi)<sub>2</sub>bpy<sup>3+</sup>, this metallointercalator was incubated with an equimolar amount of the four way junction shown in Figure 5.3(a). By labeling each strand alternately with <sup>32</sup>P, and irradiating at 313 nm in the presence and absence of magnesium, the binding location(s) of the metal complex could be easily visualized. It was found that in all cases, with and without magnesium ion, the metal complex bound preferentially to the core of the crossover junctions. This result is consistent with earlier reports showing that MPE•Fe(II), Cu(I)-(o-phenanthroline)<sub>2</sub>, and Stains-All, among other molecules, strongly binds to the core of the junction in the presence of magnesium.<sup>44-47</sup>

However, we find that the pattern and amount of reactivity is critically dependent on the concentration of magnesium, and, thus, the preferred stacking geometry. In the absence of magnesium, the metal complex tightly binds to the core of the junction uniformly, and all of the strands show equal damage at the crossover location (Figure 5.4, -Mg<sup>2+</sup> 313 lanes). Upon introduction of Mg<sup>2+</sup>, however, the direct strand scission seen in strands b and c when irradiated at 313 nm in the presence of Rh(phi)<sub>2</sub>bpy<sup>3+</sup> dramatically decreases, whereas the damage in strand d barely decreases. This contrast is consistent with strands b and c being less solvent accessible in the presence of Mg<sup>2+</sup>, and hence less accessible to Rh(phi)<sub>2</sub>bpy<sup>3+</sup>, but strand d remaining on the outside face of the crossover junction, and thus accessible to photocleavage. Tight

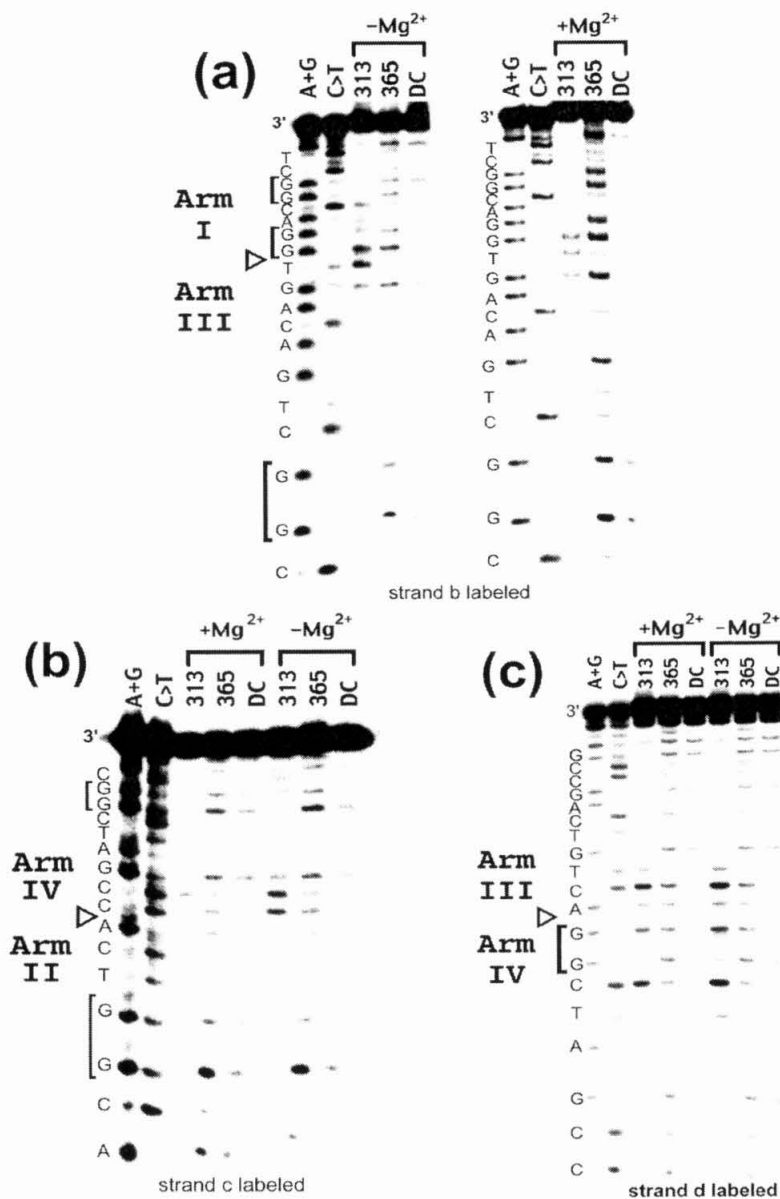
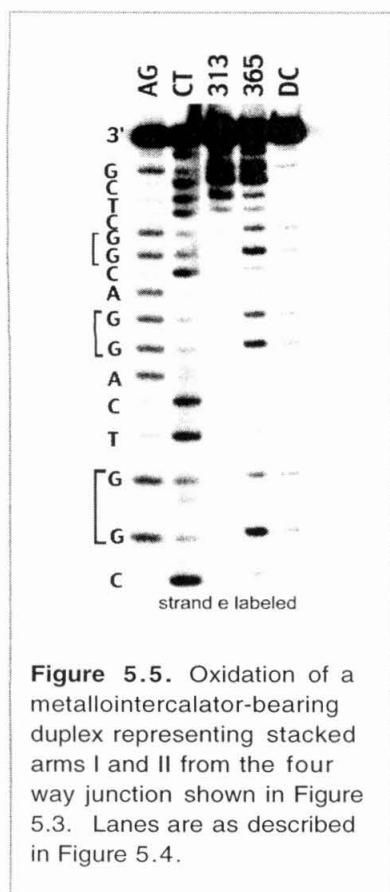


**Figure 5.4.** Direct photocleavage and piperidine induced cleavage of four way junction DNA with noncovalently bound  $\text{Rh}(\text{phi})_2\text{bpy}^{3+}$  as a function of magnesium ion concentration. (a) Phosphorimager after electrophoresis in denaturing 20% polyacrylamide gel with 5'-<sup>32</sup>P end-labeling of strand b of the four way junction in Figure 5.3 after photoirradiation. Lanes correspond to (left to right) Maxam-Gilbert A+G and C>T sequencing reactions,<sup>43</sup> photolysis at 313 nm for ten minutes, photolysis at 365 nm for two hours followed by piperidine treatment, and the same assembly without photolysis (dark control, DC) followed by piperidine treatment. Oxidatively sensitive sites are bracketed to the left of the sequencing lanes, and the site of the crossover junction is shown by a hollow triangle. The presence or absence of 5 mM  $\text{Mg}(\text{OAc})_2$  is indicated above the respective lanes, and the arm locations are indicated to the left of each gel. (b) Phosphorimager of strand c, lanes as in (a). (c) phosphorimager of strand d, lanes as in (a).



packing of the core can occur when magnesium ion is present to neutralize the core junction phosphate charges, and allow the arms that are extended and separate in the absence of magnesium ion to condense into two coaxial, antiparallel base stacks.<sup>28</sup> Interestingly, the oxidative damage seen when these assemblies are irradiated at 365 nm, with the notable exception of strand b in Figure 5.4(a), generally remains localized to the 5'-G of 5'-GG-3' doublets, and is largely independent of the magnesium ion concentration.

*5.3.3. Long Range Charge Transport Through Duplex DNA by Photoinduced Electron Transport to Covalently Bound  $Rh(phi)_2bpy^{3+}$ .* We then constructed the duplex assembly shown in Figure 5.3(c) as a positive control for photoinduced long range oxidative damage in

the sequence used to assemble four way junctions. This duplex was designed to be identical in sequence to the arm I/arm II base stack in the four way junction shown in Figure 5.3. Indeed, and as expected, the damage found at 313 nm was localized to the end of the helix that bears covalently tethered  $Rh(phi)_2bpy^{3+}$ . When irradiated at 365 nm and piperidine treated, the duplex shows guanine oxidation at all of the 5'-G of 5'-GG-3' doublets in the labeled strand complementary to the rhodium bearing strand (Figure 3), consistent with long range charge transport through the duplex.

*5.3.4. Long Range Charge Transport Through the Crossover Junction by Photoinduced Electron Transport to Covalently Bound  $Rh(phi)_2bpy^{3+}$ .* Having verified that duplex DNA of the same sequence can sustain long range charge transport, we assembled the four way junction shown in Figure 5.3(b) and performed photoirradiations on this assembly. By covalently tethering the metallointercalator to the 5'-end of strand

a, the location of radical injection into the assembly was restricted to within three base pairs of the terminus of arm I.

This restricted binding of  $\text{Rh}(\text{phi})_2\text{bpy}^{3+}$  was evident in that the only site of photocleavage in these covalent assemblies, with or without magnesium, was the end of arm I (313 lanes, Figures 5.6). Importantly, the level of photocleavage damage observed was independent of the amount of magnesium ion in solution. This independence demonstrates that the decrease in the core seen previously with noncovalent  $\text{Rh}(\text{phi})_2\text{bpy}^{3+}$  was a function of the architectural changes in the core junction upon magnesium addition that sterically preclude metal complex access to the core, and not the result of non-specific magnesium binding to the phosphate backbone.

In contrast, irradiating the covalent assemblies at 365 nm caused oxidative damage to all the guanines on strands b and c. In the absence of magnesium ion, oxidative damage was seen to occur at all three 5'-GG-3' sites in strand b. When  $\text{Mg}^{2+}$  was present, the oxidative damage appeared to increase at all of the guanines and guanine doublets. Strand c shows even more interesting behavior (Figure 5.7). In the absence of magnesium ion, the oxidative damage is seen to be rather weak, and evenly distributed between the two guanine doublets located on this strand. Magnesium ion increases the level of damage at the guanine doublet on the 3' side of this strand, located in arm IV. Most dramatically, however, the oxidative damage at the guanine doublet on the 5' end of strand c in arm II is greatly increased. This increase may reflect the stacking of this arm onto the rhodium-bearing arm I. This stacking could allow electronic coupling to occur between the site of hole injection on arm I and the affected guanine on arm II.

To verify that guanine oxidation was not occurring due to intermolecular interactions between the covalently appended metal complexes and other four way junctions, a radioactively labeled four way junction with no tethered rhodium complex and an unlabeled four way junction bearing a covalently bound metallointercalator were

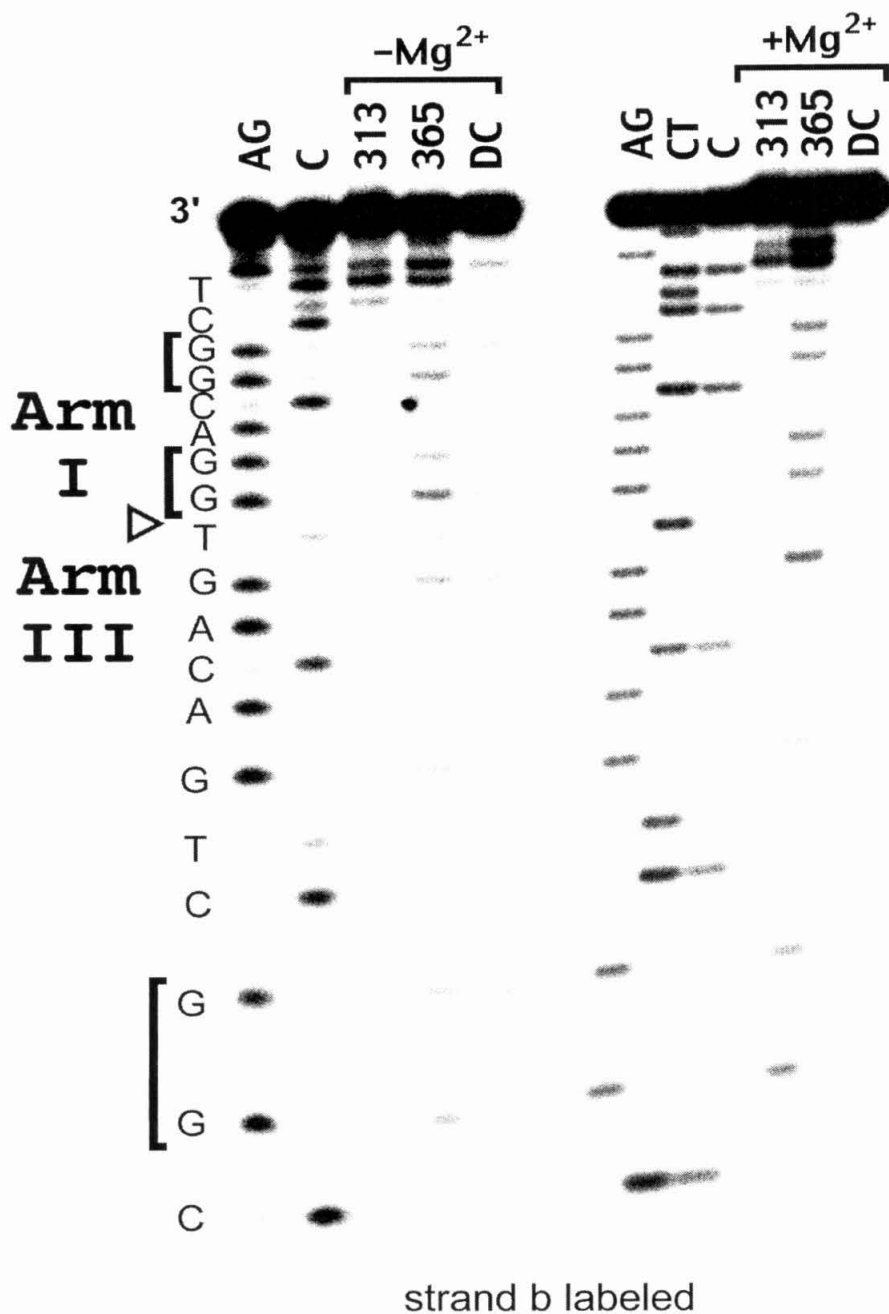


**Figure 5.6.** Long range oxidation of DNA by covalently tethered  $Rh(\phi)_2bpy^{13+}$  in four way junctions as a function of  $Mg^{2+}$  concentration. The gels are labeled as in Figure 5.4. Direct photocleavage and long range oxidation in strand b of the four way junction shown in Figure 5.3(b). The intercalation site of the tethered metal complex is visible as damage at the top of this panel in the 313 and 365 nm lanes. Long range guanine oxidation is more evenly spread across the three sites both in the absence and presence of magnesium ion.

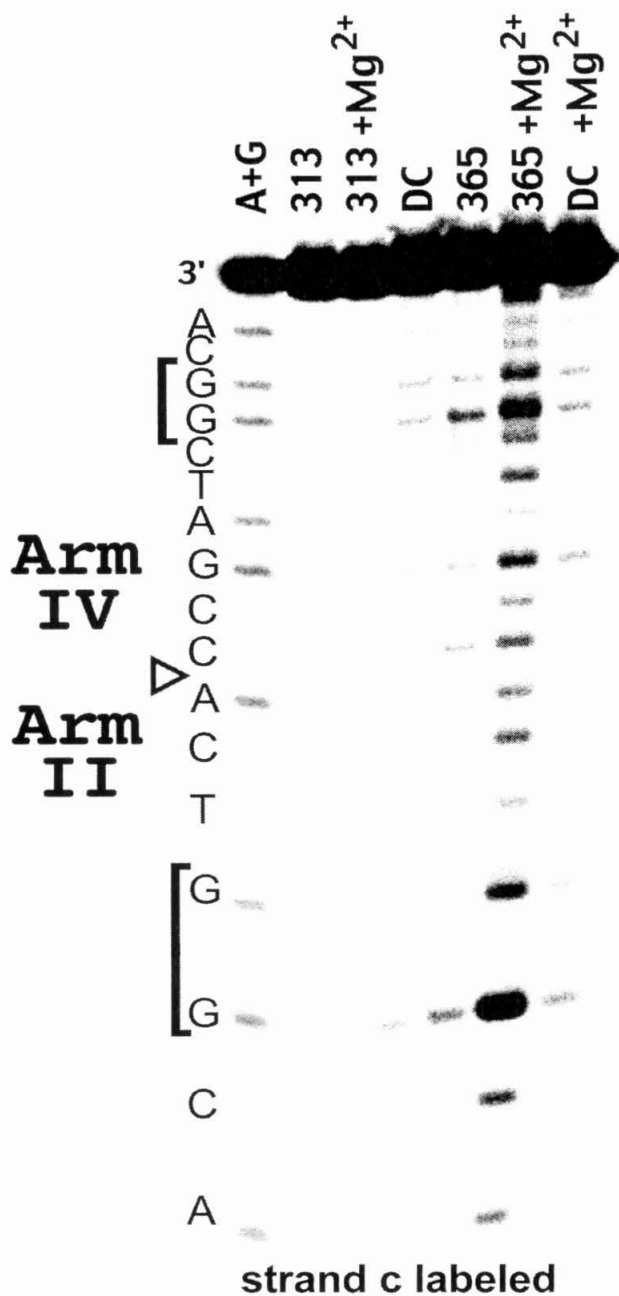


**Figure 5.7.** Long range oxidation of DNA by covalently tethered  $\text{Rh}(\text{phi})_2\text{bpy}^{3+}$  in four way junctions as a function of  $\text{Mg}^{2+}$  concentration. The gels are labeled as in Figure 5.4. Strand c of the covalently tethered four way junction is shown to be unaffected by 313 nm irradiation, but long range charge transport is evident upon 365 nm photoirradiation in the absence and, particularly, in the presence of magnesium ion.



annealed separately, mixed in equimolar amounts, and then photoirradiated. No direct strand scission or guanine oxidation was observed to the labeled strand by  $\text{Rh}(\text{phi})_2\text{bpy}^{3+}$  tethered to a separately annealed four way junction, thus demonstrating that long range charge transport proceeds only within an individual crossover assembly.

## 5.4 DISCUSSION

*5.4.1. Intercalator Exclusion from the Crossover Core in the Presence of Magnesium Ion.* Direct photocleavage of the four way junction by noncovalently bound  $\text{Rh}(\text{phi})_2\text{bpy}^{3+}$  shows that under all circumstances and salt concentrations the preferred binding site is the core of the four way junction. However, the affinity that this metal complex shows for the four stands that make up the crossover may depend on the presence or absence of magnesium ion. In the absence of magnesium ion, experiments monitoring direct strand scission show that the metal complex cleaves at the crossover junction on all of the inspected strands. By way of comparison, the addition of  $\text{Mg}^{2+}$ , which induces strands b and c to assume distorted conformations to bridge between the two separate base stacks, also leads to greatly reduced photocleavage of these strands. Importantly, strand d shows photocleavage that appears to be independent of the magnesium ion concentration.

The differing susceptibility of each of the strands to metal complex binding in the presence of magnesium ion is consistent with this junction's previously established stacking preferences. FRET experiments have demonstrated that the sequences used here favor the conformation shown in Figures 1, where arm I and arm II are stacked, and arm III and arm IV are stacked, by 20:1 over the alternate anti-parallel conformation where arm I is stacked over arm III and arm II over arm IV. Clearly, this preferred stacking pattern is reflected in the photocleavage experiments described above; when magnesium ion is present, strands b and c are inaccessible to the metal complex, but strand d remains solvent exposed.

Previous results using organic, planar DNA-binding molecules have shown that the core of the crossover junction is accessible to these intercalators in the presence of magnesium ion.<sup>44-47</sup>  $\text{Rh}(\text{phi})_2\text{bpy}^{3+}$  too uses a planar ligand to intercalate deeply into the base stack, yet the intercalating heterocycle is the extension of a larger, rigid, three dimensional object that packs into a span of the major groove of DNA.<sup>48,49</sup> We find that, in the absence of  $\text{Mg}^{2+}$ , the metal complex is very tightly bound to the crossover core, but appears to be displaced in the presence of  $\text{Mg}^{2+}$ , as seen by the 313 nm photocleavage of the core bases. In contrast, experiments conducted with organic intercalators used concentrations of magnesium ion also on the order of 10 mM, but still showed strong binding. This suggests that the  $\text{Mg}^{2+}$  dependence of the metal complex binding is a function of the matching three dimensional architecture of the DNA binding site and  $\text{Rh}(\text{phi})_2\text{bpy}^{3+}$ .

This suggestion is supported by previous studies that investigated metallointercalator binding to cruciforms. The non-intercalating metal complex, tris(4,7-diphenylphenanthroline)rhodium(III) ( $\text{Rh}(\text{DIP})_3^{3+}$ ), was shown to target cruciforms that naturally occur in supercoiled plasmids (see also Chapter 1 of this Work). When bound to a plasmid in low salt conditions and irradiated at 315 nm, this bulky, sterically demanding metal complex induced single and double strand breaks at sites previously demonstrated using other techniques to be a cruciform extrusion. This reactivity was observed with the target plasmids at all tested concentrations of sodium chloride. In a result that is remarkably similar to what is found in this study, the cleavage of the cruciform site occurred at magnesium concentrations of 1 mM, but cleavage completely disappeared when magnesium was present in 10 mM concentration. Recognition by  $\text{Rh}(\text{DIP})_3^{3+}$  of these sites is entirely based on the structure, hydrophobicity, and high charge of the open junction. The similar  $\text{Mg}^{2+}$  dependence between the  $\text{Rh}(\text{DIP})_3^{3+}$  recognition of cruciforms and the  $\text{Rh}(\text{phi})_2\text{bpy}^{3+}$  recognition of immobilized four way junctions implies that their mechanisms of recognition are also similar. However, the

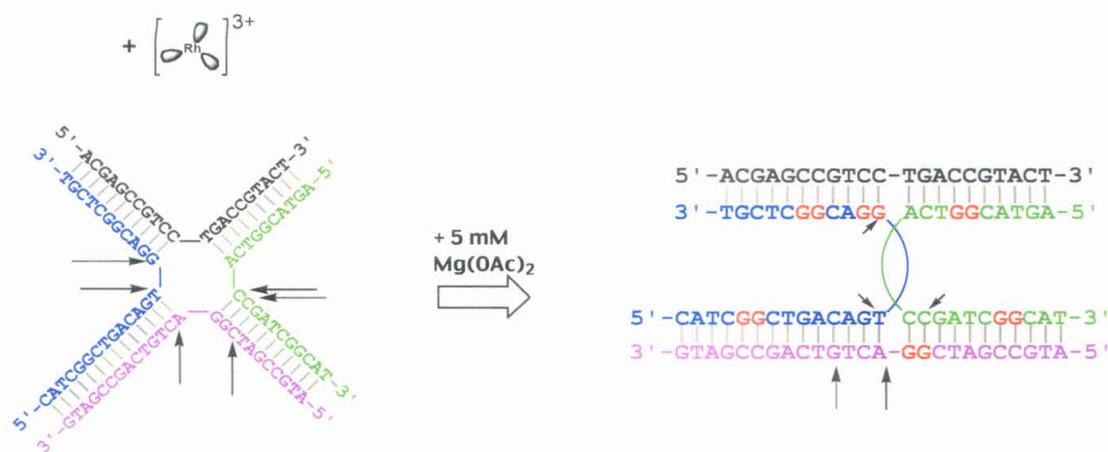
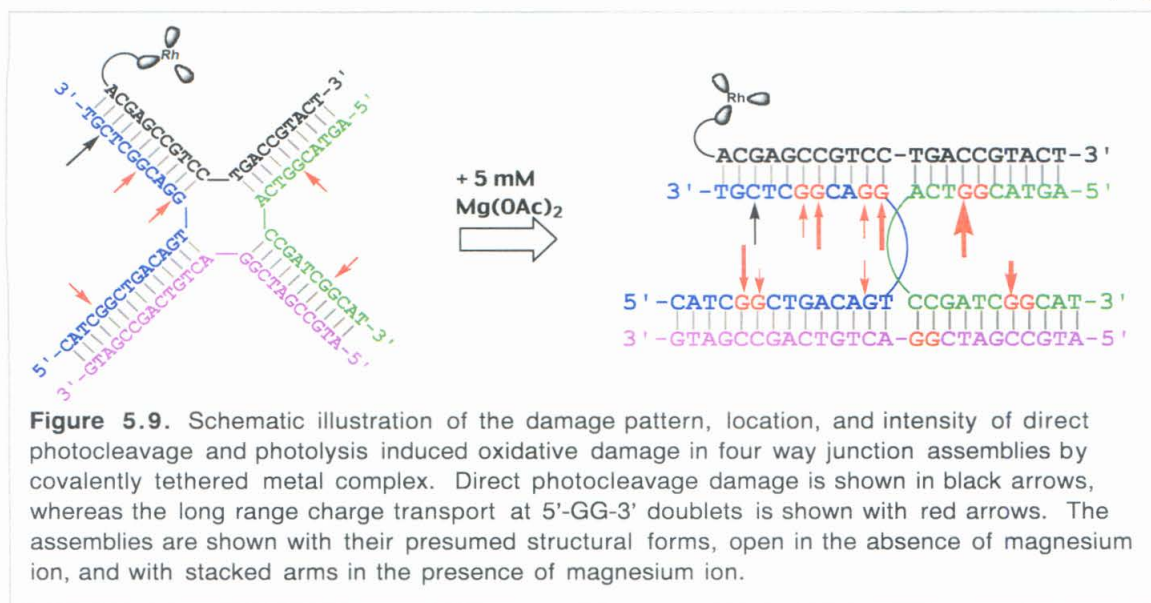


**Figure 5.8.** Schematic illustration of the damage pattern, location, and intensity of direct photocleavage and photolysis induced oxidative damage in four way junction assemblies by noncovalent metal complex. Direct photocleavage damage is shown in black arrows, whereas the long range charge transport at 5'-GG-3' doublets is shown with red arrows. The assemblies are shown with their presumed structural forms, open in the absence of magnesium ion, and with stacked arms in the presence of magnesium ion.

assymmetric  $Rh(DIP)_3^{3+}$  cleavage of cruciforms contrasts with the largely even reactivity seen in  $Rh(phi)_2bpy^{3+}$  towards four way junctions, which may be a function of the more controlled nature of the immobilized four way junction. The cruciform, as a natural extension of the supercoiled plasmid, can likely assume more conformations, including migration of the actual cruciform site, and thus be more assymmetric than immobilized, designed Holliday junctions.

**5.4.2. Long Range Charge Transport in Duplex DNA Assemblies.** Next, we assembled a duplex with a tethered metallointercalator of the same sequence and stacking as the  $Rh(phi)_2bpy^{3+}$ -bearing stack of the preferred conformer of the four way junction, but with a continuous sugar phosphate backbone on the strand complementary to the metal complex (Figure 5.3(c)). As expected, direct photocleavage mapped the rhodium binding site to the end of the helix. When photoirradiated at 365 nm, followed by piperidine treatment to reveal oxidative lesions, the duplex showed damage at all 5'-guanines in 5'-GG-3' doublets. This experiment is in effect a positive control for the



types of long range transport that would occur in single crossovers if four way junction stacking affords constructs as stable as duplex DNA.

**5.4.3. Long Range Charge Transport in Single Crossover DNA Assemblies.** In the absence of magnesium ion, four way junctions assume an extended conformation where the arms are not stacked beyond their canonical base pairing regions (Figures 5.8 and 5.9). Based on these considerations, long range charge transport experiments in the absence of magnesium would be expected to only yield damage at the guanine doublet in arm I, as radical migration should not occur across the empty, open junction. Instead, guanine oxidation is found to occur at 5'-guanines of guanine doublets in all arms. As damage is found even in arm III, the four way junction must be transiently sampling conformations that permit even the highly disfavored parallel alignment of arm I over arm III, discussed more below, to occur. Clearly, however, radical migration is occurring across the junction. Importantly, the binding location of the tethered metallointercalator, as revealed by direct strand scission at 313 nm, is exclusively at the terminus of arm I; hence, any damage seen in other locations is caused at long range.

In the presence of magnesium ion, similar experiments in four way junctions with a covalently tethered metalointercalator should afford guanine oxidation in arms I and II, and to a lesser extent in arm IV, which in general make up the favored, anti-parallel stacking partners. The core residues in these experiments were specifically chosen to favor the arm I/arm II stacking over that of the arm I/arm IV, and so it is expected that most of the damage would occur in the arm I/arm II conformer. Based on previous research indicating that parallel alignment of the backbones needed to facilitate arm I/arm III stacking cause considerable steric clashing of the backbones, the arm I/arm III stacking arrangement should be strongly disfavored regardless of magnesium ion concentration, and thus the guanine doublet located in arm III would not be expected to show oxidative damage.

The results summarized in Figure 5.9 show that addition of magnesium to this system, which presumably causes folding of the otherwise separated arms into coaxial base stacks, increases guanine oxidation overall, but especially in the guanine doublets that are located in the stacked arms I and II. Most dramatically, the guanine doublet in arm II is much more damaged by radical migration when  $Mg^{2+}$  is present. As predicted above, this increase is probably a result of the favored stacking of arm I with arm II, which would electronically couple these two base stacks much more efficiently and thus allows radical migration across the junction. Damage also increases, though more modestly, to the guanine doublet in arm IV, again, consistent with the above analysis of the arm I/arm IV stacking conformer to be the minor species. Furthermore, the differential increase, where arm II is more intensely damaged than arm IV, reflects the trend, if not the absolute numbers, of the previously determined 20:1 partition ratio of the stacking arrangements of these arms.

Notably, however, guanines are also oxidized on arm III, the highly disfavored stacking partner for arm I. This result may reflect transient sampling of this strongly disfavored stacking arrangement by the four way junction. This suggestion is quite



reasonable to explain the guanine oxidation seen in arm III in the absence of  $\text{Mg}^{2+}$ , as in the absence of highly charged cations the four way junction is extremely fluxional. It is more surprising, however, when considering the conformation of the four way junction in the presence of  $\text{Mg}^{2+}$ , where the separate arms are generally presumed to be in a more tightly packed arrangement, and the overall assembly to be much more rigid.

In some cases, especially strand b, damage also occurs in guanines at the 3' position of doublets, and single guanines as well, even ones that would be expected to be entirely orthogonal to the oxidation caused by the tethered metallointercalator. As suggested previously, the flexible junctions likely sample conformations that permit long range charge transport to proceed, but also may sample conformations that weaken the stacking geometry that concentrates HOMO localization onto the 5'-G of 5'-GG-3' doublets.<sup>13</sup> The damage seen on single guanines and 3'-guanines in 5'-GG-3' doublets on strand b, otherwise unexpected, could be the result.

*5.4.4. Magnesium Effects on Long Range Transport.* These results suggest that in general, the addition of  $\text{Mg}^{2+}$  strongly stabilizes tertiary structures with well-stacked arms, and, thus, enhances charge transport to guanines by rigidifying the base stack. This effect is especially notable when metal complexes are covalently tethered to the end of one of the base stacks. Irradiations probing the effect of magnesium on direct strand scission and thus binding, show that the tethered metallointercalator binds to the end of arm I independent of the  $\text{Mg}^{2+}$  concentration. In contrast, in the presence of  $\text{Mg}^{2+}$ , the level of guanine damage observed (Figure 5.9) is increased greatly at all positions, despite the difference in relative amount at each location. However, the largest increases are at the predicted sites of greatest oxidative sensitivity, the 5'-guanines of guanine doublets. Even in the presence of magnesium ion, charge migration can occur to disfavored sites, likely as a result of transient sampling of disfavored alignments.

Similar across the board increases in guanine oxidation are observed on strand b when noncovalent rhodium is used (Figure 5.4). This increase occurs not only at the 5'-

guanine of 5'-GG-3' guanines, but at all guanines regardless of location. Remarkably, and in contrast to the results with tethered metallointercalator, the direct strand scission in the presence of magnesium is much lower with noncovalent  $\text{Rh}(\text{phi})_2\text{bpy}^{3+}$ . In other words, it appears that lower levels of binding are yielding greater amounts of oxidative damage, consistent with the notion that magnesium ion affords a more rigid base stack that acts as a more effective conduit for charge transport. Notably, however, the oxidative damage on strand c is strictly located at the 5'-guanine of 5'-GG-3' sites, and appears to be independent entirely of the concentration of  $\text{Mg}^{2+}$ . Strand d has no oxidative damage in any case.

*5.4.5. Comparison of Charge Transport in Four Way Junctions to Double Crossover Assemblies.* DNA single crossover assemblies are considerably more flexible than their DNA double crossover counterparts. This fact accounts for why a considerable body of work exists exploring the nanostructural architecture of DX assemblies,<sup>8-11</sup> but to date few papers have been published regarding the attempted use of single crossovers as architectural elements.<sup>9,50</sup> However, considerable effort has gone into delineating the different folding behaviors that single crossover junctions undergo.<sup>26-28</sup>

Previously investigated double crossover assemblies show remarkable fidelity in radical migration across crossover junctions, due to their rigid and inflexible structures.<sup>16</sup> Notably, this rigid structure is only made possible by the presence of 10 mM  $\text{Mg}(\text{OAc})_2$ . Resistance to crosstalk in DX molecules implies that they may be used successfully in nanotechnological systems that involve charge migration. Similar considerations suggest that single crossovers are 'leakier' systems towards charge migration, and may only be appropriate for the types of architectural assemblies already investigated.

*5.4.6. Conclusions.* In summary, radical migration in the absence of magnesium is seen here to be a relatively nonspecific process, and localizes to guanine doublets with limited regard for their preferred stacking partner in the presence of magnesium.

This may reflect a constant transient sampling of conformers that allows brief, but significant, base stacking to occur between normally disfavored arms, and, thus, radical migration between normally disfavored arms. Single crossover assemblies, therefore, though interesting from a structural and architectural standpoint, would not make effective components in nanoconstruction that may demand controlled charge migration.

---

## 5.5 REFERENCES

- 1) Ames, B. *Science* (1983) **221**, 1256-1264.
- 2) Piette, J., *J. Photochem. Photobiol. B* (1991) **11**, 241-260.
- 3) Simon, M.I., Vunakis, H.V. *J. Mol. Biol.* (1962) **4**, 488-499.
- 4) Fink, H.W., Schonenberger, C. *Nature* **398**, 407-410 (1999).
- 5) Porath, D., Bezryadin, A., de Vries, S., Dekker, C. *Nature* (2000) **403**, 635-638.
- 6) Okahata, Y., Kobayashi, T., Tanaka, K., Shimomura, M. *J. Am. Chem. Soc.* (1998) **120**, 6165-6166.
- 7) Storhoff, J.J., Mirkin, C.A. *Chem. Rev.* (1999) **99**, 1849-1862.
- 8) Li, X., Yang, X., Qi, J., Seeman, N.C. *J. Am. Chem. Soc.* (1996) **118**, 6131-6140.
- 9) Mao, C., Sun, W., Shen, Z., Seeman, N.C. *Nature* (1999) **397**, 144-146.
- 10) Winfree, E., Liu, F., Wenzler, L.A., Seeman, N.C. *Nature*. (1998) **394**, 539-544.
- 11) Yang, X., Wenzler, L.A., Qi, L., Li, X., Seeman, N.C. *J. Am. Chem. Soc.* (1998) **120**, 9779-9786.
- 12) Rajski, S. R., Barton J. K. *J. Biomol. Struct. Dynam.* (2000) **S2**, 285-291.
- 13) (a) Saito, I., Takayama, M., Sugiyama, H., Nakatani, K., Tsuchida, A., Yamamoto, M. *J. Am. Chem. Soc.* (1995) **117**, 6406-6407. (b) Sugiyama, H., Saito, I. *J. Am. Chem. Soc.* (1996) **118**, 7063-7068.
- 14) Hall, D.B., Holmlin, R.E., Barton, J.K. *Nature* (1996) **382**, 731-735.
- 15) Núñez, M.E., Hall, D.B., Barton, J.K. *Chemistry & Biology* (1999) **6**, 85-97.



- 16) Odom, D.T., Dill, E.A., Barton, J.K. *Chemistry & Biology* (2000) **7** 475-481.
- 17) Odom, D.T. *Chapter 2 of this Dissertation*.
- 18) Sartor, V., Henderson, P.T. , and Schuster, G.B. *J. Am. Chem. Soc.* (1999) **121**, 11027.
- 19) Núñez, M.E., Noyes, K.T., Gianolio, D.A., McLaughlin, L.W., Barton, J.K. *Biochemistry* (2000) **39**, 6190-6199.
- 20) Yongzhi, K. Schuster, G.B. *J. Am. Chem. Soc.* (1999) **121**, 11607-11614.
- 21) Williams, T.T., Odom, D.T., Barton, J.K. *J. Am. Chem. Soc.* (2000) **122**, 9048-9049.
- 22) Rajski, S.R., Kumar, S., Roberts, R.J. Barton, J.K. *J. Am. Chem. Soc.* (1999) **121**, 5615-5616.
- 23) Hall, D.B., Barton, J.K. *J. Am. Chem. Soc.* (1997) **119**, 5045-5046.
- 24) Kelley, S.O. Boon, E.M., Barton, J.K., Jackson, N.M., Hill, M.G. *Nucleic Acids Res.* (1999) **27**, 4830-4837.
- 25) Fu, T.-J., Seeman, N.C. *Biochemistry* (1993) **32**, 3211-3220.
- 26) Lilley, D.M.J., Clegg, R.M. *Annu. Rev. Biophys. Biomol. Struct.* (1993) **22**, 299-328.
- 27) Lilley, D.M.J., Clegg, R.M., *Q. Rev. Biophys.* (1993) **26**, 131-175.
- 28) Seeman, N.C., Kallenbach, N.R. *Annu. Rev. Biophys. Biomol. Struct.* (1994) **23**, 53-86.
- 29) Holliday, R. *Genet. Res.* (1964) **5**, 282-304.
- 30) Lilley D.M.J. in *Nucleic Acid Structure* (ed. Neidle, S.) 471-498 (1999—Oxford Press).
- 31) Miick, S.M., Fee, R.S., Millar, D.P., Chazin, W.J. *Proc. Natl. Acad. Sci. USA* (1997) **94**, 9080-9084.
- 32) Seeman, N.C., Chen, J.H., Kallenbach, N.R. *Electrophoresis* (1989) **10**, 345-354.

- 33) Chen, J.H., Churchill, M.E.A., Tullius, T.D., Kallenbach, N.R., Seeman, N.C. *Biochemistry* (1988) **85**, 6032-6038.
- 34) Grainger, R.J., Murchie, A.I.H., Lilley, D.M.J. *Biochemistry* (1998) **37**, 23-32.
- 35) Ortiz-Lombardía, M., González, A., Eritja, R., Aymamí, J., Azorín F. Coll, M. *Nature Struct. Biol.* (1999) **6**, 913-917.
- 36) Eichman, B.F., Vargason, J.M., Mooers, B.H.M., Ho, P.S. *Proc. Natl. Acad. Sci. USA*. (2000) **97**, 3971-3976.
- 37) Mao, C., Sun, W., Seeman, N.C. *J. Am. Chem. Soc.* (1999) **121**, 5437-5443.
- 38) Duckett, D.R., Murchie, A.I.H., Diekman, S., von Kitzing, E., Kemper, B., Lilley, D.M.J. *Cell* (1988) **55**, 79-89.
- 39) Churchill, M.E.A., Tullius, T.D., Kallenbach, N.R., Seeman, N.C. *Proc. Natl. Acad. Sci. USA* (1988) **85**, 4653-4656.
- 40) Cooper, J.P., Hagerman, P.J. *Proc. Natl. Acad. Sci. USA* (1989) **86**, 7336-7340.
- 41) Murchie, A.I.H., Clegg, R.M., von Kitzing, E., Duckett, D.R., Diekmann, S., Lilley, D.M.J. *Nature* (1989) **341**, 763-766.
- 42) Holmlin, R.E., Dandliker, P.J. Barton, J.K. *Bioconjugate Chem.* (1999) **10**, 1122-1130.
- 43) Maxam, A.M., Gilbert, W. *Molecular Biology* (1986) **20**, 461-509.
- 44) Guo, Q., Seeman, N.C., Kallenbach, N.R. *Biochemistry* (1989) **28**, 2355-2359.
- 45) Lu, M., Guo, Q., Pasternack, R.F., Wink, D., Seeman, N.C., Kallenbach, N.R. *Biochemistry* (1990) **29**, 1614-1624.
- 46) Guo, Q., Lu, M., Seeman, N.C., Kallenbach, N.R. *Biochemistry* (1990) **29**, 570-578.
- 47) Lu, M., Guo, Q., Seeman, N.C., Kallenbach, N.R. *Biochemistry* (1990) **29**, 3407-3412.
- 48) Kielkopf, C.L., Erkkila, K.E., Hudson, B.P., Barton, J.K., Rees, D.C. *Nature Struct. Biol.* (2000) **7**, 117-121.

- 49) Erkkila, K.E., Odom, D.T., Barton, J.K. *Chem. Rev.* (1999) **99**, 2777-2795.
- 50) Petrillo, M.L., Newton, C.J., Cunningham, R.P., Ma, R.I., Kallenbach, N.R., Seeman, N.C. *Biopolymers* (1988) **27**, 1337-1352.

## CHAPTER 6

### **Oxidative Repair of a Thymine Dimer in DNA by a Covalently Attached, Organic Intercalator\***

\*Adapted from D.A. Vicic, D.T. Odom, M.E. Nunez, D.A. Gianolio, L.W. McLaughlin, J.K. Barton. *J. Am. Chem. Soc.* **2000**, 122, 8603-8611. (Note: HPLC analyses for thymine dimer repair were conducted by D. Vicic, and NDI-modified oligonucleotides were synthesized by D. Gianolio.)

## 6.1 INTRODUCTION

The thymine cyclobutane dimer (T<>T) is one of the principal photoproducts formed upon exposure of DNA to UV irradiation. This DNA lesion, if left unrepaired, can be both mutagenic and carcinogenic.<sup>1</sup> It is therefore of interest to understand the mechanisms by which UV-induced photolesions are detected and repaired. In mammalian cells, the thymine dimer lesion, once detected, is removed from DNA by dual incision of the damaged strand on both sides of the lesion, followed by filling of the resulting gap and ligation.<sup>2</sup> Extensive research has been carried out to delineate the mechanism of thymine dimer repair in bacteria, where naturally occurring photolyase enzymes can repair these lesions without excision in a catalytic process initiated by sunlight.<sup>1,3</sup>

The thymine dimer is formed as a result of a [2+2] photocycloaddition reaction between adjacent thymine bases on the same polynucleotide strand (Figure 6.1). The repair of this lesion can be triggered by electron transfer from repair proteins. Photolyase initiates the repair by direct reduction of the cyclobutane dimer, and the unstable radical anion, once formed, reverts with oxidation to the repaired form. In model systems, the repair of thymine dimers can be triggered both oxidatively and reductively,<sup>4</sup> since the cyclobutane radical cation is similarly unstable. Recently, it was shown that thymine dimers can also be repaired from a distance in a reaction involving DNA-mediated electron transfer.<sup>5</sup> Upon photoactivation with visible light, a rhodium intercalator was found to trigger oxidatively the repair of a thymine dimer site-specifically incorporated in a DNA oligonucleotide duplex. With non-covalently bound rhodium complex, the reaction is photocatalytic, consistent with electron transfer. Moreover, in assemblies in which the rhodium complex was covalently tethered and intercalated near the end of the duplex, the quantitative repair of the thymine dimer was observed with the photooxidant bound 16 to 36 Å away from the centrally located thymine dimer.

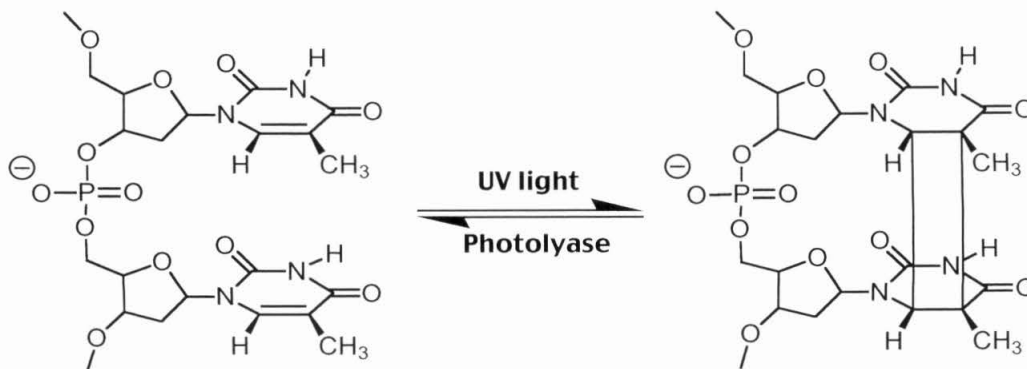


**Figure 6.1.** Photoequilibration of a *cis-syn* thymine dimer in DNA.

This long-range repair reaction is important to consider in the context of DNA-mediated electron transfer chemistry. As with other DNA charge transport reactions,<sup>6</sup> the efficiency of thymine dimer repair from a distance was found to be sensitive to perturbations in stacking by the intercalating rhodium complex and also to the integrity of the intervening base stack, but less sensitive to the distance separating the intercalator and thymine dimer. For example, repair was more efficient with the  $\Delta$ -Rh diastereomer compared to the  $\Lambda$ -Rh isomer, consistent with preferential intercalation of right-handed metal complexes into the right-handed DNA helix,<sup>7</sup> allowing more overlap with the DNA base stack. Furthermore, despite only a small variation in repair efficiency with changes in distance separating the thymine dimer and rhodium, the insertion of base bulges which perturb the base stack caused a marked decrease in the efficiency of repair.

Oxidative damage to DNA from a distance has also been demonstrated in reactions involving DNA-mediated charge transport. The 5'-G of 5'-GG-3' doublets are sites of low oxidation potential in DNA and are preferentially oxidized.<sup>8</sup> Guanine damage is a more complex reaction than thymine dimer repair, since several steps subsequent to the formation of the guanine cation radical by electron transfer are involved.<sup>9</sup> Thymine dimer repair, in contrast, may be viewed simply as a photoisomerization reaction initiated by electron transfer. Many examples of oxidative DNA damage at long range have now

been documented,<sup>6,10</sup> while the rhodium intercalator  $[\text{Rh}(\text{phi})_2(\text{bpy}') ]^{3+}$ , where  $\text{phi} = 9,10$ -phenanthrenequinone diimine and  $\text{bpy}' = 4$ -butyric acid, 4'-methylbipyridine, is the only reported oxidant demonstrated thus far to repair thymine dimers from a distance. This observation may be a consequence of differences in thermodynamics for the two reactions. The oxidation potential of guanine is estimated to be roughly 1.3 V versus NHE,<sup>11</sup> much lower than that for the thymine dimer. The oxidation potential of thymine is estimated to be  $\sim 1.7$  V vs. NHE.<sup>11</sup> It is noteworthy that another metallointercalator,  $\text{Ru}(\text{phen})(\text{bpy}')(\text{dppz})^{3+}$ , where  $\text{dppz} = \text{dipyridophenazine}$ , is capable of promoting oxidative DNA damage, but cannot repair thymine dimers.<sup>5b</sup> Based upon the estimated excited state reduction potentials for  $[\text{Rh}(\text{phi})_2(\text{dmb})]^{3+}$  ( $\text{dmb} = 4,4'$ -dimethylbipyridine)  $E_{1/2}([\text{Rh}]^{3+/2+}) = 2.0$  V vs. NHE<sup>12</sup> and ground state reduction potentials for  $\text{Ru}(\text{phen})(\text{bpy}')(\text{dppz})^{3+}$   $E_{1/2}([\text{Ru}]^{3+/2+}) = 1.6$  V vs. NHE,<sup>13</sup> we can bracket the oxidation potential for the thymine dimer in DNA to be between 1.6 - 2.0 V versus NHE.

We have recently found that a naphthalene diimide intercalator (NDI), appended to the C4 amine of a methylated cytosine base, can serve as a long range DNA photooxidant.<sup>14</sup> NDI and related compounds have been known to display anticancer<sup>15</sup> and antiviral<sup>16</sup> activities that arise from their ability to intercalate into DNA.<sup>17</sup> The photophysical properties of these compounds have also been thoroughly studied,<sup>18</sup> and it has previously been shown that a free naphthalimide chromophore can oxidize guanines via an electron transfer mechanism.<sup>19</sup> Upon irradiation at 355 nm, photoinduced electron transfer to the lowest electronically excited triplet states of an NDI chromophore from GMP occurs with a rate constant of  $2.0 \times 10^7 \text{ M}^{-1} \text{ s}^{-1}$ , considerably faster than from other nucleotides, although electron transfer was seen in all cases.<sup>18b</sup> The excited state reduction potential for this NDI chromophore in aqueous solution was estimated to be 1.9 V versus NHE, with a triplet lifetime of 100  $\mu\text{s}$ .<sup>18a</sup> Recent results, however, suggest that electron transfer involving also the excited singlet state may be important. In fact, rapid electron transfer and charge recombination processes initiated

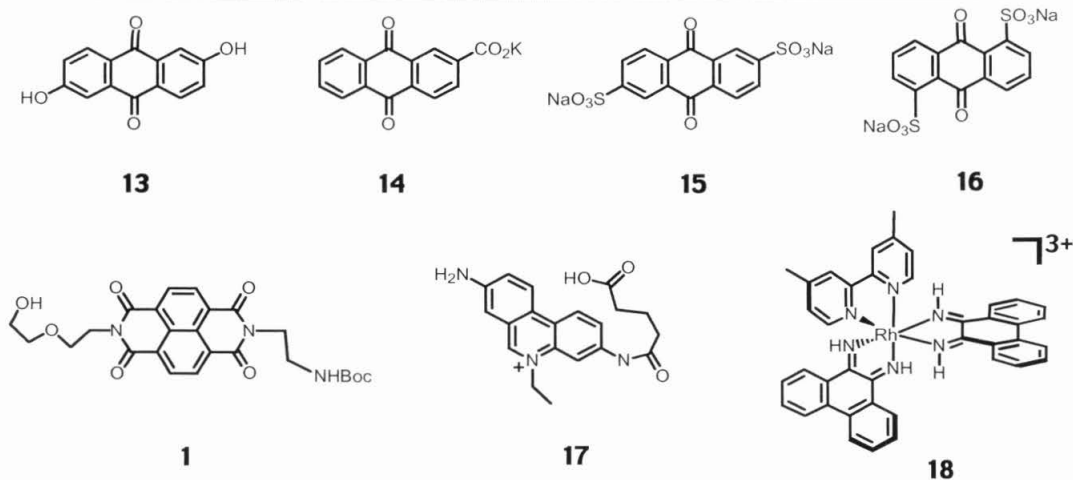


**Figure 6.2.** Photoexcitable intercalators used in this study.

by the electronically excited singlet state were found to predominate with DNA-bound NDI.<sup>18a</sup>

Both in the context of developing new synthetic molecules to repair the thymine dimer lesion and in an effort to explore further the parameters governing DNA charge transport chemistry, it was of substantial interest to find another intercalator that, as a potent photooxidant, could trigger the repair of thymine dimers in DNA from a distance. Here we describe assays for thymine dimer repair with several photooxidants (Figure 6.2) and, in particular, the demonstration of the repair of thymine dimers in DNA at a distance upon photoactivation of NDI.

## 6.2 EXPERIMENTAL

*Materials and Methods.* Oligonucleotides were prepared on an Applied Biosystems 394 DNA synthesizer, using phosphoramidite chemistry.<sup>20</sup> DNA was synthesized with a 5'-dimethoxy trityl (DMT) protective group and was purified by HPLC on a Dynamax 300 Å C<sub>18</sub> reversed-phase column (10 mm i.d. x 25 cm length) from Rainin on a Hewlett-Packard 1100 HPLC. The DMT group was removed by incubation in 80% acetic acid for 20 min at 20°C, and then the DNA was HPLC purified again. The



concentration of single stranded oligonucleotides in aqueous solution was determined by UV-visible spectroscopy on a Beckman DU 7400 Spectrophotometer;  $\epsilon$  (260 nm, L M<sup>-1</sup> cm<sup>-1</sup>) adenine = 15400; guanine = 11500, cytosine = 7400, thymine = 8700, T<>T = 0. Duplexes were formed by cooling solutions containing equimolar quantities of complementary oligonucleotides from 94 to 10°C over 120 min. [Rh(phi)<sub>2</sub>(bpy')]<sup>3+</sup> and *N*-8-glycyl ethidium were prepared according to previously published procedures.<sup>6,21,22</sup> Thymine dimer formation in synthetic oligonucleotides was performed photochemically, using acetophenone in large excess as a triplet photosensitizer as previously described.<sup>5,23</sup>

Preparations of oligonucleotides with appended naphthalene diimides and rhodium intercalators have been described elsewhere, and were performed by D. Gianolio.<sup>21,24</sup> Appending NDI onto DNA involves functionalizing a thymine nucleotide with an NDI unit, subsequently forming a 5-methylcytosine derivative. The synthesis of all NDI-containing strands was confirmed by MALDI mass spectroscopy, and were all within 2 mass units of the calculated values. Helix stabilization with covalent NDI is evident from melting temperature studies, where duplexes containing tethered NDI melted at least 3°C higher than those without. Model building indicated that NDI appended onto the base can easily intercalate within the duplex (with a minor roll of the cytosine) and the hydrophobicity of the NDI moiety would favor such intercalative stacking. Some aggregation of the conjugates has been observed over time.

*HPLC Assay for Thymine Dimer Repair.* Complementary DNA strands were annealed in buffer containing 50 mM sodium chloride, 10 mM sodium phosphate, pH 7.5. Oligonucleotide duplexes (8 μM) were irradiated with a 1000W Oriel Hg/Xe arc lamp fitted with a monochromator. Reactions run under anaerobic conditions were performed in a resealable vessel where the samples were degassed by 3 freeze-pump thaw cycles and subsequently flushed with 1 atm Ar or left under vacuum. Reaction mixtures were analyzed by HPLC at 65°C on a Sephasil C<sub>18</sub> reversed-phase column (4.6

mm i.d. x 25 cm length) from Pharmacia, eluting with a gradient of 50 mM  $\text{CH}_3\text{CO}_2\text{NH}_4/\text{MeCN}$  (98:2 to 98:7 over 20 min, isocratic at 93:7 for 10 min, to 50:50 over 5 min, isocratic at 50:50 for 1 min; flow rate = 1.1 mL/min). Under these conditions, the duplexes dissociate into single strands, each of which elutes from the column with a distinct retention time. Oligonucleotides containing a thymine dimer eluted first, followed by the corresponding repaired strand, and then the complement or the naphthalaldiimide-containing complement eluted last. Thymine dimer repair was quantitated from peak areas in the chromatograms (normalized for differences in molar absorptivity at the detection wavelength ( $\lambda = 260 \text{ nm}$ )).

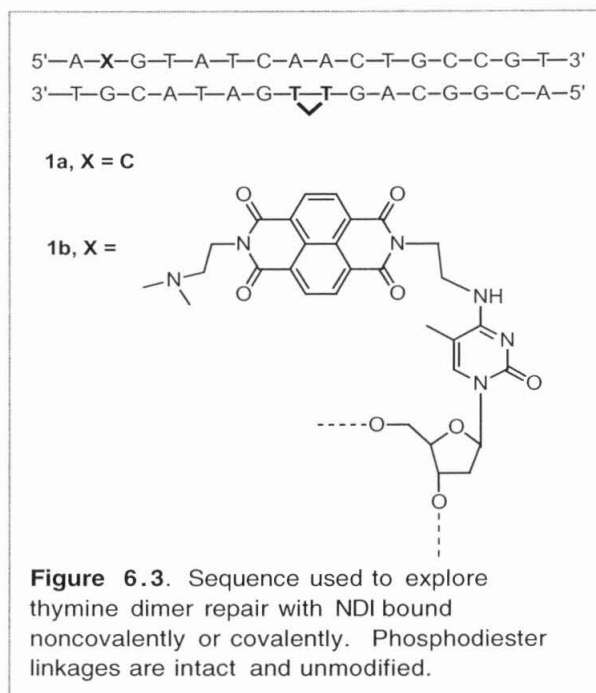
*Rapid Screen Photoligation Reversal Assay for  $T \leftrightarrow T$  Repair by Noncovalent Intercalators.* A  $^{32}\text{P}$ -endlabeled and gel purified oligonucleotide with a 3'-terminal thymidine was added to a mixture of the following: 10  $\mu\text{M}$  3'-terminal thymidine strand (unlabeled), 10  $\mu\text{M}$  oligonucleotide with a 5'-terminal thymidine, and 10  $\mu\text{M}$  splint strand complementary to their putative ligation product. This mixture was annealed as described above to form a nicked duplex oligonucleotide with a concentration of 10  $\mu\text{M}$  in 25 mM sodium phosphate at pH 7.0. This duplex mixture was then irradiated at 313 nm (4°C) to generate a  $T \leftrightarrow T$  dimer in ~25% of the duplexes. The resultant duplex mixture was used directly in experiments with noncovalent intercalators, and the disappearance of the larger molecular weight material containing the dimer was monitored versus control lanes. Experiments with noncovalent NDI used a 100  $\mu\text{M}$  stock methanolic solution of the intercalator; thus, in experiments using noncovalent NDI, the final solutions also contained ~10% methanol.

*Preparation for the Photoligation Reversal Assay for Long Range  $T \leftrightarrow T$  Repair.* A mixture of TT and  $T \leftrightarrow T$ -containing duplexes was used to screen noncovalent intercalators, as described above. To test covalently tethered intercalators for dimer repair at a distance, the photoligated dimer strand was first gel-purified and was then annealed to the oxidant-containing complementary strand. First the dimer-containing

photoligation product was formed as above. The resultant duplex after irradiation was then dried under vacuum, and the photoligation product was separated from the starting material and the complementary strand using denaturing gel electrophoresis. When electrophoresed for protracted periods, the splint strand complementary to the photoligation product containing the thymine dimer runs notably faster than the photoligation product, thus allowing their separation. The photoligated product was isolated by elution at 37°C into 10 mM Tris-HCl buffer pH 7.4, and desalted.

Oligonucleotides of the same sequence but with continuous phosphodiester backbones and lacking the T<>T lesion were used as carrier in these experiments.

Complementary strand containing bound NDI was annealed to carrier and labeled photoligation product. Irradiations were performed as described above at 1 or 10  $\mu$ M duplex in 25 mM sodium phosphate at pH 7.0. Dimer repair was monitored by denaturing gel electrophoresis as the conversion from the high molecular weight material containing the photoligated dimer to the smaller strands.



## 6.3 RESULTS

**6.3.1. HPLC Experiments with Noncovalent NDI.** Figure 6.3 illustrates the DNA duplexes prepared to examine thymine dimer repair in DNA upon photoactivation of NDI. Each duplex contains a thymine dimer site-specifically incorporated in the center of

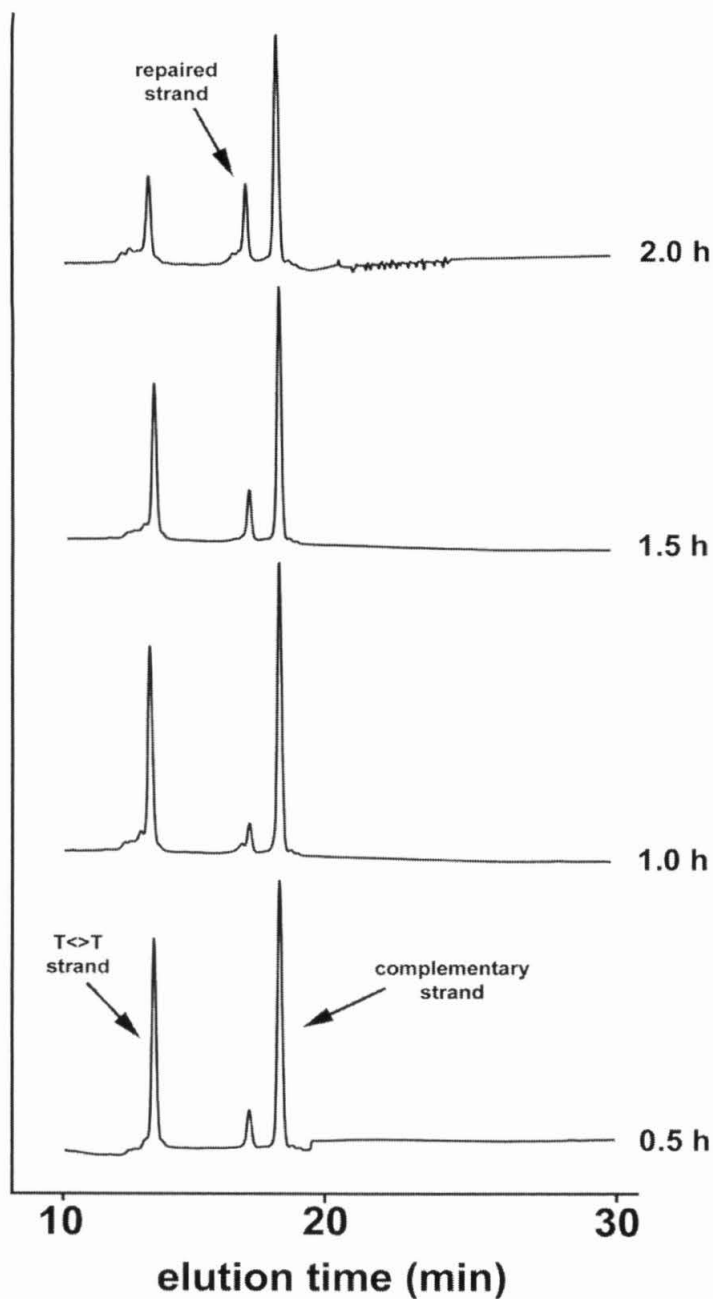


**Figure 6.4.** Photochemical repair of a thymine dimer in duplex DNA (8  $\mu$ M) containing unmodified phosphodiester buffer (10 mM) with 50 mM NaCl. Shown are (bottom to top) the HPLC chromatograms at 30, 60, 90, 120 minutes of irradiation at 380 nm. Experiments by D. Vicić, figure courtesy of D. Vicić.

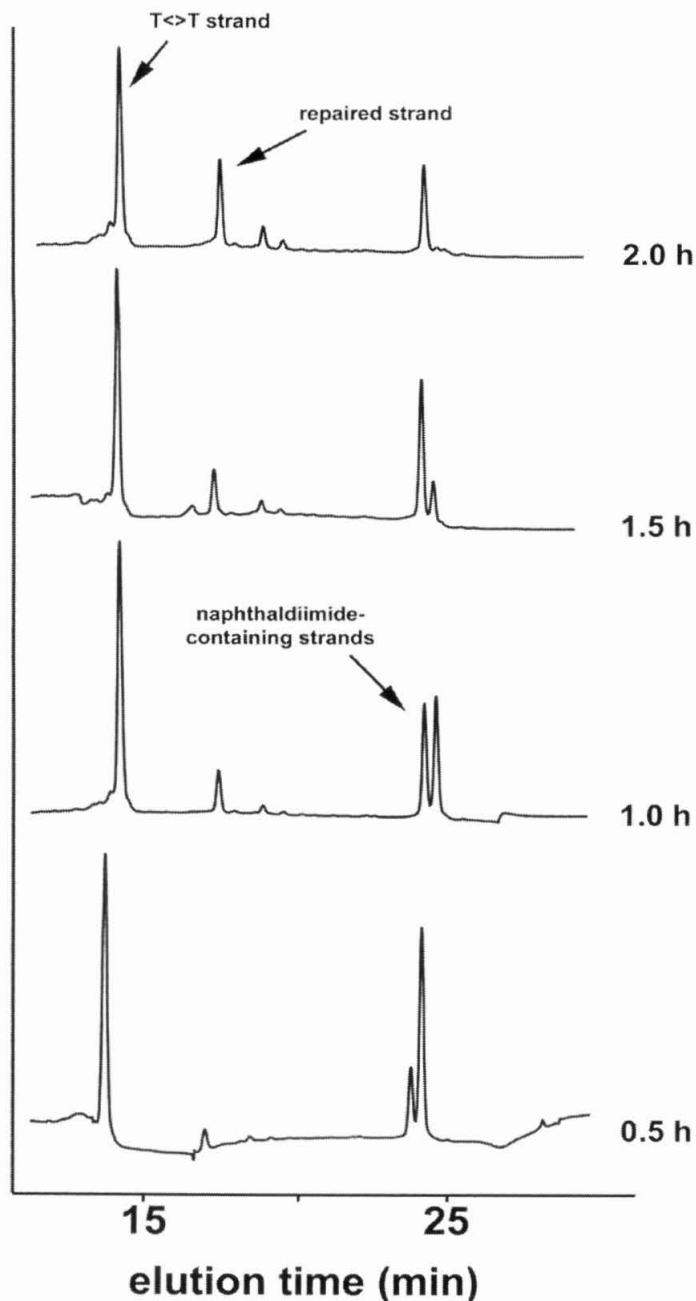


**Figure 6.5** Photochemical repair of a thymine dimer in DNA containing unmodified phosphodiester linkages by tethered NDI (8  $\mu$ M duplex) in sodium phosphate buffer (10 mM) with 50 mM NaCl. In the DNA assembly, covalently attached NDI is separated from the thymine dimer by  $\sim 22$  Å. Shown are (top to bottom) the HPLC chromatograms after 30, 60, 90, 120 minutes of irradiation at 380 nm. Experiments by D. Vicic, figure courtesy of D. Vicic.

the oligomer as well as a 5'-GG-3' doublet site. This sequence was used earlier in studies to test the competition between guanine damage and thymine dimer repair by a tethered rhodium intercalator.<sup>5b</sup> In this assay we examine repair by monitoring the conversion of the lesion-containing strand to the repaired strand by HPLC at denaturing temperatures (65°C) using free or tethered NDI.

As is evident in Figure 6.4, irradiating duplex **2** under anaerobic conditions with 380 nm light in the presence of free NDI (**1**) results in a substantial amount of dimer repair. We observe both the loss of thymine dimer-containing strand and the formation of the repaired strand. After 2 hours irradiation at 380 nm in the presence of **1** (8 µM), 38% repair of the T<>T containing strand can be seen. No significant damage to the complementary strand could be detected, although minor peaks do appear in the HPLC traces near both parent DNA strands, which we attribute to background oxidative damage under the relatively long irradiations. Interestingly, no repair is evident at low NDI concentrations (< 2 µM).

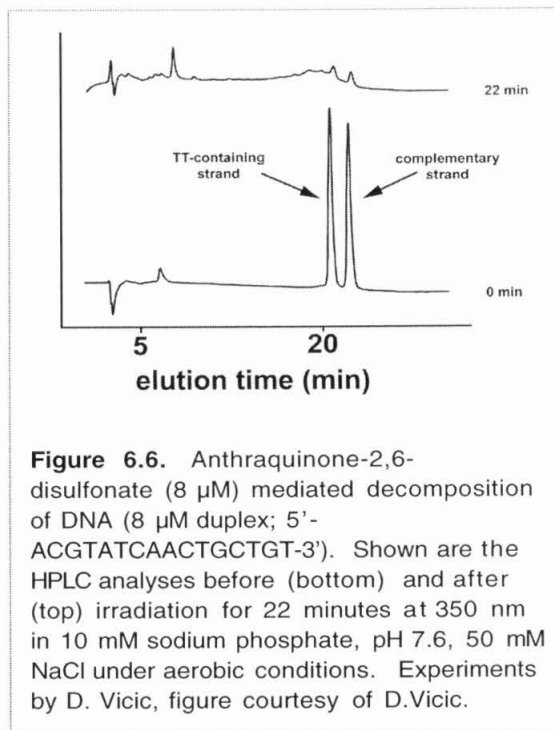
*6.3.2. HPLC Experiments with Covalent NDI.* Irradiating duplex **3**, which contains a covalently incorporated NDI spatially well-separated from the thymine dimer, at 380 nm under anaerobic conditions also results in a significant repair of the thymine dimer (Figure 6.5). After 2 h, 25% of the thymine dimer-containing strand was repaired, similar to the extent of repair seen for noncovalent NDI. It should also be noted that the duplex contains a 5'-GG-3' site, and we observed in gel experiments that oxidation of the 5'-G in the 5'GG-3' site does take place under aerobic conditions (not shown), consistent with the fact that charge transfer is occurring from the tethered NDI group.<sup>14</sup> Under anaerobic conditions, the oxidation of guanine is suppressed, thus simplifying the HPLC analyses.

The HPLC traces also reveal that during this repair process, the NDI-functionalized strand converts to a new species. The new, naphthalldiimide-containing strand was found to be 14 mass units less than the NDI-containing parent strand, as

measured by MALDI-TOF mass spectrometry. A similar mass loss was seen in experiments by Saito and coworkers, who found that irradiating a thymine derivative in the presence of a nitro-substituted 1,8-naphthalimide chromophore led to a demethylated product which arose from hydrogen atom abstraction from the thymine methyl group.<sup>25</sup> Given that the 5-methyl cytosine is in close proximity to the naphthalimide chromophore, such a demethylation reaction in this system seems quite

feasible. The persistence of the absorbance at 380 and 365 nm after irradiation suggests that the NDI chromophore remains intact. Additionally, given the high molecular weight of the DNA strand, it can be concluded that the chromophore is still attached to DNA. Conversion of the NDI-containing parent strand to the new strand is also evident upon irradiation of the NDI-containing parent strand in the absence of its complement.<sup>26</sup> It is noteworthy that repair of the thymine dimer continues even after complete conversion to the new naphthalimide-containing strand.

These results were also compared to those obtained upon irradiation of DNA in the presence of an anthraquinone for much shorter irradiation times. Anthraquinones are also potent photooxidants which have been used in studies of DNA charge transport. As is evident in Figure 6.6, and in contrast to previous NDI results, efficient decomposition of DNA by free anthraquinones appears to be the predominant reaction when the irradiations were monitored by HPLC. These conditions are comparable to those used in previous studies, and anthraquinones require oxygen for efficient charge



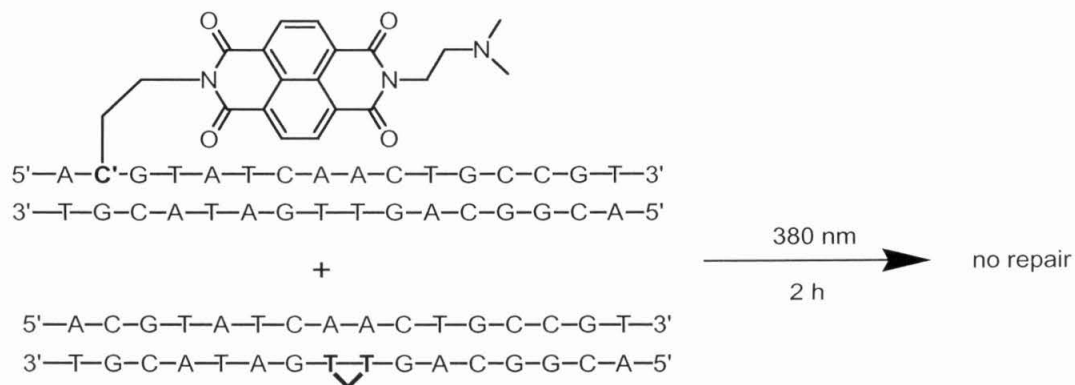


**Figure 6.7.** Control experiment demonstrating the intraduplex nature of the repair process. About 2% repair was observed in this control versus 25% repair for intraduplex reactions.

separation in DNA. Given these HPLC analyses, we are concerned about any application of anthraquinones as sensitizers for oxidative thymine dimer repair in DNA.

A critical issue to establish was whether the repair reaction occurs only in an intraduplex fashion. This was a concern, as a small amount of decomposition of the NDI strand could be detected with long time irradiations (Fig. 6.5, retention time ~17 min, mass = 4854.3). To test this question, a control reaction under the same conditions and total concentration of reagents was conducted in which the tethered naphthalendiimide-containing strand was annealed to the native strand, and subsequently mixed together with an equal amount of duplex containing the thymine dimer but lacking bound NDI (Figure 6.7). Upon irradiation at 380 nm for 2 hours under anaerobic conditions, only 2% repair was measured, confirming the intraduplex nature of the reaction described above. This control reaction demonstrates that a diffusible species cannot be responsible for repair of the thymine dimer. Therefore, while a small level of interduplex repair can be measured, it is insufficient to account for the greater than 10-fold higher level of repair seen with covalently bound NDI.

Hence, these data establish that, with photoactivation, NDI can promote the repair of a thymine dimer incorporated in a DNA duplex from a remote site. Here the



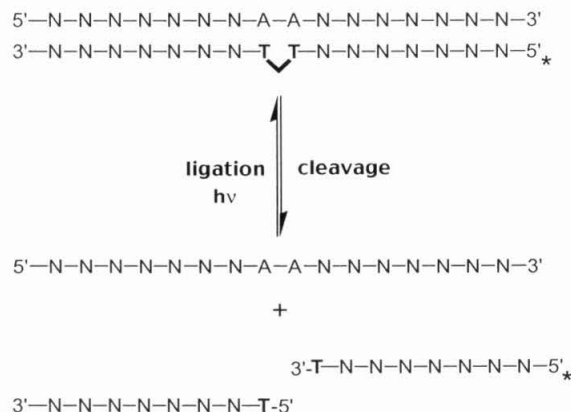


**Figure 6.8.** Schematic diagram showing the template directed photoligation of oligonucleotides effected by cyclobutane dimer formation. An asterisk indicates the site of a  $^{32}\text{P}$  radioactive label. Because there is no phosphodiester linkage between the thymine dimer's sugars, ligated versus cleaved strands are readily visualized by gel electrophoresis.

distance separating NDI and the thymine dimer (taken as the distance between an intercalated NDI and the center of the cyclobutane ring and assuming 3.4 Å stacking between bases) is ~22 Å.

**6.3.3 Photoligation Reversal Assay for Thymine Dimer Repair.** An additional, convenient assay to test for thymine dimer repair by tethered and nontethered intercalators using gel electrophoresis was developed. It has been shown in previous research that DNA can act as a template to ligate photochemically two strands of oligonucleotides containing 5'- and 3'-terminal thymidines (Figure 6.8).<sup>27</sup> Notably, the resultant thymine dimer lacks a phosphodiester linkage. The proportions of different possible thymine dimer isomers obtained by photoligation have not been established. If two strands of DNA are held together by a bridging thymine dimer without a phosphodiester linkage, then one can assay thymine dimer repair simply by monitoring the conversion of the high molecular weight strand to the "repaired," and therefore, smaller molecular weight species using denaturing gel electrophoresis. Figure 6.9 shows the duplexes prepared to test for repair. This assay provides a rapid and general screen for thymine dimer repair activity of candidate molecules.

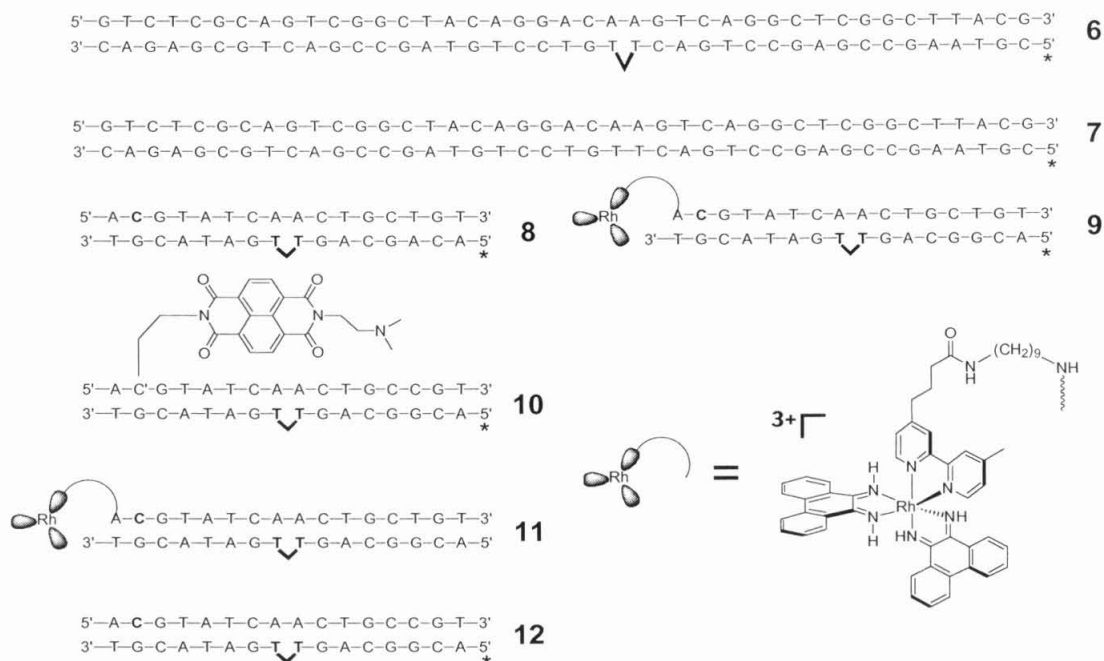


**Figure 6.9.** Sequences of the duplexes used to monitor the repair of photoligated thymine dimers. **10** and **12** are identical in sequence to duplexes **3** and **4**, respectively, except for the absence of a phosphodiester linkage between the sugars of the thymine dimer.

The first set of experiments employed a 41-mer duplex with the photoligated strands consisting of one 18-mer and one 23-mer, and the complementary strand consisting of 41 bases (duplex **6**, Figure 6.9). The 18-mer was radioactively end-labeled, mixed with the unlabeled 23-mer, and then annealed to the 41-mer complement splint. After irradiating this nicked duplex for 1 h at 313 nm, photoligation of the 18-mer and 23-mer to form a new 41-mer is evident. The photoligation can be monitored by denaturing gel electrophoresis, since the labeled, photoligated 41-mer runs more slowly than the parent 18-mer (Figure 6.10). For this assay, the 41-mer duplex product was not subsequently separated from the reactants used for the photoligation. Hence, signal from background radiolabeled 18-mer is evident in all lanes. Nonetheless the extent of repair can be quantitated by measuring changes in the ratio of 41-mer to 18-mer. With

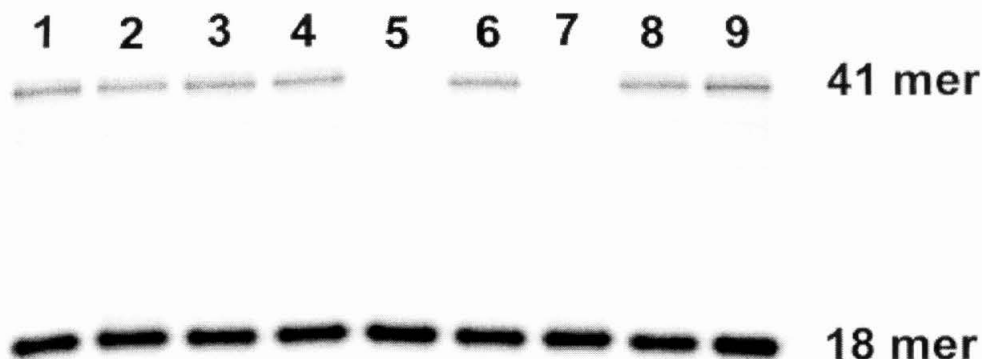


**Figure 6.10.** Autoradiogram of the denaturing gel illustrating the reversal of the thymine dimer in duplex **6**, which does not contain a phosphodiester linkage between the thymine dimer. All experiments were done under aerobic conditions, with DNA (10  $\mu$ M) and intercalators (10  $\mu$ M) in sodium phosphate buffer (25 mM). Top band represents the 41-mer while the bottom band represents the 18 mer. The loss of the 41-mer band is indicative of repair. Lanes 1-6, irradiation at 350 nm for 30 min in the presence of anthraflavic acid (**13**), anthraquinone-2-carboxylate (**14**), 2,6-disulfate anthraquinone (**15**), and 1,5-disulfate anthraquinone (**16**), NDI (**1**), N-8-glycyl ethidium (**17**). Lane 7, irradiation for 30 min at 365 nm in the presence of  $[\text{Rh}(\text{phi})_2(\text{dmb})]^{3+}$  (**18**). Lane 8, irradiation at 313 for 1 h to form T<>T ligation, then irradiation for 30 min at 350 nm. Lane 9, irradiation at 313 nm for 1 h.

this sample containing the photoligated duplex **6**, we then screened a variety of intercalating compounds to test for thymine dimer repair activity.

Four different anthraquinones were tested for their ability to repair thymine dimers, since anthraquinones have previously been shown to oxidize guanines from a distance in double stranded DNA.<sup>10</sup> Anthraflavic acid (**13**), anthraquinone-2-carboxylate (**14**), 2,6-disulfate anthraquinone (**15**), and 1,5-disulfate anthraquinone (**16**) (see Figure 6.2) were all tested, but as shown in Figure 6.10, no repair of the thymine dimer could be detected with these anthraquinones after 30 minutes' irradiation at 350 nm. To verify that the anthraquinones were bound to DNA under these conditions, a separate experiment was performed where **14** was added to the native 41-mer duplex **7**, irradiated for up to 60 minutes at 350 nm, and piperidine-treated to reveal DNA damage. Under these conditions, it was observed that the anthraquinone oxidized the 5'-G of 5'-

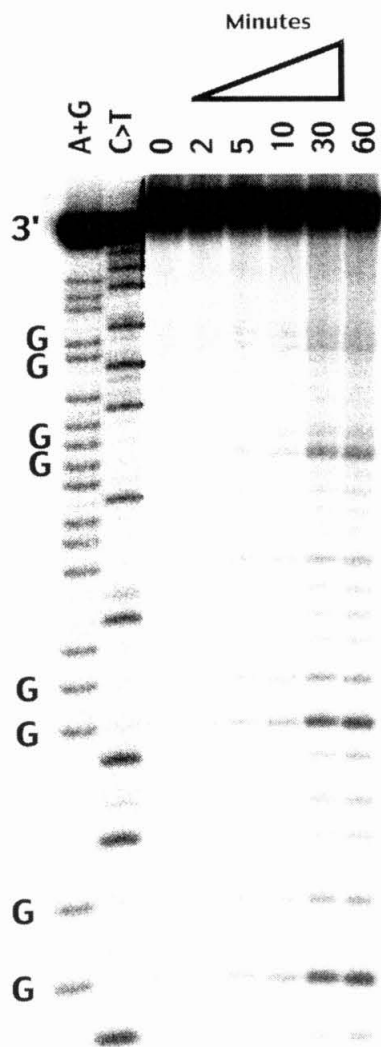


**Figure 6.11.** Guanine oxidation demonstrating noncovalent binding of anthraquinones. Lanes A+G and C>T are Maxam-Gilbert sequencing lanes, and the lanes increase in time (left to right) from a non-irradiated lane to one hour. Conditions were identical to those in Figure 6.10.

GG-3' sites, consistent with an electron transfer reaction (Figure 6.11). Thus, although the anthraquinone was able to bind to and oxidize guanine in the 41-mer duplex **7**, it was unable to repair the thymine dimer duplex in **6**. It is noteworthy that the anthraquinones used in this study are very similar in composition to anthraquinone-2-sulfonate, a complex that was used to split thymine dimers in model systems.<sup>28</sup>

Figure 6.10 also reveals the results of irradiating duplex **6** with noncovalent NDI, *N*-8-glycyl ethidium (**17**), and  $[\text{Rh}(\text{phi})_2(\text{dmb})]^{3+}$  (**18**). As is shown on the gel, only NDI and  $[\text{Rh}(\text{phi})_2(\text{dmb})]^{3+}$  were capable of repairing the photoligation, as indicated by the loss of the 41-mer band. Upon repair of the thymine dimer, the labeled 18-mer is released and travels much faster in the denaturing gel. No significant repair was observed with *N*-8-glycyl ethidium upon irradiation at 350 nm. At 313 nm, where photolysis of bound ethidium promotes the oxidation of guanine, dimer repair could not be distinguished from photoequilibration of the dimer. This assay is a simple screen, and may provide a means to test rapidly other compounds for thymine dimer repair activity.<sup>29</sup>

*6.3.4 Long Distance Repair Assayed by Photoligation Reversal.* We were interested in testing thymine dimer repair with covalently bound oxidants using the photoligation reversal assay as well as in examining the repair of DNA duplexes that were similar in composition to those used in the HPLC experiments. To prepare duplexes **8-10**, an 8-mer was radiolabeled and gel purified, and then mixed together with the second 8-mer and annealed to the appropriate 16-mer complement that did not contain functionalized chromophore. The photoligation was effected for 2 hours at 313 nm (4°C), and then the radiolabeled, ligated 16-mer was gel purified a second time under denaturing conditions. Thus the photoligated products were isolated from the 8-mer starting material and the 16-mer splint. The labeled, photoligated 16-mer was then annealed to the appropriate complements giving duplexes **8-10**.

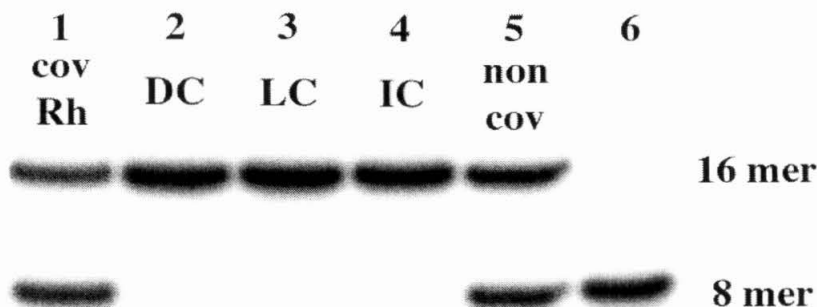


**Figure 6.12.** Autoradiogram of the denaturing gel showing reversal of a thymine dimer with free and tethered  $[\text{Rh}(\text{phi})_2(\text{bpy}') ]^{3+}$ . All experiments were done under aerobic conditions, with DNA that does not contain a phosphate linkage between the thymine dimer (1  $\mu\text{M}$ ) and intercalator (1  $\mu\text{M}$ ) in sodium phosphate buffer (25 mM). Repair is assayed by monitoring cleavage to form the 8-mer. Lanes 1 and 2, irradiation of duplex **9** at 365 nm for 1 h and 0 h, respectively. Lane 3, irradiation of duplex **10** for 1 h. Lane 4, interduplex control, irradiation of duplexes **8** and **11** for 1 h. Lane 5, irradiation of duplex **8** with an equimolar amount of  $[\text{Rh}(\text{phi})_2(\text{bpy}') ]^{3+}$ . Lane 6, dark control containing radiolabeled 8 mer.

Long-range thymine dimer repair initiated by  $[\text{Rh}(\text{phi})_2(\text{bpy}') ]^{3+}$  was tested using the photoligation reversal assay. Figure 6.12 shows the result of irradiating duplexes **8** (with free rhodium complex **18**) and **9** for 1 hour at 365 nm. Repair for covalently bound rhodium was 66%, while that for noncovalently bound rhodium was 44%. An interduplex control reaction (lane 4, Figure 6.12) revealed only 2% repair, demonstrating that a diffusible species in the reaction mixture cannot account for the observed repair. It is noteworthy that the ratio of repair seen between covalent and non-covalent rhodium in the photoligation reversal assay is much greater than that seen previously,<sup>5</sup> and may be a consequence of the structural and electronic properties of the DNA sequence employed. The photoligation experiment with rhodium involves a somewhat different base sequence, but also a thymine dimer, or a mixture of thymine dimer isomers, that do not contain a phosphodiester linkage. These structural properties may serve to insert the thymine dimer deeper into the base stack and thus render it more accessible to migrating charge.

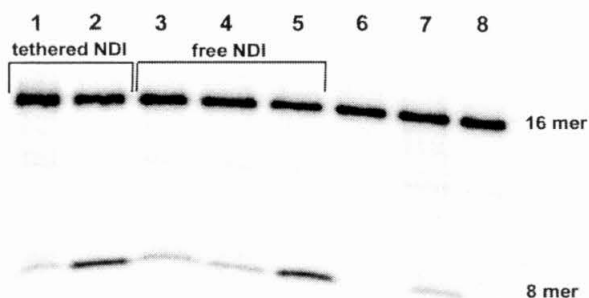


**Figure 6.13.** Autoradiogram of the denaturing gel showing reversal of a thymine dimer with free and tethered NDI. All experiments were done under anaerobic conditions, with DNA containing a thymine dimer lacking the interresidue phosphate linkage (10  $\mu$ M) and intercalator (10  $\mu$ M) in sodium phosphate buffer (25 mM). Repair is assayed by monitoring cleavage to form the 8-mer. Lanes 1 and 2, irradiation of duplex **10** at 380 nm for 0 and 2 h, respectively. Lanes 3-5, irradiation of duplex **12** at 380 nm for 0 h, 0 h in the presence of free NDI, and 2 h in the presence of free NDI. Lane 6, interduplex control (mixture of duplexes **5** and **12**) after 2 h irradiation at 380 nm. Lane 7, Duplex **12** irradiated in the absence of intercalator. Lane 8, irradiation of anthraquinone-2-carboxylate and duplex **12** for 2 h at 350 nm.

We examined dimer repair upon anaerobic irradiation of duplexes **10** and **12**, which contain covalent and noncovalent NDI, respectively (Figure 6.13). Substantial repair occurred after 2 hours in both cases (27% for both covalent and noncovalent NDI) and is readily apparent, since under the denaturing conditions of the gel, the radiolabeled 8-mer migrates much faster than the ligated 16-mer. Duplex **5** was irradiated in the presence of an equimolar amount of duplex **12** for 2 hours at 380 nm as a control to test for any interduplex repair. Only 1% of interduplex repair could be detected by gel electrophoresis. The results, shown in Figure 6.13, demonstrate that the repair due to a diffusible species produced throughout the course of the reaction, or from any interduplex interactions with the tethered naphthalendiimide, cannot account for the reaction of the covalently bound assembly. Here too, under anaerobic conditions, no repair could be observed by irradiating duplex **12** in the presence of free anthraquinone-2-carboxylate for 2 hours at 350 nm.

## 6.4 DISCUSSION

### 6.4.1. Repair of Thymine Dimers with NDI and $[Rh(phi)_2(bpy)]^{3+}$ at a Distance.

Here we have demonstrated that a thymine dimer in DNA can be repaired by long-range electron transfer to NDI with photoactivation. The repair is triggered from an oxidant located  $\sim 22$  Å from the lesion, using duplex DNA as a bridge for charge transport. A rapid screening assay for thymine dimer repair was additionally developed. Using this assay, noncovalently bound NDI as well as the rhodium intercalator were demonstrated to repair thymine dimers in DNA, where under the same conditions, a variety of anthraquinones could not.

Given that both the phi complex of rhodium<sup>5</sup> and the organic NDI intercalator have now been shown to promote oxidative repair of thymine dimers, it is interesting to compare their reactivity. HPLC experiments reveal that the efficiency of repair by the noncovalent NDI oxidant appears to be somewhat lower than that found for the rhodium complex, and gel assays on the thymine dimers lacking a phosphodiester linkage show the repair efficiencies to be roughly comparable. Perhaps more noteworthy is the comparison between repair from a distance versus non-covalently with both oxidants. Earlier we observed that the repair efficiency with non-covalently bound metal complex was  $\sim 30$  times greater than that observed from long range.<sup>5</sup> Here the sequence differs slightly from that studied earlier, but in the case of covalently bound rhodium, we are now monitoring the repair of the mixture of thymine dimers lacking phosphodiester linkages.

It was found for the rhodium intercalator, as with NDI, that repair from a distance or with non-covalently bound oxidant is comparable. In the case of the gel assays, possibly the conformation of these presumably more flexible thymine dimers permit better overlap within the base pair stack. For NDI, however, equivalent efficiencies using covalent and non-covalent oxidants were seen also in the HPLC assays using true thymine dimers with the phosphodiester linkage. It may then also be the case that,



compared to the metallointercalator, where the tether on the metal complex may somewhat restrict optimal overlap of the intercalating unit with the base stack, the NDI-based intercalators have greater surface area available for stacking; certainly they are extremely hydrophobic.

*6.4.2. Reductive Repair of Thymine Dimers with Flavins at a Distance.* It was recently shown that covalently tethered flavins in an anaerobic environment were able to repair thymine dimers in duplex DNA when photoirradiated to inject an electron into the base stack.<sup>30</sup> This reductive repair was seen to occur in cases where the lesion was directly abutting the photoexcitable flavin, and where the lesion was removed by an A•T base pair. The repair was attributed to a hopping mechanism similar to that suggested by Giese. No evidence, however, was found that long range hole transport in this system could repair dimers.

*6.4.3. Anthraquinones and  $[Ru(phen)(bpy')(dppz)]^{3+}$  Lack of Reactivity.* It is also important to consider those photooxidants for which no repair is observed, either from a distance or directly when non-covalently bound. We saw earlier that for  $[Ru(phen)(bpy')(dppz)]^{3+}$ , although efficient guanine oxidation by DNA-mediated charge transport can be observed, no thymine dimer repair is evident. We ascribed that result to the reduction potential of the  $Ru^{3+}$  species, estimated to be 1.6 V vs. NHE and thus insufficient to oxidize the dimer. In the case of NDI, which can promote thymine dimer repair, the reduction potential is at least 1.9 V versus NHE. Our results with anthraquinones, however, suggest that redox potential may not be the sole determinant for predicting candidate molecules for thymine dimer repair. Anthraquinone-2,6-disulfonate (**15**) is reported to have an excited state triplet reduction potential of 2.4 V versus NHE in aqueous solution,<sup>31</sup> yet repair with noncovalent anthraquinones could not be detected under our experimental conditions.

In addition to achieving the appropriate thermodynamics, the excited-state character of the oxidant may also have to be tailored to suit the electronic properties of

the substrate. Thymine dimer formation and splitting via a concerted mechanism are photochemically allowed *via* an excited singlet state.<sup>32</sup> There are many examples that suggest thymine dimerization/splitting reactions result from an excited singlet state.<sup>33,34</sup> In fact, the naturally occurring enzyme photolyase repairs thymine dimers by electron transfer from the singlet excited state of FADH<sub>2</sub> in high quantum yields.<sup>35</sup> It should be noted that oxidative reactions of NDI bound to DNA have recently been proposed to proceed from the excited singlet state.<sup>18a</sup> In contrast, triplet energy transfer to thymine dimers in DNA is known to be an inefficient process.<sup>33</sup> This could be the reason why we were unable to detect repair using anthraquinones, molecules whose intersystem crossing to the triplet state is extremely efficient, particularly within DNA.<sup>36</sup> It is noteworthy that anthraquinones have been shown to repair thymine dimers in model systems, albeit with irradiation in the UV range, but not in DNA. Our results caution against relating repair in a DNA duplex to these models. In fact, Schuster has questioned studies of rhodium repair from a distance based upon the poor repair efficiency of anthraquinones.<sup>37</sup> It should, however, be self-evident that repair from a distance within a DNA duplex cannot be achieved if the non-covalently bound oxidant is unable to promote repair in DNA.

*6.4.4. Mechanistic Considerations and Future Directions.* Given that the oxidant has the necessary characteristics to repair thymine dimers in DNA, oxidative repair of thymine dimers from a distance appears now to be a more general phenomenon and not specific to rhodium intercalators. How then does the charge migrate from one end of the DNA duplex to the thymine dimer located in the middle of the duplex? The fact that thymine dimer repair can occur from a remote site implies that charge is not localized exclusively on guanines, the base of lowest oxidation potential. It has previously been suggested that long range charge transfer occurs via a hopping mechanism in which charge tunnels between DNA bases of low redox potentials.<sup>10f,g</sup> Here, the thymine dimer is of significantly higher oxidation potential than the guanine, and yet repair is observed.

Hence, some charge, however transient, must reside on the thymine dimer. A mechanism which involves a hole hopping from base to base from an oxidant capable of oxidizing all the bases in DNA can account for our long range repair results, as could a mechanism that invokes a delocalized band model.

Previous work has demonstrated that the NDI chromophore does have the appropriate redox potential to oxidize all of the bases in DNA in aqueous solution.<sup>18a</sup> Alternatively, the mechanism of thymine dimer repair may require a combination of hopping and delocalized band formation, and such mechanistic models are starting to emerge.<sup>10b-c,38</sup> It is also interesting that a model has appeared which explains preferential thymine dimer formation in long pyrimidine tracts by invoking delocalization of adsorbed singlet energy through the pi-stack in DNA.<sup>32a</sup> Given these results, it will be important also to understand the fundamental principles governing this chemistry in the context of other DNA-mediated electron transfer reactions. Measurements of rates and efficiencies of repair with different oxidants, and as a function of intervening DNA sequence and structure, will be critical in delineating mechanisms of DNA charge transport.

Finally, these results raise the intriguing possibility that DNA-targeted therapeutics can be designed to function from a distance, using DNA as a bridge for charge transport. This would constitute a new approach to drug design, since most DNA-targeted therapeutics rely on site-specific interactions between the drug and DNA to carry out a specific transformation.<sup>39</sup> Moreover, electron transfer reactions need not be directed only to the site of lowest thermodynamic potential within the duplex. Indeed, in the case of thymine dimer repair, the reaction must be kinetically, rather than thermodynamically, limited. In the systems examined thus far, however, it is the case that guanine oxidation may occur along with repair of the dimer. This poses limitations for the utility of rhodium and NDI-based photochemistry for the therapeutic repair of thymine dimers. However, our results with anthraquinones also suggest that one may

be able to tune the acceptor molecule to carry out a *specific* reaction in DNA (*i.e.*, guanine oxidation versus thymine dimer repair). In this regard, a better understanding of the salient features of DNA-mediated electron transfer chemistry may make it possible to develop redox active chemotherapeutic agents that function from a distance. Certainly, the photoligation assay developed in this study may prove to be helpful in finding such molecules.

## 6.5 REFERENCES

- 1) (a) Taylor, J.-S. *Acc. Chem. Res.* **1994**, 27, 76-82. (b) Begley, T. P. *Acc. Chem. Res.* **1994**, 27, 394-401. (c) Taylor, J.-S. *Pure & Applied Chem.* **1995**, 67, 183-190. (d) Friedberg, E. C.; Walker, G. C.; Siede, W. *DNA Repair and Mutagenesis* American Society for Microbiology, Washington, DC. 1995.
- 2) (a) Mu, D.; Hsu, D. S.; Sancar, A. *J. Biol. Chem.* **1996**, 271, 8285-8294. (b) Szymkowski, D. E.; Lawrence, C. W.; Wood, R. D. *Proc. Natl. Acad. Sci. USA* **1993**, 90, 9823-9827. (c) Sancar, A. *Ann. Rev. Biochem.* **1996**, 65, 43-81.
- 3) (a) Heelis, P. F.; Hartman, R. F.; Rose, S. D. *Chem. Soc. Rev.* **1995**, 24, 289. (b) Sancar, A. *Biochemistry* **1994**, 33, 2-9.
- 4) (a) Charlier, M.; Hélène, C. *Photochem. Photobiol.* **1975**, 21, 31-37. (b) Hélène, C.; Charlier, M. *Photochem. Photobiol.* **1977**, 25, 429-434. (c) Jacobsen, J. R.; Cochran, A. G.; Stephans, J. C.; King, D. S.; Schultz, P. G. *J. Am. Chem. Soc.* **1995**, 117, 5453-5461. (d) Kim, S.-T.; Rose, S. D.; *J. Phys. Org. Chem.* **1990**, 3, 581-586. (e) Carell, T.; Epple, R. *Eur. J. Org. Chem.* **1998**, 1245-1258. (f) Carell, T. *Angew. Chem. Int. Ed. Engl.* **1995**, 34, 2491-2494. (g) Yeh, S. R.; Falvey, D. E. *J. Am. Chem. Soc.* **1992**, 114, 7313-7314. (h) Scannell, M. P.; Fenick, D. J.; Yeh, S. R. *J. Am. Chem. Soc.* **1997**, 119, 1971-1977.

- 5) (a) Dandliker, P. J.; Homlin, R. E.; Barton, J. K. *Science* **1997**, 275, 1465-1468. (b) Dandliker, P. J.; Núñez, M. E.; Barton, J. K. *Biochemistry* **1998**, 37, 6491-6502.
- 6) (a) Hall, D. B.; Holmlin, R. E.; Barton, J. K. *Nature* **1996**, 382, 731-735. (b) Hall, D. B.; Barton, J. K. *J. Am. Chem. Soc.* **1997**, 119, 5045-5046. (c) Núñez, M. E.; Hall, D. B.; Barton, J. K. *Chem. Biol.* **1999**, 6, 85-97. (d) Holmlin, R. E.; Dandliker, P. J.; Barton, J. K. *Angew. Chem. Int. Ed. Eng.* **1997**, 36, 2714-2730.
- 7) Barton, J. K. *Science* **1986** 233, 727.
- 8) Sugiyama, H.; Saito, I. *J. Am. Chem. Soc.* **1996**, 118, 7063-7068.
- 9) (a) Cadet, J.; Berger, M.; Douki, T.; Gasparutto, D.; Pouget, J.P.; Ravanat, J.L.; Sauvaigo, S. *J. Phys. IV*, **1999**, 9, 91-95. (b) Cadet, J.; Berger, M.; Douki, T.; Morin, B.; Raoul, S.; Ravanat, J.L.; Spinelli, S.; *Biol. Chem.* **1997**, 378, 1275-1286. (c) Burrows, C. J.; Muller, J. G. *Chem. Rev.* **1998**, 98, 1109-1151. (d) Kino, K.; Saito, S.; Sugiyama, H. *J. Am. Chem. Soc.* **1998**, 120, 7373-7374.
- 10) (a) Gasper, S. M.; Schuster, G. B. *J. Am. Chem. Soc.* **1997**, 119, 12762-12771. (b) Henderson, P. T.; Jones, D.; Hampikian, G.; Kan, Y.; Schuster, G. B. *Proc. Natl. Acad. Sci., USA* **1999**, 96, 8353-8358. (c) Ly, D.; Sanii, L.; Schuster, G. B. *J. Am. Chem. Soc.* **1999**, 121, 9400-9410. (d) Kan, Y.; Schuster, G. B. *J. Am. Chem. Soc.* **1999**, 121, 10857-10864. (e) Sartor, V.; Henderson, P. T.; Schuster, G. B. *J. Am. Chem. Soc.* **1999**, 121, 11027-11032. (f) Meggers, E.; Michel-Beyerle, M. E.; Giese, B. *J. Am. Chem. Soc.* **1998**, 120, 12950-12955. (g) Giese, B.; Wessely, M.; Spormann, M.; Lindermann, U.; Meggers, E.; Michel-Beyerle, M. E.; *Angew. Chem. Int. Ed. Eng.* **1999**, 38, 996-998. (h) Meggers, E.; Kusch, D.; Spichty, M.; Wille, U.; Giese, B. *Angew. Chem. Int. Ed. Eng.* **1998**, 37, 460-462. (i) Arkin, M. R.; Stemp, E. D. A.; Pulver, S. C.; Barton, J. K. *Chem. Biol.* **1997**, 4, 389-400. (j) Hall, D. B.; Kelley, S. O.; Barton, J. K. *Biochemistry* **1998**, 37, 15933-15940.
- 11) (a) Steenken, S.; Jovanovic, S.V. *J. Am. Chem. Soc.* **1997**, 119, 617-618. (b) Johnston, D. H.; Cheng, C. -C.; Campbell, K. J.; Thorp, H. H. *Inorg. Chem.* **1994**, 33,

- 6388-6390. (c) Brabec, V.; Dryhurst, G. *J. Electroanal. Chem.* **1978**, 89, 161-173. (d) Brabec, V. *Biophys. Chem.* **1979**, 9, 289-297.
- 12) Turro, C.; Enezhahav, A.; Bossman, S. H.; Barton, J. K.; Turro, N. J. *Inorg. Chim. Acta* **1996**, 243, 101-108.
- 13) Murphy, C. J.; Arkin, M. R.; Ghatlia, N. D.; Bossman, S.; Turro, N. J.; Barton, J. K. *Proc. Natl. Acad. Sci. USA* **1994**, 91, 5315-5319.
- 14) Núñez, M. E.; Noyes, K. T.; Gianolio, D. A.; McLaughlin, L. W.; Barton, J. K. *Biochemistry* **2000**, 39, 6190-6199.
- 15) (a) Brana, M. F.; Sanz, A. M.; Castellano, J. M.; Roldan, C. M. *Eur. J. Med. Chem.* **1981**, 16, 207-212. (b) Kirshenbaum, M. R.; Chen, S.-F.; Behrens, C. H.; Papp, L. M.; Stafford, M. M.; Sun, J.-H.; Behrens, D. L.; Fredericks, J. R.; Polkus, S. T.; Sipple, P.; Patten, A. D.; Dexter, D.; Seitz, S. P.; Gross, J. L. *Cancer Res.* **1994**, 54, 2199-2206.
- 16) (a) Rideout, D.; Schinazi, R.; Pauza, C. D.; Lovelace, K.; Chiang, L.-C.; Calogeropoulou, T.; McCarthy, M.; Elder, J. H. *J. Cell. Biochem.* **1993**, 51, 446-457. (b) Lewis, D. E.; Utecht, R. E.; Judy, M. M.; Matthews, J. L.; Chanh, T. C. *Spectrum J. State Gov.* **1993**, 6, 8-14.
- 17) (a) Waring, M. J.; Gonzalez, A.; Jimenez, A.; Vazquez, D. *Nucleic Acids Res.* **1979**, 7, 217-233. (b) Yen, S.-F.; Gabbay, E. J.; Wilson, W. D. *Biochemistry* **1982**, 21, 2070-2076. (c) Tanious, F. A.; Yen, S.-F.; Wilson, W. D. *Biochemistry* **1991**, 30, 1813-1819.
- 18) (a) Rogers, J. E.; Weiss, S. J.; Kelly, L. A. *J. Am. Chem. Soc.* **2000**, 122, 427-436. (b) Rogers, J. E.; Kelly, L. A. *J. Am. Chem. Soc.* **1999**, 121, 3854-3861. (b) Rodrigues, M. A.; Brochsztain, S.; Barros, T. C.; Baptista, M. S.; Politi, M. J. *Photochem. Photobiol.* **1999**, 70, 35-39. (c) Aveline, B. M.; Matsugo, S.; Redmond, R. W. *J. Am. Chem. Soc.* **1997**, 119, 11785-11795. (d) Hasharoni, K.; Levanon, H.; Greenfield, S. R.; Gosztola, D. J.; Svec, W. A.; Wasielewski, M. R. *J. Am. Chem. Soc.* **1996**, 118, 10228-10235. (e) Barros, T. C.; Brochsztain, S.; Toscano, V. G.; Filho, P. B.; Politi, M. J. *Photochem. Photobiol. A: Chem.* **1997**, 111, 97-104.

- 19) Saito, I.; Takayama, M.; Sugiyama, H.; Nakatani, K.; Tsuchida, A.; Yamamoto, M. *J. Am. Chem. Soc.* **1995**, *117*, 6406-6407.
- 20) (a) Beaucage, S. L.; Caruthers, M. H. *Tetrahedron Let.* **1981**, *22*, 1859-1802. (b) Caruthers, M.; Beaton, G.; Wu, J. V.; Wiesler, W. *Methods Enzymol.* **1992**, *211*, 3-20. (c) Goodchild, J. *Bioconj. Chem.* **1990**, *1*, 165-187.
- 21) Holmlin, R. E.; Dandliker, P. J.; Barton, J. K. *Bioconj. Chem.* **1999**, *10*, 1122-1130.
- 22) Kelley, S. O.; Holmlin, R. E.; Stemp, E. D. A.; Barton, J. K. *J. Am. Chem. Soc.* **1997**, *119*, 9861-9870.
- 23) (a) Banerjee, S. K.; Borden, A.; Christensen, R. B.; LeClerc, J. E.; Lawrence, C. W. *J. Bacteriol.* **1990**, *172*, 2105-2112. (b) Banerjee, S. K.; Christensen, R. B.; Lawrence, C. W.; LeClerc, J. E. *Proc. Natl. Acad. Sci. USA* **1988**, *85*, 8141-8145.
- 24) (a) Bevers, S.; O'Dea, T.; McLaughlin, L. *J. Am. Chem. Soc.* **1998**, *120*, 11004-11005. (b) Gianolio, D.; McLaughlin, L. *J. Am. Chem. Soc.* **1999**, *121*, 6334-6335. (c) Gianolio, D.; Segismundo, J.; McLaughlin, L. W. *Nucleic Acids Res.* **2000**, *28*, 2128-2134.
- 25) Saito, I.; Takayama, M.; Kawanishi, S. *J. Am. Chem. Soc.* **1995**, *117*, 5590-5591.
- 26) In separate experiments where an NDI chromophore was end-linked to the 5'-hydroxyl group of an adenine base of an oligonucleotide, the irradiations did not lead to the loss of 14 mass units (unpublished results).
- 27) (a) Lewis, R. J.; Hanawalt, P. C. *Nature* **1982**, *298*, 393-396. (b) Liu, J.; Taylor, J.-S. *Nucleic Acids Res.* **1998**, *26*, 3300-3304.
- 28) Young, T.; Nieman, R.; Rose, S. *Photochem. Photobio.* **1990**, *52*, 661-668.
- 29) To minimize possible degradation of those oxidants that are efficient sensitizers of singlet oxygen, reactions may be run anaerobically.
- 30) Schwogler, A.; Burgdorf, L.T.; Carrell, T. *Angew. Chem. Int. Ed. Engl.* **2000**, *39*, 3918-3920.

- 31) Moore, J. N.; Phillips, D.; Nakashima, N.; Yoshihara, K. *J. Chem. Soc., Faraday Trans. 2* **1986**, 82, 745-761.
- 32) (a) Texter, J. *Biopolymers* **1992**, 32, 53-59. (b) Hoffman, R.; Woodward, R. B. *J. Am. Chem. Soc.* **1965**, 87, 2046-2048.
- 33) Lamola, A. A. *Photochem. Photobiol.* **1968**, 7, 619-632.
- 34) (a) Lamola, A. A.; Eisinger, J. *Proc. Natl. Acad. Sci. USA* **1968**, 59, 46-51. (b) Eisinger, J.; Lamola, A. A. *Biochem. Biophys. Res. Commun.* **1967**, 28, 558. (c) Eisinger, J.; Schulman *Proc. Natl. Acad. Sci. USA* **1967**, 58, 895.
- 35) (a) Payne, G.; Sancar, A. *Biochemistry* **1990**, 29, 7715-7727. (b) Kim, S.-T.; Heelis, P. F.; Okamura, T.; Hirata, Y.; Mataga, N.; Sancar, A. *Biochemistry* **1991**, 30, 11262-11270. (c) Ramsey, A. J.; Alderfer, J. L.; Jorns, M. S. *Biochemistry* **1992**, 31, 7134-7142.
- 36) Armitage, B. A.; Yu, C.; Devadoss, C.; Schuster, G. B. *J. Am. Chem. Soc.* **1994**, 116, 9847-9859.
- 37) Dotse, A.K., Boone E.K., Schuster G.B. *J. Am. Chem. Soc.* **2000**, 122, 6825-6833.
- 38) Wan, C.; Fiebig, T.; Kelley, S. O.; Treadway, C. R.; Barton, J. K. *Proc. Natl. Acad. Sci. USA* **1999**, 96, 6014-6019.
- 39) Travers, A. *DNA-Protein Interactions*. Pubs. Chapman and Hall, London, 1993.



## **CHAPTER 7**

### **Conclusions and Further Directions**

Research conducted in many laboratories over the last twenty years has unambiguously shown that radical migration through the base stack of DNA is a general phenomenon, and in duplex DNA can damage oxidatively sensitive sites more than 60 base pairs away from the site of radical introduction. Similar experiments with thymine dimer containing oligonucleotides resulted in the remarkable discovery that photoinduced charge transport from a bound metallointercalator could catalyze the repair of this lesion at a distance. Predictably for such a dramatic discovery, questions soon arose as to the generality of the ability of radical migration to repair thymine dimers. This concern was addressed here by repeating the same reactions with an organic photooxidant, which showed that this independent photooxidant can induce the same repair in approximately the same yield as its metallointercalator counterpart.

Base bulges, base deletions, and base mismatches have all been investigated as barriers to charge transport prior to the work in this dissertation. The parameters for radical migration and possible mechanisms of long range charge transport were further probed by similar experiments with oligonucleotides designed to have A-tracts in various orientations, RNA and chimeric RNA•DNA duplex second strands, and AT tracts were all used in experiments to systematically determine the sequence and structural requirements for radical migration. The results of these investigations supported previous suggestions that charge transport must be, first and foremost, an inherent property of stacked nucleic acids, regardless of conformation. One ramification of these results is that, because strong guanine oxidation was observed across A-tract DNA, mechanistic proposals must not be limited strictly to guanine hopping, which would clearly preclude electron transport across A-track DNA. Other bases, however transiently, must be employed to assist charge transport.

Concurrently, complementary work that applied a very different methodology to DNA ropes and isolated duplexes demonstrated direct conductivity of DNA. Further, other research groups were beginning to suggest numerous possible nanotechnological

applications of larger DNA assemblies to construct arrays and ordered chips for possible use in microelectronics. The parameters of radical migration in isolated duplex oligonucleotides are increasingly well-understood. Research conducted here delineated the requirements a multistranded substrate must have to show robust, stable charge transport. DNA double crossovers were found to serve as excellent media for charge transport; indeed, the three-dimensional architecture of the assembly limited the inhibitory effect that mismatches have on radical migration. Guanine oxidation observed in DX assemblies, though slightly lower than duplex DNA of the same sequence, nevertheless showed that radical migration could occur at distances up to  $\sim 110$  Å. Interestingly, parallel experiments with smaller, single crossovers showed that radical migration may occur in more flexible systems, but that this flexibility in effect allows nonspecific transfer of charge between duplexed domains. Guanine oxidation was found to partition among the four arms that make up the junction with only limited dependence on the preferred stacking conformations. This lack of specificity probably precludes stack-specific control over charge transport in any assembly that uses single four way junctions as building blocks.

Long range charge transport in nucleic acids is here shown to be not only a general phenomenon, but also a phenomenon inherent to many different heteroaromatic base stacks. In total, it was found that radical migration proceeds through A-tracts, mixed RNA/DNA hybrids, four way junctions, and double crossover junctions. Proteins have also been shown to be able to participate in long range charge transport in previous research. This result, bolstered by the wide variety of nucleic acid forms able to conduct charge transport, as demonstrated in this work, raises the interesting possibility that natural systems may somehow employ radical migration to detect base lesions or other stack disruptions. However, considerable hurdles exist to harnessing this facet of nucleic acid chemistry to help treat disease, to use as a diagnostic tool, or to develop tools for molecular biology.

The metallointercalators that have been applied so frequently here and previously to probe long range charge transport were originally designed as small molecule mimics of DNA-binding proteins; as such, technological application of their chemistry should be considerably more direct. Extensive research reviewed here found that not only did these metal complexes bind to DNA with very high affinity, but that binding sites could be targeted based on a combination of factors, including (most notably) the presence of mismatches, the conformation of bases at particular sites, the hydrogen bonding patterns these bases make in the major groove, and potential van der Waals contacts between bases and metallointercalators. In addition, one site-specific metal complex,  $\Delta$ -1-Rh(MGP)<sub>2</sub>phi<sup>5+</sup>, was found here to prevent transcription factors from binding to an initiation site by steric occlusion. The metal complex, which has a similar affinity for the DNA binding site of the protein, in effect competes with the transcription factor  $\gamma$ AP-1, and thus could easily serve to disrupt transcription initiation complexes, possibly even *in vivo*.

This work begins to address some of the demands that will need to be met in order for charge transport to be applicable in microarray technologies, in techniques for screening potential molecules for repair of thymine dimers at a distance, and in novel applications of the recognition of metallointercalators as potential therapeutic agents. Developing DNA recognition by metallointercalators or radical migration within DNA into applications that will promote the betterment of humanity will require knowledge of the fundamental science behind applications, imagination and discipline to reliably exploit promising discoveries, and the wisdom to choose the correct questions and techniques to pursue. The scope of this challenge should serve to inspire and to frustrate researchers for many years.

## **APPENDIX 1**

### **Variations in DNA Charge Transport with Nucleotide Composition and Sequence\***














\*Adapted from T. T. Williams, D. T. Odom, J. K. Barton. *J. Am. Chem. Soc.* (2000) **122**,  
9048-9049.

Long range oxidative damage to DNA has been demonstrated in experiments using a variety of remotely bound oxidants.<sup>1-5</sup> However, the mechanism(s) by which charge is transported through the base pair stack needs still to be established. Recent theoretical proposals bring together tunneling and hopping mechanisms to describe charge transport over various distance and energetic regimes.<sup>6</sup> Based upon measurements of oxidative damage yield, it has been proposed that charge transport occurs by hopping between guanine sites and tunneling through TA steps.<sup>7</sup> In accord with the notion that low energy guanine “stepping stones” are required for efficient long-range charge transport, oxidative damage over long distance was not observed when 5'-TATATA-3' intervened between G sites.<sup>8</sup> Phonon-assisted polaron hopping has been suggested as an alternative mechanism by which charge propagates through DNA.<sup>9</sup> In this model, the sequence-dependent conformational dynamics of DNA upon hole injection are expected to aid in charge transport, but no sequence-dependent effects have been documented.

These different proposals have led us to investigate systematically the effect of intervening base composition and sequence on long-range oxidative DNA damage. Here, we vary the intervening sequence between two oxidatively sensitive sites without varying overall base composition. Previous experiments have shown that oxidative damage can occur up to 200 Å from the site of hole injection; the sequence-dependent effects we observed were attributed to variations in sequence-dependent structure and flexibility.<sup>10</sup> Recent ultrafast spectroscopic studies have shown that base dynamics may gate charge transport,<sup>11</sup> and fluorescence studies on DNA assemblies containing bound donors and acceptors have underscored the sensitivity of fluorescence quenching to the stacking of the donor, acceptor, and intervening bases.<sup>12</sup>

Table 1 shows substrates that were designed to examine long-range charge transport through sequences rich in AT base pairs. Each sequence contains two 5'-CGGC-3' doublets,<sup>13</sup> one proximal and one distal to the tethered intercalating

Table 8.1. Long Range Oxidative Damage in DNA Sequences Functionalized with the Tethered Photooxidant Rh(phi)<sub>2</sub>bpy'<sup>3+</sup>

Sequence <sup>a</sup>	Assembly <sup>b</sup>	Distal/Proximal Oxidation Ratio <sup>c</sup>
 AC GAGCCGAAAAAGCCGTAT-3' 3'-TG CTCGGCTTTTCGGCATA-5' *	TT-2	0.9 ± 0.1
 AC GAGCCGTTTGTCCGTAT-3' 3'-TG CTCGGCAAAACGGCATA-5' *	AA-2	2.5 ± 0.2
 AC GAGCCGTATAGCCGTAT-3' 3'-TG CTCGGCATATCGGCATA-5' *	AT-2	0.6 ± 0.2
 AC GAGCCGAAAAAGCCGTAT-3' 3'-TG CTCGGCTTTTTCGGCATA-5' *	TT-3	1.2 ± 0.3
 AC GAGCCGTTTTTGTCCGTAT-3' 3'-TG CTCGGCAAAAAACGGCATA-5' *	AA-3	3.5 ± 0.5
 AC GAGCCGTATATAGCCGTAT-3' 3'-TG CTCGGCATATATCGGCATA-5' *	AT-3	1.0 ± 0.2
 AC GAGCCGAAAAAAAAAGCCGTAT-3' 3'-TG CTCGGCTTTTTTTCGGCATA-5' *	TT-4	2.2 ± 0.4
 AC GAGCCGTTTTTTTGTCCGTAT-3' 3'-TG CTCGGCAAAAAAACGGCATA-5' *	AA-4	2.3 ± 0.1
 AC GAGCCGTATATATAGCCGTAT-3' 3'-TG CTCGGCATATATATCGGCATA-5' *	AT-4	1.8 ± 0.2
 AC GAGCCGAAAAAAAAAGCCGTAT-3' 3'-TG CTCGGCTTTTTTTCGGCATA-5' *	TT-5	0.4 ± 0.3
 AC GAGCCGTTTTTTTTTGTCCGTAT-3' 3'-TG CTCGGCAAAAAAACGGCATA-5' *	AA-5	1.2 ± 0.1
 AC GAGCCGTATATATATAGCCGTAT-3' 3'-TG CTCGGCATATATATATCGGCATA-5' *	AT-5	1.3 ± 0.1
 AC GAGCCGTATAGCTATAGCCGTAT-3' 3'-TG CTCGGCATATCGATATCGGCATA-5' *	TAGC	0.6 ± 0.1

**a** Sequences isolated and purified as described previously (13). Only the  $\Delta$  diastereomer was used in these studies. The photooxidant is schematically shown intercalated into its primary binding site based on the photocleavage patterns. \* denotes the site of <sup>32</sup>P labeling.

**b** Abbreviations are based on the identity and repetition of the two base pair units spanning the distal and proximal guanine doublets on the strand complementary to the metallointercalator bearing strand.

**c** Intensity ratios of the DNA damage at the 5'-G of guanine doublets proximal and distal to the rhodium complex were measured after photooxidation using conditions described in Figure 1. Values represent averages of three trials.

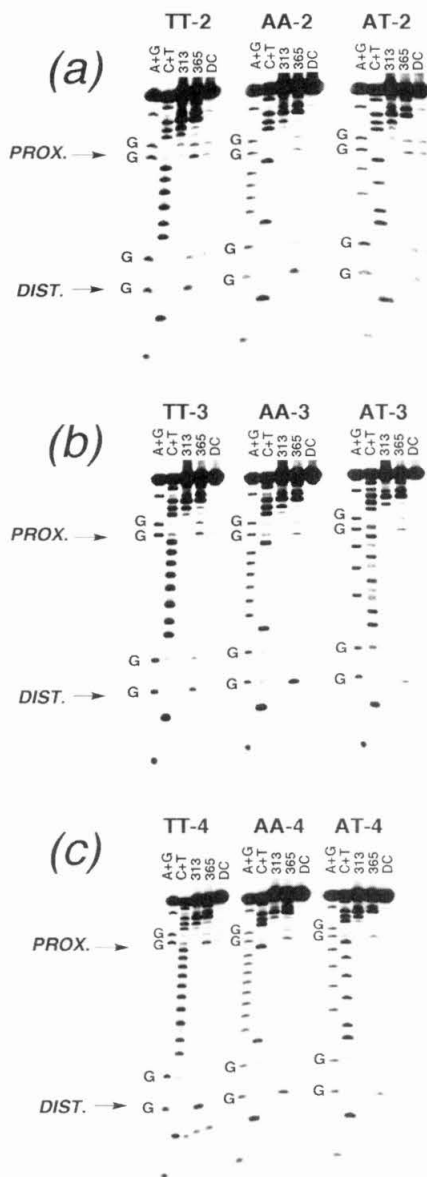


photooxidant,  $Rh(\phi)_2bpy^{3+}$  ( $\phi$  = phenanthrenequinone diimine);<sup>15</sup> the rhodium complex promotes damage to the 5'-G of a guanine doublet by photoinduced electron transport. Irreversible trapping of the guanine radical by  $O_2$  and  $H_2O$ , once generated, is assumed to be independent of variations in the global DNA sequence, since each 5'-GG-3' is identical in its local sequence context. The ratio in yield of damage at the 5'-G of the 5'-GG-3' site for the distal versus proximal sites provides a measure of relative transport efficiency through the intervening sequence.<sup>16</sup> The damage yield can be determined by treatment of the 5'-<sup>32</sup>P labeled oligonucleotide with piperidine, followed by polyacrylamide gel electrophoresis and phosphorimager analysis.<sup>1,17-19</sup>

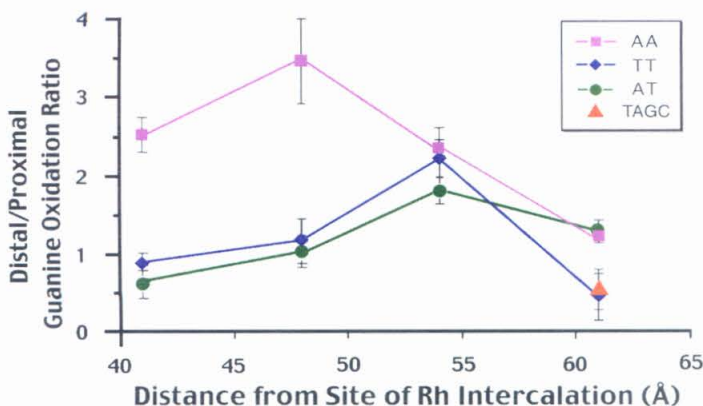
Figure 8.1 shows the phosphorimager after photooxidation of AA-2, TT-2, and AT-2. For these assemblies, the base pair composition between proximal and distal guanine doublets is constant, although the sequence of bases varies (Table 8.1). If the mechanism of charge transport were strictly a function of hopping between guanine sites,<sup>6,7</sup> one would expect the distal/proximal ratio of oxidative damage for these assemblies to be equal. In fact, based upon data obtained by others for charge transport across 5'-ATAT-3',<sup>7</sup> minimal distal oxidation might be expected for all assemblies.<sup>20</sup> As is evident in Figure 8.1 and quantitated in Table 8.1, this is not the case. Instead, we find significant distal oxidation and in particular the ratio to be consistently higher for the AA assemblies and lower for the TT and AT assemblies. Based upon energetic considerations<sup>21</sup> as well as poor stacking overlap, the TT sequences might be expected to be the poorest conduits for charge transport.<sup>22</sup> Similar considerations dictate that adenine tracts should yield efficient charge transport, and duplexes containing AT tracts might be expected to show damage in the intermediate range.

Table 8.1 also shows the effect of increasing the length of the intervening segment. Based upon a guanine hopping model,<sup>6,7</sup> increasing the number of adenines





**Figure 8.1.** Phosphorimager of a denaturing 20% polyacrylamide gel showing the sequence dependence of long range oxidative damage in assemblies containing tethered  $\Delta$ -Rh(phi)<sub>2</sub>bpy<sup>13+</sup>. Shown are the results from (a) sequences containing 4 base pairs intervening between distal and proximal guanine doublets, AA-2, AT-2, and TT-2, (b) sequences containing 6 base pairs intervening between distal and proximal guanine doublets, AA-3, AT-3, and TT-3, (c) sequences containing 8 base pairs intervening between distal and proximal guanine doublets, AA-4, AT-4, and TT-4. Sequence designations are as in Table 8.1, where the strand containing guanine doublets is 5'-<sup>32</sup>P end-labeled. For each assembly, lanes are as follows: A+G, C+T, C show Maxam-Gilbert sequencing reactions (34); 313 shows the fragment after direct photocleavage by the photoexcited metallointercalator at 313 nm for 10 min without piperidine treatment; 365 nm shows the fragment after irradiation at 365 nm for 1 h at 23°C, followed by piperidine treatment; DC (dark control) shows samples not irradiated but treated with piperidine. All samples contained 4  $\mu$ M metal complex-tethered duplex, 20 mM Tris-HCl, pH 8, 10 mM NaCl. Sites of proximal and distal 5'-GG-3' damage are indicated.



**Figure 8.2.** A plot of the distal/proximal guanine oxidation ratio versus the distance from the intercalation site, based upon data given for the assemblies in Table 8.1. Distances are estimated from the primary intercalation site, established by direct photocleavage at 313 nm, and assuming 3.4 Å stacking.

through TA sequences were tunneling, as proposed,<sup>7</sup> one would expect negligible oxidative damage at the distal site. However, as is evident in Figure 8.2, it is the *sequence* of bases that is critical. Increasing the length of the AA sequence only slightly

decreases the guanine oxidation ratio, consistent with the shallow distance dependence expected for hole hopping through *all* the bases. Remarkably, in the case of the TT and AT assemblies, there appears to be an *increase* in oxidation ratios with increasing oligonucleotide length from 4 to 8 intervening base pairs.<sup>24,25</sup> Furthermore, in contrast to that predicted by a guanine-hopping model, insertion of a GC step into the otherwise A•T bridge actually *decreases* the efficiency of charge transport (Table 8.1, TAGC). This result provides clear evidence that strict guanine hopping cannot describe long-range DNA-mediated charge transport in this system.<sup>26</sup> Alternative mechanisms which involve hopping also among other bases are required.<sup>29</sup>

The variations observed with sequence and length must depend also upon the conformational dynamics associated with these sequences. In contrast to hole hopping models developed primarily for aromatic crystals,<sup>30</sup> here electronic coupling between bases is dynamic and sequence-dependent. For the AA oligonucleotides, the efficiency of charge transport may depend upon the extensive overlap of the stacked purines. Moreover, A-tracts are well known to adopt conformations that differ from that of canonical B-form DNA.<sup>31</sup> The increase in damage ratios with increasing length for TT

sequences is consistent with the cooperative formation of conformational domains in longer A-tract DNA structures; generation of structures that introduce bends into DNA seems to require a nucleating core of five adenines before the A-tract stabilizes into a bend.<sup>32</sup> In our system, convergence of the oxidation ratios occurs in the duplexes containing six or more A•T base pairs between the guanine doublets. However, the results we obtain with 5'-TATA-3' can now be viewed in a systematic context;<sup>33</sup> in contrast to previous reports<sup>7</sup> using a slightly different sequence that did not address the effects of increasing the length of the domain. As with the A tracts, the increase in transport efficiency with lengthening of this segment may also reflect some conformational transition associated with the longer, ordered sequence, but no precedence for such a finding is available. Rather than considering hopping from guanine to guanine within a DNA segment, then, we might consider hopping between domains. Our results strongly suggest that a simple guanine hopping model is insufficient to model long-range charge transport in DNA. The observations made here underscore the need to consider the impact on DNA charge transport of sequence-dependent conformational domains and their dynamics.

## REFERENCES AND FOOTNOTES

- 1) Hall, D. B.; Holmlin, R. E.; Barton, J. K. *Nature* **1996**, 382, 731-735.
- 2) Gasper, S. M.; Schuster, G. B. *J. Am. Chem. Soc.* **1997**, 119, 12762-12771.
- 3) a) Hall, D. B.; Kelley, S. O.; Barton, J. K. *Biochemistry* **1998**, 37, 15933-15940. b) Arkin, M. R.; Stemp E. D. A.; Barton, J. K. *Chem. Biol.* **1997**, 4, 389-400.
- 4) Meggers, E.; Kusch, D.; Spichy, M.; Wille, U.; Giese, B. *Angew. Chem., Int. Engl. Ed.* **1998**, 37, 460-462.
- 5) Saito, I; Nakamura, T.; Nakatani, K.; Yoshioka, Y.; Yamaguchi, K.; Sugiyama, H. *J. Am. Chem. Soc.* **1998**, 120, 12686-12687.

- 6) a) Bixon, M.; Jortner, J. *J. Phys. Chem. B* **2000**, *104*, 3906-3913. b) Bixon, M.; Giese, B.; Wessely, S.; Langenbacher, T.; Michel-Beyerle, M. E.; Jortner, J. *Proc. Natl. Acad. Sci. USA* **1999**, *96*, 11713-11716. c) Berlin, Y. A.; Burin, A. L.; Ratner, M. A. *J. Phys. Chem. A* **2000**, *104*, 443-445. d) see also Felts, A. K.; Pollard, W. T.; Friesner, R. A. *J. Phys. Chem.* **1995**, *99*, 2929-2940.
- 7) a) Meggers, E.; Michel-Beyerle, M. E.; Giese, B. *J. Am. Chem. Soc.* **1998**, *120*, 12950-12955. b) Giese, B.; Wessely, S.; Spormann, M.; Lindemann, U.; Meggers, E.; Michel-Beyerle, M. E. *Angew Chem., Int. Ed. Engl.* **1999**, *38*, 996-998.
- 8) Nakatani, K.; Dohno, C.; Saito, I. *J. Am. Chem. Soc.* **1999**, *121*, 10854-10855.
- 9) a) Henderson, P. T.; Jones, D.; Hampikian, G.; Kan, Y.; Schuster, G. B. *Proc. Natl. Acad. Sci. USA* **1999**, *96*, 8353-8358. b) Ly, D.; Sanii, L.; Schuster, G. B. *J. Am. Chem. Soc.* **1999**, *121*, 9400-9410. c) Conwell, E. M.; Rakhmanova, S. V. *Proc. Natl. Acad. Sci. USA* **2000**, *97*, 4556-4560.
- 10) Núñez, M. E.; Hall, D. B.; Barton, J. K. *Chem. Biol.* **1998**, *6*, 85-97.
- 11) Wan, C.; Fiebig, T.; Kelley, S. O.; Treadway, C. R.; Barton, J. K.; Zewail, A. H. *Proc. Natl. Acad. Sci.* **1999**, *96*, 6014-6019.
- 12) a) Kelley, S. O.; Barton, J. K. *Science* **1999**, *283*, 375-381. b) Kelley, S. O.; Holmlin, R. E.; Stemp, E. D. A.; Barton, J. K. *J. Am. Chem. Soc.* **1997**, *119*, 9861-9870. c) Kelley, S. O.; Barton, J. K. *Chem. Biol.* **1998**, *5*, 413-425.
- 13) Both empirical and theoretical studies have shown that the 5'-G of 5'-GG-3' sites are preferentially oxidized.<sup>1,14</sup>
- 14) Sugiyama, H.; Saito, I. *J. Am. Chem. Soc.* **1996**, *118*, 7063-7068.
- 15) Holmlin, R. E.; Dandliker, P. J.; Barton, J. K. *Bioconjugate Chem.* **1999**, *10*, 1122-1130.
- 16) a) Hall, D. B.; Barton, J. K. *J. Am. Chem. Soc.* **1997**, *119*, 5045-5046. b) Rajski, S. R.; Kumar, S.; Roberts, R. J.; Barton, J. K. *J. Am. Chem. Soc.* **1999**, *121*, 5615-5616.

- 17) Chung, M.-H.; Kiyosawa, H.; Ohtsuka, E.; Nishimura, S.; Kasai, H. *Biochem. Biophys. Res. Commun.* **1992**, 188, 1-7.
- 18) Cullis, P. M.; Malone, M. E.; Merson-Davies, L. A. *J. Am. Chem. Soc.* **1996**, 118, 2775-2781.
- 19) These piperidine labile lesions correlate linearly with oxidative damage as revealed by enzymatic treatment; Rajski, S. R. unpublished results.
- 20) Sequence contexts, oxidants, and reaction conditions vary.
- 21) a) Steenken, S.; Jovanovic, S. V. *J. Am. Chem. Soc.* **1997**, 119, 617-618. b) Seidel, C. A. M.; Schultz, A.; Sauer, M. H. M. *J. Phys. Chem.* **1996**, 100, 5541-5553.
- 22) We assay charge transport to the strand containing the 5'-GG-3' doublet. However, phi complexes of rhodium intercalate over both strands,<sup>23</sup> and thus, some hole injection may occur into both strands; interstrand charge transfer is also possible.<sup>12a</sup>
- 23) Kielkopf, C. L.; Erkkila, K. E.; Hudson, B. P.; Barton, J. K.; Rees, D. C. *Nat. Struct. Biol.* **2000**, 7, 117-121.
- 24) Local denaturation might arise in longer AT segments. However, parallel experiments carried out at 5°C yielded analogous results.
- 25) Interstrand electron transfer may occur in longer oligonucleotides.
- 26) The rhodium excited state appears to be sufficiently potent to oxidize all of the bases.<sup>27</sup> Nonetheless, hole hopping must be fast relative to thermal relaxation at a site to account for oxidative damage at a distal guanine.<sup>28</sup>
- 27) Turro, C.; Evenzahav, A.; Bossman, S. H.; Barton, J. K.; Turro, N. J. *Inorg. Chim. Acta* **1996**, 243, 101-108.
- 28) Dee, D.; Baur, M. E. *J. Chem. Phys.* **1974**, 60, 541-560.
- 29) Our data provide neither support nor refutation of the phonon-assisted polaron hopping model.
- 30) a) Le Blanc, O. H. *J. Chem. Phys.* **1961**, 35, 1275-1279 b) Katz, J. L.; Rice, S. A.; Choi, S. I.; Jortner, J. *J. Chem. Phys.* **1963**, 39, 1683-1688.

- 31) a) Crothers, D. M.; Drak, J.; Kahn, J. D.; Levene, S. D. *Meth. Enzym.* **1992**, 212, 3-29 b) Koo, H. S.; Drak, J.; Rice, J. A.; Crothers, D. M. *Biochemistry* **1990**, 29, 4227-4234.
- 32) a) Crothers, D. M. personal communication b) Price, M. A.; Tullius, T. D. *Biochemistry* **1993**, 32, 127-136. c) Nadeau, J. G.; Crothers, D. M. *Proc. Natl. Acad. Sci. USA* **1989**, 86, 2622-2626.
- 33) The low charge transport efficiency for AT-2 seen here, on a relative basis, may be consistent with earlier reports.<sup>7,8</sup> The explanation may rest on the increased flexibility and poor overlap associated with 5'-TATA-3'.<sup>34</sup>
- 34) a) Dickerson, R. E. *Structure, Motion, Interaction, and Expression of Biological Macromolecules*. **1998**, 17-36. b) Dickerson, R. E. *Nucleic Acids Res.* **1998**, 26, 1906-1926. c) Kim, J. L.; Nikolov, D. B.; Burley, S. K. *Nature* **1993**, 365, 520-527. d) Kim, Y. C.; Geiger, J. H.; Hahn S.; Sigler, P. B. *Nature* **1993**, 365, 512-520.